Mitteilungen aus dem Institut für Mechanik

Claus Oberste-Brandenburg

Thermomechanical modeling of shape memory alloys at different length scales

Heft Nr. 144

RUHR-UNIVERSITÄT BOCHUM

Institut für Mechanik
Ruhr-Universität Bochum

Claus Oberste-Brandenburg

Thermomechanical modeling of shape memory alloys at different length scales

Mitteilungen aus dem Institut für Mechanik Nr. 144

Juli 2007

Herausgeber:

Institut für Mechanik
Ruhr-Universität Bochum
D-44780 Bochum

ISBN 978-3-935892-19-3

Printed in Germany

Zusammenfassung

Diese Arbeit zeigt verschiedene Aspekte der kontinuumsmechanischen Modellierung von Phasentransformationen auf. Basierend auf den kontinuumsmechanische Grundlagen werden, abhängig von der zu beantwortenden Fragestellung, zwei Beschreibungen erarbeitet.

Der erste entwickelte Ansatz basiert auf einer expliziten Nachverfolgung des Bewegung der Phasengrenze und ermöglicht daher eine sehr genaue Betrachtung lokaler Phänomene in einem Einkristall. Er kann z.B. im Rahmen eines Werkstoffdesigns verwendet werden. Zur Beschreibung der Einzelphasen wird die Randelementemethode verwendet; die numerische Beschreibung der Bewegung der Phasengrenze verwendet die selbe Diskretisierung.

Die zweite Beschreibung setzt auf einer anderen Beschreibungsebene an. Hier steht die Verwendbarkeit der entwickelten Größen in einem Stoffgesetz zur Beschreibung ausgedehnter Strukturen im Vordergrund. Daher wird eine geeignete Homogenisierung der mikromechanisch hergeleiteten Größen durchgeführt und korrespondierende makroskopische Größen erarbeitet. Der Zusammenhang zwischen klassischen Beschreibungen und diesen Größen werden aufgezeigt.

Summary

This Thesis covers diffrent aspect of the continuum-mechanical modeling of phase transformations. Based on the principles of continuum mechanics, two descriptions are developed based on the problem statement to be answered.

The first approach is based on the explicit tracking of the movement of the phase boundary. Therefore, it allows to examine local phenomena within the grain with high accuracy and may be used in a material design process. The boundary element method is employed to describe the bulk material; the same discretization is used to track the movement of the phase boundary.

The second described approach is focused on another length scale. The use of the description within a material law to describe large structures is the main focus. Thus, an appropriate homogenization scheme is employed in order to bridge the micro-mechanically developed measures to the macroscopic scale. The relations between classical descriptions an the newly developed measures are shown.

Vorwort

Die vorliegende Arbeit entstand während meiner Tätigkeit am Institut für Mechanik der Ruhr-Universität Bochum. Sie wurde von der Fakultät für Maschinenbau der Ruhr-Universität Bochum als Habilitationsschrift angenommen.

Ich möchte mich an dieser Stelle besonders bei Prof. Dr.-Ing. Otto T. Bruhns für die Möglichkeit, die Arbeit zu erstellen, das Umfeld und die beständige Motivation bedanken.
Prof. Dr.-Ing. Gunther Eggeler und Prof. Dr.-Ing. Senator h.c. Günther Kuhn danke ich für das Interesse an der Arbeit und die Übernahme der Koreferate.

Die Freude an der Arbeit wird sehr stark durch das direkte Umfeld geprägt. Diese habe ich am Lehrstuhl immer empfunden und möchte mich bei allen Kollegen herzlich bedanken, die mich während dieser Zeit begleitet haben.

Langenargen, im Juli 2007 Claus Oberste-Brandenburg

Referenten: Prof. Dr.-Ing. Otto T. Bruhns
Prof. Dr.-Ing. Gunther Eggeler
Prof. Dr.-Ing. Senator h.c. Günther Kuhn

Tag der Einreichung: 27.10.2005
Tag der mündlichen Prüfung: 26.06.2006

Contents

List of Figures

List of Tables

List of Symbols

scalar variables	
c	material parameter for the interfacial velocity
c_p	specific heat capacity at constant pressure
c_v	specific heat capacity at constant volume
$\mathrm{d}a$	area of infinitesimal area element in $\mathcal{B}$
$\mathrm{d}A$	area of infinitesimal area element in $\mathcal{B}_0$
$\mathrm{d}v$	infinitesimal volume element in $\mathcal{B}$
$\mathrm{d}V$	infinitesimal volume element in $\mathcal{B}_0$
g	specific Gibbs free energy
h	specific enthalpy
$\dot{h}_{lat}$	latent heat
m	mass
n_{reg}	number of regions
q^*	prescribed value for $\boldsymbol{\nabla} u \cdot \mathbf{n}$
$\hat{q}$	derivative of fundamental solution, i.e. $\boldsymbol{\nabla} \hat{u} \cdot \mathbf{n}$ (section 4.3.2.1)
r	specific volumetric heat sources
s	specific entropy
u	specific internal energy
u	unknown measure (section 4.3.2.1)
u^*	prescribed value for u (section 4.3.2.1)
$\hat{u}$	fundamental solution (section 4.3.2.1)
u_Λ	interface velocity
w	specific deformation energy
A_s^0	austenite start temperature at zero stress
A_f^0	austenite finish temperature at zero stress
A_Λ	surfacial area
E	Young's modulus
E	kinetic energy (chapter 2)
E^t	total energy
F^ξ	threshold value
G	shear modulus
I_1^A, I_2^A, I_3^A	invariants of $\mathbf{A}$

J_2^A, J_3^A	invariants of the deviator of $\mathbf{A}$
J	Jacobian
M	molar mass (section 3.2)
M_s^0	martensite start temperature at zero stress
M_f^0	martensite finish temperature at zero stress
M_{tot}	total mass of body
N_I	shape functions
P	work rate
P^ξ	potential
$\dot{Q}$	thermal energy supply
R	special gas constant
R_m	gas constant
S	entropy
T	temperature
U	internal energy (chapter 2)
U	interface velocity (chapter 4)
U_Λ	interface velocity in $\mathcal{B}_0$
U^perp	tangential interface velocity
$\dot{W}$	rate of the deformation energy
α	parameter of isotropic thermal expansion
α^{P0}	penalty factor
α^{PBC}	penalty factor
Δs	parameter for to the entropy difference of the phases
φ	specific Helmholtz free energy
φ_c	difference of the Helmholtz free energy of the phases
λ^A	eigenvalue of $\mathbf{A}$
λ	twinning-ratio (section 4.2.2.2)
λ	Lamé-parameter
λ^ξ	Lagrange multiplier
μ	Lamé-parameter
ν	Poisson's ratio
ρ	mass density in $\mathcal{B}$
ρ_0	mass density in $\mathcal{B}_0$
ζ^Λ	dissipation due to interfacial movement
Λ	interface or level set function describing interface
Θ	temperature
Θ_0	reference temperature or equilibrium temperature
Θ_D	Debye temperature
$\hat{\Theta}$	dimensionless temperature

first order tensors

$\mathbf{a}$	general vector
$\mathbf{b}$	general vector
$\mathbf{b}$	volumetric force
$\boldsymbol{c}$	movement of observer
$\mathrm{d}\mathbf{a}$	infinitesimal area element in $\mathcal{B}$
$\mathrm{d}\mathbf{A}$	infinitesimal area element in $\mathcal{B}_0$
$\mathrm{d}\mathbf{x}$	infinitesimal line element $\mathcal{B}$
$\mathrm{d}\mathbf{X}$	infinitesimal line element in $\mathcal{B}_0$
$\mathbf{e}$	unit base vector
$\mathbf{f}$	force vector (chapter 2)
$\mathbf{g}_i$	covariant base vector
$\mathbf{g}^i$	contravariant base vector
$\mathbf{n}$	unit normal vector
$\mathbf{n}_\Lambda$	unit normal vector on Λ
$\mathbf{n}^\perp$	unit vector normal to $\mathbf{n}$
$\mathbf{q}$	heat flux in $\mathcal{B}$
$\mathbf{q}_0$	heat flux in $\mathcal{B}_0$
$\mathbf{r}^H$	approximation of $\mathbf{r}$
$\mathbf{r}$	position vector for point on interface
$\mathbf{r}^*$	weighting function
$\dot{\mathbf{r}}_c$	constraint on the movement of the interface
$\mathbf{v}$	velocity of a material point
$\mathbf{v}_\Lambda$	velocity of point on interface
$\mathbf{x}$	position of a material point in $\mathcal{B}$
$\mathbf{x}_\Lambda$	position of a point on the interface
$\mathbf{N}_\Lambda$	unit normal vector on Λ in $\mathcal{B}_0$
$\mathbf{N}^A$	eigenvector of $\mathbf{A}$
$\mathbf{V}_\Lambda$	velocity of point on interface in $\mathcal{B}_0$
$\mathbf{X}$	position of a material point in $\mathcal{B}_0$
$\boldsymbol{\alpha}$	tensor of thermal expansion

second order tensors

$\mathbf{1}$	second order unit tensor
$\mathbf{b}$	left Cauchy-Green tensor
$\mathbf{e}^{(m)}$	Hills strain measure in $\mathcal{B}$
$\mathbf{C}_M$	right Cauchy-Green tensor due to phase transition
$\mathbf{C}$	right Cauchy-Green tensor
$\mathbf{D}$	stretching tensor, symmetric part of velocity gradient tensor
$\mathbf{E}^{(m)}$	Hills strain measure in $\mathcal{B}_0$
$\mathbf{F}$	deformation gradient
$\mathbf{L}$	velocity gradient tensor
$\mathbf{P}$	nominal stress tensor
$\mathbf{P}_c$	projection tensor
$\mathbf{Q}$	proper orthogonal tensor
$\mathbf{R}$	rotation tensor
$\mathbf{S}$	second Piola-Kirchhoff stress
$\mathbf{T}_X$	triplet of infinitesimal vectors
$\mathbf{T}$	first Piola-Kirchhoff stress
$\mathbf{U}$	right stretch tensor
$\mathbf{U}_0$	stretch tensor due to crystallographic change
$\mathbf{V}$	left stretch tensor
$\mathbf{W}$	antimetric part of velocity gradient tensor
$\boldsymbol{e}$	general strain
$\boldsymbol{\varepsilon}^{pt}$	strain due to phase transition
$\boldsymbol{\sigma}$	Cauchy stress tensor
$\boldsymbol{\kappa}$	eigenstrain
$\boldsymbol{\mu}$	Eshelby tensor
$\boldsymbol{\mu}^{\Delta}$	difference of the Eshelby tensor between the phases
$\dot{\boldsymbol{\xi}}$	macroscopic flux conjugated to $\boldsymbol{\mu}^{\Delta}$
$\boldsymbol{\tau}$	Kirchhoff stress
$\boldsymbol{\Pi}$	general stress

fourth order tensors

$\mathbf{1}^{(4)}$	fourth order unit tensor
$\mathbb{C}$	fourth order elastic stiffness tensor or elastic tangent

$\mathbb{C}_0$	$\mathbb{C}$ at reference temperature
$\mathbb{C}_\Theta$	temperature dependence of $\mathbb{C}$
$\mathbb{D}$	elastic compliance tensor

matrices, etc.

$\mathbf{f}$	vector related to tangential interfacial movement
$\mathbf{f}^{FN}$	vector related to normal interfacial movement
$\mathbf{f}^{P0}$	vector related to tangential interfacial movement
$\tilde{\mathbf{f}}$	predictor for
$\mathbf{p}$	position vector of interfacial nodes
$\tilde{\mathbf{p}}$	predictor for $\mathbf{p}$
$\hat{\mathbf{p}}$	corrector for $\mathbf{p}$
$\mathbf{q}$	BEM-vector (chapter 4)
$\mathbf{u}$	BEM-vector (chapter 4)
$\mathbf{C}$	BEM-matrix (chapter 4)
$\hat{\mathbf{E}}$	BEM-kernel (chapter 4)
$\mathbf{G}$	BEM-matrix (chapter 4)
$\mathbf{H}$	BEM-matrix (chapter 4)
$\hat{\mathbf{H}}$	BEM-matrix (chapter 4)
$\mathbf{M}$	matrix related to interfacial movement
$\mathbf{M}^N$	matrix related to normal interfacial movement
$\mathbf{M}^{PBC}$	matrix related to normal interfacial movement
$\tilde{\mathbf{M}}$	predictor for $\mathbf{M}$
$\mathbf{U}$	BEM-kernel (chapter 4)
$\delta(\bullet)$	Dirac-Delta function
δ_{ij}	Kronecker-delta
$g_{ij}, g^{ij}, G_{ij}, G^{ij},$	metric tensors
δ_{ij}	Kronecker-delta
ϵ_{ijk}	Levi-Civita symbol
$\boldsymbol{\epsilon}$	Levi-Civita symbol, symbolic notation
$\boldsymbol{\xi}^\beta$	$\beta \in \{h, p, q\}$ set of internal variables
$\mathcal{B}$	actual configuration
$\mathcal{B}_0$	reference configuration
$\mathcal{R}$	region
Ω	domain of body under consideration
Γ	domain boundary
$\emptyset$	empty set

$\overset{\circ}{(\bullet)}$	objective time derivative
$\dot{(\bullet)}$	material time derivative

Operators etc.

$\otimes$	dyadic product
$\times$	cross product
$\cdot$	single contraction, scalar product
:	double contraction
$(\bullet)^T$	transpose
$(\bullet)^{-1}$	inverse
$(\bullet)^{-T}$	inverse of transpose
$\mathrm{tr}\,(\bullet)$	trace of a second order tensor
$(\bullet)'$	deviator
$\mathrm{sym}\,(\bullet)$	symmetric part
$\mathrm{skew}\,(\bullet)$	antimetric part
$\det(\bullet)$	determinant
$\mid \bullet \mid$	absolute value
$[\bullet]$	jump at interface
$\langle\bullet\rangle$	mean value at interface
$\boldsymbol{\nabla}$	gradient in $\mathcal{B}$
$\boldsymbol{\nabla}_0$	gradient in $\mathcal{B}_0$
$\phi^*(\bullet)$	pull back
$\phi_*(\bullet)$	push forward
$\mathbf{L}_\nu(\bullet)$	Lie derivative

superscripts

$(\bullet)^*$	measure in new observer frame
$(\bullet)^+$	$\bullet$ is related to region $+$
$(\bullet)^-$	$\bullet$ is related to region $-$
$(\bullet)^A$	measure specific to austenitic phase
$(\bullet)^M$	measure specific to martensitic phase

subscripts

$(\bullet)_r$	reversible part
$(\bullet)_i$	irreversible part
$(\bullet)_\Lambda$	measure related to interface Λ

$(\bullet)_k$	measure at time step k

abbreviations	
bcc	body-centered-cubic
fcc	face-centered-cubic
BEM	boundary element method
CTM	crystallographic theory of martensite
DSC	differential scanning calorimeter
FEM	finite element method
GWMFE	gradient-weighted moving finite elements
RVE	representative volume element
SMA	shape memory alloys
XFEM	extended finite element method

1 Introduction

When a mathematical description of the behavior of a material is to be developed, different views regarding the material at different length scales might be considered. This choice may depend on the material considered, the task the material law is designed for, and the educational background of the developer of the material law. Classically, the following definitions are common, the denotations might be used differently:

- The *macroscopic scale* which is observable with unarmed eye. On this scale, the material is treated as a continuum. Models developed solely following a descriptive design on this scale are often termed phenomenological, as they do not incorporate the underlying scales. This leads sometimes to the problem, that only the phenomena observed during the modeling process can be described appropriately but fail when other situations are present. However, as these models are derived on the macroscale, they allow to be incorporated into finite element codes to model structures at a larger scale.

- The *mesoscopic scale* is the scale underlying the macroscopic scale. Here, the inhomogeneities due to the fact that a polycrystal consist of differently oriented single crystals is taken into account. Models derived on this scale often incorporate the behavior of the single crystal and use a scale transition scheme to reach the macroscopic scale. Due to the modeling scale and the scale transition, the numerical effort may be too large on the macroscopic scale for some applications.

- The *microscale* explicitly incorporates defects in the arrangement of the atoms as dislocations. Furthermore, phase boundaries within grains are explicitly captured, leading to a relatively exact description of the phenomena on this scale.

- On the *atomistic scale*, the interaction of the atoms are explicitly taken into account. Thus, a model developed on this scale may explain the reorientation and occurrence of certain atomic arrangements. Therefore, it may serve as a base for a model which predicts the crystallographic structure.

- Below the atomistic scale, a description based on electrons, neutrons, positrons or even quarks and leptons is possible and necessary if the problem to be solved can be most easily described on this scale.

As each modeling scale has an underlying physical scale, heterogeneities are *always* present on the modeling scale due to this underlying scale. Thus, since a start at an infinitesimal material point is physically not possible, an assumption about a representative volume element (RVE), with certain assumptions about its homogeneity is always necessary. Taking this into account, *such thing as THE right modeling scale which does not need any assumptions related to an underlying scale does not exist.* However, one may ask if all physical phenomena of the underlying scales are important for the questions posed in the problem to be solved, or *is the exact knowledge of the exact position of each atom of a bridge necessary to predict its behavior when loaded by a train*? Thus a proper choice for the modeling scale highly depends on the question, if the material response can be correctly predicted for the given problem. If the material response can not be predicted with the material law developed, the underlying scale has to be taken into consideration.

An important aim of this monograph is to clarify the motivation for the choice of the scale of the description. The presented examples are concerned with the description of shape memory alloys (SMA). However, in chapter 4, a problem related to the movement of the transition front within a grain is discussed whereas in chapter 5, a modeling strategy for a macroscopic, phenomenological description is presented. As the observations on the various length scales are quite different, a brief introduction to the observed phenomena, relevant to the problem to be addressed, is given in each section.

The outline of this work is as follows: in chapter 2, the general foundation for the further derivations and examples presented in chapter 4 and 5 is laid out. In chapter 3, some constitutive assumptions and derivations for a material point, or homogeneous material on the length scale considered, are derived. These chapters are important for the following two chapters in which two different approaches to the description of shape memory alloy are presented: in chapter 4, an approach is presented which focuses on the description on the scale of a single crystal. The evolution of the austenite-martensite interface is explicitly tracked and a numerical scheme to describe the process is proposed. In chapter 5, a macroscopic approach is presented which may be used to supply a macroscopic description used to model structures.

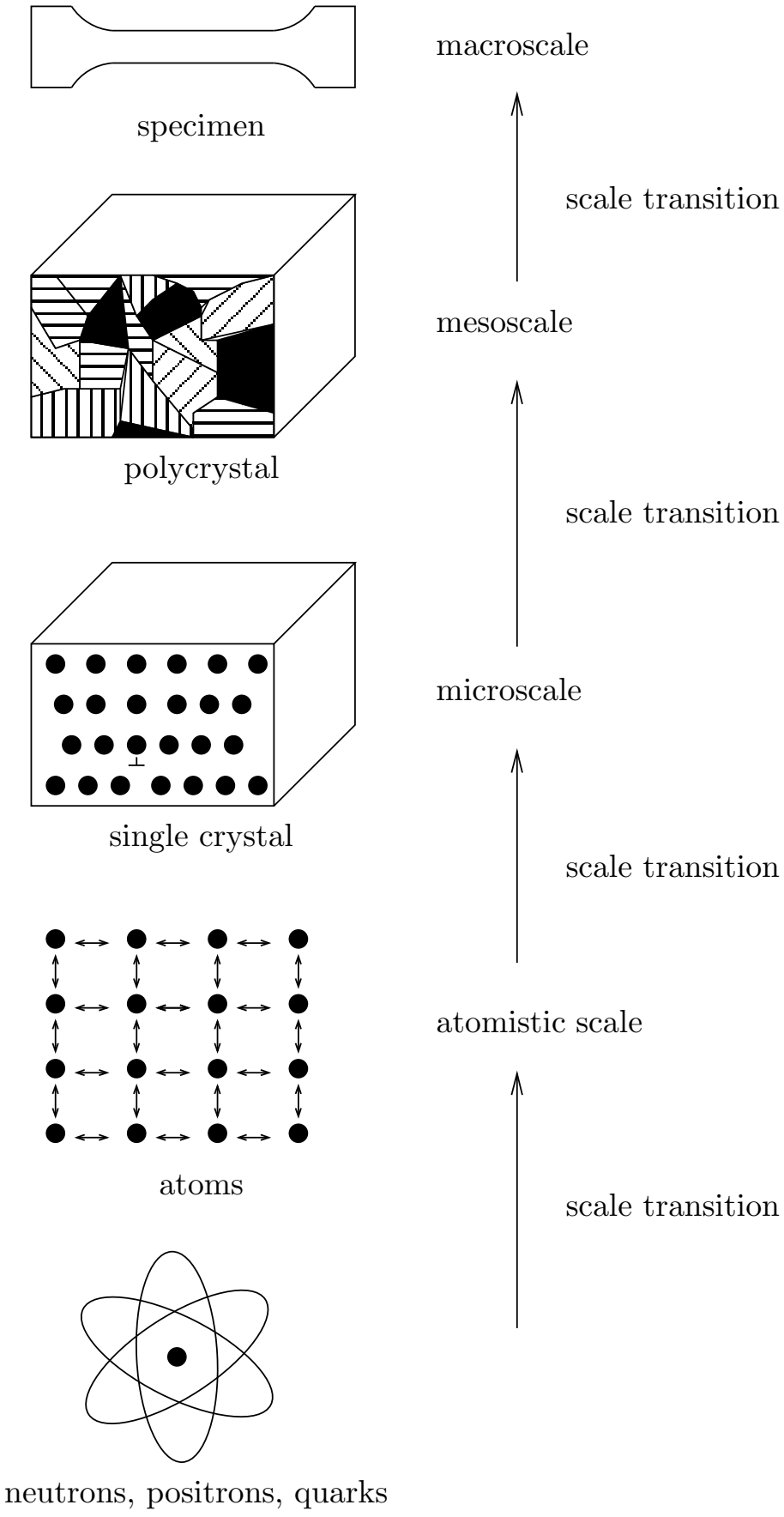

Figure 1.1: Different modeling scales

2 Thermomechanical frame

The chapter provides the continuum-mechanical foundation necessary to understand the examples presented in sections 4 and 5. It is not intended as a replacement for a textbook. It is only included to ensure a degree of self containment of this monograph and to put special emphasis on the aspects important for the examples. For a more extensive discussion on the subject, the reader may refer to textbooks on continuum mechanics, as e.g. Eringen (1975), Becker & Bürger (1975), Marsden & Hughes (1983), Ogden (1984), Altenbach & Altenbach (1994), Šilhavý (1997), Wilmanski (1998), or Başar & Weichert (2000).

After fixing the notation, the kinematics of deformation, balance laws and thermomechanical aspects for a homogeneous body are discussed. This path is followed as it allows a natural development from the description of motion, the introduction of the concept of stress by the balance laws of momentum, and bridging to thermodynamics via the energy balances. As this monograph is concerned with the description of phase transformations, the extension to bodies which include discontinuities is a vital part of this chapter. These derivations close this chapter as they are the starting point for the considerations in section 4 as well as 5, therein interpreting the same foundation on different scales.

2.1 General preliminaries

This section provides the definitions and notation related to vectors and tensors and is only included for reference to achieve a certain degree of self-containment of this monograph. However, some aspects are treated more in detail as they are important for the derivations done in this monograph. More extensive details on this subject can be found in books on tensor calculus as e.g in Betten (1987) or Altenbach & Altenbach (1994).

2.1.1 Mathematical notation

Throughout this text, an orthonormal coordinate system is used if not otherwise stated. The scalar product of two base vectors $\mathbf{e}_i$ and $\mathbf{e}_j$ of this system

follow

$$\mathbf{e}_i \cdot \mathbf{e}_j = \delta_{ij} \tag{2.1}$$

where δ_{ij} denotes the Kronecker-delta

$$\delta_{ij} = \begin{cases} 1 & \text{if } \; i = j \\ 0 & \text{otherwise.} \end{cases} \tag{2.2}$$

A first order tensor can be described by

$$\mathbf{a} = a_i \, \mathbf{e}_i \tag{2.3}$$

where a_i are the tensor components of $\mathbf{a}$ in a coordinate system with the orthonormal base vectors $\mathbf{e}_i$. If not otherwise stated, the summation convention is implicitly employed. The length of $\mathbf{a}$ is denoted by

$$|\mathbf{a}| \quad = \quad \sqrt{a_i \, a_i}. \tag{2.4}$$

A second order tensor can be understood as a "dyadic product" of two vectors such that

$$\mathbf{A} = \mathbf{a} \otimes \mathbf{b} \tag{2.5}$$

the dyadic product being

$$\mathbf{A} = \mathbf{a} \otimes \mathbf{b} = a_i \, b_j \, \mathbf{e}_i \; \otimes \mathbf{e}_j = A_{ij} \, \mathbf{e}_i \; \otimes \mathbf{e}_j. \tag{2.6}$$

Contraction operators are defined such that a single dot "$\cdot$" denotes a single contraction

$$\begin{aligned} \mathbf{a} \cdot \mathbf{b} \quad &= \quad a_i \, b_i \\ \mathbf{A} \cdot \mathbf{B} \quad &= \quad A_{ij} \, B_{jk} \, \mathbf{e}_i \; \otimes \mathbf{e}_k \\ \mathbf{A} \cdot \mathbf{b} \quad &= \quad A_{ij} \, b_j \, \mathbf{e}_i \end{aligned} \tag{2.7}$$

and a double dot ":" denotes a double contraction

$$\mathbf{A} : \mathbf{B} = A_{ij} \, B_{ij}. \tag{2.8}$$

Some properties of these contractions are

$$\begin{aligned}
(\mathbf{A}\cdot\mathbf{B})^T &= \mathbf{B}^T\cdot\mathbf{A}^T \\
(\mathbf{A}\cdot\mathbf{B})^{-1} &= \mathbf{B}^{-1}\cdot\mathbf{A}^{-1} \\
\mathbf{A}:\mathbf{B} &= \mathrm{tr}\left(\mathbf{A}\cdot\mathbf{B}^T\right) \\
(\mathbf{A}:\mathbf{B})^T &= \mathbf{B}^T:\mathbf{A}^T \\
(\mathbf{A}:\mathbf{B})^{-1} &= \mathbf{B}^{-1}:\mathbf{A}^{-1}.
\end{aligned} \tag{2.9}$$

Special second order tensors, some common operators on second order tensors, and some definitions and properties are

$$\begin{aligned}
\mathbf{1} &= \delta_{ij}\,\mathbf{e}_i\otimes\mathbf{e}_j \\
\mathrm{tr}\,(\mathbf{A}) &= A_{ii} \\
\mathbf{A}' &= \mathbf{A}-\frac{1}{3}\,\mathbf{1}\,\mathrm{tr}\,(\mathbf{A}) \\
\left(\mathbf{A}^T\right)_{ij} &= A_{ji} \\
\mathbf{A}\cdot\mathbf{A}^{-1} &= \mathbf{1} \\
\mathbf{A}^{-T} &= \left(\mathbf{A}^{-1}\right)^T = \left(\mathbf{A}^T\right)^{-1} \\
\mathrm{sym}\,(\mathbf{A}) &= \frac{1}{2}\left(\mathbf{A}+\mathbf{A}^T\right) \\
\mathrm{skew}\,(\mathbf{A}) &= \frac{1}{2}\left(\mathbf{A}-\mathbf{A}^T\right)
\end{aligned} \tag{2.10}$$

2.1.2 Vector products

The scalar product of two vectors is defined as (cf. Bronstein et al. (1997))

$$\mathbf{a}\cdot\mathbf{b} = |\mathbf{a}|\,|\mathbf{b}|\cos\varphi \tag{2.11}$$

where φ with $0\le\varphi\le\pi$ denotes the angle enclosed by $\mathbf{a}$ and $\mathbf{b}$.

The cross product is defined by

$$\mathbf{a}\times\mathbf{b} = |\mathbf{a}|\,|\mathbf{b}|\,\mathbf{n}\sin\varphi \tag{2.12}$$

where $\mathbf{n}\cdot\mathbf{a}=0$, $\mathbf{n}\cdot\mathbf{b}=0$, and $|\mathbf{n}|=1$. $(\mathbf{a},\mathbf{b},\mathbf{n})$ constitute a right hand system. Thus, the cross product yields a vector of the length of the area

of the parallelogram spanned by $\mathbf{a}$ and $\mathbf{b}$ and perpendicular to both vectors. Combining (2.11) and (2.12) such that

$$v = (\mathbf{a} \times \mathbf{b}) \cdot \mathbf{c} = \det(\mathbf{a}, \mathbf{b}, \mathbf{c}) \tag{2.13}$$

leads to the conclusion that v denotes the signed volume spanned by $\mathbf{a}$, $\mathbf{b}$ and $\mathbf{c}$. The cross product $\mathbf{c} = c_i \mathbf{e}_i$ of two vectors $\mathbf{a} = a_i \mathbf{e}_i$ and $\mathbf{b} = b_i \mathbf{e}_i$ can also be determined by

$$\mathbf{c} = c_k \, \mathbf{e}_k = \mathbf{a} \times \mathbf{b} = a_i \, b_j \, \epsilon_{ijk} \, \mathbf{e}_k \tag{2.14}$$

where ϵ_{ijk} denotes the Levi-Civita symbol

$$\epsilon_{ijk} = \begin{cases} 1 & \text{if } i, j, k \text{ are clockwise} \\ -1 & \text{if } i, j, k \text{ are counter-clockwise} \\ 0 & \text{otherwise.} \end{cases} \tag{2.15}$$

Employing the symbolic notation $\boldsymbol{\epsilon} = \epsilon_{ijk} \, \mathbf{e}_i \otimes \mathbf{e}_j \otimes \mathbf{e}_k$, equation (2.14) can be expressed as

$$\mathbf{c} = \mathbf{a} \times \mathbf{b} = (\mathbf{a} \otimes \mathbf{b}) : \boldsymbol{\epsilon}. \tag{2.16}$$

An important aspect is that the double tensor product of a symmetric second order tensor and the Levi-Civita tensor yields zero, i.e.

$$\frac{1}{2} \left(\mathbf{A} + \mathbf{A}^T \right) : \boldsymbol{\epsilon} = \mathbf{0}. \tag{2.17}$$

2.1.3 Tensor invariants

The eigenvalues λ^A and eigenvectors $\mathbf{N}^A$ of the second order tensor $\mathbf{A}$ satisfy the equation

$$\mathbf{A} \cdot \mathbf{N}^A = \lambda^A \, \mathbf{N}^A. \tag{2.18}$$

In general, the length of the eigenvectors is not defined. In what follows $|\mathbf{N}^A| = 1$ is chosen. The three eigenvalues λ_1^A, λ_2^A, and λ_3^A can be determined by solving the characteristic equation

$$\det(\mathbf{A} - \lambda^A \, \mathbf{1}) = 0. \tag{2.19}$$

This equation is cubic in λ^A and leads to the three, not necessarily nonequal, eigenvalues of $\mathbf{A}$. It can be expressed as

$$\lambda^{A\,3} - I_1^A\,\lambda^{A\,2} + I_2^A\lambda^A - I_3^A = 0 \tag{2.20}$$

where the invariants of $\boldsymbol{A}$

$$\begin{aligned} I_1^A &= \operatorname{tr}(\boldsymbol{A}) && (2.21)\\ I_2^A &= -\frac{1}{2}\left(\operatorname{tr}(\boldsymbol{A}\cdot\boldsymbol{A}) - \operatorname{tr}(\boldsymbol{A})^2\right) && (2.22)\\ I_3^A &= \frac{1}{3}\left(\operatorname{tr}(\boldsymbol{A}\cdot\boldsymbol{A}\cdot\boldsymbol{A}) - \frac{3}{2}\operatorname{tr}(\boldsymbol{A}\cdot\boldsymbol{A})\,\operatorname{tr}(\boldsymbol{A}) + \frac{1}{2}\operatorname{tr}(\boldsymbol{A})^3\right) && (2.23) \end{aligned}$$

are used. These invariants are often called principal invariants whereas $\operatorname{tr}(\boldsymbol{A})$, $\operatorname{tr}(\boldsymbol{A}\cdot\boldsymbol{A})$, and $\operatorname{tr}(\boldsymbol{A}\cdot\boldsymbol{A}\cdot\boldsymbol{A})$ are termed invariants of $\boldsymbol{A}$. However, as the invariants I_1^A, I_2^A, and I_3^A can be expressed as a linear combination of $\operatorname{tr}(\boldsymbol{A})$, $\operatorname{tr}(\boldsymbol{A}\cdot\boldsymbol{A})$, and $\operatorname{tr}(\boldsymbol{A}\cdot\boldsymbol{A}\cdot\boldsymbol{A})$, these descriptions are equivalent. The invariants of the deviator of $\boldsymbol{A}$

$$\boldsymbol{A}' = \boldsymbol{A} - \frac{1}{3}\,\mathbf{1}\operatorname{tr}(\boldsymbol{A}) \tag{2.24}$$

read

$$\begin{aligned} J_1^A &= \operatorname{tr}(\boldsymbol{A}') = 0 && (2.25)\\ J_2^A &= -\frac{1}{2}\operatorname{tr}(\boldsymbol{A}'\cdot\boldsymbol{A}') = I_2^A - \frac{1}{3}\,I_1^{A\,2} && (2.26)\\ J_3^A &= \frac{1}{3}\operatorname{tr}(\boldsymbol{A}'\cdot\boldsymbol{A}'\cdot\boldsymbol{A}') = I_3^A - \frac{1}{3}\,I_1^A\,I_2^A + \frac{2}{27}\,I_1^{A\,3}. && (2.27) \end{aligned}$$

The derivatives of the invariants of $\boldsymbol{A}$ and its deviator $\boldsymbol{A}'$ with respect to $\boldsymbol{A}$ read

$$\frac{\partial I_1^A}{\partial \boldsymbol{A}} = \mathbf{1} \tag{2.28}$$

$$\frac{\partial I_2^A}{\partial \boldsymbol{A}} = -\boldsymbol{A}^T + \mathbf{1}\, I_1^A \tag{2.29}$$

$$\frac{\partial I_3^A}{\partial \boldsymbol{A}} = (\boldsymbol{A}\cdot\boldsymbol{A})^T - \boldsymbol{A}^T\, I_1^A + I_2^A\, \mathbf{1} \tag{2.30}$$

$$\frac{\partial J_2^A}{\partial \boldsymbol{A}} = -\boldsymbol{A}'^T \tag{2.31}$$

$$\frac{\partial J_3^A}{\partial \boldsymbol{A}} = \left(\boldsymbol{A}'\cdot\boldsymbol{A}'\right)^T + \frac{2}{3}\, J_2^A\, \mathbf{1}. \tag{2.32}$$

Furthermore, the identity

$$\frac{\partial \det(\mathbf{A})}{\partial \mathbf{A}} = \det(\mathbf{A})\, \mathbf{A}^{-T} \tag{2.33}$$

will be of later use.

For symmetric second order tensors, the eigenvalues are real and the eigenvectors mutually orthogonal. The orthogonality of the eigenvectors can be used to derive the spectral decomposition[1] of $\boldsymbol{A}$. By using

$$\mathbf{A} = \sum_{i=1}^{3} \mathbf{A}\cdot\mathbf{N}_i^A \otimes \mathbf{N}_i^A \tag{2.34}$$

for $\mathbf{N}_1^A \perp \mathbf{N}_2^A \perp \mathbf{N}_3^A \perp \mathbf{N}_1^A$ in conjunction with (2.18) yields the spectral decomposition of $\mathbf{A}$

$$\mathbf{A} = \sum_{i=1}^{3} \lambda_i^A\, \mathbf{N}_i^A \otimes \mathbf{N}_i^A. \tag{2.35}$$

[1]The form presented here for the spectral decompositions assumes that three independent eigenvalues exist in order to keep the presentation as clear as possible. An approach addressing the situation where this does not hold can be found in Hoger (1986) or Carlson & Hoger (1986).

The orthogonality of the eigenvectors can only be assured if no multiple eigenvalues are determined. A geometrical interpretation of the spectral decomposition can be found if the preceding relation is rewritten as

$$\mathbf{A} = \mathbf{Q}^{A^T} \cdot \mathrm{diag}(\lambda_1^A, \lambda_2^A, \lambda_3^A) \cdot \mathbf{Q}^A \tag{2.36}$$

where $\mathbf{Q}^A = (\mathbf{N}_1^A, \mathbf{N}_2^A, \mathbf{N}_3^A)^T$ is an orthogonal rotation matrix, interpreting the spectral representation as a representation in a rotated configuration.

2.2 Deformation and motion

The following derivations are based on the assumption that the body under consideration is continuously filled with matter, i.e. the principles of continuum mechanics are followed. In addition, it is required that all relevant measures within the examined region $\mathcal{R}$ are $\mathcal{C}^0$ continuous. Thus, in addition to the first assumption which rules out the existence of strong discontinuities, i.e. gaps, the existence of weak discontinuities, i.e. jump of stresses, strains, etc., is ruled out by the second requirement. However, the region $\mathcal{R}$ might be only a part of the whole domain involved in the problem. In section 2.4 approaches are presented which deal with the violation of the latter requirement.

2.2.1 Kinematical frame

The basic definitions and derivations presented here are well accepted and in common use without any objections. Thus, the following section related to the kinematical frame is added only for, at least partial, self completeness of this monograph. For further details, refer to the textbooks mentioned at the beginning of this chapter.

2.2.1.1 Reference configuration and deformation gradient

The description of the deformation of the material is parametrized by the introduction of a referential configuration $\mathcal{B}_0$ in addition to the time dependent actual configuration $\mathcal{B}$ which describes the current state of the material. A material point P in the actual configuration is uniquely identified by its position in the referential configuration (cf. figure 2.1). Thus, given a position $\mathbf{X}$

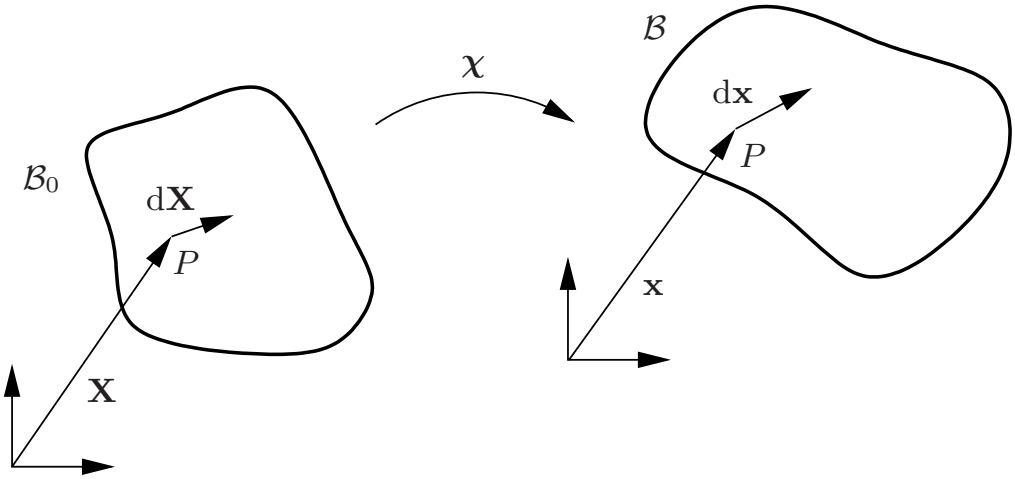

Figure 2.1: Reference configuration $\mathcal{B}_0$ and actual configuration $\mathcal{B}$.

of a particle P in a time-independent referential configuration, the position of the material point can be specified by the mapping $\boldsymbol{\chi}$ as

$$\mathbf{x}(\mathbf{X}, t) = \boldsymbol{\chi}(\mathbf{X}, t). \tag{2.37}$$

The description in material coordinates $\mathbf{X}$ is termed *Lagrangian description* where as the denotation *Eulerian description* is used when the spatial coordinates $\mathbf{x}$ are employed. Since the comparison of actual and reference configuration does not require the knowledge of intermediate stages of deformation, the time dependence is dropped for the implicit introduction of the deformation gradient $\mathbf{F}$ by the total derivative of $\mathbf{x}$

$$\mathrm{d}\mathbf{x} = \frac{\partial \mathbf{x}}{\partial \mathbf{X}} \cdot \mathrm{d}\mathbf{X} = \mathbf{F} \cdot \mathrm{d}\mathbf{X}. \tag{2.38}$$

Thus, the definition of the deformation gradient $\mathbf{F}$ reads

$$\mathbf{F} = \frac{\partial \boldsymbol{\chi}(\mathbf{X}, t)}{\partial \mathbf{X}} = \boldsymbol{\chi}(\mathbf{X}, t) \otimes \boldsymbol{\nabla}_0 = \mathbf{x} \otimes \boldsymbol{\nabla}_0. \tag{2.39}$$

2.2.1.2 Deformation of area and volume elements

Consider an infinitesimal area element $\mathrm{d}\mathbf{a}$ in $\mathcal{B}$ such that

$$\mathrm{d}\mathbf{a} = \mathbf{n}\, \mathrm{d}a \tag{2.40}$$

where $\mathbf{n}$ describes the normal to the material surface and $\mathrm{d}a$ its area. Let $\mathrm{d}\mathbf{x}$ be an arbitrary material line cutting the edge of $\mathrm{d}\mathbf{a}$ such that $\mathrm{d}\mathbf{x}^T \cdot \mathrm{d}\mathbf{a} > 0$, one may calculate the volume $\mathrm{d}v$ of an infinitesimal element with the base area $\mathrm{d}a$ and the generator $\mathrm{d}\mathbf{x}$ as

$$\mathrm{d}v = \mathrm{d}\mathbf{x}^T \cdot \mathrm{d}\mathbf{a}. \tag{2.41}$$

Considering the same area element in the referential configuration, one may state

$$\mathrm{d}\mathbf{A} = \mathbf{N}\, \mathrm{d}A \tag{2.42}$$

where $\mathbf{N}$ describes the normal to the material surface and $\mathrm{d}A$ its area. The same arguments applied to the undeformed arbitrary line element $\mathrm{d}\mathbf{X} = \mathbf{F}^{-1} \cdot \mathrm{d}\mathbf{x}$ leads to

$$\mathrm{d}V = \mathrm{d}\mathbf{X}^T \cdot \mathrm{d}\mathbf{A}. \tag{2.43}$$

Introduction of a measure for the relative volume change J such that

$$\mathrm{d}v = J\, \mathrm{d}V \tag{2.44}$$

leads, by using (2.41) and (2.43), to

$$\mathrm{d}\mathbf{x}^T \cdot \mathrm{d}\mathbf{a} = J\, \mathrm{d}\mathbf{X}^T \cdot \mathrm{d}\mathbf{A}. \tag{2.45}$$

Use of the transpose of equation (2.39) and considering the arbitrariness of $\mathbf{X}$ leads to

$$\mathbf{F}^T \cdot \mathrm{d}\mathbf{a} = J\, \mathrm{d}\mathbf{A}. \tag{2.46}$$

Thus, one may relate the infinitesimal area element in the current and the referential configuration by

$$\mathrm{d}\mathbf{a} = \mathbf{n}\, \mathrm{d}a = J\, \mathbf{F}^{-T} \cdot \mathbf{N}\, \mathrm{d}A = J\, \mathbf{F}^{-T} \cdot \mathrm{d}\mathbf{A}, \tag{2.47}$$

a relation often referred to as *Nanson's formula*.

Constituting a triplet $\mathbf{T}_X$ of infinitesimal vectors in the referential configuration $\mathbf{T}_X = (\,\mathrm{d}\boldsymbol{X}_1,\ \mathrm{d}\boldsymbol{X}_2,\ \mathrm{d}\boldsymbol{X}_3)$, by the use of equation (2.13), the volume $\mathrm{d}V$ spanned by them can be determined to be

$$\mathrm{d}V = (\,\mathrm{d}\mathbf{X}_1 \times \mathrm{d}\mathbf{X}_2) \cdot \mathrm{d}\mathbf{X}_3 = \det \mathbf{T}_X. \tag{2.48}$$

The triplet may be chosen such that $\mathrm{d}V > 0$. In the actual configuration, each vector $\mathrm{d}\mathbf{x}_i$ is deformed according to $\mathrm{d}\mathbf{x}_i = \mathbf{F} \cdot \mathrm{d}\mathbf{X}_i$ and the volume $\mathrm{d}v$ spanned by the triplet is

$$\mathrm{d}v = (\,\mathrm{d}\mathbf{x}_1 \times \mathrm{d}\mathbf{x}_2) \cdot \mathrm{d}\mathbf{x}_3 = [(\mathbf{F} \cdot \mathrm{d}\mathbf{X}_1) \times (\mathbf{F} \cdot \mathrm{d}\mathbf{X}_2)] \cdot (\mathbf{F} \cdot \mathrm{d}\mathbf{X}_3). \tag{2.49}$$

Using the relation $\det(\mathbf{A} \cdot \mathbf{B}) = \det \mathbf{A}\, \det \mathbf{B}$, one may express equation (2.49) as

$$\mathrm{d}v = \det(\mathbf{F} \cdot \mathbf{T}_X) = \det \mathbf{F}\, \mathrm{d}V \tag{2.50}$$

and, using (2.44)

$$J = \det \mathbf{F}. \tag{2.51}$$

2.2.2 Material frame indifference

The invariance of the used measures with respect to changes of the position and orientation of the observer is crucial in a continuum mechanical description. Thus, presuming that the reference configuration is independent of the observer[2], the position vector $\mathbf{x}$ must transform according to

$$\mathbf{x}^*(\mathbf{X}, t^*) = \mathbf{c}(t) + \mathbf{Q}(t) \cdot \mathbf{x}(\mathbf{X}, t), \tag{2.52}$$

where the vector $\mathbf{c}$ describes the movement and $\mathbf{Q}$, a proper orthogonal tensor with $\mathbf{Q} \cdot \mathbf{Q}^T = \mathbf{1}$ and $\det(\mathbf{Q}) = 1$, the rotation of the observer. Measures which follow this rule are said to be *objective* or *material frame indifferent*.

[2]Refer to Ogden (1984) for a more elaborate discussion on the subject.

For Lagrangian scalars α_0, first order tensors $\boldsymbol{\alpha}_0$, and second order tensors $\mathbf{A}_0$ the objectivity requirements may be formulated as

$$\begin{aligned} \alpha_0^* &= \alpha_0 \\ \boldsymbol{\alpha}_0^* &= \boldsymbol{\alpha}_0 \\ \mathbf{A}_0^* &= \mathbf{A}_0. \end{aligned} \tag{2.53}$$

For Eulerian scalars α, first order tensors $\boldsymbol{\alpha}$, and second order tensors $\mathbf{A}$ the transformations rules are

$$\begin{aligned} \alpha^* &= \alpha \\ \boldsymbol{\alpha}^* &= \mathbf{Q} \cdot \boldsymbol{\alpha} \\ \mathbf{A}^* &= \mathbf{Q} \cdot \mathbf{A} \cdot \mathbf{Q}^T. \end{aligned} \tag{2.54}$$

Following the idea that a second order tensor can be understood as the dyadic product of two first order tensors, a second order tensor may not necessarily solely belong to one configuration as the two vectors constituting the second order tensor may belong to different configurations. Such a tensor is called "two-point tensor". The objectivity requirements can be derived following the idea mentioned above, i.e by describing a two-point tensor as

$$\hat{\mathbf{A}} = \boldsymbol{\alpha} \otimes \boldsymbol{\alpha}_0 \tag{2.55}$$

or

$$\tilde{\mathbf{A}} = \boldsymbol{\alpha}_0 \otimes \boldsymbol{\alpha}. \tag{2.56}$$

Now, (2.53b) and (2.54b) can be used to yield

$$\hat{\mathbf{A}}^* = \mathbf{Q} \cdot \hat{\mathbf{A}} \tag{2.57}$$

and

$$\tilde{\mathbf{A}}^* = \tilde{\mathbf{A}} \cdot \mathbf{Q}^T. \tag{2.58}$$

For example, the deformation gradient transforms as

$$\mathbf{F}^* = \mathbf{Q} \cdot \mathbf{F}. \tag{2.59}$$

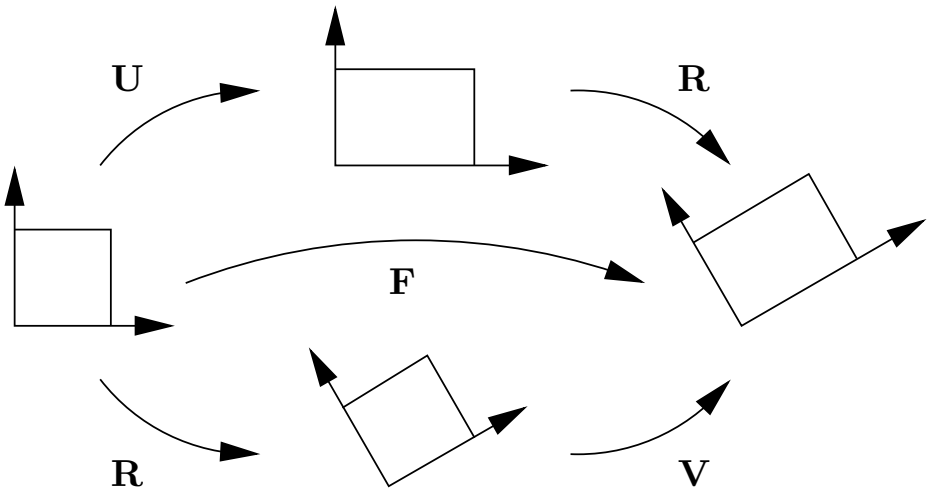

Figure 2.2: Polar decomposition of **F**

As the left component of the dyadic product in the definition of the deformation gradient (2.39) belongs to the actual configuration, the deformation gradient follows the correct transformation rule confirming the requirement of objectivity (2.57). For the Jacobian J,

$$J^* = \det(\mathbf{Q} \cdot \mathbf{F}) = \det(\mathbf{Q}) \det(\mathbf{F}) = \det(\mathbf{F}) = J \tag{2.60}$$

holds, yielding the proper transformation rule for a scalar.

2.2.3 Strain measures

The deformation gradient **F** can be uniquely decomposed by the polar decomposition[3]

$$\mathbf{F} = \mathbf{R} \cdot \mathbf{U} = \mathbf{V} \cdot \mathbf{R} \tag{2.61}$$

where **R** is a proper orthogonal tensor and **U** and **V** are both symmetric and positive definite. Based on these measures, the right Cauchy-Green tensor

$$\mathbf{C} = \mathbf{U}^T \cdot \mathbf{U} = \mathbf{F}^T \cdot \mathbf{F} \tag{2.62}$$

[3]For the two decompositions introduced in (2.61), the rotation tensor generally may be different. However, it can be shown (Ogden (1984)) that they are identical.

and left Cauchy-Green tensor

$$\mathbf{b} = \mathbf{V} \cdot \mathbf{V}^T = \mathbf{F} \cdot \mathbf{F}^T \tag{2.63}$$

are defined. For $\mathbf{b}$,

$$\mathbf{b}^* = \mathbf{F}^* \cdot \mathbf{F}^{*T} = \mathbf{Q} \cdot \mathbf{F} \cdot \mathbf{F}^T \cdot \mathbf{Q}^T = \mathbf{Q} \cdot \mathbf{b} \cdot \mathbf{Q}^T, \tag{2.64}$$

the proper transformation rule for an Eulerian tensor, holds whereas for $\mathbf{C}$,

$$\mathbf{C}^* = \mathbf{F}^{*T} \cdot \mathbf{F} = \mathbf{F}^T \cdot \mathbf{Q}^T \cdot \mathbf{Q} \cdot \mathbf{F} = \mathbf{F}^T \cdot \mathbf{F} = \mathbf{C} \tag{2.65}$$

the proper transformation rule for a Lagrangian tensor, can be derived. As $\mathbf{b}$ and $\mathbf{V}$ are coaxial as well as $\mathbf{C}$ and $\mathbf{U}$, $\mathbf{V}$ and $\mathbf{U}$ are also objective measures of their respective configurations.

Following Hill (1978), a general class of strain measures can be defined employing the spectral decomposition of $\mathbf{V}$ and $\mathbf{U}$. A scaling function $f(\lambda)$ is defined. It may be used to define Eulerian strain measures

$$\mathbf{e}^{(m)} = \sum_{i=1}^{3} f(\lambda_i^V)\, \mathbf{N}_i^V \otimes \mathbf{N}_i^V \tag{2.66}$$

or Lagrangian strain measures

$$\mathbf{E}^{(m)} = \sum_{i=1}^{3} f(\lambda_i^U)\, \mathbf{N}_i^U \otimes \mathbf{N}_i^U. \tag{2.67}$$

As the resulting strain measure is coaxial either to $\mathbf{V}$ or to $\mathbf{U}$, it is an objective measure within its corresponding configuration. The scaling function is chosen such that the measures yield zero for rigid body motions and coincide to the measure for small deformations when $\mathbf{F} = \mathbf{1}$ is approached. These conditions can be fulfilled if

$$f(\lambda) = \begin{cases} \dfrac{1}{m}\left(\lambda^m - 1\right) & \text{if } m \neq 0 \\ \ln \lambda & \text{otherwise} \end{cases} \tag{2.68}$$

is chosen. For example, the Green-Lagrange strain tensor $\mathbf{E}$ can be derived for $m = 2$ such that

$$\mathbf{E}^{(2)} = \frac{1}{2} \sum_{i=1}^{3} \left({\lambda_i^U}^2 - 1 \right) \mathbf{N}_i^U \otimes \mathbf{N}_i^U = \frac{1}{2} \left(\mathbf{C} - \mathbf{1} \right) = \mathbf{E}, \tag{2.69}$$

for $m = -2$, the approach yields the Almansi strain tensor $\mathbf{e}$

$$\mathbf{e}^{(-2)} = -\frac{1}{2} \sum_{i=1}^{3} \left({\lambda_i^V}^{-2} - 1 \right) \mathbf{N}_i^V \otimes \mathbf{N}_i^V = \frac{1}{2} \left(\mathbf{1} - \mathbf{b}^{-1} \right) = \mathbf{e}. \tag{2.70}$$

2.2.4 Velocities

The velocity of a material point P is denoted by

$$\mathbf{v} = \frac{\mathrm{d}}{\mathrm{d}t} \mathbf{x}. \tag{2.71}$$

For later use, it is convenient to define the velocity gradient tensor by

$$\mathbf{L} = \mathbf{v} \otimes \boldsymbol{\nabla} = \frac{\partial \mathbf{v}}{\partial \mathbf{x}} = \frac{\partial \mathbf{v}}{\partial \mathbf{X}} \cdot \frac{\partial \mathbf{X}}{\partial \mathbf{x}} = \dot{\mathbf{F}} \cdot \mathbf{F}^{-1}. \tag{2.72}$$

Its symmetric part is denoted by

$$\mathbf{D} = \frac{1}{2} \left(\mathbf{L} + \mathbf{L}^T \right), \tag{2.73}$$

its antimetric part by

$$\mathbf{W} = \frac{1}{2} \left(\mathbf{L} - \mathbf{L}^T \right). \tag{2.74}$$

By applying relation (2.33) to the deformation gradient, post-multiplying by $\dot{\mathbf{F}}^T$ and making use of the definition (2.72), one may derive

$$\frac{\partial J}{\partial \mathbf{F}} \cdot \dot{\mathbf{F}}^T = J \, \mathbf{F}^{-T} \cdot \dot{\mathbf{F}}^T = J \, \mathbf{L}^T. \tag{2.75}$$

As $J = J(\mathbf{F})$, its time derivative can be calculated to be

$$\dot{J} = \frac{\partial J}{\partial \mathbf{F}} : \dot{\mathbf{F}} = \mathrm{tr} \left(\frac{\partial J}{\partial \mathbf{F}} \cdot \dot{\mathbf{F}}^T \right) = \mathrm{tr} \left(J \, \mathbf{L}^T \right) = J \, \mathrm{tr} \left(\mathbf{L} \right). \tag{2.76}$$

2.2.5 Objective time derivative

To better understand the motivation behind the concepts introduced in this section, one may consider the following example. Given an objective Eulerian second order tensor $\mathbf{A}$, i.e.

$$\mathbf{A}^* = \mathbf{Q} \cdot \mathbf{A} \cdot \mathbf{Q}^T \tag{2.77}$$

holds. For a large class of problems, the formulation of the material law in rate form is useful. This introduces the time derivative of $\mathbf{A}$. The check of the requirement of material frame indifference for the material time derivative $\dot{\mathbf{A}}$ yields

$$\begin{aligned} \frac{\mathrm{d}}{\mathrm{d}t}\mathbf{A}^* &= \frac{\mathrm{d}}{\mathrm{d}t}\left(\mathbf{Q} \cdot \mathbf{A} \cdot \mathbf{Q}^T\right) \\ &= \dot{\mathbf{Q}} \cdot \mathbf{A} \cdot \mathbf{Q}^T + \mathbf{Q} \cdot \dot{\mathbf{A}} \cdot \mathbf{Q}^T + \mathbf{Q} \cdot \mathbf{A} \cdot \dot{\mathbf{Q}}^T \\ &\neq \mathbf{Q} \cdot \dot{\mathbf{A}} \cdot \mathbf{Q}^T \end{aligned} \tag{2.78}$$

as the orientation of the observer might change in time. Thus, the material time derivative $\dot{\mathbf{A}}$ of a general second order tensor $\mathbf{A}$ may not be objective. This problem leads to the introduction of a so called *objective time derivative* $\overset{\circ}{(\bullet)}$ (in contrast to the *material time derivative* $\mathrm{d}(\bullet)/\,\mathrm{d}t = \dot{(\bullet)}$). The material law is now formulated in terms of the objective time derivative instead of the material time derivative, employing objective measures. The first objective time derivative was the *Zaremba-Jaumann* derivative

$$\overset{\circ}{\mathbf{A}} = \dot{\mathbf{A}} - \mathbf{W} \cdot \mathbf{A} + \mathbf{A} \cdot \mathbf{W}. \tag{2.79}$$

However, this derivative yields non-physical results in a shear test, thus its use was discouraged. Other objective derivatives have been proposed in the past, as e.g. the Green-Naghdi derivative

$$\overset{\triangledown}{\mathbf{A}} = \dot{\mathbf{A}} - \boldsymbol{\Omega} \cdot \mathbf{A} + \mathbf{A} \cdot \boldsymbol{\Omega}. \tag{2.80}$$

with $\boldsymbol{\Omega} = \dot{\mathbf{R}} \cdot \mathbf{R}^T$. The existing objective time derivatives can be categorized in two classes: the convective and the corotational time derivatives. %indexLie concept

Objective rates can be developed based on the assumption that the material time derivate suffices when applied to a tensor in the referential description. However, the application of the material time derivative is not limited to the referential description; any configuration coaxial with the referential configuration qualifies for the application of the concept, the so called Lie concept.

In order to understand the ideas behind the Lie concept, first it is necessary to introduce the concept of the "pull-back" and the "push-forward" of a tensor. These operations transfer the components of a tensor from the deformed into the undeformed base and vice versa. As the resulting push-forward or pull-back operation is bound to the way the indices are chosen, the concept of the co- and contravariant description of tensors is given here, as far as it is necessary to follow the ideas introduced in this section. A more elaborate description can be found in numerous textbooks, refer for example to Başar & Weichert (2000).

The assumption that the base vectors of the underlying base system are orthonormal is explicitly not used within this section, i.e. the metric does not collapse to the Kronecker-delta. In addition, two base systems are introduced. The covariant base system is constituted by $\mathbf{g}_i$, where the metric g_{ij} is defined by

$$g_{ij} = \mathbf{g}_i \cdot \mathbf{g}_j. \tag{2.81}$$

Generally $g_{ij} \neq \delta_{ij}$ holds. The contravariant base system is constituted by $\mathbf{g}^i$, where the metric g^{ij} is defined as

$$g^{ij} = \mathbf{g}^i \cdot \mathbf{g}^j. \tag{2.82}$$

The metrics can be used to yield

$$\mathbf{g}_i = g_{ij}\, \mathbf{g}^j \text{ and } \mathbf{g}^i = g^{ij}\, \mathbf{g}_j. \tag{2.83}$$

Furthermore, it can be shown that

$$\mathbf{g}_i \cdot \mathbf{g}^j = \delta_j^i \tag{2.84}$$

holds. An Eulerian second order tensor $\mathbf{A}$ may thus be equivalently represented by a combination of co- or contravariant base vectors

$$\mathbf{A} = A_{ik}\, \mathbf{g}^i \otimes \mathbf{g}^k = A^i_{\cdot k}\, \mathbf{g}_i \otimes \mathbf{g}^k = A_i^{\cdot k}\, \mathbf{g}^i \otimes \mathbf{g}_k = A^{ik}\, \mathbf{g}_i \otimes \mathbf{g}_k. \tag{2.85}$$

In the referential configuration, the base vectors are denoted by $\mathbf{G}_i$ and $\mathbf{G}^i$. The metric in the referential configuration reads

$$G_{ik} = \mathbf{G}_i \cdot \mathbf{G}_k \text{ and } \quad G^{ik} = \mathbf{G}^i \cdot \mathbf{G}^k \tag{2.86}$$

with properties equivalent to those defined for $\mathbf{g}_i$ and $\mathbf{g}^i$ in (2.83) and (2.84).

The deformation gradient can now be expressed in terms of the base vectors such that

$$\mathbf{F} = \mathbf{g}_i \otimes \mathbf{G}^i. \tag{2.87}$$

Its transpose, inverse, and transpose of inverse read

$$\mathbf{F}^T = \mathbf{G}^i \otimes \mathbf{g}_i, \;\; \mathbf{F}^{-1} = \mathbf{G}_i \otimes \mathbf{g}^i, \;\; \mathbf{F}^{-T} = \mathbf{g}^i \otimes \mathbf{G}_i, \tag{2.88}$$

respectively. Using (2.87) and (2.88), one may derive

$$\mathbf{g}_i = \mathbf{F} \cdot \mathbf{G}_i, \;\; \mathbf{G}_i = \mathbf{F}^{-1} \cdot \mathbf{g}_i, \;\; \mathbf{g}^i = \mathbf{F}^{-T} \cdot \mathbf{G}^i, \text{ and } \quad \mathbf{G}^i = \mathbf{F}^T \cdot \mathbf{g}^i. \tag{2.89}$$

The pull-back $\phi^*(\mathbf{A})$ of $\mathbf{A}$ can be interpreted as the expression of the Eulerian tensor $\mathbf{A}$ in terms of the referential base system $\mathbf{G}^i$ or $\mathbf{G}_i$. For covariant components, one may derive

$$\mathbf{A} = A_{ik}\, \mathbf{g}^i \otimes \mathbf{g}^k = A_{ik}\, \mathbf{F}^{-T} \cdot \mathbf{G}^i \otimes \mathbf{G}^k \cdot \mathbf{F}^{-1} \tag{2.90}$$

and finally

$$\mathbf{A}_0 = A_{ik} \mathbf{G}^i \otimes \mathbf{G}^k = \mathbf{F}^T \cdot \mathbf{A} \cdot \mathbf{F}. \tag{2.91}$$

The push forward $\phi_*(\mathbf{A}_0)$ of the Lagrangian Tensor $\mathbf{A}_0$, i.e. the description of $\mathbf{A}_0$ in terms of the Eulerian base vectors $\mathbf{g}^i$ or $\mathbf{g}_i$, can be derived in the same manner. Obviously, the choice of the proper push-forward or pull-back operation depends on the choice of the tensor components, leading to four different operations, depending on the representation of the tensor. For second order tensors the resulting operations are summarized in table 2.1.

components (in $\mathcal{B}$)	pull-back	push-forward
$\mathbf{A} = A_{ik}\,\mathbf{g}^i \otimes \mathbf{g}^k$	$\phi^*(\mathbf{A}) = \mathbf{F}^T \cdot \mathbf{A} \cdot \mathbf{F}$	$\phi_*(\mathbf{A}_0) = \mathbf{F}^{-T} \cdot \mathbf{A}_0 \cdot \mathbf{F}^{-1}$
$\mathbf{A} = A^{ik}\,\mathbf{g}_i \otimes \mathbf{g}_k$	$\phi^*(\mathbf{A}) = \mathbf{F}^{-1} \cdot \mathbf{A} \cdot \mathbf{F}^{-T}$	$\phi_*(\mathbf{A}_0) = \mathbf{F} \cdot \mathbf{A}_0 \cdot \mathbf{F}^T$
$\mathbf{A} = A^{i}_{.k}\,\mathbf{g}_i \otimes \mathbf{g}^k$	$\phi^*(\mathbf{A}) = \mathbf{F}^{-1} \cdot \mathbf{A} \cdot \mathbf{F}$	$\phi_*(\mathbf{A}_0) = \mathbf{F} \cdot \mathbf{A}_0 \cdot \mathbf{F}^{-1}$
$\mathbf{A} = A^{.k}_{i}\,\mathbf{g}^i \otimes \mathbf{g}_k$	$\phi^*(\mathbf{A}) = \mathbf{F}^T \cdot \mathbf{A} \cdot \mathbf{F}^{-T}$	$\phi_*(\mathbf{A}_0) = \mathbf{F}^{-T} \cdot \mathbf{A}_0 \cdot \mathbf{F}^T$

Table 2.1: Push/Pull operations for second order tensors

The results of table 2.1 imply a new interpretation of the left and the right Cauchy-Green tensor: using the proper indices for $\mathbf{C}$, it can be expressed as

$$\mathbf{C} = \mathbf{F}^T \cdot \mathbf{F} = \phi^*(\mathbf{1}), \tag{2.92}$$

leading to the interpretation that it is the pull back of the unit tensor into the referential configuration. For the left Cauchy-Green tensor, one obtains

$$\mathbf{b} = \mathbf{F} \cdot \mathbf{F}^T = \phi_*(\mathbf{1}), \tag{2.93}$$

implying the interpretation that it is the push forward of the unit tensor of the referential description.

The idea underlying the Lie concept may be described as follows:

- the Eulerian tensor $\mathbf{A}$ is pulled back into a configuration in which the use of the material time derivative is objective,
- the material time derivative is applied, and
- a push-forward is applied to the resulting term.

This procedure yields an objective time derivative of $\mathbf{A}$. Mathematically, the procedure can be described by

$$\mathbf{L}_\nu(\mathbf{A}) = \phi_* \left(\frac{\mathrm{d}}{\mathrm{d}t} \{\phi^*(\mathbf{A})\} \right) \tag{2.94}$$

Using the Lagrangian configuration as the reference configuration described in the steps above, one may obtain the derivatives as stated in table 2.2.

components	Lie derivative		
$\mathbf{A} = A_{ik}\,\mathbf{g}^i \otimes \mathbf{g}^k$	$\mathbf{L}_\nu(\mathbf{A})$	$=$	$\dot{\mathbf{A}} + \mathbf{L}^T \cdot \mathbf{A} + \mathbf{A} \cdot \mathbf{L}$
$\mathbf{A} = A^{ik}\,\mathbf{g}_i \otimes \mathbf{g}_k$	$\mathbf{L}_\nu(\mathbf{A})$	$=$	$\dot{\mathbf{A}} - \mathbf{L} \cdot \mathbf{A} - \mathbf{A} \cdot \mathbf{L}^T$
$\mathbf{A} = A^{i}_{\cdot k}\,\mathbf{g}_i \otimes \mathbf{g}^k$	$\mathbf{L}_\nu(\mathbf{A})$	$=$	$\dot{\mathbf{A}} - \mathbf{L} \cdot \mathbf{A} + \mathbf{A} \cdot \mathbf{L}$
$\mathbf{A} = A_{i}^{\cdot k}\,\mathbf{g}^i \otimes \mathbf{g}_k$	$\mathbf{L}_\nu(\mathbf{A})$	$=$	$\dot{\mathbf{A}} + \mathbf{L}^T \cdot \mathbf{A} - \mathbf{A} \cdot \mathbf{L}^T$

Table 2.2: Lie derivatives for co-, contra-, and mixed indices.

However, the choice of the configuration used for the pull-back is only bound to the requirement, that the material time derivative leads to objective measures. This broadens the applicability of the Lie concept. One example for such a rate, even though the choice of the referential frame is not explicitly defined within the frame described by the authors, is the recently introduced logarithmic time derivative (Xiao, Bruhns & Meyers (1997a; 1997b; 1999; 2000a; 2000b)).

2.3 Thermomechanical frame for homogeneous material

Before developing the thermomechanical frame, some introductory remarks on the nature of the introduced measures have to be made. One important distinction in thermodynamics is the question whether a parameter is *intensive* or *extensive*. An intensive parameter has a distinct value depending on the spatial position, i.e. it may vary from point to point within the body. The corresponding extensive parameter can be constructed by integrating the intensive parameter over a volume of the body. A prominent example for such a pair, also addressed in the following section, is the extensive parameter mass and the intensive parameter mass density. The mass of a body is determined by a volume integration of the mass density over the domain of the body. An intensive parameter, where the corresponding extensive parameter lacks the prominence of its counterpart, is the temperature. The volume integration of the temperature does seldomly appear in balance relations. However, it may be divided by the volume of the body, interpreted as a mean value of its intensive counterpart for the domain considered. Due to arbitrariness of the domain integration, the intensive description is often favored in continuum mechanics. Nevertheless, the correspondence to the physical intuition is often more facile to grasp when the balance laws are expressed in their extensive representation. Thus, the derivations often start with the extensive form and yield the intensive form.

An extensive parameter is homogeneous of degree one with respect to mass or volume. Thus, an extensive parameter describing the state within a certain region can be additively composed from the extensive partial parameter of arbitrary subregions of the body. From this, it follows immediately that all balance relations must be linear with respect to all extensive parameters appearing in the equations. This highlights the importance of the extensive parameters when governing equations at the discontinuity are derived in section 2.4. Since not only the discontinuity itself, but also its neighborhood has to be considered, only extensive parameters can serve as valid parameters for these derivations.

2.3.1 Transport theorem

For the following balance laws, time derivatives of integrals over the control volume are necessary. The derivation with respect to time is worked into the integral and further used in a similar fashion for the different balance relations. To keep the focus on the balance laws in their respective sections and keep the notation and derivations as simple as possible, the used procedure is derived here in a slightly more general form. Let $\mathbf{A}$ be an n-th order Tensor, i.e. $\mathbf{A} = A_{i\cdots j}\,\mathbf{e}_i \otimes \cdots \otimes \mathbf{e}_j$, the Gauss theorem for the domain $\mathcal{R}$ may be expressed as

$$\int_{\partial\mathcal{R}} \mathbf{A} \odot \mathbf{n}\, \mathrm{d}a = \int_{\mathcal{R}} \mathbf{A} \odot \boldsymbol{\nabla}\, \mathrm{d}v \tag{2.95}$$

where $\odot \in \{\cdot, \otimes, \times\}$. It may be noted that the use of the Gauss theorem is not bound to a specific configuration, i.e. it might be used in any configuration. The three terms can be replaced by the proper counterparts of any arbitrary configuration, as e.g. $\mathrm{d}A$, $\mathrm{d}V$, and $\boldsymbol{\nabla}_0$ for the referential configuration, as long as the continuity of the measures is assured. The material time derivative of

the volume integration of $\mathbf{A}$ can be expressed as

$$\begin{aligned}
\frac{\mathrm{d}}{\mathrm{d}t}\int\limits_{\mathcal{R}} \mathbf{A}\ \mathrm{d}v &= \frac{\mathrm{d}}{\mathrm{d}t}\int\limits_{\mathcal{R}_0} \mathbf{A}\, J\ \mathrm{d}V \\
&= \int\limits_{\mathcal{R}_0} \left(\frac{\mathrm{d}\mathbf{A}}{\mathrm{d}t}\, J + \mathbf{A}\,\frac{\mathrm{d}J}{\mathrm{d}t}\right)\ \mathrm{d}V \\
&= \int\limits_{\mathcal{R}_0} \Big(\dot{\mathbf{A}}\, J + \mathbf{A}\, J \,\mathrm{tr}\,(\mathbf{L})\Big)\ \mathrm{d}V \\
&= \int\limits_{\mathcal{R}} \Big(\dot{\mathbf{A}} + \mathbf{A}\,\mathrm{tr}\,(\mathbf{L})\Big)\ \mathrm{d}v \\
&= \int\limits_{\mathcal{R}} \Big(\dot{\mathbf{A}} + \mathbf{A}\,\mathrm{tr}\,(\mathbf{D})\Big)\ \mathrm{d}v. \qquad (2.96)
\end{aligned}$$

This relation will be frequently used in the following relations. An alternative form can be derived by use of the point that the tensor $\mathbf{A}$ depends on time t and the spatial position $\mathbf{x}$, i.e. $\mathbf{A} = \mathbf{A}(\mathbf{x}, t)$. One may use

$$\dot{\mathbf{A}} = \frac{\partial \mathbf{A}}{\partial t} + (\boldsymbol{\nabla}\mathbf{A}) \cdot \mathbf{v} \qquad (2.97)$$

and write

$$\begin{aligned}
\frac{\mathrm{d}}{\mathrm{d}t}\int\limits_{\mathcal{R}} \mathbf{A}\ \mathrm{d}v &= \int\limits_{\mathcal{R}} \Big(\dot{\mathbf{A}} + \mathbf{A}\,\mathrm{tr}\,(\mathbf{L})\Big)\ \mathrm{d}v \\
&= \int\limits_{\mathcal{R}} \left(\frac{\partial \mathbf{A}}{\partial t} + (\boldsymbol{\nabla}\mathbf{A}) \cdot \mathbf{v} + \mathbf{A}\,\boldsymbol{\nabla} \cdot \mathbf{v}\right)\ \mathrm{d}v \\
&= \int\limits_{\mathcal{R}} \left(\frac{\partial \mathbf{A}}{\partial t} + \boldsymbol{\nabla} \cdot (\mathbf{A}\mathbf{v})\right)\ \mathrm{d}v \\
&= \int\limits_{\mathcal{R}} \frac{\partial \mathbf{A}}{\partial t}\ \mathrm{d}v + \int\limits_{\partial\mathcal{R}} \mathbf{A}\,\mathbf{v} \cdot \mathbf{n}\,\mathrm{d}a. \qquad (2.98)
\end{aligned}$$

This relation will be of use when the relations for nonhomogeneous regions are derived.

2.3.2 Balance of mass

The region $\mathcal{R}$ is homogeneously filled with matter with a time and spatially varying mass density $\rho = \rho(\mathbf{x}, t) \geq 0$. The total mass of the region can be calculated to be

$$m = \int_{\mathcal{R}} \rho(\mathbf{x}, t) \, \mathrm{d}v. \tag{2.99}$$

It is noteworthy that the integral bounds are not fixed in time. As the region deforms, they may change. Since no reference is made to an observer in its definition, the mass m in $\mathcal{R}$ is intrinsic to the region $\mathcal{R}$, independent of the motion of $\mathcal{R}$ and therefore an objective scalar. As the mass contained inside the region may not change[4], one may introduce

$$\dot{m} = \frac{\mathrm{d}}{\mathrm{d}t} m = \frac{\mathrm{d}}{\mathrm{d}t} \int_{\mathcal{R}} \rho(\mathbf{x}, t) \, \mathrm{d}v = 0. \tag{2.100}$$

This statement is the principle of the conservation of mass. As the choice of the control volume is arbitrary, one may also choose an infinitesimal control volume and write relation (2.100) as

$$\frac{\mathrm{d}}{\mathrm{d}t} \left(\rho \, \mathrm{d}v \right) = 0. \tag{2.101}$$

Using (2.44) and (2.76), one may derive the local form of the mass balance

$$\dot{\rho} + \rho \, \mathrm{tr} \left(\mathbf{L} \right) = \dot{\rho} + \rho \, \boldsymbol{\nabla} \cdot \mathbf{v} = 0 \tag{2.102}$$

or, by the use of (2.97),

$$\frac{\partial \rho}{\partial t} + \boldsymbol{\nabla} \cdot \left(\rho \, \mathbf{v} \right) = 0. \tag{2.103}$$

As equation (2.102) may be valid for any homogeneous region, one may derive an alternative extensive form of the mass balance as

$$\int_{\mathcal{R}} \left(\dot{\rho} + \rho \, \mathrm{tr} \left(\mathbf{L} \right) \right) \, \mathrm{d}v = 0. \tag{2.104}$$

[4] An extension not restricted to this issue is presented in section 2.4.

Since the mass m within $\mathcal{R}$ is independent of the choice of the configuration, one may state for the referential configuration

$$m = \int_{\mathcal{R}} \rho(\mathbf{x}, t) \, \mathrm{d}v = \int_{\mathcal{R}_0} \rho_0(\mathbf{X}) \, \mathrm{d}V \tag{2.105}$$

where ρ_0 denotes the mass density for the arbitrarily chosen referential configuration $\mathcal{R}_0$. Employing equation (2.44), one may express the mass density in the referential configuration as

$$\rho_0 = J\rho. \tag{2.106}$$

2.3.3 Balance of linear momentum

The balance of linear momentum can be stated as

$$\frac{\mathrm{d}}{\mathrm{d}t} \int_{\mathcal{R}} \rho \, \mathbf{v} \, \mathrm{d}v = \int_{\partial\mathcal{R}} \mathbf{f} \, \mathrm{d}a + \int_{\mathcal{R}} \rho \, \mathbf{b} \, \mathrm{d}v. \tag{2.107}$$

The left hand side describes the resulting forces due to inertia, the first term on the right hand side the resultant of the force $\mathbf{f}(\mathbf{x}, t)$ acting on the surface of the region $\mathcal{R}$, and the second term the resultant due to volumetric forces $\mathbf{b}(\mathbf{x}, t)$ acting in $\mathcal{R}$.

The Cauchy stress tensor $\boldsymbol{\sigma}$ is introduced such that

$$\boldsymbol{\sigma}^T \cdot \mathbf{n} = \mathbf{f}. \tag{2.108}$$

Making use of the mass balance in the form (2.101) leads to

$$\int_{\mathcal{R}} \rho \, \dot{\mathbf{v}} \, \mathrm{d}v = \int_{\partial\mathcal{R}} \boldsymbol{\sigma}^T \cdot \mathbf{n} \, \mathrm{d}a + \int_{\mathcal{R}} \rho \, \mathbf{b} \, \mathrm{d}v. \tag{2.109}$$

By employing the Gauss theorem (2.95), i.e. substituting

$$\int_{\partial\mathcal{R}} \mathbf{f} \, \mathrm{d}a = \int_{\partial\mathcal{R}} \boldsymbol{\sigma}^T \cdot \mathbf{n} \, \mathrm{d}a = \int_{\mathcal{R}} \boldsymbol{\nabla} \cdot \boldsymbol{\sigma} \, \mathrm{d}v, \tag{2.110}$$

one arrives at another extensive form of the balance of momentum

$$\int_{\mathcal{R}} \rho\, \dot{\mathbf{v}}\ \mathrm{d}v = \int_{\mathcal{R}} (\boldsymbol{\nabla} \cdot \boldsymbol{\sigma} + \rho\, \mathbf{b})\ \mathrm{d}v. \tag{2.111}$$

Using again the arbitrariness of the control volume leads to the intensive form of the balance of linear momentum in the actual configuration

$$\rho\, \dot{\mathbf{v}} = \boldsymbol{\nabla} \cdot \boldsymbol{\sigma} + \rho\, \mathbf{b}. \tag{2.112}$$

In some publications, this relation is referred to as *Cauchy's first law of motion*.

By using Nanson's formula (2.47) and the relations (2.44) and (2.106), equation (2.109) may by expressed as

$$\int_{\mathcal{R}_0} \rho_0\, \dot{\mathbf{v}}\ \mathrm{d}V = \int_{\partial\mathcal{R}_0} J\, \boldsymbol{\sigma}^T \cdot \mathbf{F}^{-T} \cdot \mathbf{N}\ \mathrm{d}A + \int_{\mathcal{R}_0} \rho_0\, \mathbf{b}\ \mathrm{d}V. \tag{2.113}$$

By introducing the nominal stress tensor

$$\mathbf{P} = J\, \mathbf{F}^{-1} \cdot \boldsymbol{\sigma}, \tag{2.114}$$

one may express the extensive form of the balance of linear momentum in terms of the reference configuration as

$$\int_{\mathcal{R}_0} \rho_0\, \dot{\mathbf{v}}\ \mathrm{d}V = \int_{\partial\mathcal{R}_0} \mathbf{P}^T \cdot \mathbf{N}\ \mathrm{d}A + \int_{\mathcal{R}_0} \rho_0\, \mathbf{b}\ \mathrm{d}V, \tag{2.115}$$

the referential counterpart to relation (2.109). By using the Gauss theorem with respect to the referential configuration, one may derive a relation in close analogy to equation (2.111)

$$\int_{\mathcal{R}_0} \rho_0\, \dot{\mathbf{v}}\ \mathrm{d}V = \int_{\mathcal{R}_0} \boldsymbol{\nabla}_0 \cdot \mathbf{P}\ \mathrm{d}V + \int_{\mathcal{R}_0} \rho_0\, \mathbf{b}\ \mathrm{d}V. \tag{2.116}$$

This leads directly to the local form of the linear momentum balance for the referential configuration

$$\rho_0\, \dot{\mathbf{v}} = \boldsymbol{\nabla}_0 \cdot \mathbf{P} + \rho_0\, \mathbf{b}. \tag{2.117}$$

It is noteworthy that, even though the Cauchy stress is symmetric for a large class of problems as shown in the next section, the nominal stress tensor is generally non symmetric. Its transpose

$$\mathbf{T} = \mathbf{P}^T \tag{2.118}$$

is denoted first Piola-Kirchhoff stress[5]. The pull-back of the traction vector $\mathbf{f}$ into the referential configuration, which is energetically motivated as later shown, denoted by $\mathbf{f}_0 = \mathbf{F}^{-1} \cdot \mathbf{f}$, leads to the introduction of the second Piola-Kirchhoff stress

$$\mathbf{S} = \mathbf{F}^{-1} \cdot \mathbf{T} = J\,\mathbf{F}^{-1} \cdot \boldsymbol{\sigma}^T \cdot \mathbf{F}^{-T}. \tag{2.119}$$

The motivation behind the introduction of the second Piola-Kirchhoff stress tensor will be more extensively discussed in section 2.3.5. Note that this tensor is symmetric if the Cauchy stress tensor is symmetric. One example for another stress definition is the Kirchhoff stress or weighted Cauchy stress

$$\boldsymbol{\tau} = J\,\boldsymbol{\sigma}. \tag{2.120}$$

A more detailed discussion on other possible choices for the stress description can be found in Ogden (1984).

2.3.4 Balance of angular momentum

In this monograph, volumetric and surfacial moments are not taken into account for the homogeneous region $\mathcal{R}$. Due to this restriction, only the resulting moments of body and surface forces are taken into account to express the change of the angular momentum as

$$\frac{\mathrm{d}}{\mathrm{d}t}\int_{\mathcal{R}} \rho\,(\mathbf{x}-\mathbf{x}_0)\,\times\mathbf{v}\;\mathrm{d}v \;=\; \int_{\partial\mathcal{R}} (\mathbf{x}-\mathbf{x}_0)\,\times\,\mathbf{f}\;\mathrm{d}a + \int_{\mathcal{R}} \rho\,(\mathbf{x}-\mathbf{x}_0)\,\times\,\mathbf{b}\;\mathrm{d}v \tag{2.121}$$

[5]The use of the denotation "First Piola-Kirchhoff stress" and "nominal stress" is not fixed and sometimes used reversed, i.e. the First Piola-Kirchhoff stress is defined as the transposed tensor.

or, for a fixed point $\mathbf{x}_0$ by making use of the identity $\mathbf{v} \times \mathbf{v} = \mathbf{0}$ and employing relation (2.101) as

$$\int_{\mathcal{R}} \rho \left(\mathbf{x} - \mathbf{x}_0\right) \times \dot{\mathbf{v}} \, \mathrm{d}v = \int_{\partial\mathcal{R}} \left(\mathbf{x} - \mathbf{x}_0\right) \times \mathbf{f} \, \mathrm{d}a + \int_{\mathcal{R}} \rho \left(\mathbf{x} - \mathbf{x}_0\right) \times \mathbf{b} \, \mathrm{d}v. \tag{2.122}$$

Substitution of the balance of linear momentum (2.112) and the definition of the Cauchy stress (2.108) yields

$$\int_{\mathcal{R}} \left(\mathbf{x} - \mathbf{x}_0\right) \times \left(\boldsymbol{\nabla} \cdot \boldsymbol{\sigma}\right) \, \mathrm{d}v = \int_{\partial\mathcal{R}} \left(\mathbf{x} - \mathbf{x}_0\right) \times \left(\boldsymbol{\sigma}^T \cdot \mathbf{n}\right) \, \mathrm{d}a. \tag{2.123}$$

Conversion of the surface integral into a volume integral by means of the Gauss theorem and by introduction of the Levi-Civita Tensor $\boldsymbol{\epsilon}$ (cf. equation (2.15)) leads to

$$\int_{\mathcal{R}} \boldsymbol{\sigma} : \boldsymbol{\epsilon} \, \mathrm{d}v = \mathbf{0}. \tag{2.124}$$

As the control volume may be chosen arbitrarily,

$$\boldsymbol{\sigma} : \boldsymbol{\epsilon} = \mathbf{0} \tag{2.125}$$

holds, which can generally only be fulfilled if

$$\boldsymbol{\sigma}^T = \boldsymbol{\sigma}. \tag{2.126}$$

Thus, the restriction imposed in the opening of this section leads to the conclusion that the Cauchy stress tensor is symmetric. In some publications, this relation is referred to as *Cauchy's second law of motion*.

Even though this relation could be incorporated into the preceding equations, it is not used in order to clarify the similarities between equations in the actual and their corresponding relations in the reference configuration.

2.3.5 Balance of energy

2.3.5.1 Balance of kinetic energy

One possible point of departure for the notion of energy is the balance of linear momentum. Multiplying relation (2.112) by $\mathbf{v}$ and using the mass balance yields a work rate, the mechanical stress power

$$\frac{1}{2}\,\rho\,(\mathbf{v}\cdot\mathbf{v})^{\cdot} = \rho\,\mathbf{v}\cdot\mathbf{b} + \mathbf{v}\cdot(\boldsymbol{\nabla}\cdot\boldsymbol{\sigma}). \tag{2.127}$$

Integrating this term over the volume $\mathcal{R}$, use of the Gauss theorem, the balance of mass, and integration by parts leads to

$$\frac{\mathrm{d}}{\mathrm{d}t}\int\limits_{\mathcal{R}}\frac{1}{2}\,\rho\,\mathbf{v}^2\,\mathrm{d}v = \int\limits_{\mathcal{R}}\rho\,\mathbf{b}\cdot\mathbf{v}\,\mathrm{d}v + \int\limits_{\partial\mathcal{R}}(\boldsymbol{\sigma}^T\cdot\mathbf{n})\cdot\mathbf{v}\,\mathrm{d}a - \int\limits_{\mathcal{R}}\boldsymbol{\sigma}:\mathbf{L}\,\mathrm{d}v. \tag{2.128}$$

By introducing the kinetic energy

$$E = \int\limits_{\mathcal{R}}\frac{1}{2}\,\rho\,\mathbf{v}^2\,\mathrm{d}v, \tag{2.129}$$

the work rate due to the mechanical external forces

$$P = \int\limits_{\mathcal{R}}\rho\,\mathbf{b}\cdot\mathbf{v}\,\mathrm{d}v + \int\limits_{\partial\mathcal{R}}\mathbf{v}\cdot(\boldsymbol{\nabla}\cdot\boldsymbol{\sigma})\,\mathrm{d}a, \tag{2.130}$$

and the rate of the deformation energy

$$\dot{W} = \int\limits_{\mathcal{R}}\boldsymbol{\sigma}:\boldsymbol{L}\,\mathrm{d}v, \tag{2.131}$$

relation (2.128) may be restated in the form

$$\frac{\mathrm{d}}{\mathrm{d}t}\,E = P - \dot{W}. \tag{2.132}$$

Use of the same procedure leads to the balance of mechanical energy in terms of the referential description[6]

$$\frac{\mathrm{d}}{\mathrm{d}t}\int\limits_{\mathcal{R}_0}\frac{1}{2}\,\rho_0\,\mathbf{v}^2\,\mathrm{d}V=\int\limits_{\mathcal{R}_0}\rho_o\,\mathbf{b}\cdot\mathbf{v}\,\mathrm{d}V+\int\limits_{\partial\mathcal{R}_0}(\mathbf{P}\cdot\mathbf{N})\cdot\mathbf{v}\,\mathrm{d}A-\int\limits_{\mathcal{R}_0}\mathbf{P}^T\,:\,\dot{\mathbf{F}}\,\mathrm{d}V. \tag{2.133}$$

Equations (2.128) and (2.133) are called balance of kinetic energy (Gyarmati (1970)) or mechanical balance of energy (Schade (1970)).

2.3.5.2 Conjugate stress analysis

The last part of equations (2.128) and (2.133) may also be expressed as

$$\dot{W}=\int\limits_{\mathcal{R}}\rho\,\dot{w}\,\mathrm{d}v=\int\limits_{\mathcal{R}_0}\rho_0\,\dot{w}\,\mathrm{d}V \tag{2.134}$$

where the definition of the specific mechanical work rate, i.e. per unit mass,

$$\dot{w}=\frac{1}{\rho}\,\boldsymbol{\sigma}\,:\,\mathbf{L}=\frac{1}{\rho}\,\boldsymbol{\sigma}\,:\,\mathbf{D}=\frac{1}{\rho_0}\,\boldsymbol{\tau}\,:\,\mathbf{D} \tag{2.135}$$

is used. This scalar can also be expressed in terms of the referential configuration as

$$\dot{w}=\frac{1}{\rho_0}\,\mathbf{P}\,:\,\dot{\mathbf{F}}^T=\frac{1}{\rho_0}\,\mathbf{T}^T\,:\,\dot{\mathbf{F}}^T. \tag{2.136}$$

The Kirchhoff stress $\boldsymbol{\tau}$ and the stretching tensor $\mathbf{D}$ form a pair of variables which are, due to the fact that their double contraction yields a work rate, energetically conjugate. The same applies for the pair consisting of the first Piola-Kirchoff stress $\mathbf{T}$ (or the nominal stress $\mathbf{P}$) and the material time derivative of the deformation gradient $\dot{\mathbf{F}}$. This grouping is not unique. One may also find other pairs, e.g. the second Piola-Kirchhoff stress $\mathbf{S}$ and the Green-Lagrange strain $\mathbf{E}$

$$\dot{w}=\frac{1}{\rho_0}\,\mathbf{S}^T\,:\,\dot{\mathbf{E}} \tag{2.137}$$

[6] The symmetry of the Cauchy stress tensor was implicitly used to derive relation (2.133).

which provides the energetic motivation for the introduction of the second Piola-Kirchhoff stress.

Apart from the possible addition of an arbitrary antimetric tensor, the grouping of the quantities to yield an expression for $\dot{w}$ is unique providing that one component of the pair is fixed. However, the grouping is no longer unique when a relation for w with $\dot{w} = \mathrm{d}w/\,\mathrm{d}t$ is to be derived. For descriptions in the referential frame, no difficulties arise. The material time derivative of a quantity is replaced by the quantity itself to yield w. For the Eulerian description, this is not possible as the use of the material time derivative leads to a non-objective measure. Thus, the objective time derivative $\overset{\circ}{(\bullet)}$ of a tensor is introduced, presuming that

$$\dot{w} = \frac{1}{\rho_0}\,\mathbf{\Pi} : \overset{\circ}{\boldsymbol{e}}\,. \tag{2.138}$$

holds. Considering in this section only the constraints due to thermodynamics, $\mathbf{\Pi}$ and $\boldsymbol{e}$ are pairs of stresses and strains as described above, $\overset{\circ}{(\bullet)}$ may be either an objective time derivative or, for measures in the referential configuration, the material time derivative. Furthermore, it is required that the chain rule can be applied to a potential $\phi = \phi(\mathbf{A})$ such that

$$\dot{\phi} = \frac{\partial \phi}{\partial \mathbf{A}} : \overset{\circ}{\mathbf{A}} \tag{2.139}$$

holds. For corotational rates, which can be derived following the Lie concept employing a configuration in which the material time derivative is sufficient as described in section 2.2.5, Bruhns (2003) has shown that this holds true. However, it may not be possible to prove the existence and uniqueness for any objective rate.

2.3.5.3 First law of thermodynamics

Turning the focus to thermodynamics, the first law of thermodynamics states, that the sum of work done by the external forces and the thermal energy supplied to the region have to equal the change of the total energy of the body $\mathcal{R}$. The thermal energy supplied to the region $\dot{Q}$ can be described by

$$\dot{Q} = \int_{\mathcal{R}} \rho\, r \;\mathrm{d}v - \int_{\partial\mathcal{R}} \mathbf{q}\cdot\mathbf{n}\;\mathrm{d}a \tag{2.140}$$

where r denotes volumetric, specific heat sources (e.g. due to chemical reactions) and $\mathbf{q}$ the heat flux within the region $\mathcal{R}$. Thus, the term $-\mathbf{q}\cdot\mathbf{n}$ describes the heat flux into the region $\mathcal{R}$ through its surface. In contrast to section 2.3.5.1 where only the total energy was taken into account, the energy stored due to atomistic or micro processes is considered. In order to reflect this, an additional energy term is introduced, the internal energy U. Classically, this term accounts for the thermal energy stored in the body due to e.g. atomic oscillation. The total energy E^t of the region $\mathcal{R}$ can be expressed as

$$E^t = E + U. \tag{2.141}$$

The first law of thermodynamics is now to be postulated as

$$\frac{\mathrm{d}}{\mathrm{d}t}\,E^t = \frac{\mathrm{d}}{\mathrm{d}t}\,(E+U) = P + \dot{Q}. \tag{2.142}$$

Combination of this equation with the mechanical form (2.132) leads to the form

$$\frac{\mathrm{d}}{\mathrm{d}t}\,U = \dot{W} + \dot{Q}. \tag{2.143}$$

By introducing the specific internal energy implicitly by

$$U = \int\limits_{\mathcal{R}} \rho\, u \,\mathrm{d}v, \tag{2.144}$$

one may rewrite relation (2.142) as

$$\frac{\mathrm{d}}{\mathrm{d}t}\left\{\int\limits_{\mathcal{R}} \frac{1}{2}\rho\,\mathbf{v}^2\,\mathrm{d}v + \int\limits_{\mathcal{R}} \rho\, u\;\mathrm{d}v\right\} = \tag{2.145}$$

$$\int\limits_{\mathcal{R}} \rho\,\mathbf{b}\cdot\mathbf{v}\,\mathrm{d}v + \int\limits_{\partial\mathcal{R}} (\boldsymbol{\sigma}^T\cdot\mathbf{n})\cdot\mathbf{v}\,\mathrm{d}a + \int\limits_{\mathcal{R}} \rho\, r\;\mathrm{d}v - \int\limits_{\partial\mathcal{R}} \mathbf{q}\cdot\mathbf{n}\;\mathrm{d}a.$$

The combination of this variant of the first law of thermodynamics with the balance of the mechanical kinetic energy (2.128) leads to the continuum-mechanical version of the first law of thermodynamics in the extensive form

$$\frac{\mathrm{d}}{\mathrm{d}t}\int\limits_{\mathcal{R}} \rho\, u\,\mathrm{d}v = \int\limits_{\mathcal{R}} \rho\, r\;\mathrm{d}v - \int\limits_{\partial\mathcal{R}} \mathbf{q}\cdot\mathbf{n}\;\mathrm{d}a + \int\limits_{\mathcal{R}} \rho\,\dot{w}\,\mathrm{d}v. \tag{2.146}$$

The intensive form can be derived after application of the Gauss theorem (2.95) and the mass-balance as

$$\dot{u} - \dot{w} - r + \frac{1}{\rho} \, \boldsymbol{\nabla} \cdot \mathbf{q} = 0. \tag{2.147}$$

Again, these relations can also be obtained in terms of the reference configuration in extensive form

$$\frac{\mathrm{d}}{\mathrm{d}t} \int\limits_{\mathcal{R}_0} \rho_0 \, u \, \mathrm{d}V = \int\limits_{\mathcal{R}_0} \rho_0 \, r \, \mathrm{d}V - \int\limits_{\partial\mathcal{R}_0} \mathbf{q}_0 \cdot \mathbf{N} \, \mathrm{d}A + \int\limits_{\mathcal{R}_0} \rho_0 \, \dot{w} \, \mathrm{d}V \tag{2.148}$$

and in intensive form

$$\dot{u} - \dot{w} - r + \frac{1}{\rho_0} \, \boldsymbol{\nabla}_0 \cdot \mathbf{q}_0 = 0. \tag{2.149}$$

Here, the referential heat flux $\mathbf{q}_0 = J \, \mathbf{F}^{-1} \cdot \mathbf{q}$ is introduced.

2.3.5.4 Thermal energy

The local form of the first law of thermodynamics (2.147) may be stated as

$$\dot{u} = \dot{w} + \dot{q} \tag{2.150}$$

where the thermal flux

$$\dot{q} = r - \frac{1}{\rho} \, \boldsymbol{\nabla} \cdot \mathbf{q} \tag{2.151}$$

has been introduced. In section 2.3.5.2, a pair of variables is identified which lead in proper combination to the notion of the mechanical work rate $\dot{w}$. Following the ideas of rational thermodynamics (cf. Muschik et al. (2001)), two scalar variables s and Θ are introduced such that

$$\dot{q} = \Theta \, \dot{s}. \tag{2.152}$$

The variable Θ is an intensive variable, s an intensive, specific variable. Thus, an extensive variable entropy

$$S = \int_{\mathcal{R}} \rho s \, \mathrm{d}v \tag{2.153}$$

can be defined as well. Both specific entropy s and temperature Θ are primitive concepts, i.e. nothing is said how to define or measure these quantities. Especially regarding the temperature it is important to note that the connection to the usual notion of temperature is yet to be established and may only be shown for equilibrium thermodynamics. However, within this monograph, the measure Θ is adopted as the thermodynamic temperature without further derivation.

2.3.6 The second law of thermodynamics

The second law of thermodynamics is not a fundamental relation derived from basic physical considerations. It is merely a statement following experimental observations, which does not make it less strict as violations of the rule could not be experimentally justified. The balance of entropy is adopted in the extensive form

$$\frac{\mathrm{d}}{\mathrm{d}t} \int_{\mathcal{R}} \rho \, s \, \mathrm{d}v \geq \int_{\mathcal{R}} \frac{\rho \, r}{\Theta} \, \mathrm{d}v - \int_{\partial\mathcal{R}} \frac{\mathbf{q} \cdot \mathbf{n}}{\Theta} \, \mathrm{d}a. \tag{2.154}$$

This statement can be interpreted such that the change of total entropy within the region under consideration must be always larger or equal to the entropy change due to external entropy supply or drain due to heat transfer. A local form of relation (2.154) can be derived as

$$\rho \, \Theta \, \dot{s} \geq \rho r - \boldsymbol{\nabla} \cdot \mathbf{q} + \frac{1}{\Theta} \, \mathbf{q} \cdot \boldsymbol{\nabla} \Theta, \tag{2.155}$$

a relation often referred to as the *Clausius-Duhem inequality*. The referential forms of equations (2.154) and (2.155) are

$$\frac{\mathrm{d}}{\mathrm{d}t} \int_{\mathcal{R}_0} \rho_0 \, s \, \mathrm{d}V \geq \int_{\mathcal{R}_0} \frac{\rho_0 \, r}{\Theta} \, \mathrm{d}V - \int_{\partial\mathcal{R}_0} \frac{\mathbf{q}_0 \cdot \mathbf{N}}{\Theta} \, \mathrm{d}A \tag{2.156}$$

and

$$\rho_0 \, \Theta \, \dot{s} \geq \rho_0 r - \boldsymbol{\nabla}_0 \cdot \mathbf{q}_0 + \frac{1}{\Theta} \, \mathbf{q}_0 \cdot \boldsymbol{\nabla}_0 \Theta. \tag{2.157}$$

If a material law is developed in accordance to inequalities stated in this section, it is said to be *thermodynamically consistent*[7]..

2.3.7 State space

The state space is introduced in order to describe the problem completely, i.e. the material behavior at time t can be expressed in terms of the variables in the state space at time t (cf . Muschik et al. (2001)). The variables contained in the state space are independent variables. However, the spatial derivative of a variable may be included as well as the variable itself. This is in conflict with the fact that the value of the scalar quantity at two different points and the spatial gradient of the quantity are not independent. Thus, the requirement of independence of the variables within the state is only locally valid. The requirement of independence yields certain restrictions on the choice of the variables. The inclusion of both the mass density ρ and the deformation gradient $\mathbf{F}$ would violate this requirement as the mass density can be expressed in terms of the deformation gradient as $\rho_0/\rho = \det \mathbf{F}$.

A state space Z is called *large* (cf. Muschik et al. (2001)) if the material properties are defined by maps local in time, i.e. the state of the substance can be completely described by the state variables. A state space Z is called *small* if the material properties depend on the history of the state variables. In the following, the focus will be on large state spaces as the functional dependence involved in small state spaces is not convenient. Thus, the process history may be captured by the introduction of an appropriate set of internal variables into the state space. As the use of a large state space prohibits the use of functionals, the total strain may generally not be included into the space. Instead, only its reversible part[8] may be included in the state and the inelastic behavior is described by an appropriate set of internal variables which are part of the state space.

[7] In addition, the Maxwell relations (2.185)-(2.188) have to fulfilled as well. However, they are not included in this definition of thermodynamic consistency as they are restrictions due to the introduction of the concept of potentials and not due to physical observations.

[8] The definition of the reversible part is based on thermodynamical considerations as amplified later.

As a consequence of the requirement that the chosen state space may completely describe the material, all other variables can be described in terms of the chosen state. If, for example, the state space consists of the scalar x, the Eulerian first order tensor $\mathbf{y}$ and the Eulerian second order tensor $\mathbf{Z}$, i.e.

$$Z = \{x, \mathbf{y}, \mathbf{Z}\}, \tag{2.158}$$

then a variable ϕ arising in the problem description can be expressed in terms of the state, i.e. $\phi = \phi(x, \mathbf{y}, \mathbf{Z})$. Consequently, all measures derived from ϕ can also be derived from the state space, as e.g.

$$\dot{\phi} = \frac{\partial \phi}{\partial x}\, \dot{x} + \frac{\partial \phi}{\partial \mathbf{y}} \cdot \overset{\circ}{\mathbf{y}} + \frac{\partial \phi}{\partial \mathbf{Z}} \,:\overset{\circ}{\mathbf{Z}}, \tag{2.159}$$

providing that the chain rule as noted in section 2.2.5 holds, or

$$\boldsymbol{\nabla}\phi = \frac{\partial \phi}{\partial x}\, \boldsymbol{\nabla} x + \frac{\partial \phi}{\partial \mathbf{y}} \cdot (\mathbf{y} \otimes \boldsymbol{\nabla}) + \frac{\partial \phi}{\partial \mathbf{Z}} \,:\, (\mathbf{Z} \otimes \boldsymbol{\nabla}). \tag{2.160}$$

In order to simplify the notation, the expression

$$\dot{\phi} = \frac{\partial \phi}{\partial Z} \;\overset{\circ}{Z} \tag{2.161}$$

shall be used equivalently to equation (2.159).

2.3.8 Affinities and fluxes

Within the theory of the description of inelastic continua, it is fundamental that general processes are not reversible. Thus, the mechanical work rate arising in such a process may be additively split into a reversible and an irreversible part

$$\dot{w} = \dot{w}_r + \dot{w}_i. \tag{2.162}$$

As the working variable in relation (2.135) is the velocity gradient tensor $\mathbf{L}$, the decomposition (2.162) implies a decomposition of $\mathbf{L}$ into a reversible part

$\mathbf{L}_r$ and an irreversible part $\mathbf{L}_i$. Equivalently, providing that $\boldsymbol{\tau} = \boldsymbol{\tau}^T$ holds, a decomposition of the the stretching tensor $\mathbf{D}$ such that

$$\mathbf{D} = \mathbf{D}_r + \mathbf{D}_i \tag{2.163}$$

is implied. Using this decomposition in relation (2.162) yields the forms

$$\dot{w}_r = \frac{1}{\rho_0}\,\boldsymbol{\tau} : \mathbf{D}_r \quad \text{and} \quad \dot{w}_i = \frac{1}{\rho_0}\,\boldsymbol{\tau} : \mathbf{D}_i. \tag{2.164}$$

It is important to note that the reversible part of the deformation rate tensor $\mathbf{D}_r$ is, from the thermodynamical point of view, chosen such that it qualifies to be included into the large state describing the material behavior. Furthermore, the irreversible part $\mathbf{D}_i$ can be expressed in terms of an appropriately chosen set of internal variables. Thus, it does not qualify as a state variable. A pair of thermodynamically conjugated variables consists of a thermodynamic force, or affinity, and a thermodynamic flux. Focussing on $\dot{w}_r$, one may define $\boldsymbol{\tau}$ as the thermodynamic force and $\mathbf{D}_r$ as the associated thermodynamic flux.

Employing the same motivational ground and using (2.152), one might rewrite the first law of thermodynamics (2.150) as

$$\dot{u} = \frac{1}{\rho_0}\,\boldsymbol{\tau} : \mathbf{D}_r + \dot{w}_i + \Theta\,\dot{s}. \tag{2.165}$$

Using the terms affinities (or thermodynamic forces) and associated fluxes, it should be mentioned that the choice of the corresponding pairs is not unique. Thus the idea may not be accepted unquestioningly (Eringen (1967)).

2.3.9 Thermodynamic potentials

2.3.9.1 The internal energy as a thermodynamic potential

It is now necessary to define the large state describing the state of the material. We might use

$$Z = \{\boldsymbol{e}_r, s, \boldsymbol{\xi}^h\}. \tag{2.166}$$

Here, it is assumed that a connection $\overset{\circ}{\boldsymbol{e}}_r = \mathbf{D}_r$ for the general strain introduced in section 2.3.5.2 is possible. $\boldsymbol{\xi}^h$ denotes a set of internal variables necessary to

describe the thermomechanical behavior of the material appropriately. What follows from this choice of the state space is that the internal energy can be expressed as

$$u = u(\boldsymbol{e}_r, s, \boldsymbol{\xi}^h). \tag{2.167}$$

The choice of $\boldsymbol{e}_r$ and s can be supplied if relation (2.165) is rewritten using the general stress $\boldsymbol{\Pi}$ introduced in section 2.3.5.2 as

$$\dot{u} = \frac{1}{\rho_0}\,\boldsymbol{\Pi} : \overset{\circ}{\boldsymbol{e}}_r + \dot{w}_i + \Theta\,\dot{s}, \tag{2.168}$$

where the working variables for $\dot{w}_r$ and $\dot{q}$ in this relation are the objective and material time derivative of $\boldsymbol{e}_r$ and s, respectively. Taking the total derivative of u based on the definition (2.167) yields

$$\dot{u} = \frac{\partial u}{\partial \boldsymbol{e}_r} : \overset{\circ}{\boldsymbol{e}}_r + \frac{\partial u}{\partial s}\,\dot{s} + \frac{\partial u}{\partial \boldsymbol{\xi}^h}\ \overset{\circ}{\boldsymbol{\xi}}{}^h\ . \tag{2.169}$$

Comparison with (2.168) leads to the relations for the partial derivatives of u

$$\frac{\partial u}{\partial \boldsymbol{e}_r} = \frac{1}{\rho_0}\boldsymbol{\Pi} \quad \text{and} \quad \frac{\partial u}{\partial s} = \Theta. \tag{2.170}$$

2.3.9.2 The Legendre transform

The Legendre transform may be explained here for the one dimensional case as a motivating example. The extension to more dimensions is rather straightforward and not covered here. A more elaborate discussion of the subject can be found e.g. in Aavatsmark (1995).

One may consider a relation between a measure x and a measure y described by

$$y = f(x). \tag{2.171}$$

The measure x shall be subject to a substitution: for each x with $\partial f/\partial x \neq \infty$, a tangent to the curve with the slope

$$a = \frac{\partial f}{\partial x} \tag{2.172}$$

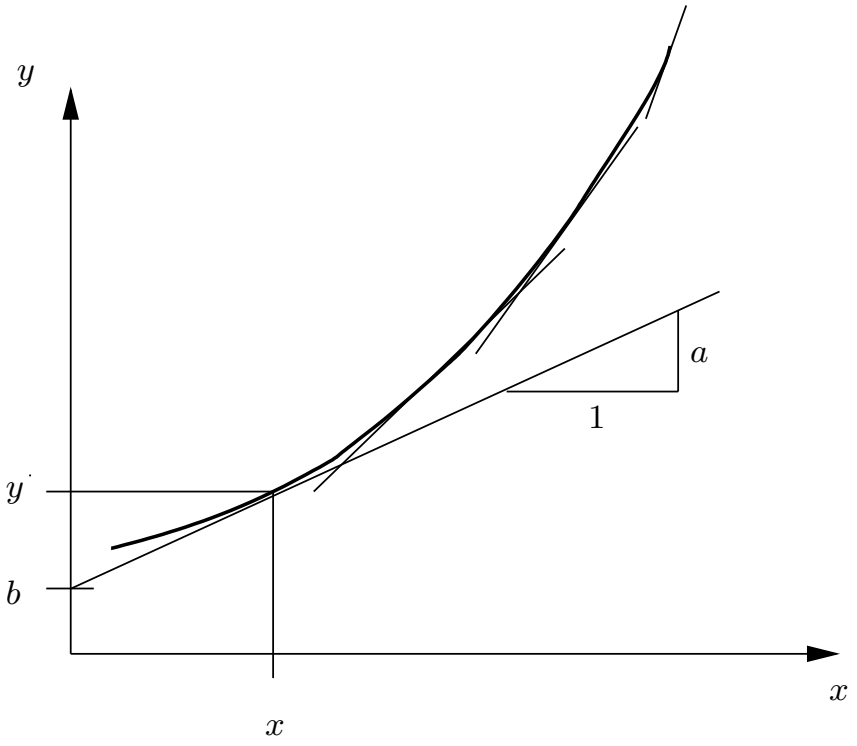

Figure 2.3: Tangents to curve $y = f(x)$

and the axis intercept

$$b = f(x) - \frac{\partial f}{\partial x} x = y - ax \tag{2.173}$$

can be constructed (cf. figure 2.3). Thus, a function $b = b(a)$ can be defined such that the relation is no longer described by $y = f(x)$ but by $b = b(a)$.

2.3.9.3 Application of the Legendre transform to the internal energy

As described in section 2.3.9.1, the internal energy can be identified as a potential which depends on the entropy s, the reversible part of the strain $\boldsymbol{e}_r$ and an appropriate set of internal variables which describe the dissipative processes of the thermal and the mechanical problem $\boldsymbol{\xi}^h$, i.e.

$$u = u(s, \boldsymbol{e}_r, \boldsymbol{\xi}^h). \tag{2.174}$$

The partial derivatives are

$$\frac{\partial u}{\partial \boldsymbol{e}_r} = \frac{1}{\rho_0}\boldsymbol{\Pi} \quad \text{and} \quad \frac{\partial u}{\partial s} = \Theta. \tag{2.175}$$

Applying the Legendre transform to u in order to substitute s leads to the introduction of the Helmholtz free energy

$$\varphi = u - \frac{\partial u}{\partial s}\, s = u - \Theta\, s. \tag{2.176}$$

As the variable s has been substituted by $\partial u/\partial s = \Theta$, the Helmholtz free energy depends on the variables

$$\varphi = \varphi(\Theta, \boldsymbol{e}_r, \boldsymbol{\xi}^h). \tag{2.177}$$

The partial derivatives read

$$\frac{\partial \varphi}{\partial \boldsymbol{e}_r} = \frac{1}{\rho_0}\boldsymbol{\Pi} \quad \text{and} \quad \frac{\partial \varphi}{\partial \Theta} = -s. \tag{2.178}$$

The application of the Legendre transform to φ in order to substitute $\boldsymbol{e}_r$ leads to the Gibbs free energy $g = g(\Theta, \boldsymbol{\Pi}, \boldsymbol{\xi}^h)$ with

$$g = \varphi - \frac{\partial \varphi}{\partial \boldsymbol{e}_r} : \boldsymbol{e}_r = \varphi - \frac{1}{\rho_0}\boldsymbol{\Pi} : \boldsymbol{e}_r \tag{2.179}$$

The partial derivatives are

$$\frac{\partial g}{\partial \boldsymbol{\Pi}} = -\frac{1}{\rho_0}\boldsymbol{e}_r \quad \text{and} \quad \frac{\partial g}{\partial \Theta} = -s. \tag{2.180}$$

The Legendre transform may be applied again to lead to the introduction of the enthalpy $h = h(s, \boldsymbol{\Pi}, \boldsymbol{\xi}^h)$ by

$$h = g - \frac{\partial g}{\partial \Theta}\Theta = g + s\,\Theta. \tag{2.181}$$

The partial derivatives of h are

$$\frac{\partial h}{\partial \boldsymbol{\Pi}} = -\frac{1}{\rho_0}\boldsymbol{e}_r \quad \text{and} \quad \frac{\partial h}{\partial s} = \Theta. \tag{2.182}$$

A fourth application of the Legendre transform to the enthalpy in order to substitute $\mathbf{\Pi}$ leads again to the internal energy. Thus, the enthalpy could also be derived by applying the Legendre transform to the internal energy in order to substitute $\boldsymbol{e}_r$. Therefore, the four potentials constitute a "closed circle" of all four possible potentials when the arguments $\mathbf{\Pi}$, $\boldsymbol{e}_r$, Θ, or s are varied. Naturally, the introduction of further potentials is possible by applying the transform with respect to the internal variables.

It is noteworthy, that the concept that the working variables are chosen as the independent variables is still valid for the potentials introduced in this section. This may be exemplarily shown for the Helmholtz free energy. Using the definition of the first law of thermodynamics in the form (2.168) leads to

$$\dot{\varphi} = \frac{1}{\rho_0}\,\mathbf{\Pi} : \overset{\circ}{\boldsymbol{e}}_r + \dot{w}_i - \dot{\Theta}\, s, \tag{2.183}$$

an alternative form of the first law suggesting the use of $\boldsymbol{e}_r$, Θ, and $\boldsymbol{\xi}^h$ as the independent variables.

As u, φ, g and h are potentials, they have to satisfy the integrability conditions, i.e.

$$\frac{\partial}{\partial x}\left(\frac{\partial \phi}{\partial y}\right) = \frac{\partial}{\partial y}\left(\frac{\partial \phi}{\partial x}\right) \tag{2.184}$$

if ϕ is a potential $\phi = \phi(x, y, ...)$. This leads to the Maxwell-relations, here only stated with respect to the variables u, φ, g and h,

$$\frac{\partial}{\partial s}\frac{\partial u}{\partial \boldsymbol{e}_r} = \frac{1}{\rho_0}\frac{\partial \mathbf{\Pi}}{\partial s} = \frac{\partial \Theta}{\partial \boldsymbol{e}_r} = \frac{\partial}{\partial \boldsymbol{e}_r}\frac{\partial u}{\partial s} \tag{2.185}$$

$$\frac{\partial}{\partial \Theta}\frac{\partial \varphi}{\partial \boldsymbol{e}_r} = \frac{1}{\rho_0}\frac{\partial \mathbf{\Pi}}{\partial \Theta} = -\frac{\partial s}{\partial \boldsymbol{e}_r} = \frac{\partial}{\partial \boldsymbol{e}_r}\frac{\partial \varphi}{\partial \Theta} \tag{2.186}$$

$$\frac{\partial}{\partial \Theta}\frac{\partial g}{\partial \mathbf{\Pi}} = -\frac{1}{\rho_0}\frac{\partial \boldsymbol{e}_r}{\partial \Theta} = -\frac{\partial s}{\partial \mathbf{\Pi}} = \frac{\partial}{\partial \mathbf{\Pi}}\frac{\partial g}{\partial s} \tag{2.187}$$

$$\frac{\partial}{\partial s}\frac{\partial h}{\partial \mathbf{\Pi}} = -\frac{1}{\rho_0}\frac{\partial \boldsymbol{e}_r}{\partial \Theta} = \frac{\partial \Theta}{\partial \mathbf{\Pi}} = \frac{\partial}{\partial \mathbf{\Pi}}\frac{\partial h}{\partial s}. \tag{2.188}$$

It is also possible to state these relations with respect to the internal variables. These relations pose, in addition to the second law of thermodynamics, important restrictions on the choice of the constitutive assumptions employed.

2.3.9.4 Thermodynamic consistency

As already stated in section 2.3.6, a material law is said to be thermodynamically consistent when developed in accordance to the restriction imposed by the second law of thermodynamics. As the validity of the second law is widely accepted, a material law should be developed in accordance to this rule. Thus, its exploitation within this framework should be discussed more in detail.

Introducing the Gibbs free energy g by use of the definitions (2.176) and (2.179) in local form of the balance of energy (2.147) yields

$$\dot{g} + \dot{\Theta} s + \Theta \dot{s} + \frac{1}{\rho_0} \overset{\circ}{\mathbf{\Pi}} : \boldsymbol{e}_r + \frac{1}{\rho_0} \mathbf{\Pi} : \overset{\circ}{\boldsymbol{e}}_r = \frac{1}{\rho_0} \mathbf{\Pi} : \overset{\circ}{\boldsymbol{e}}_r + \dot{w}_i + r - \frac{1}{\rho} \boldsymbol{\nabla} \cdot \boldsymbol{q}. \tag{2.189}$$

Use of the total differential of g

$$\dot{g} = \frac{\partial g}{\partial \mathbf{\Pi}} : \overset{\circ}{\mathbf{\Pi}} + \frac{\partial g}{\partial \Theta} \dot{\Theta} + \frac{\partial g}{\partial \boldsymbol{\xi}^h} \overset{\circ}{\boldsymbol{\xi}}^h \tag{2.190}$$

and its partial derivatives (2.180a) and (2.180b) yields

$$r - \frac{1}{\rho} \boldsymbol{\nabla} \cdot \boldsymbol{q} = \Theta \dot{s} + \frac{\partial g}{\partial \boldsymbol{\xi}^h} \overset{\circ}{\boldsymbol{\xi}}^h - \dot{w}_i. \tag{2.191}$$

Defining now the entropy change in a, possible fictive, reversible process as $\dot{s}_r$ leads, considering the inequality (2.155) as an equality and substituting $\dot{s}$ by $\dot{s}_r$, to

$$\Theta \, \dot{s}_r = r - \frac{1}{\rho} \boldsymbol{\nabla} \cdot \mathbf{q} + \frac{1}{\rho \, \Theta} \, \mathbf{q} \cdot \boldsymbol{\nabla} \Theta. \tag{2.192}$$

Presuming an additive decomposition of the entropy change

$$\dot{s} = \dot{s}_r + \dot{s}_i \tag{2.193}$$

yields

$$\Theta \, \dot{s}_i \geq 0. \tag{2.194}$$

Employing (2.192) in (2.191) gives

$$0 = \Theta\, \dot{s}_i + \frac{1}{\rho\,\Theta}\, \mathbf{q} \cdot \boldsymbol{\nabla}\Theta + \frac{\partial g}{\partial \boldsymbol{\xi}^h}\, \overset{\circ}{\boldsymbol{\xi}}{}^h - \dot{w}_i \tag{2.195}$$

leading to

$$\Theta \dot{s}_i = \dot{w}_i - \frac{\partial g}{\partial \boldsymbol{\xi}^h}\, \overset{\circ}{\boldsymbol{\xi}}{}^h - \frac{1}{\rho\,\Theta}\, \mathbf{q} \cdot \boldsymbol{\nabla}\Theta \geq 0. \tag{2.196}$$

Usually, the set of internal variables $\boldsymbol{\xi}^h$ is decomposed into a non-interfering set describing the mechanical process $\boldsymbol{\xi}^p$ and a set describing the thermal process $\boldsymbol{\xi}^q$, thus

$$\boldsymbol{\xi}^h = \{\boldsymbol{\xi}^p, \boldsymbol{\xi}^q\} \tag{2.197}$$

follows and relation (2.196) reads

$$\Theta \dot{s}_i = \dot{w}_i - \frac{\partial g}{\partial \boldsymbol{\xi}^p}\, \overset{\circ}{\boldsymbol{\xi}}{}^p - \frac{\partial g}{\partial \boldsymbol{\xi}^q}\, \overset{\circ}{\boldsymbol{\xi}}{}^q - \frac{1}{\rho\,\Theta}\, \mathbf{q} \cdot \boldsymbol{\nabla}\Theta \geq 0. \tag{2.198}$$

Using decomposition (2.197), a stronger assumption with respect to inequality (2.196) is done. It is assumed that the mechanical part and the thermal part independently satisfy inequality (2.196), i.e. that

$$\dot{w}_i - \frac{\partial g}{\partial \boldsymbol{\xi}^p}\, \overset{\circ}{\boldsymbol{\xi}}{}^p \quad \geq \quad 0 \tag{2.199}$$

$$-\frac{\partial g}{\partial \boldsymbol{\xi}^q}\, \overset{\circ}{\boldsymbol{\xi}}{}^q - \frac{1}{\rho\Theta}\mathbf{q} \cdot (\boldsymbol{\nabla}\Theta) \quad \geq \quad 0 \tag{2.200}$$

must be fulfilled independently.

2.3.10 Thermomechanical coupling

To close the considerations related to homogeneous media, the coupling between the thermodynamic process and the mechanical process has to be established. Taking the time derivative of the definition of the Helmholtz free energy (2.176), using the first law of thermodynamics in the form (2.150), and

inserting the total derivative of $\dot{\varphi}$ in conjunction with definition (2.178) and decomposition (2.162) leads to

$$\Theta\,\dot{s} = \dot{w}_i + \dot{q} - \frac{\partial \varphi}{\partial \boldsymbol{\xi}^h} \overset{\circ}{\boldsymbol{\xi}}{}^h \,. \tag{2.201}$$

Using the form (2.178b) for s leads to

$$-\Theta\,\frac{\partial \dot{\varphi}}{\partial \Theta} = \dot{w}_i + \dot{q} - \frac{\partial \varphi}{\partial \boldsymbol{\xi}^h} : \overset{\circ}{\boldsymbol{\xi}}{}^h \,. \tag{2.202}$$

Making use again of the total derivative of φ yields

$$c_p\,\dot{\Theta} = \dot{q} + \dot{w}_i + \Theta\,\frac{\partial^2 \varphi}{\partial \Theta\,\partial \boldsymbol{e}_r} : \overset{\circ}{\boldsymbol{e}}_r + \Theta\,\frac{\partial^2 \varphi}{\partial \Theta\,\partial \boldsymbol{\xi}^h} : \overset{\circ}{\boldsymbol{\xi}}{}^h - \frac{\partial \varphi}{\partial \boldsymbol{\xi}^h} : \overset{\circ}{\boldsymbol{\xi}}{}^h \tag{2.203}$$

where the definition of the specific heat capacity c_p (cf. relations (3.36) and (3.37))

$$c_p = \frac{\partial h}{\partial \Theta} = \Theta\,\frac{\partial s}{\partial \Theta} = -\Theta\,\frac{\partial^2 \varphi}{\partial \Theta^2} \tag{2.204}$$

is used. In relation (2.203), the two terms containing mixed partial derivatives represent the coupling terms between the thermal and their respective subprocess. For example, the first term describes the piezocaloric coupling.

Relating this derivation to the form of the field equation usually used for thermal problems

$$c_p\,\dot{\Theta} = -\frac{1}{\rho}\,\boldsymbol{\nabla}\cdot\mathbf{q} + \dot{h}_{lat} \tag{2.205}$$

one may identify

$$\dot{h}_{lat} = r + \dot{w}_i + \Theta\,\frac{\partial^2 \varphi}{\partial \Theta\,\partial \boldsymbol{e}_r} : \overset{\circ}{\boldsymbol{e}}_r + \Theta\,\frac{\partial^2 \varphi}{\partial \Theta\,\partial \boldsymbol{\xi}^h} : \overset{\circ}{\boldsymbol{\xi}}{}^h - \frac{\partial \varphi}{\partial \boldsymbol{\xi}^h} : \overset{\circ}{\boldsymbol{\xi}}{}^h \tag{2.206}$$

or its equivalent, employing the Gibbs energy g (cf. Müller (2003)),

$$\dot{h}_{lat} = r + \dot{w}_i + \Theta\,\frac{\partial^2 g}{\partial \Theta\,\partial \boldsymbol{\Pi}} : \overset{\circ}{\boldsymbol{\Pi}} + \Theta\,\frac{\partial^2 g}{\partial \Theta\,\partial \boldsymbol{\xi}^h} : \overset{\circ}{\boldsymbol{\xi}}{}^h - \frac{\partial g}{\partial \boldsymbol{\xi}^h} : \overset{\circ}{\boldsymbol{\xi}}{}^h \,. \tag{2.207}$$

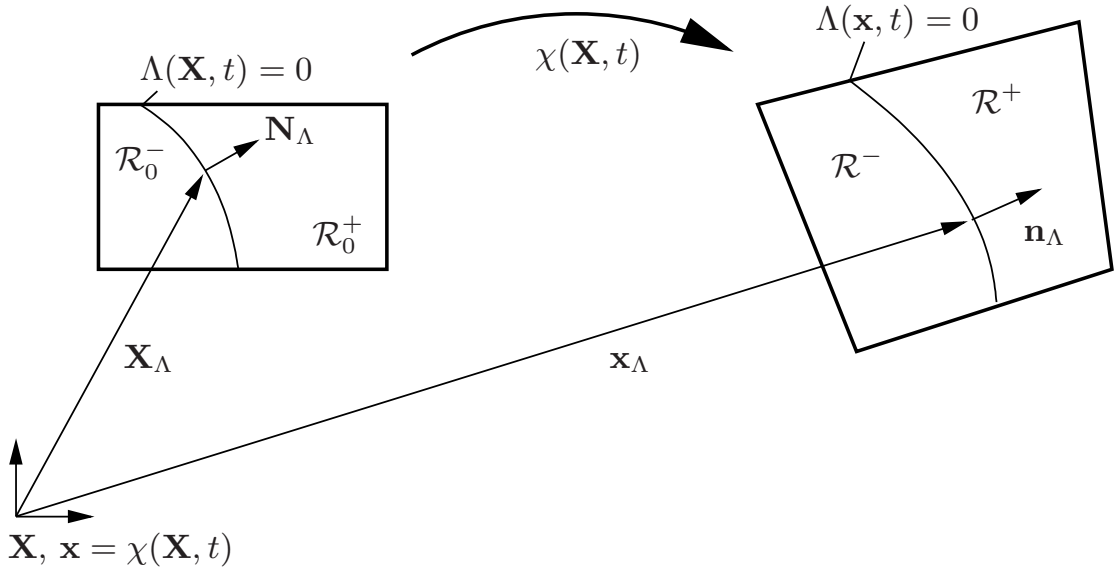

Figure 2.4: Region surrounding $\mathbf{x}_\Lambda$ in $\mathcal{B}_0$ and $\mathcal{B}$.

2.4 Local considerations at a discontinuity

In the following section, local relations at a discontinuity, often termed jump conditions, are derived. These relations can be found in various publications or books (see e.g. Truesdell & Toupin (1960), Becker & Bürger (1975), Šilhavý (1997)) and is included for later reference. In order to derive them, a sufficiently small region $\mathcal{R}$ around the point of interest $\mathbf{x}_\Lambda$ located on the discontinuity Λ is considered. The region is chosen such that no discontinuity other than Λ can be found in $\mathcal{R}$. Therefore, $\mathcal{R}$ may be subdivided into two homogeneous subregions[9] $\mathcal{R}^+$ and $\mathcal{R}^-$ such that $\mathcal{R}=\mathcal{R}^+\cup\mathcal{R}^-$ and $\mathcal{R}^+\cap\mathcal{R}^-=\emptyset$. Consequently, the discontinuity is defined by $\Lambda=\partial\mathcal{R}^+\cap\partial\mathcal{R}^-$ (cf. figure 2.4) and the boundary of the composed region $\mathcal{R}$ by $\partial\mathcal{R}=(\partial\mathcal{R}^+\backslash\Lambda)\cup(\partial\mathcal{R}^-\backslash\Lambda)$.

2.4.1 Mathematical description of the spatial position of the discontinuity

As the interface might move within the body, the distinction between the position of a material point $\mathbf{x}$ and the position of a point on the interface $\mathbf{x}_\Lambda$ is crucial. For each discontinuity, a function $\Lambda=\Lambda(\mathbf{x},t)$ is defined. For a point

[9] The term homogeneous is used to describe a region without discontinuity.

on the discontinuity with the vector $\mathbf{x}_\Lambda$ describing its position, the condition

$$\Lambda(\mathbf{x}_\Lambda, t) = 0 \tag{2.208}$$

holds. For the region $\mathcal{R}^+$, $\Lambda(\mathbf{x}, t) > 0$ holds whereas for the region $\mathcal{R}^-$ $\Lambda(\mathbf{x}, t) < 0$ holds. The unit vector normal to the discontinuity $\mathbf{n}_\Lambda$ pointing towards $\mathcal{R}^+$ is defined by

$$\mathbf{n}_\Lambda = \frac{\boldsymbol{\nabla}\Lambda}{|\boldsymbol{\nabla}\Lambda|}. \tag{2.209}$$

The sign convention for $\mathbf{n}_\Lambda$ leads to

$$\mathbf{n}_\Lambda = \mathbf{n}^- = -\mathbf{n}^+ \quad \text{on} \quad \Lambda \tag{2.210}$$

where $\mathbf{n}^-$ and $\mathbf{n}^+$ are the usual unit vectors normal to $\partial\mathcal{R}^-$ and $\partial\mathcal{R}^+$ pointing outwards. In terms of the referential description, this position may be described by

$$\Lambda(\mathbf{X}_\Lambda, t) = 0. \tag{2.211}$$

Equivalently, a normal vector $\mathbf{N}_\Lambda$ can be defined in the referential configuration. Its connection to $\mathbf{n}_\Lambda$ can be established by virtue of Nanson's formula (2.47) as

$$\mathbf{n}_\Lambda = \frac{\mathbf{F}^{-T} \cdot \mathbf{N}_\Lambda}{|\mathbf{F}^{-T} \cdot \mathbf{N}_\Lambda|} \tag{2.212}$$

and

$$\mathbf{N}_\Lambda = \frac{\mathbf{F}^{T} \cdot \mathbf{n}_\Lambda}{|\mathbf{F}^{T} \cdot \mathbf{n}_\Lambda|}. \tag{2.213}$$

The velocity of a point on the interface is denoted by

$$\mathbf{v}_\Lambda = \frac{\partial \mathbf{x}_\Lambda}{\partial t}, \tag{2.214}$$

the relative velocity of the interface by

$$u_\Lambda = (\mathbf{v}_\Lambda - \mathbf{v}) \cdot \mathbf{n}_\Lambda. \tag{2.215}$$

In the referential configuration the velocity of a point on the interface is denoted by

$$\mathbf{V}_\Lambda = \frac{\partial \mathbf{X}_\Lambda}{\partial t}, \tag{2.216}$$

the velocity of the interface in the referential description by

$$U_\Lambda = \mathbf{V}_\Lambda \cdot \mathbf{N}_\Lambda. \tag{2.217}$$

A jump at the discontinuity is denoted by square brackets,

$$[\bullet] = \bullet^+ - \bullet^- \tag{2.218}$$

where the superscript "+" denotes a value at the discontinuity approaching from the region $\mathcal{R}^+$, whereas the superscript "–" is used in the same manner regarding region $\mathcal{R}^-$. The average value is denoted by angle brackets

$$\langle \bullet \rangle = \frac{\bullet^+ + \bullet^-}{2}. \tag{2.219}$$

Some additional rules regarding the jump of a measure might prove useful in the following:

$$[a\, b] = [a]\, \langle b \rangle + \langle a \rangle\, [b] \tag{2.220}$$

where a and b are scalars and

$$[\mathbf{a} \odot \mathbf{b}] = [\mathbf{a}] \odot \langle \mathbf{b} \rangle + \langle \mathbf{a} \rangle \odot [\mathbf{b}] \tag{2.221}$$

where $\mathbf{a}$ and $\mathbf{b}$ are vectors and $\odot \in \{\cdot, \times\}$.

2.4.2 Transport theorem

In section 2.3.1, a transport theorem is developed under the assumption that the involved region is homogeneous. However, this does not apply for the situation discussed in this section, thus an extension based on these derivations is to be done. As in section 2.3.1, $\mathbf{A}$ denotes an n-th order tensor, i.e. $\mathbf{A} = A_{i\ldots j}\, \mathbf{e}_i \otimes \cdots \otimes \mathbf{e}_j$, as well as $\mathbf{B}$ and $\mathbf{G}$.

In the present monograph, only the transport theorem for volumes is used. Thus, the main focus is on this theorem, refer to Schade (1970) for other theorems. One may formulate the transport theorem for homogeneous regions in the form (2.98) independently for each region $\alpha \in \{+, -\}$ such that

$$\frac{\mathrm{d}}{\mathrm{d}t} \int\limits_{\mathcal{R}^\alpha} \mathbf{A} \, \mathrm{d}v = \int\limits_{\mathcal{R}^\alpha} \frac{\partial \mathbf{A}}{\partial t} \, \mathrm{d}v + \int\limits_{\Lambda \cap \partial\mathcal{R}^\alpha} \mathbf{A}^\alpha \, \mathbf{v}_\Lambda \cdot \mathbf{n}^\alpha \, \mathrm{d}a + \int\limits_{\partial\mathcal{R}^\alpha \cap \partial\mathcal{R}} \mathbf{A}\, \mathbf{v} \cdot \mathbf{n} \, \mathrm{d}a. \tag{2.222}$$

The superscript α is introduced to distinguish the values approaching Λ from region $+$ from those approaching from region $-$. It is noteworthy that the velocity of the boundary of the region $\mathbf{v}_\Lambda$ and not the velocity of a material particle on the boundary at time t must be used in the second term of the right hand side of this relation as the boundary might move within the body. The third term on the right hand side of this equation can be reformulated using Gauss theorem (2.95). Note that an additional term arises containing velocity of a material point $\mathbf{v}$ and not the velocity $\mathbf{v}_\Lambda$ of Λ. Thus, one may rewrite relation (2.222)

$$\frac{\mathrm{d}}{\mathrm{d}t} \int\limits_{\mathcal{R}^\alpha} \mathbf{A} \, \mathrm{d}v = \int\limits_{\mathcal{R}^\alpha} \frac{\partial \mathbf{A}}{\partial t} \, \mathrm{d}v + \int\limits_{\Lambda \cap \partial\mathcal{R}^\alpha} \mathbf{A}^\alpha \mathbf{v}_\Lambda \cdot \mathbf{n}^\alpha \, \mathrm{d}a + \int\limits_{\mathcal{R}^\alpha} \mathbf{A}\, \mathbf{v} \cdot \boldsymbol{\nabla} \, \mathrm{d}v - \int\limits_{\Lambda \cap \partial\mathcal{R}^\alpha} \mathbf{A}^\alpha \, \mathbf{v} \cdot \mathbf{n}^\alpha \, \mathrm{d}a. \tag{2.223}$$

Evaluating this relation for both regions $\mathcal{R}^+$ and $\mathcal{R}^-$ and adding the resulting two equations leads to

$$\frac{\mathrm{d}}{\mathrm{d}t} \int\limits_{\mathcal{R}} \mathbf{A} \, \mathrm{d}v = \int\limits_{\mathcal{R}} \left(\frac{\partial \mathbf{A}}{\partial t} + \mathbf{A}\boldsymbol{\nabla} \cdot \mathbf{v} \right) \, \mathrm{d}v - \int\limits_{\Lambda} [\mathbf{A}] \, (\mathbf{v}_\Lambda - \mathbf{v}) \cdot \mathbf{n}_\Lambda \, \mathrm{d}a \tag{2.224}$$

where the sign convention (2.210) and definition (2.218) is used.

In the following, focus is on the balance laws which can be expressed in the form

$$\frac{\mathrm{d}}{\mathrm{d}t} \int\limits_{\mathcal{R}} \mathbf{A} \, \mathrm{d}v = \int\limits_{\mathcal{R}} \mathbf{B} \, \mathrm{d}v + \int\limits_{\partial\mathcal{R}} \mathbf{G} \cdot \mathbf{n} \, \mathrm{d}a, \tag{2.225}$$

which applies to the balances of mass, momentum, and angular momentum. Furthermore, this relation can also be applied to the entropy inequality when correctly stated as shown later. The tensors $\mathbf{A}$ and $\mathbf{B}$ are of order n, the tensor $\mathbf{G}$ of order $n+1$. The last term in (2.225) may be rewritten as

$$\begin{aligned}\int\limits_{\partial\mathcal{R}} \mathbf{G}\cdot\mathbf{n}\,\mathrm{d}a &= \int\limits_{\partial\mathcal{R}^+} \mathbf{G}\cdot\mathbf{n}\,\mathrm{d}a - \int\limits_{\Lambda} \mathbf{G}^+\cdot\mathbf{n}^+\,\mathrm{d}a \\ &\quad + \int\limits_{\partial\mathcal{R}^-} \mathbf{G}\cdot\mathbf{n}\,\mathrm{d}a - \int\limits_{\Lambda} \mathbf{G}^-\cdot\mathbf{n}^-\,\mathrm{d}a \\ &= \int\limits_{\mathcal{R}} \mathbf{G}\cdot\boldsymbol{\nabla}\,\mathrm{d}v + \int\limits_{\Lambda} [\mathbf{G}]\cdot\mathbf{n}_\Lambda\,\mathrm{d}a. \end{aligned} \tag{2.226}$$

The previous relation is not bound to the use of the single contraction as presented above. One may also use e.g. the dyadic product, providing that $\mathbf{G}$ is a tensor of order $n-1$. Use of (2.224) and (2.226) in equation (2.225) yields

$$\begin{aligned}\int\limits_{\mathcal{R}} \left(\frac{\partial\mathbf{A}}{\partial t} + \mathbf{A}\boldsymbol{\nabla}\cdot\mathbf{v} - \mathbf{G}\cdot\boldsymbol{\nabla} - \mathbf{B}\right)\,\mathrm{d}v &= \\ \int\limits_{\Lambda} \left([\mathbf{A}]\,(\mathbf{v}_\Lambda - \mathbf{v})\cdot\mathbf{n}_\Lambda + [\mathbf{G}]\cdot\mathbf{n}_\Lambda\right)\,\mathrm{d}a.\end{aligned} \tag{2.227}$$

This statement is valid for regions containing discontinuities as well as homogeneous regions $\mathcal{R}^h$, $h \in \{+,-\}$. For the homogeneous region, the right hand side is zero, yielding

$$\frac{\partial\mathbf{A}}{\partial t} + \mathbf{A}\boldsymbol{\nabla}\cdot\mathbf{v} - \mathbf{G}\cdot\boldsymbol{\nabla} - \mathbf{B} = 0, \tag{2.228}$$

or equivalently by employing (2.97)

$$\dot{\mathbf{A}} - \mathbf{G}\cdot\boldsymbol{\nabla} - \mathbf{B} = 0. \tag{2.229}$$

Thus, for a nonhomogeneous region,

$$\int\limits_{\Lambda} \left([\mathbf{A}]\,(\mathbf{v}_\Lambda - \mathbf{v})\cdot\mathbf{n}_\Lambda + [\mathbf{G}]\cdot\mathbf{n}_\Lambda\right)\,\mathrm{d}a = 0 \tag{2.230}$$

must hold. Due to the arbitrariness of the choice of the region $\mathcal{R}$ containing Λ, the general form of the jump relations

$$[\mathbf{A}]\,(\mathbf{v}_\Lambda - \mathbf{v}) \cdot \mathbf{n}_\Lambda + [\mathbf{G}] \cdot \mathbf{n}_\Lambda + \psi = 0 \tag{2.231}$$

or

$$[\mathbf{A}]\,u_\Lambda + [\mathbf{G}] \cdot \mathbf{n}_\Lambda + \psi = 0 \tag{2.232}$$

can be derived. The term ψ is added to account for the formation of surfacial area. Examples for this term will be given below. An equivalent form in the referential configuration can be derived by considering that the position of a material point in the referential configuration is fixed. It follows, that if a statement of the form

$$\frac{\mathrm{d}}{\mathrm{d}t} \int\limits_{\mathcal{R}_0} \mathbf{A}\ \mathrm{d}V = \int\limits_{\mathcal{R}_0} \mathbf{B}\ \mathrm{d}V + \int\limits_{\partial\mathcal{R}_0} \mathbf{G} \cdot \mathbf{N}\ \mathrm{d}A, \tag{2.233}$$

is valid, the relation at the discontinuity can be expressed as

$$[\mathbf{A}]\,\mathbf{V}_\Lambda \cdot \mathbf{N}_\Lambda + [\mathbf{G}] \cdot \mathbf{N}_\Lambda + \psi = 0 \tag{2.234}$$

or

$$[\mathbf{A}]\,U_\Lambda + [\mathbf{G}] \cdot \mathbf{N}_\Lambda + \psi = 0. \tag{2.235}$$

2.4.3 Balance of mass

Application of equation (2.231) to the balance of mass in its form (2.100), i.e. by comparison of (2.225) to (2.100) and setting $\mathbf{A} = \rho$, $\mathbf{G} = 0$, and $\psi = 0$ in (2.231), leads to

$$[\rho]\,(\mathbf{v}_\Lambda - \mathbf{v}) \cdot \mathbf{n}_\Lambda = 0\,. \tag{2.236}$$

For a description in the referential description, one gets ($\mathbf{A} = \rho_0$ and $\mathbf{G} = 0$)

$$[\rho_0]\,\mathbf{V}_\Lambda \cdot \mathbf{N}_\Lambda = 0\,. \tag{2.237}$$

2.4.4 Balance of linear momentum

The application of equation (2.107) with use of equation (2.108) ($\mathbf{A} = \rho\mathbf{v}$, $\mathbf{G} = \boldsymbol{\sigma}^T$, and $\psi = 0$ in (2.231)) yields

$$[\rho\,\mathbf{v}]\,(\mathbf{v}_\Lambda - \mathbf{v})\cdot\mathbf{n}_\Lambda + [\boldsymbol{\sigma}^T]\cdot\mathbf{n}_\Lambda = \mathbf{0}\,. \tag{2.238}$$

For the referential configuration, by setting $\mathbf{A} = \rho_0\mathbf{v}$ and $\mathbf{G} = \mathbf{P}^T$ in (2.234), one gets

$$[\rho_0\,\mathbf{v}]\,\mathbf{V}_\Lambda\cdot\mathbf{N}_\Lambda + [\mathbf{P}^T]\cdot\mathbf{N}_\Lambda = \mathbf{0}\,. \tag{2.239}$$

2.4.5 Balance of angular momentum

Using the balance of angular momentum in the form (2.121), thus setting $\mathbf{A} = \rho\,(\mathbf{x}-\mathbf{x}_0)\times\mathbf{v}$, $\mathbf{G} = (\mathbf{x}-\mathbf{x}_0)\times\boldsymbol{\sigma}^T$, and $\psi = 0$ in (2.231), yields

$$[\rho\,(\mathbf{x}-\mathbf{x}_0)\times\mathbf{v}]\,(\mathbf{v}_\Lambda - \mathbf{v})\cdot\mathbf{n}_\Lambda + [(\mathbf{x}-\mathbf{x}_0)\times\boldsymbol{\sigma}]\cdot\mathbf{n}_\Lambda = \mathbf{0}\,. \tag{2.240}$$

This equation yields no new jump relations after proper simplification (cf. Eringen (1967)).

2.4.6 Balance of energy

For the balance of energy, a surfacial energy production term due to the formation of interfacial area ψ^u is included. The energy balance is adopted in its form (2.146), thus $\mathbf{A} = \rho\,u + \rho\,\mathbf{v}^2/2$ $\mathbf{G} = \boldsymbol{\sigma}\cdot\mathbf{v} - \mathbf{q}$, and $\psi = \psi^u$ is set in (2.231). At the interface, one gets

$$[\rho\,u + \frac{1}{2}\,\rho\,\mathbf{v}^2]\,(\mathbf{v}_\Lambda - \mathbf{v})\cdot\mathbf{n}_\Lambda + [\boldsymbol{\sigma}\cdot\mathbf{v} - \mathbf{q}]\cdot\mathbf{n}_\Lambda + \psi^u = 0\,. \tag{2.241}$$

For a description in the referential configuration,

$$[\rho_0\,u + \frac{1}{2}\,\rho_0\,\mathbf{v}^2]\,\mathbf{V}_\Lambda\cdot\mathbf{N}_\Lambda + [\mathbf{P}\cdot\mathbf{v} - \mathbf{Q}]\cdot\mathbf{N}_\Lambda + \psi^u = 0\,. \tag{2.242}$$

can be derived.

2.4.7 The entropy inequality

The adaption of the procedure used above to the entropy inequality (2.154) is realized by the decomposition of the entropy production into a reversible and an irreversible part by relation (2.193) as $\dot{s}_r = \dot{s} - \dot{s}_i$ and the definition (2.192), restating the entropy inequality as

$$\frac{\mathrm{d}}{\mathrm{d}t}\int\limits_{\mathcal{R}} \rho\, s_r \,\mathrm{d}v = \int\limits_{\mathcal{R}} \frac{\rho\, r}{\Theta}\,\mathrm{d}v - \int\limits_{\partial\mathcal{R}} \frac{\mathbf{q}\cdot\mathbf{n}}{\Theta}\,\mathrm{d}a. \tag{2.243}$$

with the additional condition (2.194), $\dot{s}_i \geq 0$. The procedure can now be applied by setting $\mathbf{A} = \rho\, s_r$, $\mathbf{G} = -\mathbf{q}/\Theta$, and $\psi = \psi^s$, introducing the non-negative dissipation due to the movement of the interface ψ^s. This leads to

$$[\rho\, s]\,(\mathbf{v}_\Lambda - \mathbf{v})\cdot\mathbf{n}_\Lambda - \left[\frac{\mathbf{q}}{\Theta}\right]\cdot\mathbf{n}_\Lambda + \psi^s = [\rho\, s_i]\,(\mathbf{v}_\Lambda - \mathbf{v})\cdot\mathbf{n}_\Lambda \geq 0. \tag{2.244}$$

Grouping of the dissipative terms into

$$\dot{s}_\Lambda = \psi^s - [\rho\, s_i]\,(\mathbf{v}_\Lambda - \mathbf{v})\cdot\mathbf{n}_\Lambda \tag{2.245}$$

yields

$$[\rho\, s]\,(\mathbf{v}_\Lambda - \mathbf{v})\cdot\mathbf{n}_\Lambda - \left[\frac{\mathbf{q}}{\Theta}\right]\cdot\mathbf{n}_\Lambda = -\dot{s}_\Lambda. \tag{2.246}$$

For the applications considered within this context, it can be assumed that the term due to the jump of the entropy production is small compared to the original production term ψ^s. Thus, one may require

$$[\rho\, s]\,(\mathbf{v}_\Lambda - \mathbf{v})\cdot\mathbf{n}_\Lambda - \left[\frac{\mathbf{q}}{\Theta}\right]\cdot\mathbf{n}_\Lambda = -\dot{s}_\Lambda \leq 0. \tag{2.247}$$

In the referential description, the relation

$$[\rho_0\, s]\,\mathbf{V}_\Lambda\cdot\mathbf{N}_\Lambda - \left[\frac{\mathbf{Q}}{\Theta}\right]\cdot\mathbf{N}_\Lambda = -\dot{s}_\Lambda \leq 0. \tag{2.248}$$

can be derived.

2.4.8 Hadamard condition

Different paths lead to the introduction of the so called *Hadamard condition* which is a vital part in numerous derivations at the discontinuity. The derivation shown here follows Wilmanski (1998).

Starting with the definition of the deformation gradient (2.39)

$$\mathbf{F} = \mathbf{x} \otimes \boldsymbol{\nabla}_0 \tag{2.249}$$

one may calculate the time derivative of this relation as

$$\frac{\mathrm{d}}{\mathrm{d}t}\,\mathbf{F} = \mathbf{v} \otimes \boldsymbol{\nabla}_0. \tag{2.250}$$

A weak form can be obtained by integrating over the region $\mathcal{R}_0$ such that

$$\frac{\mathrm{d}}{\mathrm{d}t} \int\limits_{\mathcal{R}_0} \mathbf{F}\,\mathrm{d}V = \int\limits_{\mathcal{R}_0} \mathbf{v} \otimes \boldsymbol{\nabla}_0\,\mathrm{d}V. \tag{2.251}$$

Application of the Gauss theorem (2.95) in the referential form as described in section 2.3.1 and taking the time derivative yields

$$\frac{\mathrm{d}}{\mathrm{d}t} \int\limits_{\mathcal{R}_0} \mathbf{F}\,\mathrm{d}V = \int\limits_{\partial\mathcal{R}_0} \mathbf{v} \otimes \mathbf{N}\,\mathrm{d}A. \tag{2.252}$$

The general form of the balance relation can be applied to this case with the exception, that instead of the scalar product, the dyadic product has to be used as remarked in section 2.4.2. Hence,

$$U_\Lambda\,[\mathbf{F}] + [\mathbf{v}] \otimes \mathbf{N}_\Lambda = \mathbf{0} \tag{2.253}$$

or

$$[\mathbf{F}] = -\frac{1}{U_\Lambda}\,[\mathbf{v}] \otimes \mathbf{N}_\Lambda. \tag{2.254}$$

It must be noted, that the assumption the motion $\mathbf{x}$ being continuous everywhere is implicitly used. For the discontinuity, this implies

$$[\mathbf{x}] = \mathbf{0}, \tag{2.255}$$

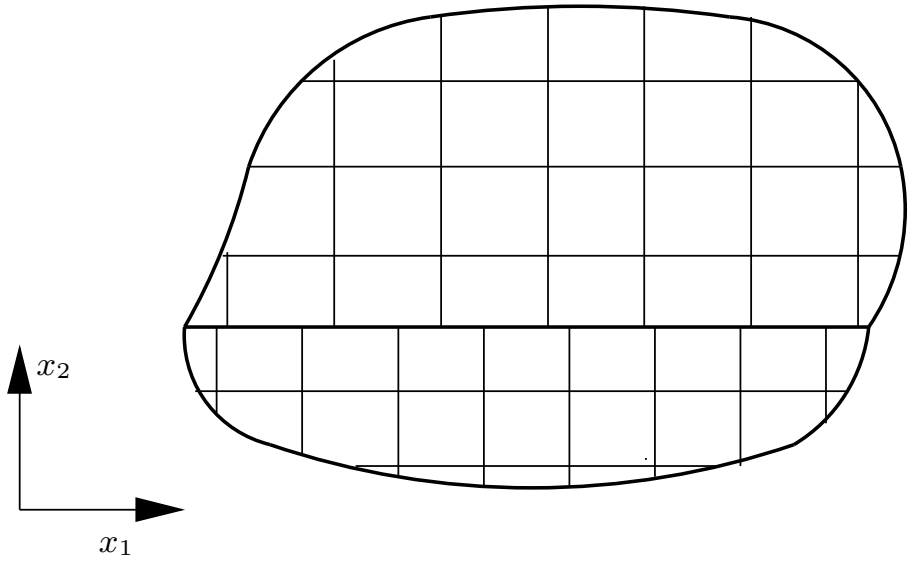

Figure 2.5: Non-coherent interface with $\{[\mathbf{F}]\}_{11} \neq 0$. The overlayed mesh consists of squares of the same size for vanishing deformation.

leading to the condition of *coherence*. Using this, it is obvious that the jump of the deformation gradient is a rank one connection, i.e.

$$[\mathbf{F}] = \mathbf{a} \otimes \mathbf{N}_\Lambda \tag{2.256}$$

with

$$\mathbf{a} = -\frac{1}{U_\Lambda} [\mathbf{v}] \,. \tag{2.257}$$

Together with the implied coherence, relation (2.256) can be interpreted by a simple example. Postmultiplying relation (2.256) by the normal vector $\mathbf{N}_\Lambda^\perp$ with $\mathbf{N}_\Lambda^\perp \cdot \mathbf{N}_\Lambda = 0$ yields zero, whereas a nonzero value violates the coherence condition as depicted in figure 2.5.

2.4.9 Discontinuity movement

Introducing the Helmholtz free energy $\varphi = u - \Theta\, s$ (cf. equation (2.176)) in the balance of energy in the form (2.242) leads, by making use of the assumption

$[\Theta] = 0$, to

$$\rho_0 U_\Lambda [\varphi + \frac{1}{2}\mathbf{v}^2] + [\mathbf{P}\cdot\mathbf{v}]\cdot\mathbf{N}_\Lambda + \psi^u + \Theta[\rho_0 s]U_\Lambda - [\mathbf{Q}]\cdot\mathbf{N}_\Lambda = 0\,. \quad (2.258)$$

The entropy balance (2.248) can be written, also under the presumption $[\Theta] = 0$, as

$$\Theta[\rho_0 s]\, U_\Lambda - [\mathbf{Q}]\cdot\mathbf{N}_\Lambda = -\Theta\,\dot{s}_\Lambda. \quad (2.259)$$

The combination of these equations leads to

$$\rho_0 U_\Lambda [\varphi + \frac{1}{2}\mathbf{v}^2] + [\mathbf{P}\cdot\mathbf{v}]\cdot\mathbf{N}_\Lambda + \psi^u = \Theta\,\dot{s}_\Lambda, \quad (2.260)$$

and yields, by employing the balance of linear momentum (2.240) and the Hadamard condition in the form (2.257) applied to the orientation of the discontinuity $\mathbf{N}_\Lambda$, the balance of linear momentum

$$\rho_0 U_\Lambda [\varphi + \frac{1}{2}\mathbf{v}^2] - \rho_0 U_\Lambda [\mathbf{v}]\cdot\langle\mathbf{v}\rangle - \langle\mathbf{P}\rangle\cdot\mathbf{N}_\Lambda U_\Lambda\ [\mathbf{F}]\cdot\mathbf{N}_\Lambda + \psi^u = \Theta\,\dot{s}_\Lambda, \quad (2.261)$$

and after some rearrangement

$$\rho_0 U_\Lambda [\varphi] - U_\Lambda\,\mathbf{N}_\Lambda\cdot\left[\mathbf{F}^T\right]\cdot\langle\mathbf{P}\rangle\cdot\mathbf{N}_\Lambda + \psi^u = \Theta\,\dot{s}_\Lambda. \quad (2.262)$$

Restricting ourselves to the quasistatic case, i.e. using (2.239) in the form $[\mathbf{P}^T]\cdot\mathbf{N}_\Lambda = \mathbf{0}$, and setting $\psi^u = 0$ yields

$$\zeta^\Lambda = \Theta\,\dot{s}_\Lambda = \rho_0 U_\Lambda\,\mathbf{N}_\Lambda\cdot[\boldsymbol{\mu}]\cdot\mathbf{N}_\Lambda \quad (2.263)$$

where the definition

$$\boldsymbol{\mu} = \varphi\mathbf{1} - \frac{1}{\rho_0}\,\mathbf{F}^T\cdot\mathbf{P} \quad (2.264)$$

is used (see Heidug & Lehner (1985), Knowles (1995), Raniecki & Tanaka (1994), Šilhavý (1997), Buratti et al. (2003)). It is noteworthy that the transpose of $\boldsymbol{\mu}$ is often denoted "Eshelby-Tensor". As this tensor is always used in conjunction with a projection in direction of the normal $\mathbf{N}_\Lambda$ (i.e. $\mathbf{N}_\Lambda\cdot[\boldsymbol{\mu}]\cdot\mathbf{N}_\Lambda$),

the asymmetric part of $\boldsymbol{\mu}$ does not influence the problem and this difference is not of importance. Heidug & Lehner (1985) have shown that the condition $\mathbf{N}_\Lambda \cdot [\boldsymbol{\mu}] \cdot \mathbf{N}_\Lambda = 0$ is a necessary condition for unconstrained thermodynamic equilibrium, i.e. for the absence of movement of the discontinuity. Thus, the projection of the tensor $\boldsymbol{\mu}$ can be x as the thermodynamic force for the local movement of the discontinuity and may be used in a concept which describes locally the movement of the phase transition front. A study which discusses potential shortcomings and possible further developments can be found in Levitas (2002), Oberste-Brandenburg (1999), and Oberste-Brandenburg & Bruhns (2004).

Different notations have been introduced for $\boldsymbol{\mu}$. The first use of a similar tensor can be traced back to Eshelby (1951, 1975), there using the term "elastic energy momentum tensor". He described the force on the movement of the boundary of an inclusion in an isothermal frame. Thus, in his original introduction, the elastic energy w was used instead of the Helmholtz free energy φ. This tensor, and later its nonisothermal form (2.264), was used to constitute a balance law, the "balance of pseudomomentum" (cf. Maugin (1993) or Gurtin (1995)). These theories have even led to the introduction of the term "mechanics in material space" in contrast to the classical "mechanics in physical space" (cf. Maugin (1993), Kienzler & Herrmann (2000); Kienzler & Maugin (2001)). As the origins of this description can be traced back to the work of Eshelby mentioned above, the term *Eshelbian mechanics* (Maugin (1993, 2002)) is frequently used, equally denoting $\boldsymbol{\mu}$ by "Eshelby tensor". Grinfeld used in (1991) the term "asymmetric chemical potential tensor", indicating that $\boldsymbol{\mu}$ has a strong connection to the scalar chemical potential as it collapses to a unit-tensor times the chemical potential for hydrostatic stress states as shown below. By using the term asymmetric, $\boldsymbol{\mu}$ is distinguished from the symmetric chemical potential tensor

$$\boldsymbol{K} := \boldsymbol{F}^{-T} \cdot \boldsymbol{\mu} \cdot \boldsymbol{F}^{T}, \tag{2.265}$$

where $\boldsymbol{F}^{-T} = (\boldsymbol{F}^{T})^{-1}$. This tensor, used in the description of materials with changes in the chemical composition, was first introduced by Bowen (1967, 1976). Hence in Grinfeld (1991), he suggested the name "Bowen's chemical potential tensor". Grinfeld (1991) also gives an extensive overview over the developments that lead to the introduction of this tensorial value.

3 Constitutive relations for a material point

3.1 Elastic behavior

If not otherwise stated, referring to elastic behavior of the material, it is assumed that it can be described by

$$\boldsymbol{\Pi} = \mathbb{C} : (\boldsymbol{e} - (\Theta - \Theta_0)\,\boldsymbol{\alpha})\,. \tag{3.1}$$

$\mathbb{C}$ denotes the fourth order elastic stiffness tensor, $\boldsymbol{\alpha}$ the tensor of thermal expansion. If not otherwise stated, the elastic behavior is assumed to be isotropic (cf. Hahn (1985)). Following this assumption, $\mathbb{C}$ can be expressed as

$$\mathbb{C} = \lambda\,\mathbf{1} \otimes \mathbf{1} + \mu\,\mathbf{1}^{(4)} \tag{3.2}$$

where $\mathbf{1}^{(4)}$ denotes the fourth order unit tensor and λ and μ the Lamé-parameters. Young's modulus E and Poisson's ratio ν may be expressed in terms of λ and μ as

$$E = \frac{\mu(3\lambda + 2\mu)}{\lambda + \mu} \quad \text{and} \quad \nu = \frac{\lambda}{2(\lambda + \mu)}. \tag{3.3}$$

The shear modulus is $G = \mu$. Inversion of (3.3) yields

$$\lambda = \frac{\nu E}{(1+\nu)(1-2\nu)} \quad \text{and} \quad \mu = \frac{E}{2(1+\nu)}. \tag{3.4}$$

The form used for the tensor of thermal expansion $\boldsymbol{\alpha}$ is based on the isotropy assumption as well. It can be described by

$$\boldsymbol{\alpha} = \mathbf{1}\,\alpha \tag{3.5}$$

where α denotes the isotropic thermal expansion.

3.2 Derivation of the Helmholtz free energy

For phase transition problems discussed in the following two chapters, the knowledge of the Helmholtz free energy is of vital importance. The procedure described here follows the path of derivation as in Raniecki & Bruhns (1991).

The classical definition of the specific heat at constant volume is (cf. e.g. Baehr (1966))

$$c_v = \left.\frac{\partial u}{\partial \Theta}\right|_V . \tag{3.6}$$

The requirement that the volume may not change is transferred into this thermomechanical context by introduction of the requirement that the reversible part of the strain $\boldsymbol{e}_r$ and the internal variables $\boldsymbol{\xi}_h$ may not change, i.e.

$$c_v = \left.\frac{\partial u}{\partial \Theta}\right|_{\boldsymbol{e}_r, \boldsymbol{\xi}_h} \tag{3.7}$$

which introduces a stronger constraint because the internal variables may not influence the change of volume of the body. Introducing the Helmholtz free energy by (2.176) and the definition of the entropy (2.178b), one may write

$$c_v = \Theta \left.\frac{\partial s}{\partial \Theta}\right|_{\boldsymbol{e}_r, \boldsymbol{\xi}_h} . \tag{3.8}$$

Integrating this relation with respect to Θ leads to

$$s = c_v \ln \frac{\Theta}{\Theta_0} - c_v^{\Theta} + s_0 \tag{3.9}$$

where $s_0 = s_0(\boldsymbol{e}_r, \Theta_0, \boldsymbol{\xi}_h)$ and $c_v^{\Theta} = c_v^{\Theta}(\Theta)$ with

$$c_v^{\Theta} = \int_{\Theta_0}^{\Theta} \frac{\partial c_v}{\partial \Theta} \ln \Theta \, \mathrm{d}\Theta \tag{3.10}$$

have been introduced. The second application of the definition of the entropy (2.178b) leads to

$$\varphi = c_v \left[\Theta - \Theta_0 - \Theta \ln \frac{\Theta}{\Theta_0}\right] + c_v^{\Theta\Theta} - s_0(T - T_0) + \varphi_0, \tag{3.11}$$

where the constant $\varphi_0 = \varphi_0(\boldsymbol{e}_r, \Theta_0, \boldsymbol{\xi}_h)$ is introduced. The function $c_v^{\Theta\Theta} = c_v^{\Theta\Theta}(\Theta)$ is determined as

$$c_v^{\Theta\Theta} = \int_{\Theta_0}^{\Theta} \frac{\partial c_v}{\partial \Theta}\, \Theta \left[\ln \frac{\Theta}{\Theta_0} - 1\right] + c_v^{\Theta}\, \mathrm{d}\Theta \tag{3.12}$$

To determine the unknowns φ_0 and s_0, the tangent $\mathbb{C} = \mathbb{C}(\boldsymbol{e}_r, \Theta, \boldsymbol{\xi}_h)$ is introduced such that

$$\mathbb{C} = \frac{\partial \boldsymbol{\Pi}}{\partial \boldsymbol{e}_r}. \tag{3.13}$$

Inserting (3.13) and (3.9) into the Maxwell-relation (2.186) and differentiation by $\boldsymbol{e}_r$ yields a differential equation for s_0

$$\frac{\partial^2 s_0}{\partial \boldsymbol{e}_r^2} = -\frac{1}{\rho_0}\, \frac{\partial \mathbb{C}}{\partial \Theta}. \tag{3.14}$$

Integrating twice with respect to $\boldsymbol{e}_r$ leads to

$$s_0 = -\frac{1}{2\rho_0} \boldsymbol{e}_r : \frac{\partial \mathbb{C}}{\partial \Theta} : \boldsymbol{e}_r + \boldsymbol{\beta}_0 : \boldsymbol{\varepsilon}_r + s_* \tag{3.15}$$

with $\boldsymbol{\beta}_0 = \boldsymbol{\beta}_0(\boldsymbol{\xi}_h)$ and $s_* = s_*(\boldsymbol{\xi}_h)$. By taking into consideration, that $s_0 = s_0(\boldsymbol{e}_r, \Theta_0, \boldsymbol{\xi}_h)$ and therefore

$$\frac{\partial s_0}{\partial \Theta} = 0, \tag{3.16}$$

one may derive, using the orthogonality of the independent variables,

$$\boldsymbol{e}_r : \frac{\partial^2 \mathbb{C}}{\partial \Theta^2} : \boldsymbol{e}_r = 0 \tag{3.17}$$

and, as $\boldsymbol{e}_r$ is an independent variable of state,

$$\frac{\partial^2 \mathbb{C}}{\partial \Theta^2} = \mathbf{0}. \tag{3.18}$$

Twice integration of this relation with respect to Θ leads to

$$\mathbb{C} = \mathbb{C}_0 + \mathbb{C}_\Theta(\Theta - \Theta_0) \tag{3.19}$$

where the constants $\mathbb{C}_0 = \mathbb{C}_0(\boldsymbol{e}_r, \boldsymbol{\xi}_h)$ and $\mathbb{C}_\Theta = \mathbb{C}_\Theta(\boldsymbol{e}_r, \boldsymbol{\xi}_h)$ with

$$\mathbb{C}_0 = \mathbb{C}(\Theta = \Theta_0) \tag{3.20}$$

and

$$\mathbb{C}_\Theta = \frac{\partial \mathbb{C}}{\partial \Theta} \tag{3.21}$$

are introduced. Using relation (3.19), the expression for s_0 (3.15) can be rewritten as

$$s_0 = -\frac{1}{2\rho_0}\boldsymbol{e}_r : \mathbb{C}_\Theta : \boldsymbol{e}_r + \boldsymbol{\beta}_0 : \boldsymbol{\varepsilon}_r + s_*. \tag{3.22}$$

The starting point in course of the derivation of the differential equation for φ_0 is the use of the definition of the stress $\mathbf{\Pi}$ (2.178a) in the definition of the tangent (3.13) leading to

$$\frac{\partial^2 \varphi}{\partial \boldsymbol{e}_r^2} = \frac{1}{\rho_0}\,\mathbb{C}. \tag{3.23}$$

Employing relation (3.11) leads to

$$\frac{\partial^2 \varphi_0}{\partial \boldsymbol{e}_r^2} - (\Theta - \Theta_0)\left(\frac{2}{\rho_0}\boldsymbol{e}_r : \mathbb{C}_{\Theta\boldsymbol{e}} + \frac{1}{\rho_0}\boldsymbol{e}_r : \mathbb{C}_{\Theta\boldsymbol{e}\boldsymbol{e}} : \boldsymbol{e}_r\right) = \frac{1}{\rho_0}\,\mathbb{C}_0 \tag{3.24}$$

where

$$\mathbb{C}_{\Theta\boldsymbol{e}} = \frac{\partial \mathbb{C}_\Theta}{\partial \boldsymbol{e}_r} = \frac{\partial^2 \mathbb{C}}{\partial \Theta\, \partial \boldsymbol{e}_r} \tag{3.25}$$

and

$$\mathbb{C}_{\Theta\boldsymbol{e}\boldsymbol{e}} = \frac{\partial^2 \mathbb{C}_\Theta}{\partial \boldsymbol{e}_r\, \partial \boldsymbol{e}_r} = \frac{\partial^3 \mathbb{C}}{\partial \Theta\, \partial \boldsymbol{e}_r\, \partial \boldsymbol{e}_r} \tag{3.26}$$

are introduced. In the following, it is assumed that the relation between $\boldsymbol{\Pi}$ and $\boldsymbol{e}$ may be described by a linear relation, i.e. $\mathbb{C}_{\Theta \boldsymbol{e}} = \mathbf{0}$ and $\mathbb{C}_{\Theta \boldsymbol{e}\boldsymbol{e}} = \mathbf{0}$. Relation (3.24) can be integrated twice with respect to $\boldsymbol{e}_r$ to yield

$$\varphi_0 = \frac{1}{2\rho_0}\, \boldsymbol{e}_r : \mathbb{C}_0 : \boldsymbol{e}_r + \boldsymbol{\varphi}'_* : \boldsymbol{e}_r + \varphi_* \tag{3.27}$$

where $\varphi_* = \varphi_*(\boldsymbol{\xi}_h)$ with

$$\varphi_* = \varphi_0(\boldsymbol{e}_r = \mathbf{0}) \tag{3.28}$$

and $\boldsymbol{\varphi}'_* = \boldsymbol{\varphi}'_*(\boldsymbol{\xi}_h)$

$$\boldsymbol{\varphi}'_* = \frac{\partial \varphi_0}{\partial \boldsymbol{e}_r}(\boldsymbol{e}_r = \mathbf{0}) \tag{3.29}$$

are used. The combination of (3.11), (3.22), and (3.27) leads to the final form of the Helmholtz free energy

$$\begin{aligned} \varphi \;\; = \;\; & c_v \left[\Theta - \Theta_0 - \Theta \ln \frac{\Theta}{\Theta_0}\right] + c_v^{\Theta\Theta} \\ & + \frac{1}{2\rho_0}\, \boldsymbol{e}_r : \mathbb{C} : \boldsymbol{e}_r - \boldsymbol{\beta}_0 : \boldsymbol{\varepsilon}_r (\Theta - \Theta_0) \\ & + \boldsymbol{\varphi}'_* : \boldsymbol{e}_r + \varphi_* - s_* (\Theta - \Theta_0). \end{aligned} \tag{3.30}$$

The caloric and thermal equations of state read for the case $\boldsymbol{\varphi}'_* = \mathbf{0}$

$$-\frac{\partial \varphi}{\partial \Theta} = s \;\; = \;\; c_v \ln \frac{\Theta}{\Theta_0} - c_v^{\Theta} - \frac{1}{2\rho_0}\, \boldsymbol{e}_r : \mathbb{C}_\Theta : \boldsymbol{e}_r + \boldsymbol{\beta}_0 : \boldsymbol{e}_r + s_* \tag{3.31}$$

$$\rho_0 \frac{\partial \varphi}{\partial \boldsymbol{e}_r} = \boldsymbol{\Pi} \;\; = \;\; \mathbb{C} : \boldsymbol{e}_r - (\Theta - \Theta_0) \boldsymbol{\beta}_0\, \rho_0. \tag{3.32}$$

The coupling between the elastic behavior of the material and the thermal behavior, the piezocaloric effect, is characterized by

$$\frac{\partial^2 \varphi}{\partial \boldsymbol{e}_r\, \partial \Theta} = \frac{1}{\rho_0} \mathbb{C}_\Theta : \boldsymbol{e}_r - \boldsymbol{\beta}_0 = \frac{1}{\rho_0}\, (\mathbb{C}_\Theta : \boldsymbol{e}_r - \mathbb{C} : \boldsymbol{\alpha}) \tag{3.33}$$

with the tensor of thermal expansion given by $\mathbb{C} : \boldsymbol{\alpha} = \rho_0 \boldsymbol{\beta}_0$. The coupling between the process described by the internal variables and the thermal process is given by

$$\frac{\partial^2 \varphi}{\partial \boldsymbol{\xi}_h \, \partial \Theta} = -\frac{1}{2\rho_0} \boldsymbol{e}_r : \frac{\partial \mathbb{C}_\Theta}{\partial \boldsymbol{\xi}_h} : \boldsymbol{e}_r + \frac{\partial \boldsymbol{\beta}_0}{\partial \boldsymbol{\xi}_h} : \boldsymbol{e}_r + \frac{\partial s_*}{\partial \boldsymbol{\xi}_h}. \tag{3.34}$$

If the thermoelastic behavior is not influenced by the process described by the internal variables, $\mathbb{C}_\Theta = \mathbb{C}_\Theta(\boldsymbol{e}_r)$ and $\boldsymbol{\beta}_0 = const$, thus

$$\frac{\partial^2 \varphi}{\partial \boldsymbol{\xi}_h \, \partial \Theta} = \frac{\partial s_*}{\partial \boldsymbol{\xi}_h} \tag{3.35}$$

remains.

A relation for the specific heat capacity at constant pressure c_p, here used in a stricter formulation as the heat capacity at constant stress, may be derived by using its definition within this thermomechanical frame

$$c_p = \left. \frac{\partial h}{\partial \Theta} \right|_{\boldsymbol{\Pi}, \boldsymbol{\xi}_h} . \tag{3.36}$$

Using the definition of the enthalpy $h = g + \Theta \, s$ (2.181) yields

$$c_p = \Theta \left. \frac{\partial s}{\partial \Theta} \right|_{\boldsymbol{\Pi}, \boldsymbol{\xi}_h} . \tag{3.37}$$

It is important to note that the potential used now is the Gibbs free energy $g = g(\boldsymbol{\Pi}, \Theta, \boldsymbol{\xi}_h)$. Thus, $\boldsymbol{e}_r$ in (3.31) is no longer a state variable and it should be replaced by the stress $\boldsymbol{\Pi}$ in equation (3.31). For doing so, relation (3.32) is used to yield

$$\boldsymbol{e}_r = \mathbb{D} : \boldsymbol{\Pi} + (\Theta - \Theta_0) \, \boldsymbol{\alpha} \tag{3.38}$$

where the elastic compliance $\mathbb{D}$ with $\mathbb{C} : \mathbb{D} = \mathbf{1}^{(4)}$ is introduced. The relation for c_p then reads

$$c_p = c_v + \frac{\Theta}{\rho_0} \left(\mathbb{D} : \boldsymbol{\Pi} : \mathbb{C}_\Theta : \boldsymbol{\alpha} + \boldsymbol{\alpha} : \mathbb{C}_0 : \boldsymbol{\alpha} \right). \tag{3.39}$$

A relation for c_v has not been specified yet. Following the theory of Debye (Callen (1970),Morill (1972)), the heat capacity at constant volume can be determined as

$$c_v = 3R \left[4\, D(\Theta_D/\Theta) - \frac{3\,\Theta_D/\Theta}{\exp(\Theta_D/\Theta) - 1} \right] \tag{3.40}$$

where Θ_D denotes the Debye-temperature, R the special gas-constant with

$$R = \frac{R_m}{M}, \tag{3.41}$$

$R_m = 8.3143\, J/(mol\, K)$, and the molar mass M. $D(x)$ denotes the Debye-function

$$D(x) = \frac{3}{x^3} \int_0^x \frac{y^3}{\exp(y) - 1}\, \mathrm{d}y. \tag{3.42}$$

4 Micromechanical approach

4.1 Motivation and observations – micromechanical view

4.1.1 An introductory example

The example shall explain the motivation for the model and especially clarify the modeling space, i.e. the underlying assumptions, governing length scales and related physical observations.

Phase transitions in NiTi are usually, when the R-phase is not involved, one stage transformations, i.e. austenite transforms to martensite showing only one peak in the curve measured in a differential scanning calorimeter (DSC) experiment[1]. The same applies for the reverse transformation. Eggeler et al. (2003) have shown, that for a Ni-rich NiTi alloy in which, due to its chemical composition and the applied heat treatment, Ni_4Ti_3 precipitates of a considerable size are present, the one stage transformation converts into a two stage transformation as depicted in figure 4.1. Two possible explanations are discussed.

- It can be expected that the material around the Ni-rich precipitates has a different chemical composition than the bulk NiTi. Thus, the material around the inclusions has a different martensite start temperature which may lead to the two stage transformation.
- The Ni_4Ti_3 precipitates have different mechanical properties than the surrounding NiTi matrix. Thus, from the mechanical viewpoint they can be regarded as inhomogeneities. This leads to nonhomogeneities of the stress state around the inclusions, influencing the overall behavior.

The first explanation can only be proven by a thorough investigation of the chemical composition around the inhomogeneities which is beyond the capabilities of a mechanical investigation. The latter explanation can be verified by a micromechanical simulation of the transformation process within a grain. In

[1] For a description of a DSC-measurement, refer to section 4.1.2.

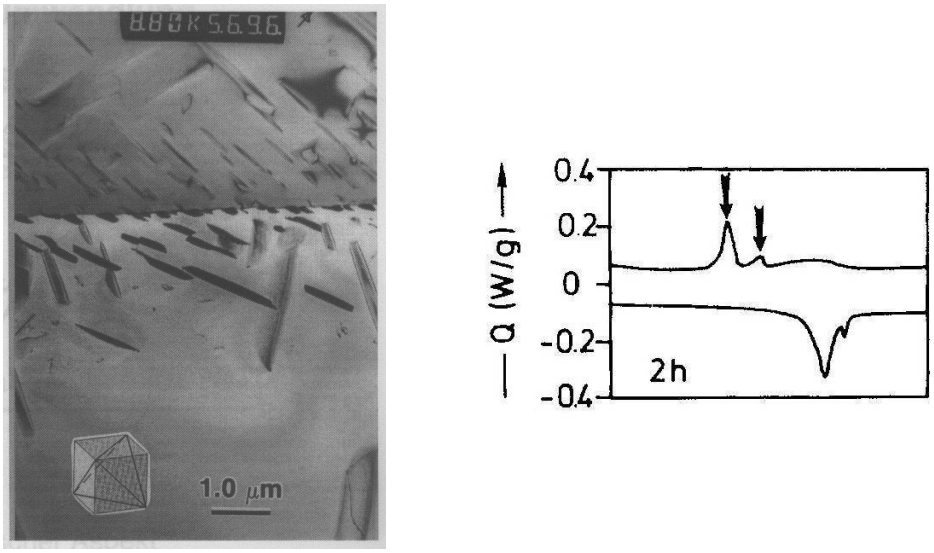

Figure 4.1: Left: Micrograph with Ni_4Ti_3 inclusions
Right: DSC measurement for the alloy shown left.

the following, this is addressed by the development of an approach which gives detailed information about the position of the transformation front within a grain (or a single crystal).

The section is organized as follows: after a description of the physical phenomena observed on the microscale during the phase transition, these observations are placed within a mechanical description in section 4.2. In section 4.3, a numerical scheme is proposed to solve the problem posed in section 4.2. Some numerical aspects of this scheme are discussed and one example problem closely related to the initial question posed in this introduction is finally presented.

4.1.2 Phase transitions in shape memory alloys – micromechanical observations

The term "phase" describes the aspect that the atomic arrangement in a material can be different for a different thermomechanical environment without change of the chemical composition. Prominent examples for such arrangements are the face-centered-cubic (fcc), the body-centered-cubic (bcc) or the orthorhombic structure (cf. Hornbogen & Warlimont (1991)). Martensite and austenite are denotations used to identify phase structures frequently observed. The austenitic phase is usually stable at higher temperatures whereas the martensitic phase is stable, if at all, at lower temperatures. The atomic

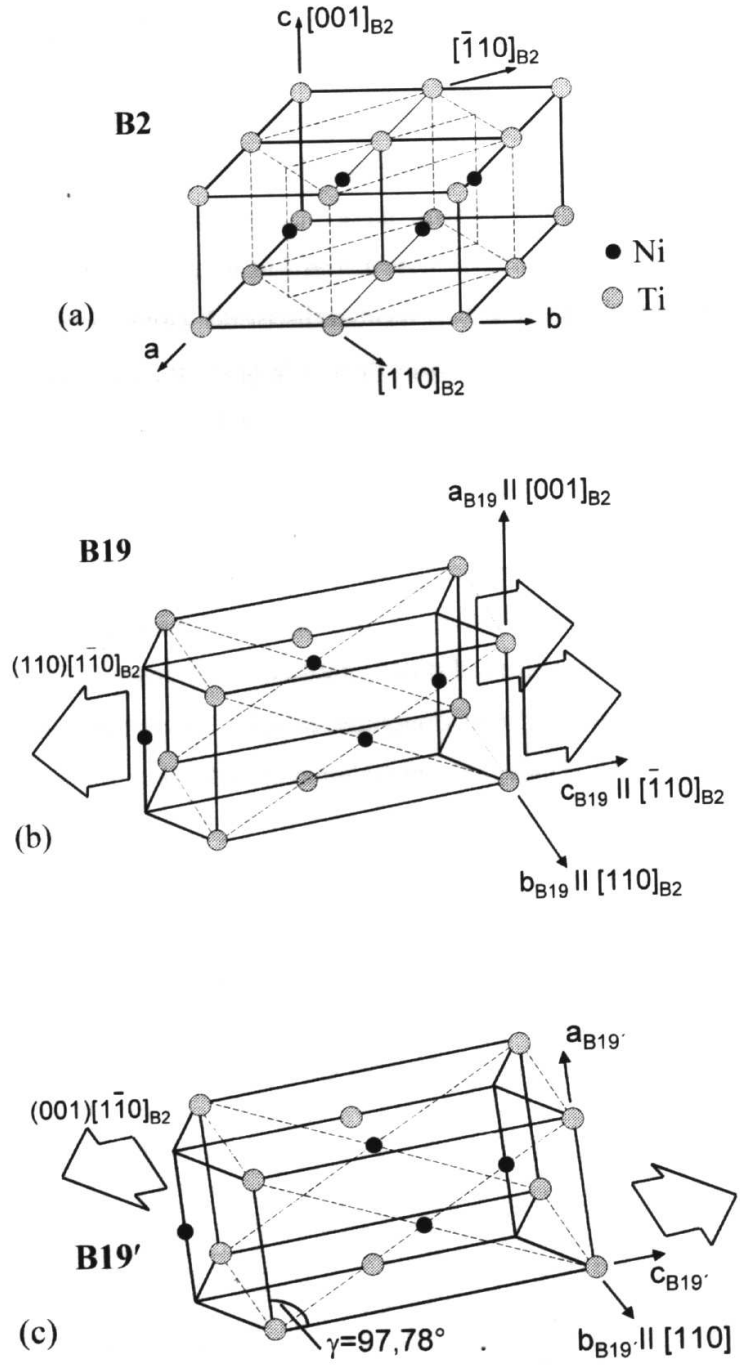

Figure 4.2: Schematic sketch of the transformation from B2-austenite to B19'-martensite (Allafi (2002)).

arrangement associated with the phase is not the same for all materials as e.g in steels austenite is fcc and martensite is a distorted bcc-arrangement. In NiTi however, austenite shows a B2 (bcc) structure, the diffusionless transformation to martensite may be either direct via the unstable orthorhombic B19 to the stress stabilized monoclinic B19' structure (cf. figure 4.2) or including an intermediate step, the R-phase. If the alloy is not freshly annealed but already thermomechanically treated, a two stage transformation via B2→R-phase→B19/B19' might be observed. The R-phase is a triclinic phase, the B2→R transformation is mechanically not well pronounced, however it is accompanied by a considerable release of latent heat. The change of the atomic arrangement, the crystallographic structure, induces a strain, the Bain strain. This strain depends on crystallographic parameters, or lattice parameters, and the crystallographic orientation of the material. The resulting strain may be determined by the *crystallographic theory of martensite* (CTM) as described by Wechsler, Lieberman, and Read (WLR) (cf. Wechsler et al. (1953), Lieberman et al. (1955)), Bowles and Mackenzie (BM) (cf. Bowles & Mackenzie (1954)), or, more recently Ball and James (BJ) (cf. Ball & James (1987), Ball & James (1992), see also section 4.2.2). Based on the crystallographic structure, only a finite number of possible values for the induced strain due to the finite number of choices for atomic arrangements are possible. These different configurations are called *martensite variants*. Ball and James have shown by a description in the stress free referential configuration, that an interface between austenite and homogeneous martensite of only one single variant is not possible. An austenite martensite interface may only exist when the martensitic phase consists of a sequence of at least two different martensitic phases with a high spatial frequency, called *twinning* of variants. This leads to nonhomogeneous martensitic domains as depicted in figure 4.3. However, the Bain strain is only the primary strain induced by the phase transition. As the martensite is embedded into an austenitic matrix, the eigenstrain in the martensite induces a stress (and therefore strain) in the austenitic matrix, leading again to an additional strain in the martensite at equilibrium. Thus, the most favorable configuration may even be a stack of self-accommodating martensite, leading to a vanishing macroscopic deformation (cf. figure 4.4 and 4.5).

The decision which phase is favored is based on an energetic criterion. For higher energetic levels, e.g. at higher temperatures, austenite is stable whereas for lower energetic levels martensite becomes stable (cf. figure 4.6). Traditionally, the Gibbs free energy g is regarded as the decisive factor. At temperature T_0 (here depicted for the stress free state) the Gibbs energies of both phases are equal. If the temperature is lowered, the Gibbs energy of the

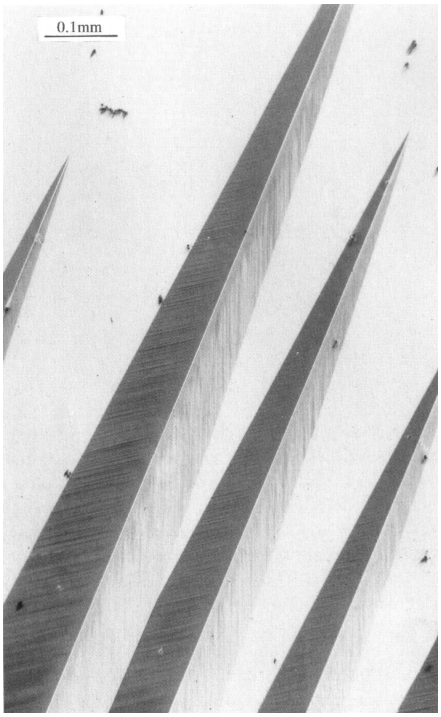

Figure 4.3: Optical micrograph of spear-like martensite (Otsuka & Wayman (1998)).

martensite is lower than the Gibbs energy of the austenite, making the martensite the favored phase. However, the transition does not follow immediately after lowering the temperature, a certain amount of undercooling under the temperature T_0 is necessary. Only if a certain threshold is reached, the transition sets in, releasing the difference of the Gibbs energies between austenitic and martensitic states as latent heat. Thus, the transformation from austenite to martensite is an exothermal process, whereas the backtransformation is an endothermal process. This leads to the behavior observed during a test in a differential scanning calorimeter (DSC) as depicted in figure 4.7.

As the energy required to induce the phase transition may by supplied by mechanical loads as well, a complex behavior in the stress-temperature space can be observed. Depending on the energy barrier necessary to induce the transition, characterized by the martensite start temperature in the stress free state M_s^0, different classes with qualitatively differing behavior, can be observed:

- For temperatures above A_f^0, thus ensuring that the austenitic phase (β) is the only phase existing in the stress free state, *pseudoelastic behavior* can

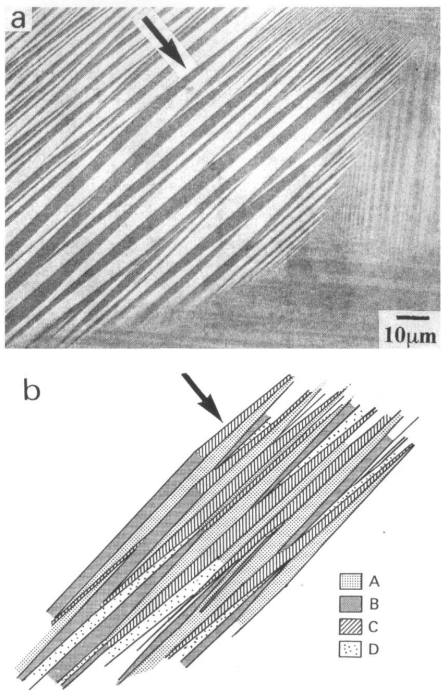

Figure 4.4: Scanning electron microscopy micrograph of twinned martensite. Four variants have been formed (Otsuka & Wayman (1998)).

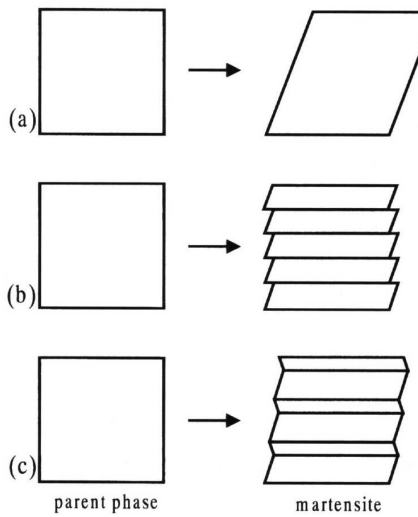

Figure 4.5: (a) shape change upon martensitic transformation;
(b) accommodation due to slip;
(c) accommodation due to twinning;
(cf. Otsuka & Wayman (1998)).

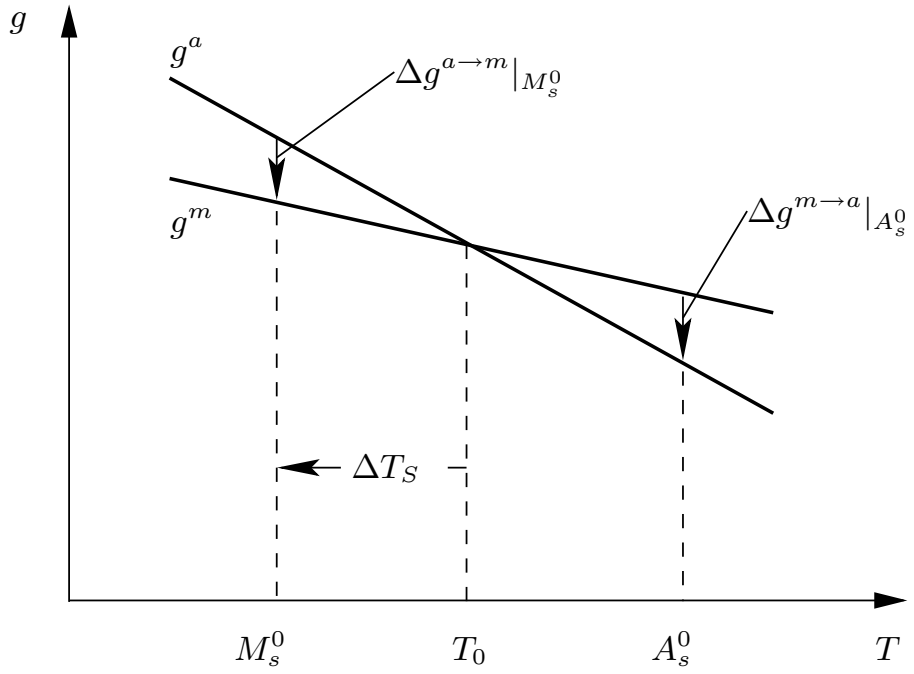

Figure 4.6: Schematic representation of free energies for both parent and product phases in the stress free state.

be observed (see figure 4.8, lower sketch). Starting from the stress free state, a mechanical load yields elastic response of the austenite. When a threshold is reached, the phase transformation is induced and proceeds with increasing load leading to an additional strain. When the phase transition is completed, elastic behavior of the martensite ($\alpha^\wedge$) can be observed. When the load is lowered, the backtransformation does not follow the same path. As for the stress free transformation in the DSC-measurement, a hysteresis can be observed, i.e. the backtransformation can be observed at a lower stress level. If the material is well prepared and trained, no permanent deformation remains when the stress free state is reached again. Hence, the denotation pseudoelastic is used even though a dissipation was induced due to the hysteretic behavior.

- Lowering the temperature from the austenitic state at zero stress below M_f^0 initiates the stress free transformation. This yields no, or only a very small, observable deformation as the twinned martensitic microstructure $\alpha^{//}$ is energetically the most favorable (see figure 4.8, upper graph). Applying mechanical load changes the situation: now, the untwinned martensitic microstructure $\alpha^\wedge$ is favored, leading to a macroscopic strain.

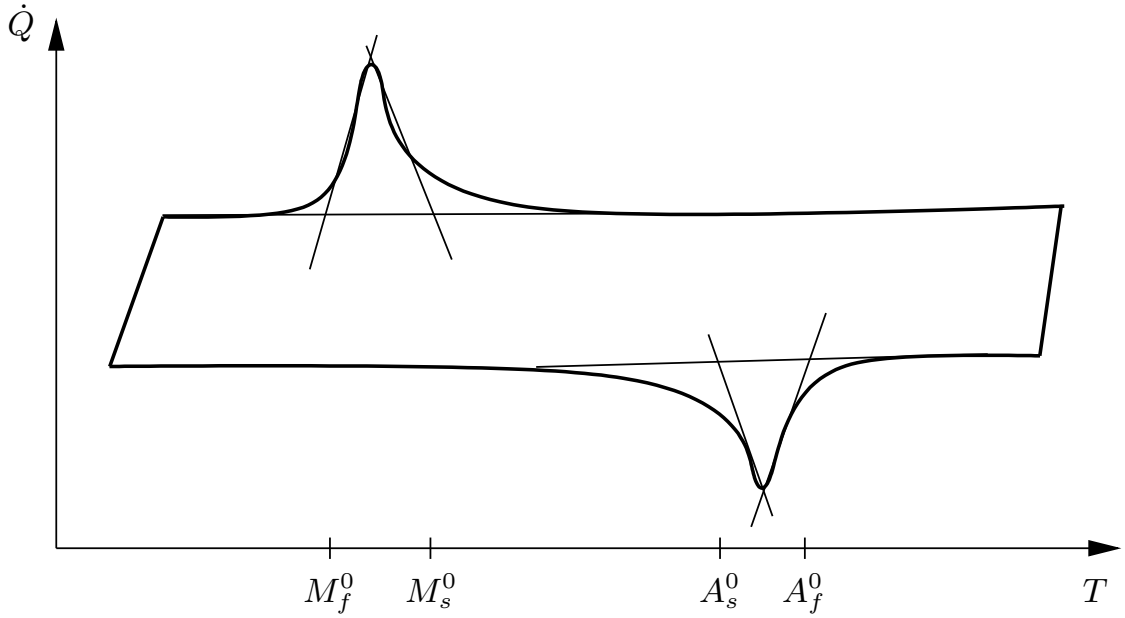

Figure 4.7: Schematic sketch of a DSC-test with the temperatures for start- and finish-temperatures for both the formation of martensite (M_s^0 and M_f^0) and austenite (A_s^0 and A_f^0) for a stress free state. Positive values for the measured heat flux $\dot{Q}$ indicate an exothermal process.

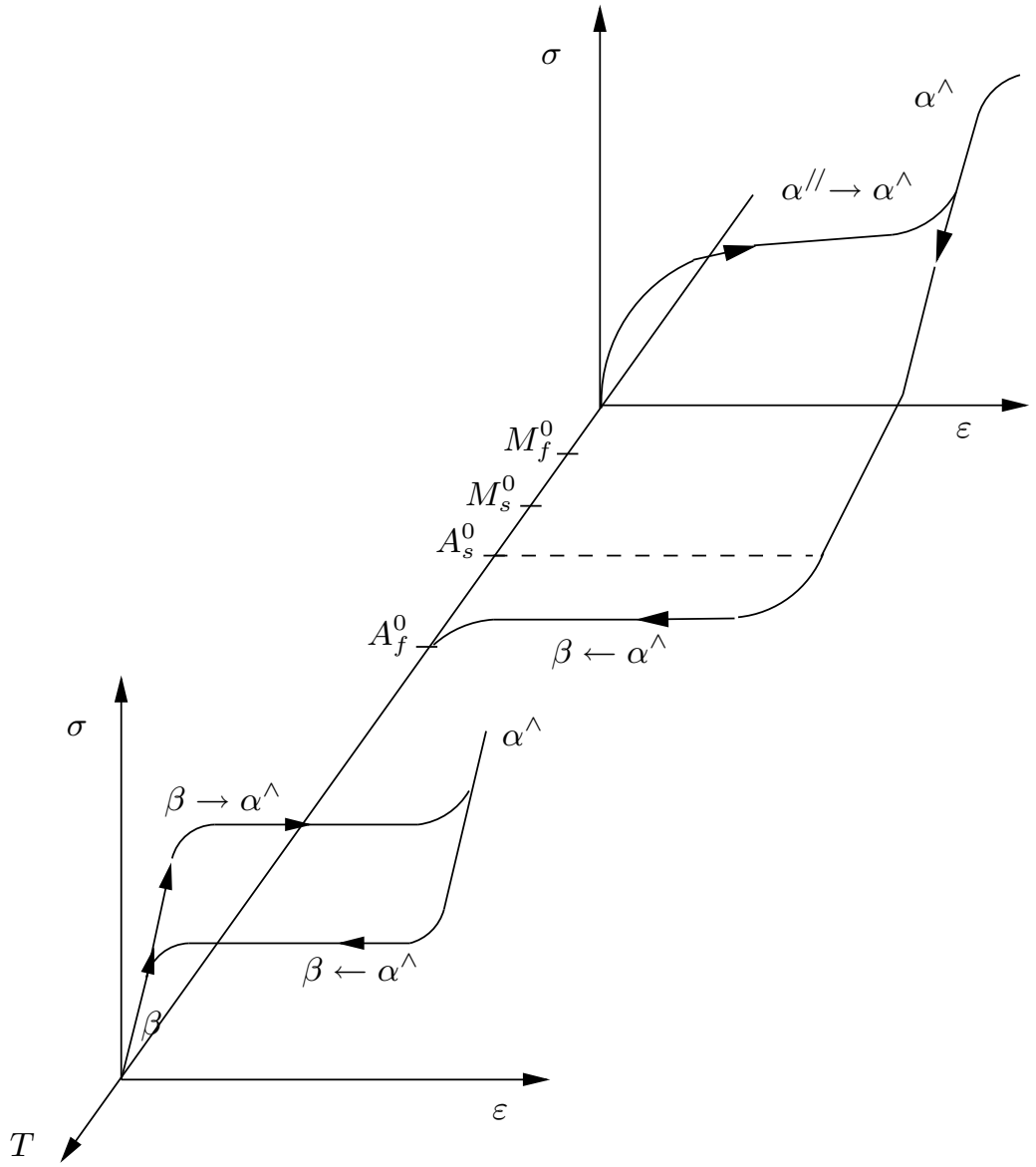

Figure 4.8: Schematic sketch of pseudoelastic ($T > M_f^0$) and pseudoplastic behavior of shape memory alloys. The deformation of material due to the thermal expansion is not depicted for clarity.

Thus, the strain observed is not primarily due to the austenite-martensite transformation but has its origin in the reorientation of martensite from a twinned to an untwinned configuration. Thus, backtransformation can not be induced by simple removal of the load. For the unloaded state, martensite is still stable as re-twinning can not be induced by removal of the load. The transformation back to austenite can only be induced by increasing the temperature above A_s^0 and finally completed by reaching A_f^0. As the behavior regarding the stress/strain plane resembles the behavior of classical plasticity, the term *pseudoplastic behavior* is used. Focusing on the functional behavior of the material, the term *one-way shape memory effect* is also used frequently.

- Considering a thermal cycle as performed in a DSC-measurement, i.e. completing a whole transformation cycle, generally no macroscopically observable deformation is present as the microscopic deformation is accommodated by the twinned structure. However, if this twinning process may be inhibited leading to a non-twinned microstructure even for a vanishing stress on the macroscale, a behavior as depicted in figure 4.9 can be achieved. As this effect is completely driven by a temperature change in either direction, the term *two-way shape memory effect* is used. The microstructure necessary to inhibit the twinning process can be established by a training process in which dislocations are induced into the material.

Of importance regarding the applicability in structures are the pseudoelastic and the pseudoplastic effect at the moment. Hence, the main focus in this monograph will be on the description of these phenomena.

To close this introductory section, it has to be noted that the observations discussed in this context are not meant to be a complete crystallographic description of the phenomena occurring during the austenite/martensite transformation in shape memory alloys. They may only serve to better understand the problem statement described in the following section and the derived solution to the problem.

4.2 Problem statement

The description of the austenite/martensite transition historically focusses on the change of the crystallographic structure and is therefore regarded as a

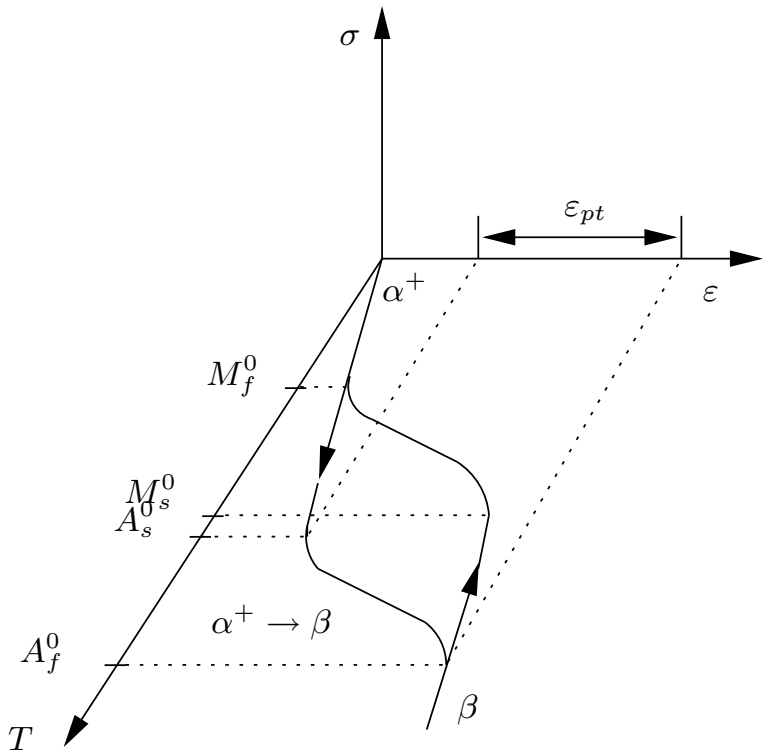

Figure 4.9: Schematic sketch of the behavior of a shape memory alloy exhibiting the two-way effect.

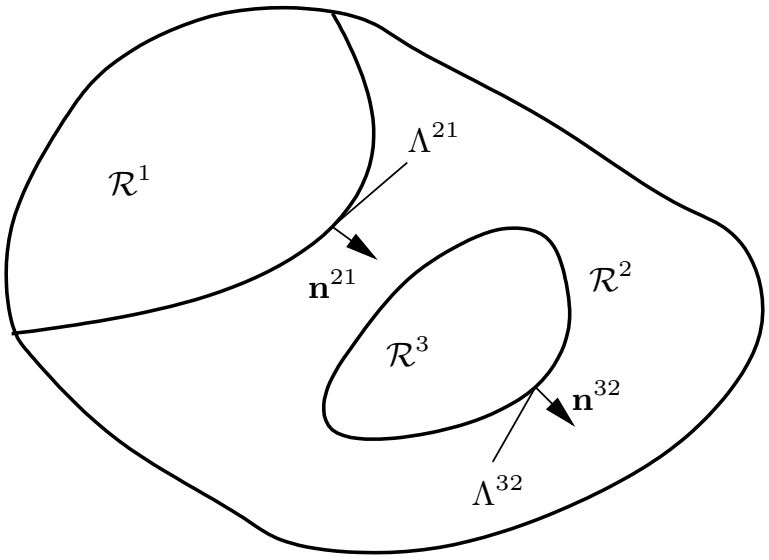

Figure 4.10: Body decomposed into three non-overlapping regions $\mathcal{R}^1$, $\mathcal{R}^2$, and $\mathcal{R}^3$.

process related to the bulk material. However, during the phase transition, usually a sharp interface can be observed between the parent and the product phase. When the phase transformation progresses, the transition front moves within the body. Thus, the phase transition can be understood as a process in which the phase transition front moves within the solid. The aim of the approach described in the remainder of this chapter is to explicitly track the movement of this interface.

The clear identification of the phase interface classifies it as a weak discontinuity, i.e. the coherency requirement is fulfilled but jumps of the deformation gradient, stress, strain, etc. might be present. This allows to use the procedures for a moving weak discontinuity derived in section 2.4, leading to a locally defined expression for the driving force of the movement of the interface.

Due to the presence of a sharp interface, the domain Ω of the body under consideration $\mathcal{B}$ can be subdivided into n_{reg} subregions $\mathcal{R}^\alpha$, $\alpha \in I$ with $I = \{1, ..., n_{reg}\}$ such that no overlapping occurs, i.e. $\Omega = \bigcup_{\alpha=1}^{n_{reg}} \mathcal{R}^\alpha$ and $\mathcal{R}^\alpha \cap \mathcal{R}^\beta = \emptyset \, \forall \, \alpha, \beta \in I, \alpha \neq \beta$. The boundary of the Region $\mathcal{R}^\alpha$ is denoted by $\partial\mathcal{R}^\alpha$. The interface between the subregions $\mathcal{R}^\alpha$ and $\mathcal{R}^\beta$ with the normal vector on the interface $\mathbf{n}^{\alpha\beta}$ pointing towards region $\mathcal{R}^\alpha$ is denoted by $\Lambda^{\alpha\beta}$, i.e. $\Lambda^{\alpha\beta} = \partial\mathcal{R}^\alpha \cap \partial\mathcal{R}^\beta \, \forall \, \alpha, \beta \in I, \alpha \neq \beta$. An example consisting of three regions is depicted in figure 4.10.

The idea that the phase transformation is regarded as movement of the transformation surface within the body poses two subproblems:

- the movement of the transformation surface has to be described locally depending on the stress, strain, and temperature jump at the transformation surface, and
- the thermoelastic behavior including eigenstrains due to the phase transformation of the bulk, i.e. the regions itself, has to be captured as well.

The coupled nature of the whole problem is evident: the thermomechanical state at the interface due to external thermomechanical loads influences (and initially initiates) the movement of the transformation front. Vice versa does the movement of the transition front lead to the induction of an additional strain due to the phase transition and a change of the material behavior when the transition occurs within a region.

4.2.1 Bulk behavior

The clear distinction between austenitic and martensitic phase allows to use different material laws for each phase. Due to restrictions of the implementation of the boundary element method, small strain theory is adopted. Thus, consequently instead of $\boldsymbol{e}$, the infinitisimal strain $\boldsymbol{\varepsilon}$ is used. The same applies for $\boldsymbol{\Pi}$ and $\boldsymbol{\sigma}$. Each phase is characterized as:

- for the austenitic phase a linear thermoelastic stress strain relation (cf. equation (3.1)) is employed

$$\boldsymbol{\sigma} = \mathbb{C}^A : \left(\boldsymbol{\varepsilon} - (\Theta - \Theta_0)\, \boldsymbol{\alpha}^A\right) \tag{4.1}$$

  where $\mathbb{C}^A$ denotes the fourth order stiffness tensor of isotropic elasticity within the austenite as described in section 3.1. The material parameters are denoted by λ^A, μ^A, and $\boldsymbol{\alpha}^A = \mathbf{1}\alpha^A$.

- for the martensitic phase a linear thermoelastic stress strain relation extended by an eigenstrain $\boldsymbol{\varepsilon}^{pt}$ due to phase transformation

$$\boldsymbol{\sigma} = \mathbb{C}^M : \left(\boldsymbol{\varepsilon} - \boldsymbol{\varepsilon}^{pt} - (\Theta - \Theta_0)\, \boldsymbol{\alpha}^M\right) \tag{4.2}$$

where $\mathbb{C}^M$ denotes the fourth order stiffness tensor of isotropic elasticity within the martensite. The material parameters are denoted by λ^M, μ^M, and $\boldsymbol{\alpha}^M = \mathbf{1}\alpha^M$. As reorientation of martensite is currently not considered, the term $\boldsymbol{\varepsilon}^{pt}$ is in general spatially not constant, but remains the same for a specific material point when chosen. For the strain $\boldsymbol{\varepsilon}^{pt}$ induced by the phase transformation, the time when the transformation takes place determines its crystallographic structure. After that, $\boldsymbol{\varepsilon}^{pt}$ remains constant. A strategy to choose a proper value for $\boldsymbol{\varepsilon}^{pt}$ is presented in the following section wherein a term for the right Cauchy Green tensor $\mathbf{C}_M$ due to the phase transition is derived. As only small deformations are taken into account, the term might be approximated in a Green-Lagrange sense as

$$\boldsymbol{\varepsilon}^{pt} = \frac{1}{2}\left(\mathbf{1} + \mathbf{C}_M\right). \tag{4.3}$$

4.2.2 Deformation induced by change of the crystallographic structure

Different theories exist in the literature which predict the deformation induced to the material due to the change of the crystallographic structure during transformation. As the most prominent approach, the Wechsler-Lieberman-Read theory should be mentioned (Wechsler et al. (1953)). A more recent approach was suggested by Ball & James (1987, 1992) which is frequently used in crystallographic theories nowadays (see eg. Shield (1995), Lusk (1996)). This approach is used in the following to determine the induced deformation.

4.2.2.1 Stretch-tensors associated with change of the crystallographic structure

The deformation induced by a change of the crystallographic structure can be described by the positive definite matrix $\mathbf{U}_0$ such that[2] $\tilde{\mathbf{x}} = \mathbf{U}_0 \cdot \mathbf{X}$ where $\mathbf{X}$ describes the position of a material point before transformation in the referential configuration and $\tilde{\mathbf{x}}$ thereafter. For lingual simplicity, we will refer to the reference configuration as austenite and the configuration after transformation as martensite.

[2]The choice of a proper coordinate system is a prerequisite for this relation.

The shape change due to the change of the crystallographic structure from cubic to orthorhombic structure $\mathbf{U}_0$ takes the form

$$\mathbf{U}_0 = \frac{\eta_i(\mathbf{e}_i + \mathbf{e}_j) \otimes (\mathbf{e}_i + \mathbf{e}_j) + \eta_j(\mathbf{e}_i - \mathbf{e}_j) \otimes (\mathbf{e}_i - \mathbf{e}_j)}{2} + \eta_k \mathbf{e}_k \otimes \mathbf{e}_k, \tag{4.4}$$

where $\mathbf{e}_i, i = 1, 2, 3$ are the unit base vectors in the orthonormal cubic basis of the parent phase. For Cu-Al-Ni, the parameters are (see Shield (1995), Sun (2001))

$$\eta_1 = 1.0619,\ \eta_2 = 1.0230,\ \eta_3 = 0.9178 \tag{4.5}$$

leading to six possible choices for $\mathbf{U}_0$.

Based on these stretches, the variants of the transformed material but also the parent phase can be described by a rotation $\mathbf{R}_i$ such that

$$\mathbf{1}, \mathbf{R}_1 \cdot \mathbf{U}_0 \cdot \mathbf{R}_1^T, ..., \mathbf{R}_\nu \cdot \mathbf{U}_0 \cdot \mathbf{R}_\nu^T, \tag{4.6}$$

where ν denotes the number of variants.

4.2.2.2 Determination of choices satisfying compatibility

The main starting point for the frame by Ball & James (1987, 1992) developed in this section is the assumption, that the interfaces within the material are coherent. These interfaces may be between austenite and martensite or different martensite variants. This leads to the coherence condition at the interface (2.256) which may be expressed here as

$$\mathbf{F}^+ - \mathbf{F}^- = \mathbf{a} \otimes \mathbf{N} \tag{4.7}$$

where $\mathbf{F}^+$ and $\mathbf{F}^-$ are the limiting values of the deformation gradient $\mathbf{F}$ from either side of the discontinuity. It is noteworthy that at the moment no restriction with respect to the type of interface is imposed. Hence, different types of interfaces may be discussed in the following:

(I) Austenite/Austenite Interfaces
For austenite, only $\mathbf{U}^+ = \mathbf{U}^- = \mathbf{1}$ is possible. Thus (4.7) reads in this case

$$\mathbf{R}^+ - \mathbf{R}^- = \mathbf{a} \otimes \mathbf{N}, \tag{4.8}$$

which implies that

$$\mathbf{R}* = \mathbf{1} + \mathbf{a} * \otimes \mathbf{N}, \tag{4.9}$$

where $\mathbf{R}* = (\mathbf{R}^-)^T \cdot \mathbf{R}^+$ and $\mathbf{a}* = (\mathbf{R}^-)^T \cdot \mathbf{a}$. Relation (4.9) implies that $\mathbf{R}* = \mathbf{1}$ (cf. Ball & James (1987)) and therefore

$$\mathbf{R}^+ = \mathbf{R}^- = \mathbf{1}, \tag{4.10}$$

which means that no austenite/austenite interfaces are possible.

(II) Martensite/Martensite Interfaces
Based on the polar decomposition of the deformation gradient, the jump relation (4.7) and the possible choices for $\mathbf{U}$ (4.6), an interface between martensite variants i and j is governed by

$$\hat{\mathbf{R}}^+ \cdot \mathbf{U}_0 \cdot \mathbf{R}_i^T - \hat{\mathbf{R}}^- \cdot \mathbf{U}_0 \cdot \mathbf{R}_j^T = \hat{\mathbf{a}} \otimes \hat{\mathbf{N}} \tag{4.11}$$

where $\hat{\mathbf{R}}^+ = \mathbf{R}^+ \cdot \mathbf{R}_i$, $\hat{\mathbf{R}}^- = \mathbf{R}^- \cdot \mathbf{R}_j$, $\hat{\mathbf{N}}$ denotes the normal vector to the interface, and $\hat{\mathbf{a}} \neq \mathbf{0}$. Premultiplying by $(\hat{\mathbf{R}}^-)^T$ and postmultiplying by $\mathbf{R}_j$ yields

$$\mathbf{R} \cdot \mathbf{U}_0 \cdot \bar{\mathbf{R}} - \mathbf{U}_0 = \mathbf{a} \otimes \mathbf{N} \tag{4.12}$$

where $\mathbf{R} = (\hat{\mathbf{R}}^-)^T \cdot \hat{\mathbf{R}}^+$, $\bar{\mathbf{R}} = \mathbf{R}_i^T \cdot \mathbf{R}_j$, $\mathbf{a} = (\hat{\mathbf{R}}^-)^T \cdot \hat{\mathbf{a}}$, and $\mathbf{N} = \mathbf{R}_j^T \cdot \hat{\mathbf{N}}$.

(III) Austenite/Martensite Interfaces
The interfaces are governed by

$$\mathbf{R} \cdot \mathbf{U}_0 \cdot \mathbf{R}_k^T - \mathbf{1} = \mathbf{a} \otimes \mathbf{N} \tag{4.13}$$

which implies that

$$\mathbf{R}_k \cdot \mathbf{U}_0^2 \cdot \mathbf{R}_k^T = (\mathbf{1} + \mathbf{N} \otimes \mathbf{a}) \cdot (\mathbf{1} + \mathbf{a} \otimes \mathbf{N}). \tag{4.14}$$

This in turn implies that a vector perpendicular to both $\mathbf{a}$ and $\mathbf{N}$ is an eigenvector of $\mathbf{R}_k \cdot \mathbf{U}_0^2 \cdot \mathbf{R}_k^T$ with an eigenvalue equal to 1. But this is impossible unless one of the eigenvalues of $\mathbf{U}_0$ equals 1. Taking into account the structure of $\mathbf{U}_0$, it renders an interface between austenite and martensite impossible. However, this is in clear contradiction to experimental observations. In the following, the approach by Ball and James to circumvent this contradiction is described.

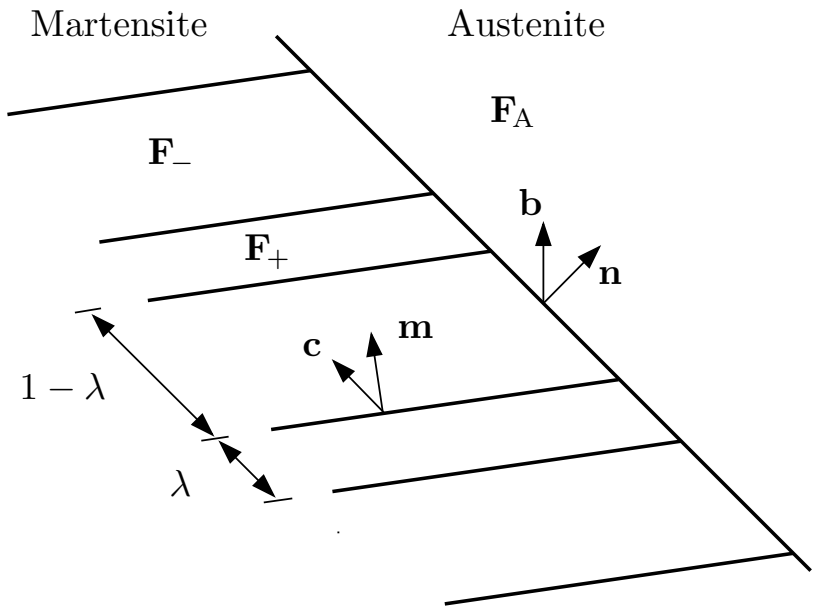

Figure 4.11: A sketch of the Austenite/Martensite interface structure.

The approach is based on the experimental observation that the martensitic phase usually exhibits a finely layered structure as depicted in figure 4.11. Thus, in the following compatibility is not sought directly between martensite and austenite but between the deformation gradient $\mathbf{F}_\mathrm{A}$ and the averaged deformation gradient $\mathbf{F}_\mathrm{M}$.

First, the focus is on the martensitic phase and the martensite/martensite interface. Using volumetric averaging, the mean deformation gradient in the martensite can be expressed as

$$\mathbf{F}_\mathrm{M} = \lambda \mathbf{F}_+ + (1-\lambda)\mathbf{F}_-, \tag{4.15}$$

where λ denotes the volumetric fraction within the martensite where a deformation gradient $\mathbf{F}_+$ was induced due to the transformation as depicted in figure 4.11. Compatibility is now required on the average between $\mathbf{F}_\mathrm{M}$ and $\mathbf{F}_\mathrm{A}$. Thus, compatibility can be expressed as

$$\mathbf{F}_\mathrm{M} - \mathbf{F}_\mathrm{A} = \mathbf{b} \otimes \mathbf{n} \tag{4.16}$$

or, considering that the austenitic state corresponds to the referential state, as

$$\mathbf{F}_\mathrm{M} - \mathbf{1} = \mathbf{b} \otimes \mathbf{n}. \tag{4.17}$$

At the martensite/martensite interface, the condition

$$\mathbf{F}_+ - \mathbf{F}_- = \mathbf{c} \otimes \mathbf{m} \tag{4.18}$$

has to be fulfilled. The combination of equations (4.15), (4.16), and (4.18) with $\mathbf{F}_\mathrm{A} = \mathbf{1}$ yields

$$\begin{aligned} \mathbf{F}_+ &= \mathbf{1} + \mathbf{b} \otimes \mathbf{n} + (1-\lambda)\,\mathbf{c} \otimes \mathbf{m} \\ \mathbf{F}_- &= \mathbf{1} + \mathbf{b} \otimes \mathbf{n} - \lambda\,\mathbf{c} \otimes \mathbf{m}. \end{aligned} \tag{4.19}$$

As stated already, the deformation gradients for martensite can be expressed as

$$\mathbf{F}_+ = \mathbf{R}_+ \cdot \mathbf{U}_+ \tag{4.20}$$

$$\mathbf{F}_- = \mathbf{R}_- \cdot \mathbf{U}_-. \tag{4.21}$$

By introducing $\mathbf{R} = \mathbf{R}_-^T \cdot \mathbf{R}_+$, $\mathbf{c}* = \mathbf{R}_-^T \cdot \mathbf{c}$, $\mathbf{m}* = \mathbf{U}_-^{-1} \cdot \mathbf{m}$, one may restate the jump relation (4.18) as

$$\mathbf{R} \cdot \mathbf{U}_+ \cdot \mathbf{U}_-^{-1} = \mathbf{1} + \mathbf{c}* \otimes \mathbf{m}*\,. \tag{4.22}$$

As the determinants of $\mathbf{R}$, $\mathbf{U}_+$, and $\mathbf{U}_-$ are larger than zero, $1 + \mathbf{c}* \cdot \mathbf{m}* > 0$ holds. Relation (4.19b) now reads

$$\mathbf{F}_- = \mathbf{R}_- \cdot \mathbf{U}_- = \mathbf{1} + \mathbf{b} \otimes \mathbf{n} - \lambda\,(\mathbf{R}_- \cdot \mathbf{c}*) \otimes (\mathbf{m}* \cdot \mathbf{U}_-) \tag{4.23}$$

leading to

$$\mathbf{U}_- + \lambda\,\mathbf{c}* \otimes (\mathbf{m}* \cdot \mathbf{U}_-) = \mathbf{R}_-^T \cdot (\mathbf{1} + \mathbf{b} \otimes \mathbf{n}). \tag{4.24}$$

This relation establishes a connection between the problem posed by the jump conditions of the martensite/martensite interface on the left hand side and the problem posed by the jump conditions of the austenite/martensite interface on the right hand side. Note that by considering relation (4.17), the term $\mathbf{1}+\mathbf{b}\otimes\mathbf{n}$ can be identified as the averaged deformation gradient in the martensitic phase. Thus, the right Cauchy-Green Tensor induced due to the phase transition can be determined as

$$\mathbf{C}_M = \mathbf{F}_\mathrm{M}^T \cdot \mathbf{F}_\mathrm{M} = (\mathbf{1} + \mathbf{n} \otimes \mathbf{b}) \cdot (\mathbf{1} + \mathbf{b} \otimes \mathbf{n}) \tag{4.25}$$

or as

$$\mathbf{C}_M = (\mathbf{U}_- + \lambda\,(\mathbf{m}*\cdot\mathbf{U}_-)\otimes\mathbf{c}*)\cdot(\mathbf{U}_- + \lambda\,\mathbf{c}*\otimes(\mathbf{m}*\cdot\mathbf{U}_-)). \tag{4.26}$$

The possible solutions of this relation have to be found. Proposition 4 by Ball and James (Ball & James (1987)) states that any matrix $\mathbf{C}$ of the form

$$\mathbf{C} = (\mathbf{1} + \mathbf{q}\otimes\mathbf{p}\,)\cdot(\mathbf{1} + \mathbf{p}\otimes\mathbf{q}\,) \tag{4.27}$$

must have eigenvalues $\lambda_1 \le \lambda_2 \le \lambda_3$ with following properties

$$\lambda_i \ge 0 \quad \text{and} \quad \lambda_2 = 1. \tag{4.28}$$

In that case, the solutions $\mathbf{p}$ and $\mathbf{q}$ are given by:

$$\begin{aligned}\mathbf{p} &= \rho\left(\sqrt{\frac{\lambda_3(1-\lambda_1)}{\lambda_3-\lambda_1}}\,\mathbf{N}_1^C + \kappa\sqrt{\frac{\lambda_1(\lambda_3-1)}{\lambda_3-\lambda_1}}\,\mathbf{N}_3^C\right)\\ \mathbf{q} &= \rho^{-1}\left(\frac{\sqrt{\lambda_3}-\sqrt{\lambda_1}}{\sqrt{\lambda_3-\lambda_1}}\right)(-\sqrt{1-\lambda_1}\,\mathbf{N}_1^C + \kappa\sqrt{\lambda_3-1}\,\mathbf{N}_3^C),\end{aligned} \tag{4.29}$$

where $\mathbf{N}_1^C$ and $\mathbf{N}_3^C$ are normalized eigenvectors of $\mathbf{C}$ corresponding to λ_1 and λ_3, respectively. The constant ρ represents an invariant scaling of the solution and will be used to choose unit normal vectors. The constant κ can take the values ± 1. Considering that $\mathbf{1} + \mathbf{p}\otimes\mathbf{q}$ can be interpreted as a deformation gradient, the requirement $1 + \mathbf{p}\cdot\mathbf{q} > 0$ follows. This requirement is already worked into (4.29).

As the matrix $\mathbf{C}_M$ fulfills equation (4.25) as well as (4.26), the condition that one eigenvalue of $\mathbf{C}_M$ has to be 1 in order to be expressible in the form stated above restricts the values for λ. To ensure that at least one eigenvalue equals one, a function $g(\lambda)$ is introduced such that

$$g(\lambda) = \det(\mathbf{C}_M - \mathbf{1}). \tag{4.30}$$

The function $g(\lambda)$ only depends on λ as the focus is on the determination of λ for given $\mathbf{b}$ and $\mathbf{n}$. One root for $g(\lambda)$ has to be found with $0 \le \lambda \le 1$ in order to be physically admissible. Generally, $g(\lambda)$ is a sixth order polynomial. By using proposition 5 in Ball & James (1987), it can be shown that it reduces to a quadratic function in λ, leading to two solutions for relation (4.30). In

addition, proposition 6 of the publication mentioned above poses restrictions on $\mathbf{C}_M$ due to the fact that $0 \leq \lambda_1 \leq 1$ and $\lambda_3 \geq 1$.

The complete "CTM-problem" consists of the determination of the rotation tensors, $\mathbf{c}$, $\mathbf{n}$, $\mathbf{b}$, and $\mathbf{m}$[3]. However, within this application, the theory is only used to determine the deformation induced by the phase transition. Thus, knowledge of $\mathbf{C}_M$ is sufficient and only the steps taken to determine the correct value for $\mathbf{C}_M$ are necessary.

4.2.2.3 Criterion choosing the existing strain

The procedure by Ball & James (1987, 1992) yields the possible values for the strain induced regardless of the stress applied. Thus no information is provided which variant is the one which will actually form within a specific region. Therefore, an additional criterion must be introduced which will be used to finally decide which variants are active. In the following, a proposition by Shield (1995) is adopted. An energy criterion is introduced: the variant which minimizes the strain energy due to the induced Bain strain is chosen. Thus, from the possible choices $\mathbf{C}_M^i$, the one which minimizes

$$\tilde{W}_M^i = \mathrm{tr}(\mathbf{C}_M^i \cdot \boldsymbol{\sigma}), \tag{4.31}$$

is selected.

4.2.3 Interfacial movement

In order to simplify the notation, the superscript $\alpha\beta$ is omitted in the following section, i.e. $[\bullet] = [\bullet]^{\alpha\beta}$, $\Lambda = \Lambda^{\alpha\beta}$, and $\mathbf{n} = \mathbf{n}^{\alpha\beta}$. The restriction on the movement of the interface imposed by the second law of thermodynamics may be described by (2.263). It is adopted in the notation used within this chapter as

$$\zeta^{\Lambda} = U\rho_0 \ \mathbf{n} \cdot [\boldsymbol{\mu}] \cdot \mathbf{n} \ \geq 0. \tag{4.32}$$

Various approaches are possible to satisfy relation (4.32): one may assume that the interfacial movement is always in equilibrium (cf. Raniecki & Lexcellent

[3]The approach by Ball and James predicts plane interfaces. This is in clear contradiction to the results presented here. However, it must be noted that the theory is developed in the referential frame. The transformation into he actual configuration leads to curved interfaces (Lusk (1996)).

(1999)), satisfying relation (4.32) by ensuring that $\mathbf{n}\cdot[\boldsymbol{\mu}]\cdot\mathbf{n} = 0$. This approach may lead to large changes or jumps of the position of the interface, which in turn may lead to numerical instabilities. Thus, a different approach is employed here. In what follows, a linear relation

$$U = c\,\mathbf{n}\cdot[\boldsymbol{\mu}]\cdot\mathbf{n} \tag{4.33}$$

with the restriction $c > 0$ to satisfy relation (4.32) is used. It changes the character of the problem: the equilibrium approach is time independent. When the equilibrium position is to be found at a different position, even infinite propagation speeds of the transformation interface may be possible. the approach (4.33) introduces a time dependence into the problem. The position of the interface does not only depend on the equilibrium position but also on the parameter c. For $c \to \infty$, this model approaches the equilibrium scheme. Thus, the choice of the parameter c is still an open issue. One may choose a value which is large enough to allow for fast approach of the equilibrium position but small enough to avoid numerical instabilities. However, regardless of the choice of c it must be noted that the equilibrium position is finally reached, as long as the numerical scheme works correctly. In addition to the preceding considerations, the choice of a linear relation may be questioned (cf. Berezovski & Maugin (2005)). But as the main focus of this chapter is on the development of the numerical scheme, this choice suffices for now. An extension to other, nonlinear approaches is straightforward.

4.3 Numerical realization

As described in section 4.2.3, the evolution of the interface can be locally described in terms of the jump of the state variables between the coexisting phases. However, these local state variables, such as stress, deformation gradient or temperature, strongly depend on the behavior of the bulk material and the externally applied boundary conditions. Thus, its movement can not solely be described by a local description at the phase boundary, which is a sufficient approach when the interfacial movement is primarily driven by its curvature (Taylor et al. (1992), Russo & Smereka (2000), Gurtin & Jabbour (2002)). Closed form solutions of the coupled problem exist only for some special cases (Raniecki & Lexcellent (1999), Berezovski & Maugin (2002, 2003)). To address problems with arbitrary geometries[4], a numerical scheme able to capture the

[4]The initial geometry might be chosen based on micrographs. After reaching the equilibrium state, the geometry reached in the simulation should again be compared to micrographs.

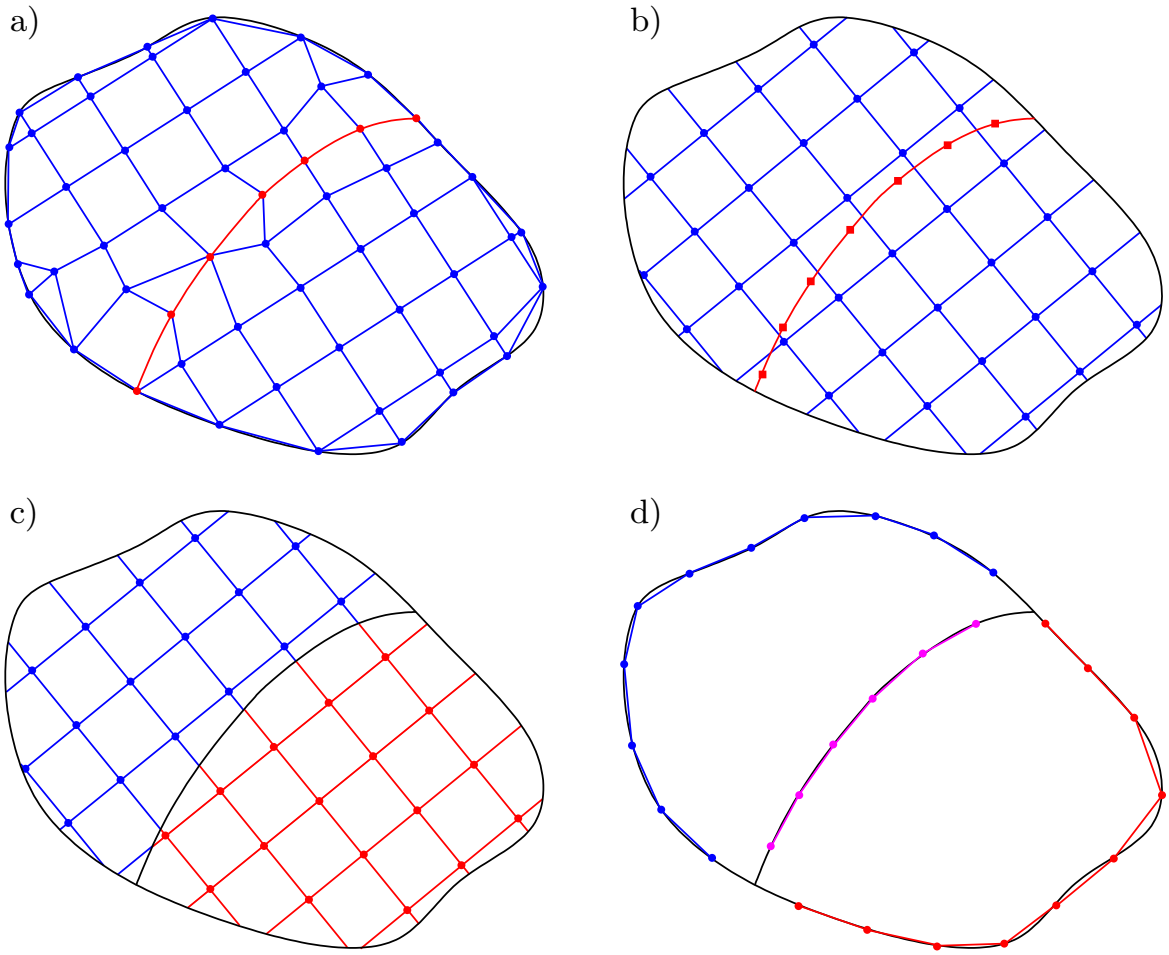

Figure 4.12: Discretization approaches discussed in section 4.3.

behavior of the bulk material must be developed. Different approaches might be possible (cf. figure 4.12):

a) The finite element method (FEM) is used to describe the bulk behavior. Its mesh coincides with the interface. Thus, the FEM-nodes can be used to constitute a mesh on the interface and establish a numerical scheme to describe the movement of the phase boundary. The state at the interface can be determined by extrapolation of the quantities at the Gauss-points to the interfacial nodes. This procedure is only an extrapolation as usually a jump of the quantity of interest can be found at the phase interface. Thus, no interpolation over the interface is possible. The values at both sides of the interface have to be extrapolated from the corresponding bulk Gauss-points. When the interface evolves, remeshing of

the generally three-dimensional FEM-mesh is necessary which renders to be difficult. An application of this approach can be found in Ghoussoub & Leroy (2001).

b) Deviating from the previous approach, a two-dimensional discretization of the interface independent of the discretization of the bulk is used. This mesh can move within the body without any restriction which may be imposed by the bulk discretization. Again, extrapolation of the quantities at the gauss-points to the interfacial points is necessary. The quality of this extrapolation varies depending on the distance of the interfacial node from the gauss-points of the corresponding bulk material. This introduces an extrapolation error which may lead to inaccurate results for the interfacial values.

c) Again, the FEM is used to solve the bulk problem, but the position of the interface is described implicitly by means of a level set function (Sethian (1998), Barles et al. (1993)). An additional degree of freedom is introduced by this level set. The movement of the interface is now solved at the gauss-points, an extrapolation of the interfacial values to the gauss-points is necessary. As also strong discontinuities can be addressed with this approach, the displacement field may be enriched by an additional term, leading to the extended finite element method (XFEM) (Sukumar et al. (2001), Chessa & Belytschko (2004)) approach. This approach has been successfully applied to crack growth problems (Sukumar & H., 2003; Huang et al., 2003; Budyn et al., 2004) or solidification problems (Chessa et al. (2002)).

d) The method proposed in the following explicitly discretizes the interface by a two-dimensional mesh as in proposal b). The same discretization is used to solve the bulk problem as the boundary element method (BEM), which generally only requires a surfacial mesh as it provides by its concept a reduction of the problem dimension. Schmidt et al. (Schmidt & Gross (1997), Gross et al. (2003)) used the same approach to calculate the equilibrium shape of an elastically inhomogeneous inclusion. Thus, the approach was similar but it lacked the evolution algorithm for the interface as the determination of the equilibrium shape was subject of their contribution.

4.3.1 Preliminaries

The developed description is not restricted to the use of an explicitly specified configuration even though it is presented here within the context of small deformations. The position vector $\mathbf{r} \in \mathbb{R}^n$, where n denotes the number of spatial dimensions, may describe the position of a material point in an Eulerian, Lagrangian or any intermediate configuration. Consequently, the measures introduced have to be well defined in the configuration employed. The approach is therefore coupled to the BEM description employed and its ability to provide values for certain measures at the interface in the chosen configuration.

4.3.2 Boundary Element Method

This section shall not be understood as an introduction to the boundary element method. The complete description of the boundary element method is beyond the scope of this contribution. Numerous textbooks exist which give a detail introduction and an overview of the current research within this field, see e.g. Gao & Davies (2000b), Beer (2001). This section is only included to give a reader, who is not familiar with the idea behind the boundary element method, an idea about the concepts followed within this approach.

4.3.2.1 Main idea of the Boundary Element Method

In order to keep the focus on the main ideas of the Boundary Element Method, an introductory example is presented in this section. Here the problem of stationary heat conduction, described by the Laplace equation, is discussed. The problem statement in strong form is as follows: the domain Ω is governed by the Laplace equation as stated below, its boundary $\partial\Omega$ can be separated into two regions such that $\partial\Omega = \Gamma_u \cup \Gamma_q$ and $\Gamma_u \cap \Gamma_q = \emptyset$. The solution for $u \in \mathbb{R}$, stated in the strong form, is sought that

$$\begin{array}{lll} \boldsymbol{\nabla}^2 u = 0 & \text{in} & \Omega \\ u = u^* & \text{on} & \Gamma_u \\ q = \boldsymbol{\nabla} u \cdot \mathbf{n} = q^* & \text{on} & \Gamma_q. \end{array} \tag{4.34}$$

is satisfied. A weak form of (4.34) can be derived by introduction of a, not yet explicitly specified, weighting function $\hat{u}(\mathbf{x}, \hat{\mathbf{x}})$ to lead to

$$\int_{\Omega} \hat{u} \left(\boldsymbol{\nabla}^2 u \right) \, \mathrm{d}\Omega(\mathbf{x}) + \int_{\Gamma_u} \hat{q} \left(u - u^* \right) \, \mathrm{d}\Gamma(\mathbf{x}) - \int_{\Gamma_q} \hat{u} \left(\boldsymbol{\nabla} u \cdot \mathbf{n} - q^* \right) \, \mathrm{d}\Gamma(\mathbf{x}) = 0 \tag{4.35}$$

with $\hat{q} = \boldsymbol{\nabla} \hat{u} \cdot \mathbf{n}$. The weighted integrals lead, due to the introduction of the weighting function $\hat{u}(\mathbf{x}, \hat{\mathbf{x}})$, funtions of the new spatial variable $\hat{\mathbf{x}}$. It is noteworthy, that not only the differential equation is part of the weak form of the problem statement but also the boundary conditions are included. Relating this aspect to the idea pursued in this section and its environment of isotropic elasticity, the tractions and stresses can be evaluated at the boundary with higher accuracy compared to an approach based on finite elements. Thus, two positive aspects are noticed: the measures are evaluated directly at the points of interest, the interface. Furthermore, the inclusion of the traction leads to a higher accuracy for the determination of the stresses. The weighting functions used for the differential equation and the boundary conditions are different and not of the same type as u, thus qualifying this method as a Petrov-Galerkin method. Twice partial integration of the first term in (4.35) yields

$$\int_{\Omega} \boldsymbol{\nabla}^2 \hat{u} \, u \, \mathrm{d}\Omega(\mathbf{x}) - \int_{\Gamma} \boldsymbol{\nabla} \hat{u} u \cdot \mathbf{n} \, \mathrm{d}\Gamma(\mathbf{x}) + \int_{\Gamma} \hat{u} \left(\boldsymbol{\nabla} u \right) \cdot \mathbf{n} \, \mathrm{d}\Gamma(\mathbf{x}) + \int_{\Gamma_u} \hat{q} \left(u - u^* \right) \, \mathrm{d}\Gamma(\mathbf{x}) - \int_{\Gamma_q} \hat{u} \left(\boldsymbol{\nabla} u \cdot \mathbf{n} - q^* \right) \, \mathrm{d}\Gamma(\mathbf{x}) = 0, \tag{4.36}$$

after rearrangement

$$\int_{\Omega} \boldsymbol{\nabla}^2 \hat{u} \, u \, \mathrm{d}\Omega(\mathbf{x}) - \int_{\Gamma_q} \hat{q} \, u \, \mathrm{d}\Gamma(\mathbf{x}) - \int_{\Gamma_u} \hat{q} \, u^* \, \mathrm{d}\Gamma(\mathbf{x}) + \int_{\Gamma_u} \hat{u} \, q \, \mathrm{d}\Gamma(\mathbf{x}) + \int_{\Gamma_q} \hat{u} \, q^* \, \mathrm{d}\Gamma(\mathbf{x}) = 0, \tag{4.37}$$

and finally

$$\int_{\Omega} \boldsymbol{\nabla}^2 \hat{u}\, u \,\mathrm{d}\Omega(\mathbf{x}) - \int_{\Gamma} \hat{q}\, u \,\mathrm{d}\Gamma(\mathbf{x}) + \int_{\Gamma} \hat{u}\, q \,\mathrm{d}\Gamma(\mathbf{x}) = 0. \tag{4.38}$$

The main idea is now to choose the weighting function $\hat{u}$ such that the remaining volume integral collapses. For the integral derived, $\hat{u}$ is chosen such that

$$\boldsymbol{\nabla}^2 \hat{u}(\hat{\mathbf{x}}) = \delta(\mathbf{x} - \hat{\mathbf{x}}) \tag{4.39}$$

holds. If the above requirement holds, $\hat{u}$ is called a fundamental solution. The derivation of the fundamental solution depends on the underlying differential equation. Thus, the formalism leading to the boundary element formulation is closely bound to the differential equation used to derive the fundamental solution and even for slight modifications, as e.g. the transition from isotropic to orthotropic behavior in elasticity, a new derivation of the fundamental solution is necessary. Furthermore, the derivation is bound to the problem dimension as well.

Assuming that a three dimensional problem has to be solved, the fundamental solution for the case considered here reads

$$\hat{u} = \frac{1}{2\,\pi}\, \ln \frac{1}{|\mathbf{x} - \hat{\mathbf{x}}|}. \tag{4.40}$$

Using (4.40), relation (4.38) can be rewritten as

$$c\, u(\hat{\mathbf{x}}) - \int_{\Gamma} \hat{q}\, u \,\mathrm{d}\Gamma(\mathbf{x}) + \int_{\Gamma} \hat{u}\, q \,\mathrm{d}\Gamma(\mathbf{x}) = 0, \tag{4.41}$$

where $c = 1$ if $\mathbf{x}$ is an interior point and $c = \frac{1}{2}$ if $\mathbf{x}$ is a point on the boundary. The transformation of the problem from one which is defined by a differential equation in the bulk and appropriate boundary conditions to a problem solely described in terms of the boundary is achieved. The integrals over the boundary are split into an element-wise integration over the elements I

$$c\, u(\hat{\mathbf{x}}) - \sum_{I} \int_{\Gamma_I} \hat{q}(\mathbf{x}, \hat{\mathbf{x}})\, u(\mathbf{x}) \,\mathrm{d}\Gamma(\mathbf{x}) + \sum_{I} \int_{\Gamma_I} \hat{u}(\mathbf{x}, \hat{\mathbf{x}})\, q(\mathbf{x}) \,\mathrm{d}\Gamma(\mathbf{x}) = 0. \tag{4.42}$$

Special care has to be taken for the singularities related to the evaluation of $\hat{u}$ and $\hat{q} = \boldsymbol{\nabla}\hat{u} \cdot \mathbf{n}$. For other elements, usual Gaussian integration can be used. The two integrals now have to be evaluated in terms of the nodal values $\mathbf{u}$ and $\mathbf{q}$ to yield the matrices

$$\mathbf{C}\mathbf{u} - \hat{\mathbf{H}}\mathbf{u} + \mathbf{G}\mathbf{q} = 0, \tag{4.43}$$

or

$$\mathbf{H}\,\mathbf{u} = \mathbf{G}\,\mathbf{q} \tag{4.44}$$

with $\mathbf{H} = \hat{\mathbf{H}} - \mathbf{C}$. Here, $\mathbf{C}$ has only nonzero components on the main diagonal which are either 1 or 1/2, depending on the associated value of c. At each node, either u^* is specified and q is unknown or q^* is specified and u is unknown. The terms which are known are multiplied with their corresponding matrix $\mathbf{H}$ or $\mathbf{G}$ and grouped into a vector $\mathbf{y}$. The unknowns are grouped into $\mathbf{x}$, leading to the equation to be solved

$$\mathbf{F}\,\mathbf{x} = \mathbf{y}. \tag{4.45}$$

4.3.2.2 Multiregion BEM for isotropic elasticity and nonhomogeneous eigenstrain

As already described in section 4.3.1, the domain Ω of the body $\mathcal{B}$ can be divided into nonintersecting regions $\mathcal{R}^\alpha$. For each region $\mathcal{R}^\alpha$, the boundary element method must provide a solution of the bulk problem, i.e. provide a solution for the vector of unknowns $\mathbf{u}$ and tractions $\mathbf{t}$ on the boundary $\partial\mathcal{R}^\alpha$ of the region. Thus, depending on the problem type, an appropriate scheme has to be chosen.

The term isotropic elasticity is used to characterize the elastic response of the region considered. In fact, a nonhomogeneous strain within the domain might be present as introduced in section 4.2.1.

Starting point for the description for isotropic elasticity is the Somigliana identity

$$\begin{aligned}\mathbf{C}\cdot\mathbf{u}(\hat{\mathbf{x}}) \;=\; & \int_\Gamma \mathbf{U}(\mathbf{x},\hat{\mathbf{x}})\cdot\mathbf{t}(\mathbf{x})\,\mathrm{d}\Gamma(\mathbf{x}) - \int_\Gamma \mathbf{T}(\mathbf{x},\hat{\mathbf{x}})\cdot\mathbf{u}(\mathbf{x})\,\mathrm{d}\Gamma(\mathbf{x}) \\ & + \int_\Omega \hat{\mathbf{E}}(\mathbf{x},\hat{\mathbf{x}}) : \boldsymbol{\varepsilon}^{pt}(\mathbf{x})\,\mathrm{d}\Omega(\mathbf{x}),\end{aligned} \tag{4.46}$$

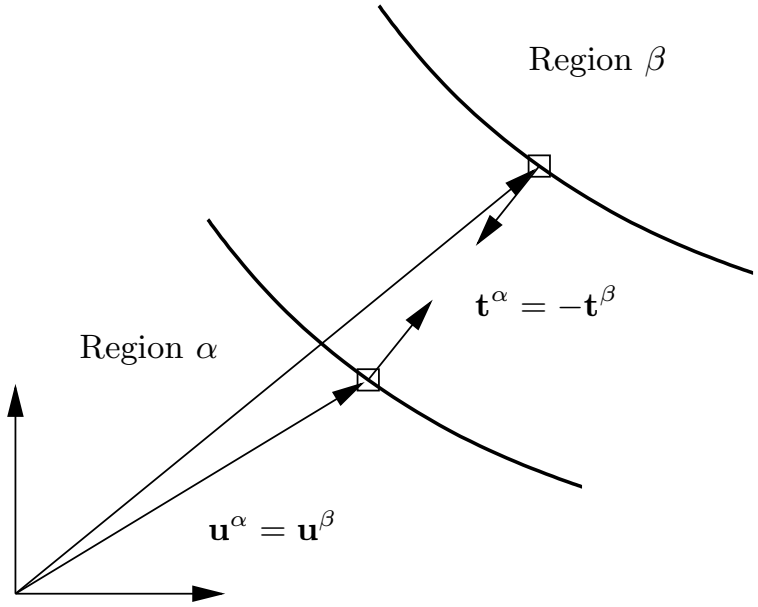

Figure 4.13: Node on the interface, the regions are drawn apart for clarity.

which is the equivalent to relation (4.41). The tensors $\mathbf{U}$, $\mathbf{T}$, and $\hat{\mathbf{E}}$, depend on the problem type and their appropriate choice is explained in appendix A. However, due to the additional strain $\boldsymbol{\varepsilon}^{pt}$, a term with a volume integration remains in the formulation which can not be transferred to the boundary. Thus, two aspects distinguish this formulation from a plain boundary element formulation: equation (4.46) is only valid for a homogeneous region α and a volume integral is still present in the formulation. Both aspects will be covered in the following section even though the underlying derivations are well established (cf. Gao & Davies (2000b,a), Kane et al. (1990), or Potrc et al. (1987)). The same discretization procedure as described in the previous section leads to

$$\mathbf{C}^\alpha\,\mathbf{u}^\alpha - \hat{\mathbf{H}}^\alpha\mathbf{u}^\alpha + \mathbf{G}^\alpha\mathbf{t}^\alpha + \mathbf{f}^{i\alpha} = 0, \tag{4.47}$$

and analogously to (4.44)

$$\mathbf{H}^\alpha\,\mathbf{u}^\alpha = \mathbf{G}^\alpha\,\mathbf{t}^\alpha + \mathbf{f}^{i\alpha}. \tag{4.48}$$

The additional term $\mathbf{f}^{i\alpha}$ stems from the integral containing $\boldsymbol{\varepsilon}^{pt}$. For multidomain problems, relation (4.48) can be formulated for each region α. However,

for nodes belonging to multiple regions, the grouping into known and unknown measures as described previously cannot be performed. This is clarified by figure 4.13. For each node on the interface belonging to region α, an associate node in region β at the same position exists. Each node provides three equations for a three dimensional problem. The number of unknowns is six for each interfacial node, $\mathbf{u}^\alpha$, $\mathbf{t}^\alpha$, $\mathbf{u}^\beta$, and $\mathbf{t}^\beta$. The connection of the nodes is brought in by the additional conditions $\mathbf{u}^\alpha = \mathbf{u}^\beta$ and $\mathbf{t}^\alpha = -\mathbf{t}^\beta$ as shown in figure 4.13. Thus $2 * 3 + 2 * 3 = 12$ equations are given for the $2 * (3 + 3) = 12$ unknowns. Thus, all displacements and tractions can be determined.

The additional constraints at the boundary provide the additional relations and rules underlying the procedure employed to combine the regional governing equations (4.48) to a global governing equation

$$\mathbf{H}\,\mathbf{u} = \mathbf{G}\,\mathbf{t} + \mathbf{f}^{pt} \tag{4.49}$$

which again can be rearranged to be solved for the unknowns at each node.

The third term on the right hand side of relation (4.46), which can only be treated by a volume integration, does not pose any special problems for this particular application. It has to be taken into account, that the additional induced strain $\boldsymbol{\varepsilon}^{pt}$ is only present in regions where the transformation has already taken place. As the simulation considers the movement of the phase transition front within the body, each part of the region where the eigenstrain is induced was once located directly behind the moving phase transition front.

The volumetric elements which are used to compute the additional term are constructed by taking the two dimensional element at the beginning and the end of the time step, thus providing two faces for the volume element. The other four faces of the element are constructed by taking the appropriate nodes of the two dimensional element as depicted in figure 4.14. No connectivity of the nodes which do not belong to the same volume element are necessary as only the volume integration is performed. Furthermore, the elements can even overlap, which might happen if the phase interface starts to reverse the transformation, accompanied by a removal of the strain induced due to the phase transformation. For the majority of the elements, the integration can be carried out by a low order Gauss integration. For elements where singularities occur, again special steps have to be taken (cf. appendix A).

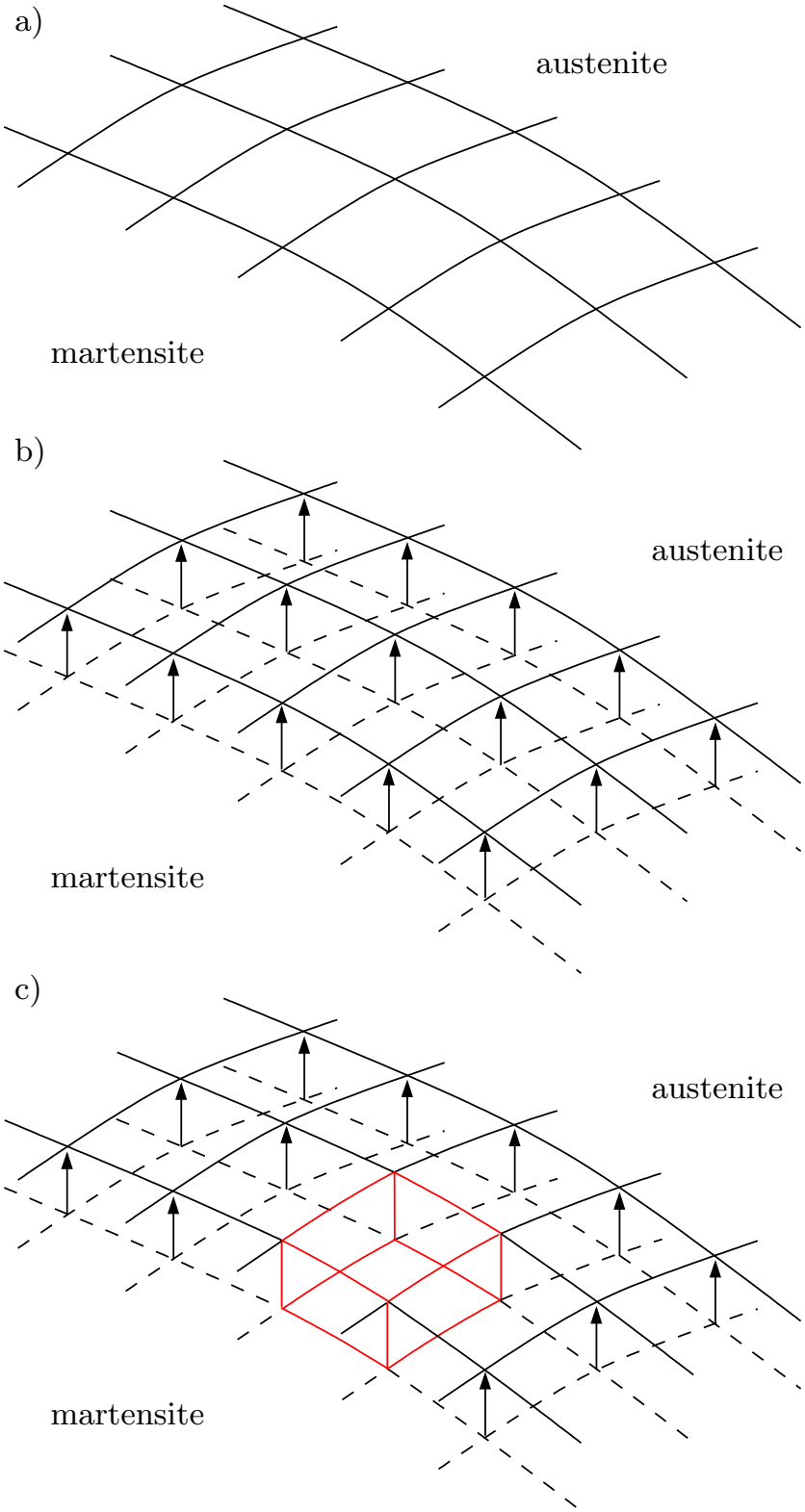

Figure 4.14: Construction of a volumetric element.
a) Interfacial mesh at the start of time step.
b) Interfacial mesh at the end of time step.
c) Construction of a volume element by use of a new and an old face.

4.3.3 Interfacial movement

The scheme proposed here is based on the gradient-weighted moving finite element (GWMFE) approach by Miller et al. (Carlson & Miller (1998a,b); Kuprat (2000)). However, due to the interaction with the BEM, the coupled problem is solved in the approach presented here. Furthermore, the remeshing due to distortion of the mesh and restrictions due to the morphology are taken into the evolution step and not handled by a separate software as proposed by Kuprat (2000).

The position of a point on the interface is denoted by $\mathbf{x}_\Lambda$. It can be described by an additive decomposition

$$\mathbf{x}_\Lambda = \mathbf{r} + \mathbf{u}, \tag{4.50}$$

where $\mathbf{u}$ describes the displacement of the point due to the deformation of the body. The remainder $\mathbf{r}$ stems from the movement of the phase boundary. It is assumed that for the description of the interfacial movement, the term $\mathbf{r}$ is sufficient to describe its position. This can be achieved in two ways:

- $\mathbf{u} \ll \mathbf{r}$, thus the error introduced by $\mathbf{u}$ can be neglected, or
- the description is a Lagrangian description, thus the position of a material point is the referential position $\mathbf{X}$ which does not change.

As the description is restricted to small deformation measures due to the capabilities of the BEM-package used, the first option is sufficient for the remainder of the section. However, a description in the referential configuration would be highly desirable (Foerster & Kuhn (1993), Köhler (1999)). Let each boundary $\partial\mathcal{R}^\alpha$ of a subregion $\mathcal{R}^\alpha$ of the body $\mathcal{B}$ be discretized by a mesh of nodes $\mathscr{J}^\alpha$, and let $\mathscr{F}^{\alpha\beta} \subset \mathscr{J}^\alpha$ be the nodes on $\Lambda^{\alpha\beta}$. The mesh is chosen such that the nodes on the interfaces between regions coincide, i.e. $\mathscr{F}^{\alpha\beta} = \mathscr{F}^{\beta\alpha}$ (cf. figure 4.15). Meshes constituted by $\mathscr{J}^\alpha$ are used for the solution of the boundary element problem described in section 4.3.2.2 whereas the mesh described by the nodes $\mathscr{F}^{\alpha\beta}$ are used to describe the evolution of the interface $\Lambda^{\alpha\beta}$ (or $\Lambda^{\beta\alpha}$). Again, to simplify the notation, the movement of a single interface within a body is considered, i.e. nodes on the interface are denoted by $\mathscr{F}$.

The movement of the interfacial nodes $\dot{\mathbf{r}}$ is split into a normal and a tangential part, i.e.

$$\dot{\mathbf{r}} = \mathbf{n}\, U + \mathbf{n}^\perp\, U^\perp \tag{4.51}$$

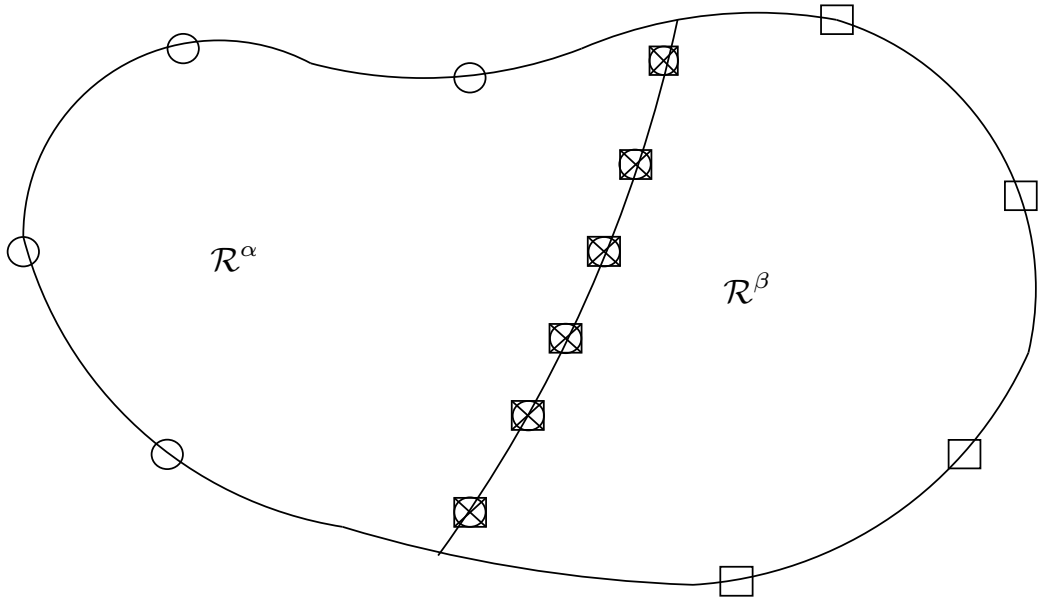

Figure 4.15: Set of nodes, region α with set $\mathscr{J}^{\alpha}$ circled, region β with set $\mathscr{J}^{\beta}$ boxed, interface with set $\mathscr{F}^{\alpha\beta}$ crossed.

where $\mathbf{n} \cdot \mathbf{n}^{\perp} = 0$ and $U^{\perp}$ denotes the tangential velocity of the interfacial node under consideration. It is important to note that $U^{\perp}$ is not physically founded. It is added to avoid a degeneration of the mesh or to satisfy restrictions imposed on the movement of the nodes, e.g. on the boundary of the body $\mathcal{B}$. It may not change the results obtained providing that the numerical solution converges to the physical solution of the system. However, the use of this term is of vital importance as degenerated elements have a tremendous influence on the accuracy the numerical solution.

4.3.3.1 Weak form

The derivation of the weak form of the problem follows a Bubnov-Galerkin approach. The use of a weak form greatly simplifies the treatment of boundaries and edges (Simha & Bhattacharya (1999, 2000)). By combination of the strong form of the governing differential equation (4.33)

$$U = c\, \mathbf{n} \cdot [\boldsymbol{\mu}] \cdot \mathbf{n} \tag{4.52}$$

with the description of the nodal positions on the interface (4.51)

$$\dot{\mathbf{r}} = \mathbf{n}\, U + \mathbf{n}^{\perp}\, U^{\perp} \tag{4.53}$$

one may, after premultiplication by a weighting function $\mathbf{r}^*$, obtain the weak form after integration over the interface

$$\int_{\Lambda} \left\{ \mathbf{r}^* \cdot \dot{\mathbf{r}} - c\,(\mathbf{r}^* \cdot \mathbf{n})\,(\mathbf{n} \cdot [\boldsymbol{\mu}] \cdot \mathbf{n}) - \mathbf{r}^* \cdot \mathbf{n}^{\perp}\, U^{\perp} \right\} \mathrm{d}A - \hat{\mathscr{B}}^{P} = 0. \tag{4.54}$$

The term $\hat{\mathscr{B}}^{P}$ is an additional penalty term introduced in order to satisfy constraints on the movement of the interfacial nodes or to avoid excessive mesh distortion. It is described in detail below. Identifying the terms

$$\hat{\mathscr{B}}^{M} = \int_{\Lambda} \mathbf{r}^* \cdot \dot{\mathbf{r}}\, \mathrm{d}A \tag{4.55}$$

$$\hat{\mathscr{B}}^{FN} = \int_{\Lambda} c\,(\mathbf{r}^* \cdot \mathbf{n})\,(\mathbf{n} \cdot [\boldsymbol{\mu}] \cdot \mathbf{n})\, \mathrm{d}A \tag{4.56}$$

$$\hat{\mathscr{B}}^{FT} = \int_{\Lambda} \mathbf{r}^* \cdot \mathbf{n}^{\perp}\, U^{\perp}\, \mathrm{d}A, \tag{4.57}$$

one may write relation (4.54) as

$$\hat{\mathscr{B}}^{M} - \hat{\mathscr{B}}^{FN} - \hat{\mathscr{B}}^{FT} - \hat{\mathscr{B}}^{P} = 0. \tag{4.58}$$

$\mathbf{r}$ is approximated by

$$\mathbf{r}^h(\mathbf{x}, t) = \sum_{I \in \mathscr{F}} \mathrm{N}_I(\mathbf{x})\, \mathbf{p}_I(t), \tag{4.59}$$

where $\mathbf{N}_I(\mathbf{x})$ are shape functions provided by the boundary element system. Equivalently, for the test functions $\mathbf{r}^*$, relation

$$\mathbf{r}^*(\mathbf{x}, t) = \sum_{I \in \mathscr{F}} \mathrm{N}_I(\mathbf{x})\, \mathbf{p}^*_I(t) \tag{4.60}$$

holds. $\mathbf{p}_I(t)$ and $\mathbf{p}_I^*(t)$ can be interpreted as nodal values, i.e. nodal positions of the interface. Considering that the choice of $\mathbf{r}^*$ is arbitrary, one may find a relation which satisfies (4.58) to be

$$\mathscr{B}^M - \mathscr{B}^{FN} - \mathscr{B}^{FT} - \mathscr{B}^P = 0. \tag{4.61}$$

The different terms occurring can be expressed as

$$\mathscr{B}^M = \mathbf{M}^N \, \dot{\mathbf{p}}, \tag{4.62}$$

where $\mathbf{M}^N = \{M_{IJ}\}$, $\mathbf{p} = \{\mathbf{p}_J\}$, and

$$M_{IJ} = \int_\Lambda \mathbf{N}_I \cdot \mathbf{N}_J \, \mathrm{d}A. \tag{4.63}$$

The term $\mathscr{B}^{FN}$ can be expressed as

$$\mathscr{B}^{FN} = \mathbf{f}^{FN}, \tag{4.64}$$

with $\mathbf{f}^{FN} = \{F_I^{FN}\}$ and

$$F_I^{FN} = \int_\Lambda c \, (\mathbf{N}_I \cdot \mathbf{n}) \, (\mathbf{n} \cdot [\boldsymbol{\mu}] \cdot \mathbf{n}) \, \mathrm{d}A. \tag{4.65}$$

Constraints on the motion of the interfacial nodes are incorporated by means of penalty functions. Three different cases, $\mathscr{B}^{P0}$, $\mathscr{B}^{PBC}$, and $\mathscr{B}^{PM}$ leading to

$$\mathscr{B}^P = \mathscr{B}^{P0} + \mathscr{B}^{PBC} + \mathscr{B}^{PM} \tag{4.66}$$

are considered in the following.

- If the nodal movement is not restricted and no special considerations due to mesh distortion are necessary,

$$U^\perp = 0 \tag{4.67}$$

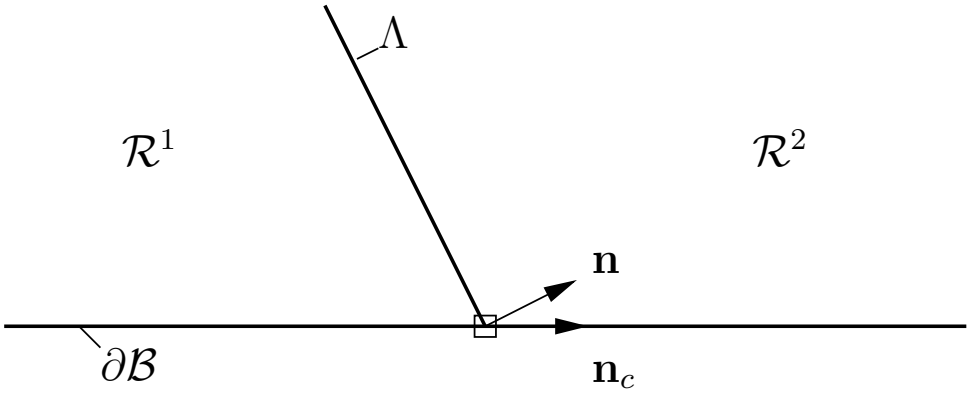

Figure 4.16: Node on the boundary of $\mathcal{B}$, restricted to a movement in direction $\mathbf{n}_c$.

may hold. For this situation, the penalty terms $\mathscr{B}^{PBC}$ and $\mathscr{B}^{PM}$ are set to zero. In general, the term $\mathscr{B}^{P0}$ is chosen as

$$\mathscr{B}^{P0} = \mathbf{f}^{P0} = -\alpha^{P0} \int_{\Lambda} \mathbf{r}^* \cdot \mathbf{n}^{\perp} U^{\perp} \, \mathrm{d}A, \tag{4.68}$$

where $\alpha^{P0} = 1$, which ensures the validity of condition (4.67) in the weak sense.

- Constraints on the nodal movement due to the morphology of the body $\mathcal{B}$ are incorporated by means of $\mathscr{B}^{PBC}$. Let for the node with the spatial position $\mathbf{r}_c$ exist a constraint on the nodal movement, a term

$$\mathscr{B}^{PBC} = \alpha^{PBC} \int_{\Lambda} \mathbf{r}^* \cdot \dot{\mathbf{r}}_c \, \delta(\mathbf{r} - \mathbf{r}_c) \, \mathrm{d}A \tag{4.69}$$

with the penalty factor $\alpha^{PBC} \gg 1$ is added. The example depicted in figure 4.16 illustrates the determination of $\dot{\mathbf{r}}_c$: for the node depicted, the movement $\dot{\mathbf{r}}$ may only be coaxial to $\mathbf{n}_c$. Thus,

$$\dot{\mathbf{r}} = \mathbf{n}_c \cdot (\mathbf{n}_c \cdot \dot{\mathbf{r}}) \tag{4.70}$$

must hold. Introducing the projection tensor $\mathbf{P}_c = \mathbf{1} - \mathbf{n}_c \otimes \mathbf{n}_c$, one may express the requirement on the movement as

$$\dot{\mathbf{r}}_c = \mathbf{P}_c \cdot \dot{\mathbf{r}} = \mathbf{0}. \tag{4.71}$$

Using again the approximations (4.59) and (4.60), equations (4.69) and (4.71) yield

$$\mathscr{B}^{PBC} = \mathbf{M}^{PBC}\dot{\mathbf{p}} \tag{4.72}$$

with $\mathbf{M}^{PBC} = \{M_{IJ}^{PBC}\}$ and

$$M_{IJ}^{PBC} = \alpha^{PBC} \int_{\Lambda} \mathbf{N}_I \cdot \mathbf{P}_c \cdot \mathbf{N}_J \, \delta(\mathbf{r} - \mathbf{r}_c) \, \mathrm{d}A. \tag{4.73}$$

The penalty α^{PBC} must be large enough to ensure approximate fulfillment of the restrictions imposed and small enough to avoid badly conditioned matrices. For now, $\alpha^{PBC} = 10^3$ is chosen, however more extensive studies might be necessary related to the choice of the penalty.

- If severe mesh distortion, leading to a badly conditioned matrix $\mathbf{M}^N$, may be the result of the current time step, additional terms might be included via $\mathscr{B}^{PM}$. As this is done due to purely numerical reasons, it is heavily coupled to the choice of the integration scheme employed. Furthermore, the constraint should not be formulated in terms of the current position $\mathbf{p}(t)$ or its change $\dot{\mathbf{p}}$, but in terms of the position at the end of the current time step $\mathbf{p}(t+\delta t)$. Possible choices are e.g. a penalty employed when a the ratio between height and width of the elements would get too large.

The combination of the components leads to

$$\mathbf{M}\,\dot{\mathbf{p}} = \mathbf{f} \tag{4.74}$$

with

$$\mathbf{M} = \mathbf{M}^N + \mathbf{M}^{PBC} \tag{4.75}$$

and

$$\mathbf{f} = \mathbf{f}^{FN} + \mathbf{f}^{P0}. \tag{4.76}$$

This equation has to be integrated in time in order to yield the solution. It is noteworthy that $\mathbf{M}$ and $\mathbf{f}$ are dependent on the solution $\mathbf{p}$.

4.3.3.2 Evaluation of M and f

The terms $\mathbf{M}^{PBC}$ and $\mathbf{f}^{P0}$ pose no special problems during the course of the evaluation of (4.75) and (4.76). $\mathbf{M}^N$ and $\mathbf{f}^{FN}$ are determined by evaluation of the surface integrals over the interface Λ. For $\mathbf{f}^{FN}$, integration has to be carried out explicitly as the term resulting from the driving force of the movement of the interface varies. The surface integration $\mathbf{M}^N$ only depends on the geometry of the interface. Thus, an explicit integration is not necessary and the element contribution to the global matrix $\mathbf{M}^N$ can be evaluated in terms of nodal positions of the elements. Further analyzing the structure of $\mathbf{M}^N$, it is obvious that the evaluation of $\mathbf{M}^N$ follows the same procedures as the evaluation of the mass matrix used in transient finite element analysis. However, a so called "lumped mass-matrix" approach is often employed there. The use of this approach within the application presented here would lead to large inaccuracies as explained by the following example.

The evolution of an interface consisting of a single element in a two dimensional case is considered. The position on the interface is described by a variable η with $-1 \leq \eta \leq 1$. Initially, the interface may be at the position $r(\eta) = 0$. As depicted in figure 4.17, the driving force for the movement of the interface $U = c\,\mathbf{n} \cdot [\boldsymbol{\mu}] \cdot \mathbf{n}$ may be described by

$$U = \begin{cases} k\,(\eta + 1) & \text{if } -1 \leq \eta \leq 1 \\ 0 & \text{otherwise.} \end{cases} \tag{4.77}$$

Denoting the nodal positions by $p_I = r(\eta = -1)$ and $p_{II} = r(\eta = 1)$, they can be grouped into the vector $\mathbf{p} = (p_I, p_{II})^T$. Furthermore, the use of linear shape functions is assumed, i.e.

$$N_I(\eta) = \begin{cases} \dfrac{1}{2}(1 - \eta) & \text{if } I = 1 \\ \dfrac{1}{2}(\eta + 1) & \text{if } I = 2. \end{cases} \tag{4.78}$$

Evaluating only the part due to the normal movement of the interface, the vector $\mathbf{f}$ can be shown to be

$$\mathbf{f} = \int_{-1}^{1} N_I(\eta) U(\eta)\,\mathrm{d}\eta = \int_{-1}^{1} N_I(\eta) k(\eta + 1)\,\mathrm{d}\eta = \frac{k}{3} \begin{pmatrix} 2 \\ 4 \end{pmatrix}. \tag{4.79}$$

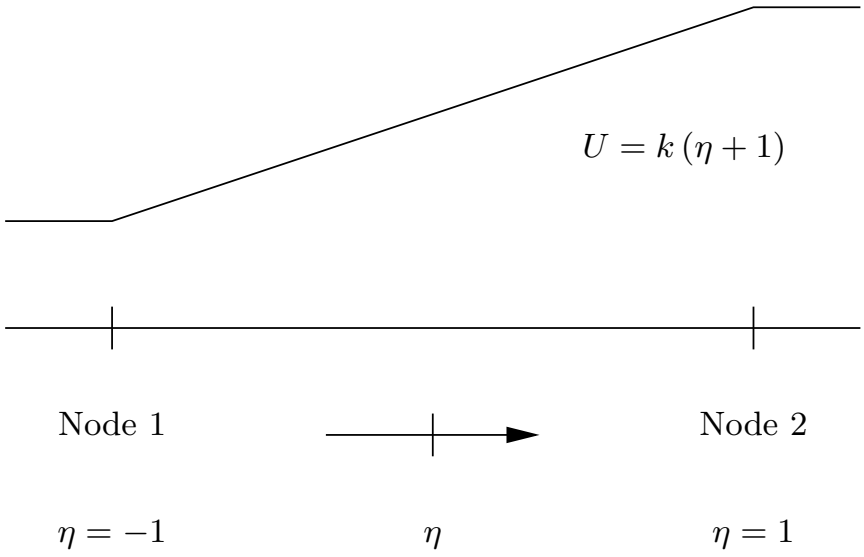

Figure 4.17: Driving force and expected movement for the example from section 4.3.3.2

The evaluation of $\mathbf{M}$ yields

$$\mathbf{M} = \int_{-1}^{1} N_I(\eta) N_J(\eta)\,\mathrm{d}\eta = \frac{1}{3}\begin{pmatrix} 2 & 1 \\ 1 & 2 \end{pmatrix}. \tag{4.80}$$

Solving $\mathbf{M}\,\Delta\mathbf{p} = \mathbf{f}$ for the unknown $\Delta\mathbf{p}$ leads to

$$\Delta\mathbf{p} = k\begin{pmatrix} 0 \\ 2 \end{pmatrix} \tag{4.81}$$

which coincides with the analytical solution. Use of the lumped matrix

$$\mathbf{M} = \begin{pmatrix} 1 & 0 \\ 0 & 1 \end{pmatrix} \tag{4.82}$$

yields

$$\Delta\mathbf{p} = k\,\frac{1}{3}\begin{pmatrix} 2 \\ 4 \end{pmatrix}. \tag{4.83}$$

Thus, the lumped approach would lead to a movement of Node 1 even though the driving force at this node is zero. As the purpose of this description is an

accurate description of the movement of the phase boundary, the use of the lumped approach is ruled out.

4.3.3.3 Time integration scheme

The purpose of the time integration scheme is to advance the problem solution in time and provide the new position of the interface at that time instance. As mentioned before, both $\mathbf{M}$ and $\mathbf{f}$ depend on the solution $\mathbf{p}$. Furthermore, the solution of the bulk problem also influences and depends on the interfacial step. Thus, stability properties are difficult to analyze. In order to at least partially resolve this problem, a numerically fast, but less stable and a more stable but computationally more expensive integration scheme for $\mathbf{p}$ are developed in the following. Both feature a constant time step Δt and start at time $t = t_0$. The denotations $\mathbf{p}_k = \mathbf{p}(t = t_0 + k\,\Delta t)$, $\mathbf{M}_k = \mathbf{M}(\mathbf{p}_k)$, and $\mathbf{f}_k = \mathbf{f}(\mathbf{p}_k)$ are used.

4.3.3.3a Staggered Integration

An explicit, staggered scheme where the descriptions of section 4.3.3 and 4.3.2.2 are completely decoupled is featured here. The term $\dot{\mathbf{p}}$ is approximated by

$$\dot{\mathbf{p}}(t) \approx \frac{\mathbf{p}(t + \Delta t) - \mathbf{p}(t)}{\Delta t}. \tag{4.84}$$

The algorithm can be described as follows:

(E1) At time $t = t_0$, the position of the interface is known. The current position $\mathbf{p}_k$ is set to $\mathbf{p}_k \leftarrow \mathbf{p}_0$ (and $k \leftarrow 0$).

(E2) (*bulk step*) Based on the position of the interface $\mathbf{p}_k$, the state at the interface is determined employing the boundary element scheme described in section 4.3.2.2. The local driving force for the movement of the interface and the local velocity of the interface can be determined.

(E3) (*interface step*) The matrix $\mathbf{M}_k$ and the vector $\mathbf{f}_k$ can be determined be means of (4.75) and (4.76), the next interfacial position can be determined using (4.74) and (4.84) such that

$$\mathbf{p}_{k+1} = \mathbf{p}_k + \Delta t\, \mathbf{M}_k^{-1}\, \mathbf{f}_k. \tag{4.85}$$

(E4) The solution is advanced by setting $k \leftarrow k + 1$ and the scheme proceeds with step (E2).

This scheme bears certain advantages, as e.g.

- the matrix $\mathbf{M}_k$ and the vector $\mathbf{f}_k$ have to be evaluated only once for each time step,
- only one inversion of the matrix $\mathbf{M}_k$ is necessary for one time step,
- the time step Δt can be easily changed from one step to another.

Possible problems might occur when

- a stepsize Δt is chosen too large resulting in instabilities,
- the solution does not converge as the scheme is a staggered scheme.

4.3.3.3b Predictor-Corrector Integration

An important aspect related to $\mathbf{M}$ and $\mathbf{f}$ is that they are in general nonlinear functions of the interfacial position $\mathbf{p}$. Thus, the explicit scheme proposed above might lead to a numerical solution which deviates significantly from the true solution due the staggered scheme. Furthermore, the stability properties are difficult to investigate. In order to relax this situation, a predictor corrector scheme which finds the solution considering both the interfacial step and the bulk step is proposed here. The scheme is based on the solution of equation (4.74) at time step $k+1$

$$\mathbf{M}_{k+1}\,\dot{\mathbf{p}}_{k+1} = \mathbf{f}_{k+1} \tag{4.86}$$

and a slightly different approximation

$$\dot{\mathbf{p}}(t) \approx \frac{\mathbf{p}(t) - \mathbf{p}(t-\Delta t)}{\Delta t}. \tag{4.87}$$

The algorithm can be described as follows:

(PC1) As for the explicit scheme, for $t = t_0$ the current position $\mathbf{p}_k$ is set to $\mathbf{p}_k = \mathbf{p}_0$.

(PC2) As in step (E2) of the explicit method, $\mathbf{M}_k$ and $\mathbf{f}_k$ are calculated.

(PC3) A predictor $\tilde{\mathbf{p}}_{k+1}$ for $\mathbf{p}_{k+1}$ is calculated by using

$$\tilde{\mathbf{p}}_{k+1} = \mathbf{p}_k + \Delta t\, \mathbf{M}_k^{-1}\, \mathbf{f}_k. \tag{4.88}$$

(PC4) Using the predictor $\tilde{\mathbf{p}}_{k+1}$ of the nodal positions on the interface, predictor values for the matrix $\tilde{\mathbf{M}}_{k+1} = \mathbf{M}(\tilde{\mathbf{p}}_{k+1})$ and $\tilde{\mathbf{f}}_{k+1} = \mathbf{f}(\tilde{\mathbf{p}}_{k+1})$ are determined.

(PC5) Using these, a corrector value

$$\hat{\mathbf{p}}_{k+1} = \mathbf{p}_k + \Delta t\, \tilde{\mathbf{M}}_{k+1}^{-1}\, \tilde{\mathbf{f}}_{k+1} \tag{4.89}$$

is calculated.

(PC6) If $norm(\hat{\mathbf{p}}_{k+1} - \tilde{\mathbf{p}}_{k+1}) > \varepsilon$, where $norm(\bullet)$ denotes an appropriately defined norm and ε a threshold value, $\tilde{\mathbf{p}}_{k+1} \leftarrow \hat{\mathbf{p}}_{k+1}$ and the iteration proceeds with step (PC4). Otherwise, $\mathbf{p}_{k+1} \leftarrow \hat{\mathbf{p}}_{k+1}$, $\mathbf{M}_{k+1} \leftarrow \tilde{\mathbf{M}}_{k+1}$, $\mathbf{f}_{k+1} \leftarrow \tilde{\mathbf{f}}_{k+1}$, and finally $k \leftarrow k+1$ is set and the scheme proceeds with step (PC3).

This scheme avoids the main two shortcomings of the staggered scheme: it avoids the possible deviation due to the uncoupling of the BEM-scheme and the interfacial scheme due to the iteration and a higher stability is achieved as the correction steps are implicit. However, unconditional stability can not be achieved due to the nonlinear nature of the problem.

4.3.4 Remeshing strategies

As the nodes which are common to the outer surface and the interface move with ongoing phase transformation, a remeshing strategy has to be used. As a first approach, two strategies are discussed (cf. figure 4.18):

a) The first approach is based on the idea that the distortion of the elements should be kept as small as possible. Only the nodes on the outer surface which also belong to the interface are moved. As long as these nodes do not destroy the elements on the outer surface they belong to, i.e. the Jacobian of the element becomes negative, nothing is done. If the element collapses, a remeshing step for the abjected surfacial elements is performed: the node which moved to far will be a node of the element

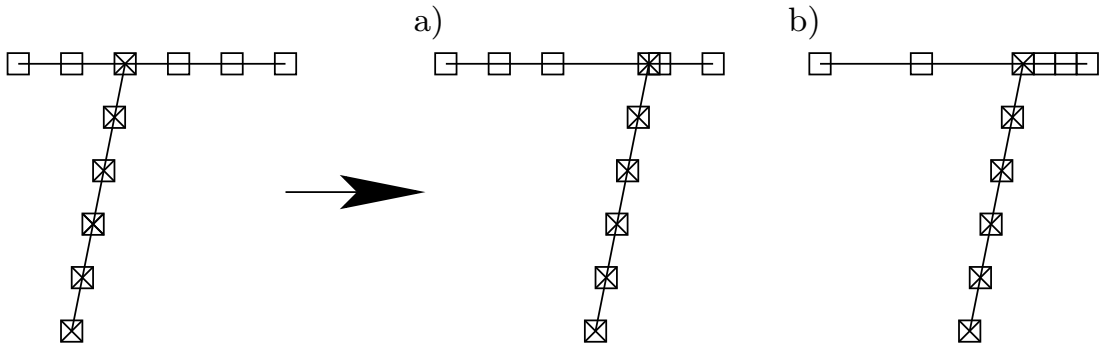

Figure 4.18: Discussed remeshing strategies. Interfacial nodes are crossed. a) Reconnecting b) Stretching

it moved into, the free node will then be a node of the element which lacks a node. This procedure has been implemented and tested. It yields numerical instabilities when the nodes are very close to each other. This situation can not be avoided as the nodal position must reach a point where the Jacobian becomes negative. More elaborate remeshing conditions based on this scheme might be considered, but those require thorough investigations. As the main scope is not on the choice of remeshing strategies, this approach will not be used further.

b) A simple proportional stretch of the elements on the outer surface of the body is performed. This simple approach bears certain disadvantages: for complex geometries the stretching is difficult to determine and the elements may become ill conditioned due to the stretching applied. However, for the studies done here, this approach has proven to be sufficient to perform simulation up to a very high percentage of martensite.

4.3.5 Convergence studies

In order to study the convergence properties of the proposed approach, a simple model is considered as depicted in figure 4.19. The outer shape of the model is a rectangular block which is separated by a transformation front dividing the block into two halves of the same size. Within the martensitic region, a homogeneous eigenstrain is assumed consistent with the crystallographic theory of martensite explained before. At the lateral faces of the block, boundary conditions are applied to lead to a constant face load on those faces. Due to

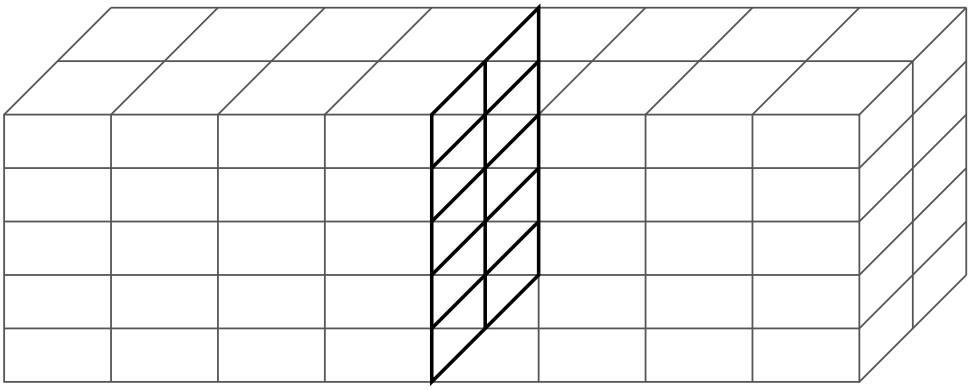

Figure 4.19: Rectangular block used for convergence studies. The mesh drawn is only symbolic, nonvisible mesh on the body surface not drawn, interfacial mesh drawn with thicker lines.

the load applied, the propagation of the transformation front is initiated. The influence of the time step and the size and ratio of the edge lengths on the accuracy of the solution is investigated in the following.

The convergence studies concerning the number of nodes used for the solution consider a different number of nodes on the transformation interface. The highest number of nodes used was 176, defining the results obtained with this number of nodes as true solution of the problem. The error is defined as

$$err^{\alpha} = \sum_{I} \left(u_I^{\alpha} - u_I^{176} \right)^2 \tag{4.90}$$

where u_I denotes the z-position of the interfacial node I at the end of the test and the superscript the number of nodes on the interface. The summation is performed over all nodes with common x and y coordinates for all meshes, which are the corner nodes. The result depicted in figure 4.20 exhibits almost linear convergence.

If the number of time steps, using the same mesh, is varied, the error measure

$$err^{\beta} = \sum_{I} \left(u_I^{\beta} - u_I^{2000} \right)^2 \tag{4.91}$$

is used where u_I^{β} denotes the result of the test with β time steps. The maximum number of time steps used is 2000, defining this result as the true solution.

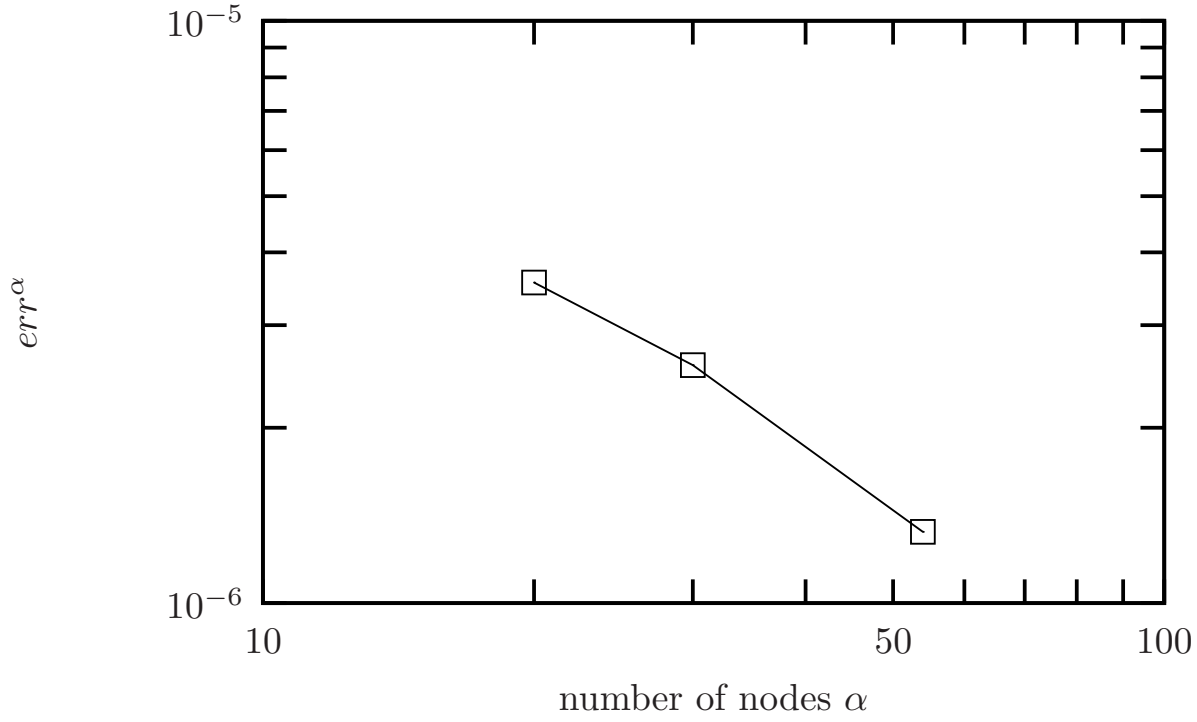

Figure 4.20: Convergence study, different number of nodes.

The result is depicted in figure 4.21, linear convergence can be observed again. The predictor-corrector scheme is not presented here as its use can not be recommended for such simple problems. The number of time steps is not the governing factor but rather the number of iterations for a given required accuracy. A comparison of the staggered scheme with the predictor-corrector scheme will be presented in the following section.

4.4 Example – Phase transition in a single crystal

To show the abilities of the presented approach, an example as depicted in figure 4.22 is considered. It can be interpreted as the model of a single crystal in which the transformation proceeded up to the half of the domain under consideration. The reasons for the existence of the martensitic domain are not part of the simulation. This example is very similar to the one considered in the preceding section, in fact only the inhomogeneity in the austenitic phase is added. In figure 4.22, the region pointing towards the observer is the austenitic region whereas the region in the back is the martensitic region. The load is

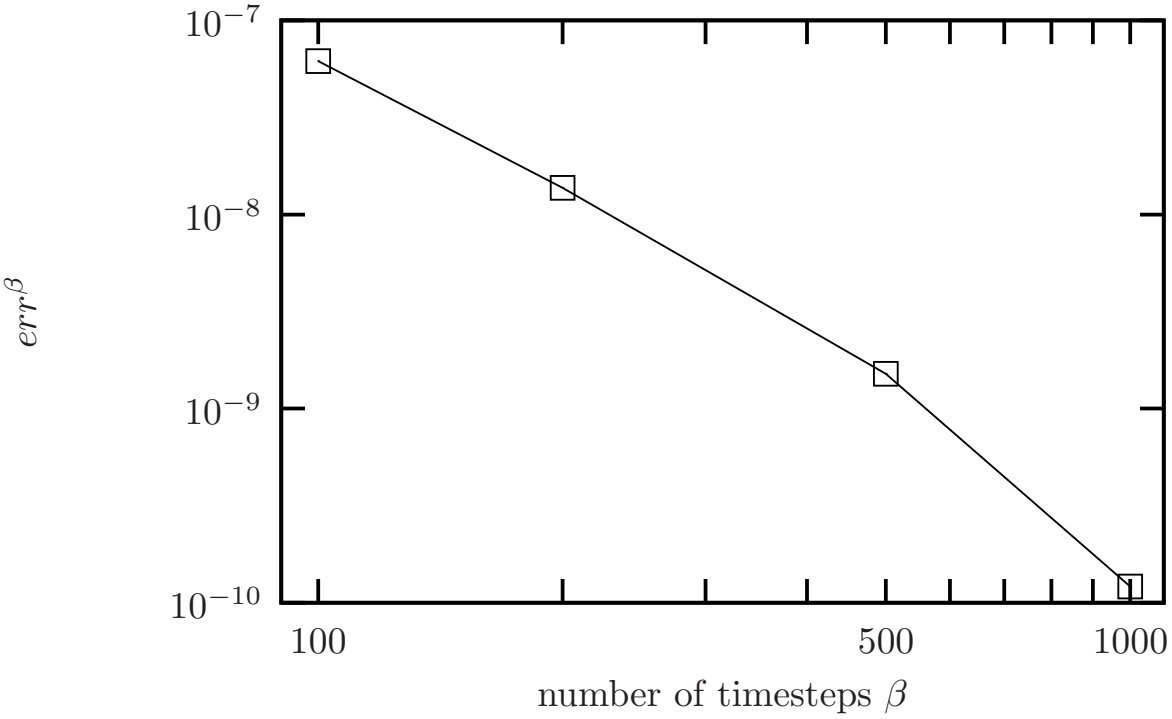

Figure 4.21: Convergence study, different number of time steps for staggered scheme.

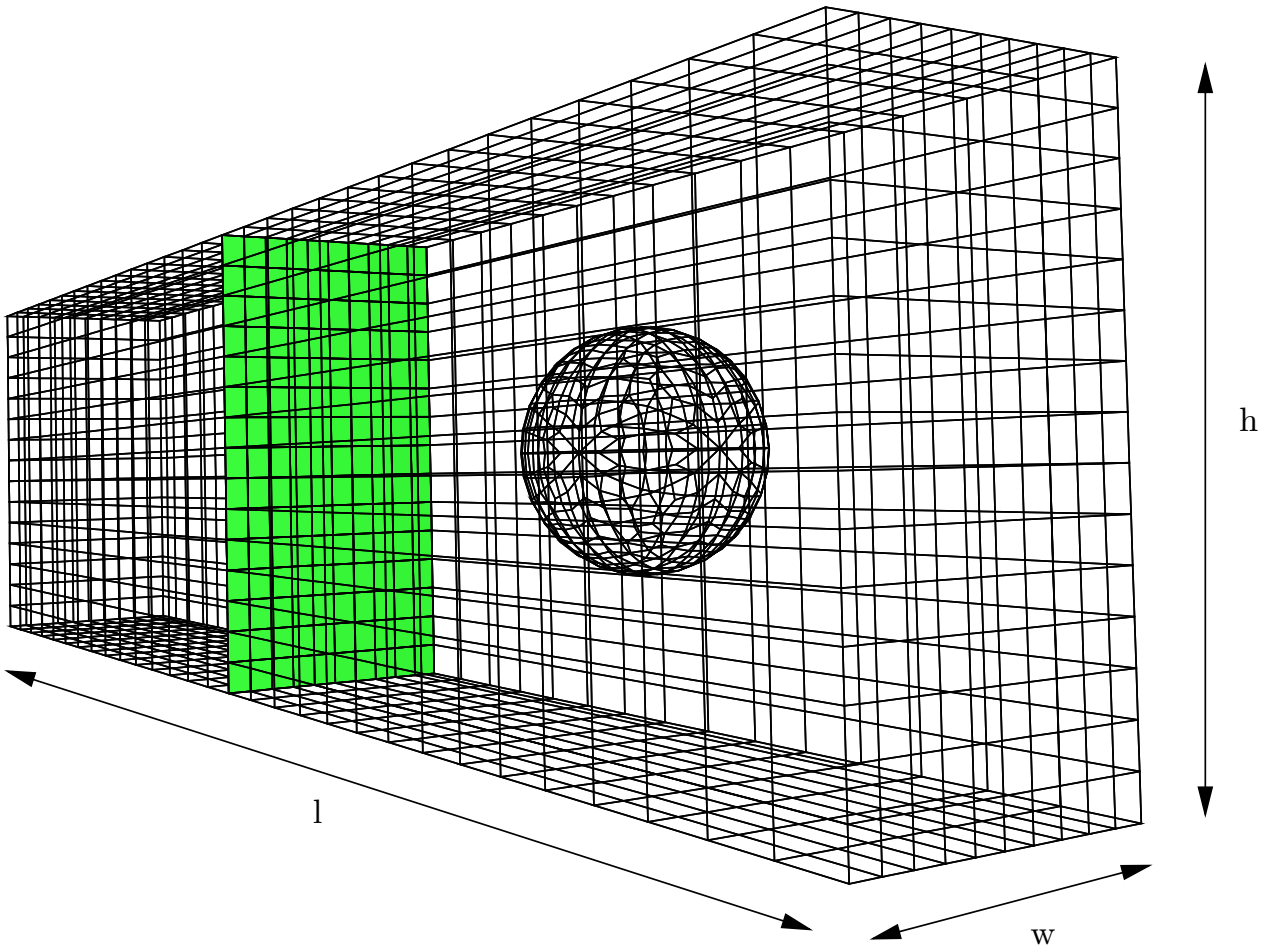

Figure 4.22: Discretization used for the studies in this section. In the figure, the dimensions are $w = 1$, $h = 2$, $l = 8$, the diameter of the sphere is $d = 0.8$.

applied at the nodes on the frontal surface (defined by its dimensions width w and height h) to yield a homogeneous traction on this surface. For a problem without inhomogeneity, this setup would lead to a homogeneous stress state within the specimen. A void of diameter d is added at the center of the austenitic phase as the most simple inhomogeneity.

4.4.1 Introductory setup

The geometry for the first setup is chosen as depicted in figure 4.22. The diameter is $d = 0.8$. Furthermore, the traction at the frontal surface is chosen

as[5] $t = 150$. The material parameters are chosen as follows:

E_A	$1 \cdot 10^5$
ν_A	0.25
E_M	$7.2 \cdot 10^4$
ν_M	0.25
c	1.0

The staggered evolution scheme is chosen with a constant stepsize of $\Delta t = 0.1$. The evolution of the transformation front is depicted in figure 4.23. At $t = 0$, the transformation plane starts moving homogeneously with a constant velocity due to the applied stress. Due to the inhomogeneous stress state around the inhomogeneity, the velocity is no longer the same for all points on the transformation surface, thus the plane character of the transformation surface is lost under the influence of the stress state around the inhomogeneity. For the dimensions chosen in this example, a state of equilibrium is reached at approximately $t = 18$ as no further movement of the interface can be detected. The inhomogeneity has not been reached by the transformation surface even though the distance is very small. Thus, the approach described here can not only track the movement of the transition front, but it is also able to calculate equilibrium shapes of the transformation surface when nonhomogeneous stress states within the grain exist.

[5] Units are omitted as the numerical solution is only a proof of concept to show its general ability to investigate the phenomena discussed in the introduction of this chapter qualitatively. A quantitative description can be done based on this approach, but would require a detailed knowledge of the micromechanical morphology and is out of the scope of this contribution.

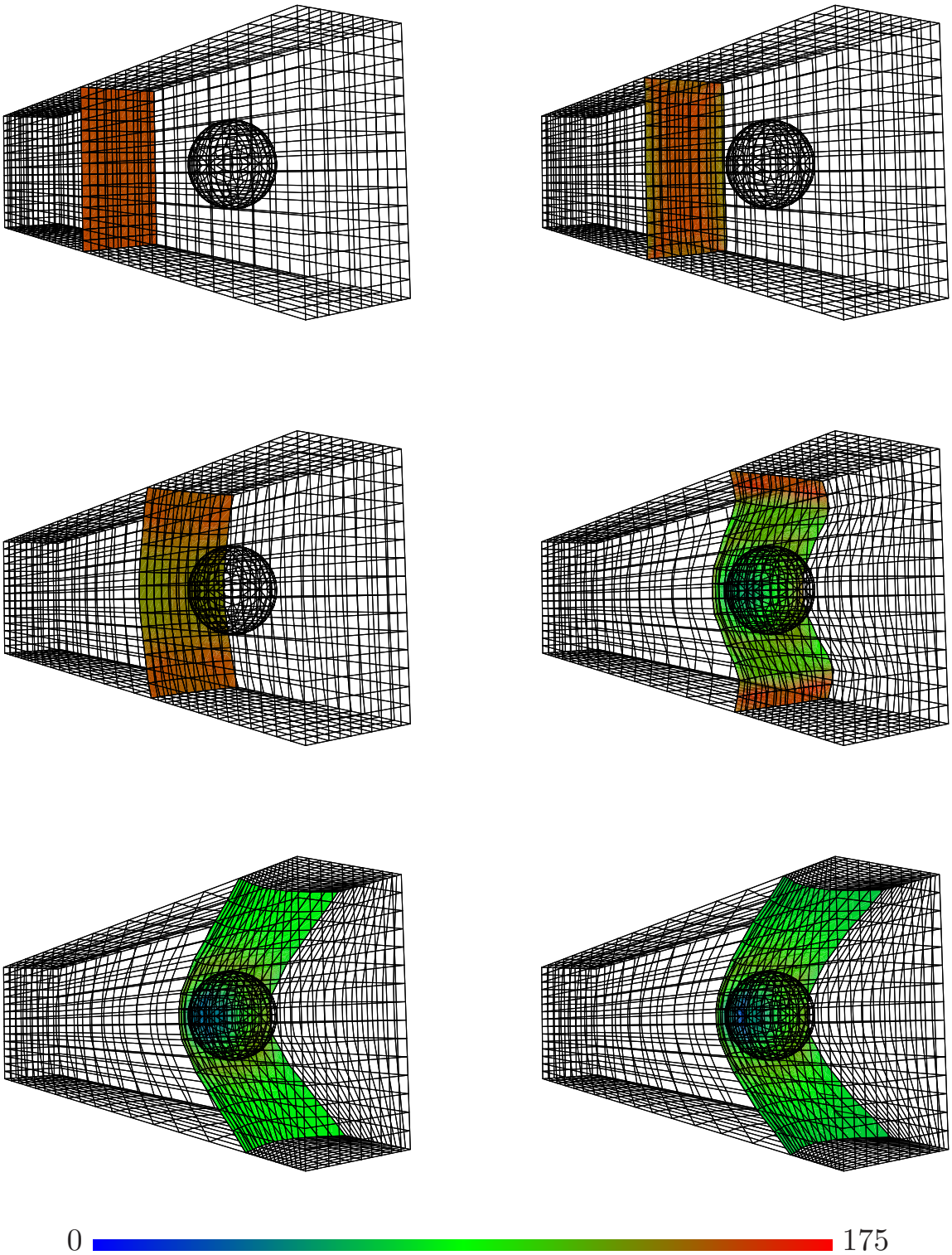

Figure 4.23: Evolution of the transformation plane for time instances $t = 0$, $t = 5$, $t = 10$, $t = 15$, $t = 20$, and $t = 25$ from upper left to lower right picture. Colors represent the value of $|\boldsymbol{\sigma} \cdot \mathbf{n}|$ on the interface.

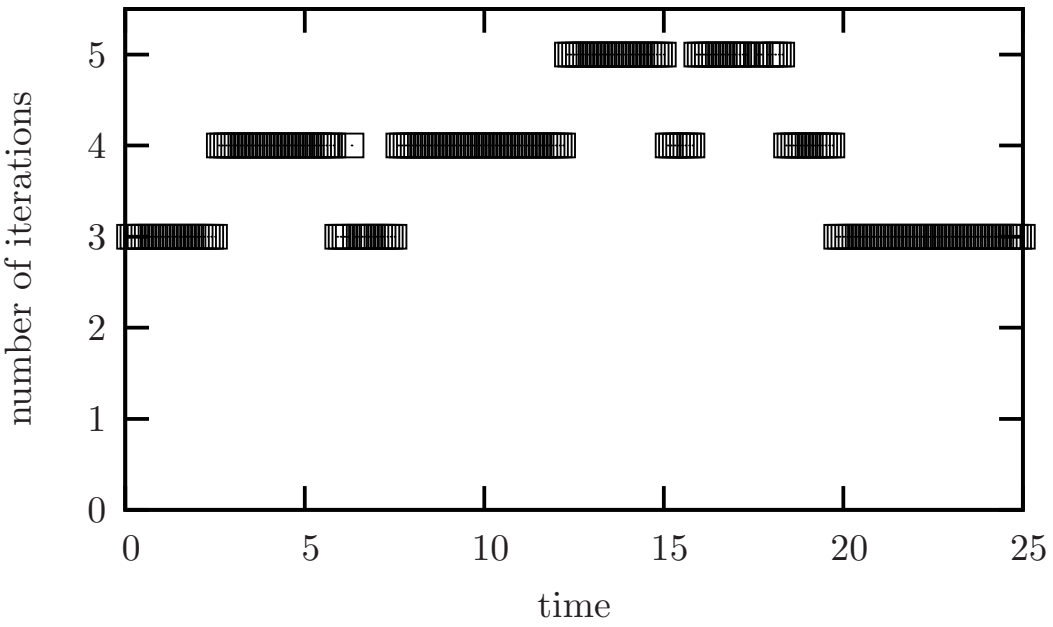

Figure 4.24: Number of iterations including "zeroth" predictor step necessary to reach the error threshold ε.

4.4.2 Integration procedure

To compare the staggered scheme with the predictor corrector scheme, the example presented in the previous section is simulated employing the predictor corrector algorithm described in section 4.3.3.3b. The norm operator introduced in section 4.3.3.3b is $norm(\bullet) = \bullet \cdot \bullet$ where $\bullet$ is a vector. The error measure ε is chosen such that three iterations are necessary including the first initial predictor step during the first phase of the simulation. The term "number of iterations" includes the first predictor step, even though the first step is not an iteration.

For the movement of the plane interface at the beginning of the simulation, the number of iterations is three or four. Keeping in mind that the minimum number of iterations is two, one may conclude that the stepsize is chosen such that it almost yields the accuracy required by the choice of ε. When the transformation front approaches the inhomogeneity and is no longer plane, the number of iterations tends towards five. This high number of iterations is necessary as long as the interface changes its shape. When for $t \approx 18$ the stationary state is reached, the number of iterations drops back to the initial value of three. One may ask why the minimum number of iterations is

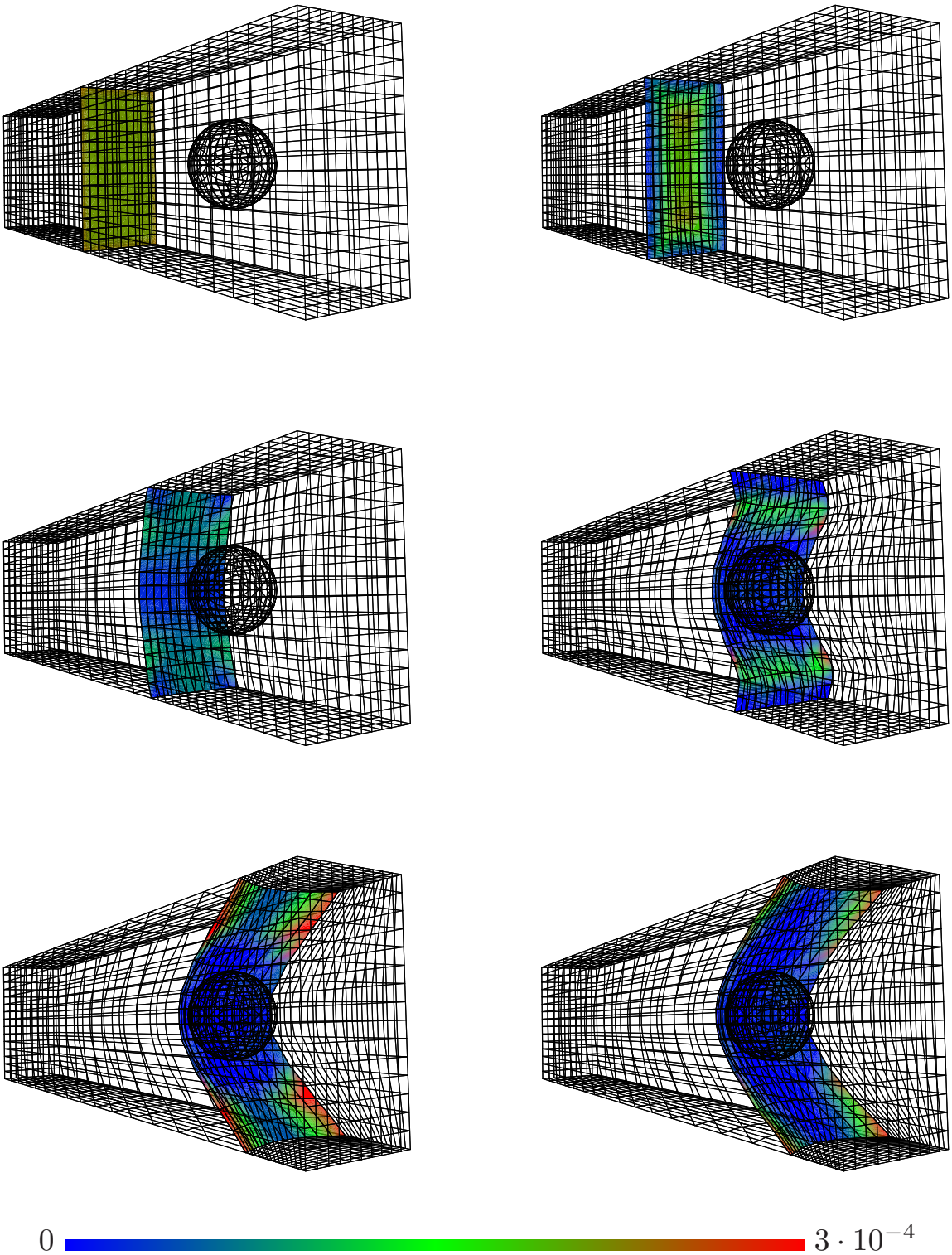

Figure 4.25: Evolution of the transformation plane for time instances $t = 0$, $t = 5$, $t = 10$, $t = 15$, $t = 20$, and $t = 25$ from upper left to lower right picture. Colors represent the value of Δ^{PCST} on the interface.

not reached for this state. It must be noted that the stationary state is not completely stationary. As no threshold is present in the material law which described the movement of the interface (4.3.3), small perturbations of the BEM-Solution, possibly due to numerical errors, lead to a movement of the transformation front. However, after a perturbation, the transformation front returns to the stationary, the equilibrium, shape.

In figure 4.25, the squared difference between the solution of the staggered scheme u_z^{ST} and the predictor corrector scheme u_z^{PD} of the horizontal position of the nodes on the interface $\Delta^{PCST} = (u_z^{PD} - u_z^{ST})^2$ is depicted. The value always remains below $3 \cdot 10^{-4}$. Considering the length scale used in this model, this result can be regarded as a small difference.

4.4.3 Influence of the value of the applied traction

It can be expected that the value of the applied tractions has an influence on the result as the transition front moves faster. However, to justify that the approach is able to capture the behavior observed in a DSC-experiment, it has to be shown that the transformation front would progress past the inclusion for an increased load.

The result for a test with an applied traction of 300 is depicted in figure 4.26. The transformation surface proceeds until it reaches the inhomogeneity, the state which is depicted in figure 4.26[6]. As extensive remeshing operations would be necessary at this point, the simulation is stopped. Those operations are not implemented yet, but are generally possible using the approach proposed. The fact that the transformation surface reached the inhomogeneity indicates that an elevated stress level yields to an ongoing phase transition.

4.4.4 Size effects regarding the inhomogeneity

To investigate the influence of the size of the inhomogeneity a simulation with an inhomogeneity with reduced size is performed. The results are shown in figure 4.27. At $t = 15.2$, the interface reaches the inhomogeneity and the simulation is stopped due to the reasons described in the previous paragraph. The transformation surface is relatively plane, the influence of the inhomogeneity on the state of the transformation front is relatively small, as e.g. the traction

[6]The state depicted for comparison is based on the velocity of the transformation plane observed for the homogeneous case.

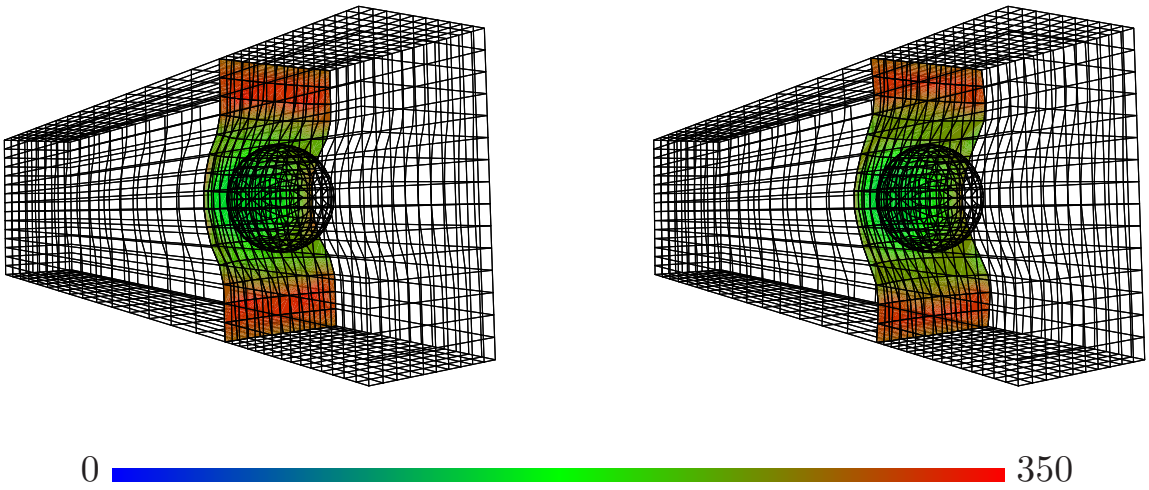

Figure 4.26: State at $t = 0.35$ for an applied stress of 300. For comparison, the state at $t = 1.4$ for the load 150 is depicted right. Colors represent the value of $|\boldsymbol{\sigma} \cdot \mathbf{n}|$ an the interface.

depicted in figure 4.27. A further progress of the transformation front can be expected.

4.5 Summary and outlook

Based on this simple model, some phenomena discussed in the opening could be verified:

- If an inhomogeneity in the austenitic phase exists, the surrounding stress state can stop the progress of the transformation front if the external thermomechanical loads remain constant. This may explain the transition from a one stage to a two stage transformation as in this case, the thermomechanical load on the specimen had to be increased further in order to show a proceeding phase transition.

- The behavior may not be apparent if the size of the inhomogeneity is below a certain size compared to the size of the grain. This corresponds well to the experimental observations as inhomogeneities of different sizes

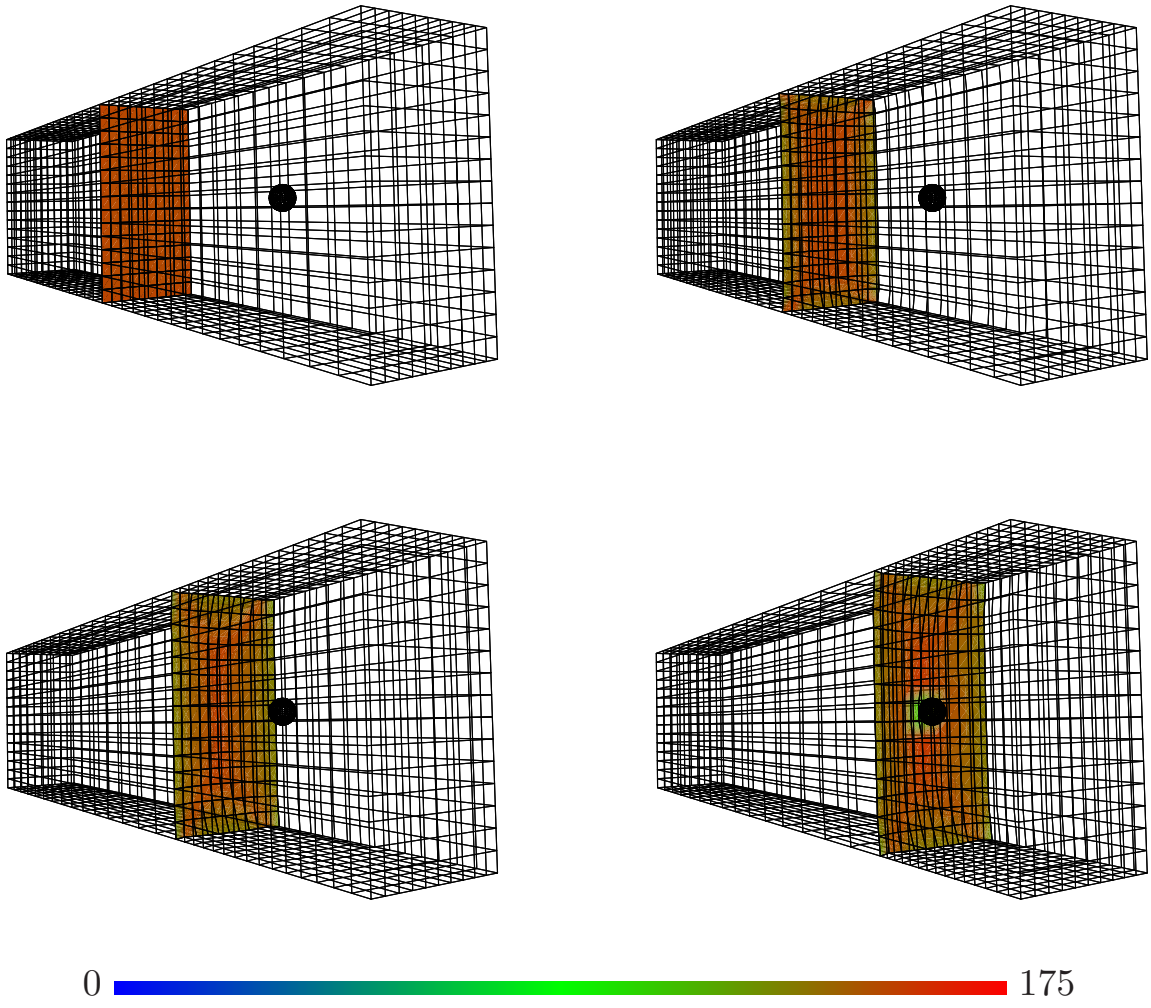

Figure 4.27: Evolution of the transformation plane for time instances $t = 0$, $t = 5$, $t = 10$, and $t = 15$ from upper left to lower right picture with $d = 0.2$. Colors represent the value of $|\boldsymbol{\sigma} \cdot \mathbf{n}|$ an the interface.

are always present in the material. However only inhomogeneities of a considerable size lead to a visible macroscopic effect.

The current implementation is restricted to isothermal processes due to the limitations of the BEM-package. As the phase transition problem is strongly coupled, an extension to cover heat conduction as well is highly desirable.

5 Macroscopic approach

5.1 Motivation and observations – macroscopic view

The approach developed in this chapter focuses, even though meso- or micromechanical observations serve as the motivational base, on a macroscopic description of the material. Thus, in this introductory section, only macroscopically observable phenomena are shown whereas the underlying crystallographic mechanisms are discussed in section 4.1.

The three basic classes categorizing the behavior of SMA also apply to polycrystals. Thus, SMA show pseudoelastic, pseudoplastic and the two way effect. In comparison to single crystals, the transformation strain observed is usually smaller. For single crystals, transformation strains range up 17% whereas for polycrystals only strain up to 7% (Luig et al. (2005)) can be achieved. The behavior strongly depends on the heat treatment used for the material during preparation. To conclude, it must be noted that the observations from the micromechanical, single crystal[1] scale can only be transferred to the macroscopic, polycrystal level to a certain extent. This can be traced back to

- the interaction of the grains,
- grain boundaries induce, from a mechanical viewpoint, inhomogeneities which lead to nonhomogeneous stress states,
- the unique crystallographic orientation of each grain which may range from a completely randomized structure with no distinct orientation to a situation where the orientation of the grains coincides relatively well.

These aspects lead to macroscopically observable phenomena which can not solely be explained on the microscopic level, but stem from the scale transition. Two aspect might be mentioned here:

[1] Even though it is nowadays possible to manufacture single crystals of macroscopic size, in this context the term single crystal shall denote a single crystal within a polycrystal. Thus, the use of the term single crystal corresponds to observations on the microlevel.

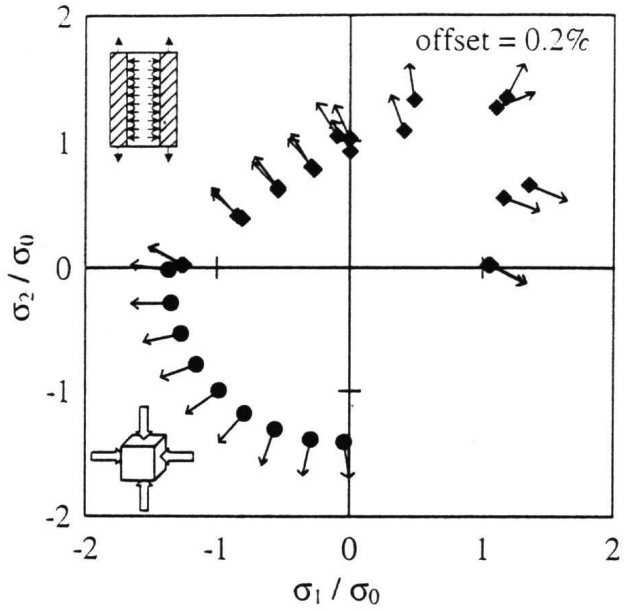

Figure 5.1: Curve characterizing the onset of the phase transition for a CuAlNi-SMA, measured by Lexcellent et al. (2002).

- For multiaxial behavior, the transition from the region where elastic austenite is the only phase present to the region where already martensite is present (the transformation regime) may be characterized, borrowing the term from plasticity even though the effects observed do not primarily stem from plastic deformations, as a yield surface. Such a curve, measured for a CuAlNi-SMA, is depicted in figure 5.1. The shape of the yield limit can not be explained by a J_2-theory based on the value of the applied stress even for a specified temperature. Furthermore, the "normality-rule" frequently used in plasticity does not apply for this behavior in stress space (cf. figure 5.2). The description may even get more complicated when cycles in stress- or strain-space are considered (cf. figure 5.3). Strong cross-effects between the behavior in tension and torsion are present which can not be explained with simple theories adapted from plasticity.

- In figure 5.4, the stress and temperature evolution during a test in simple tension is depicted. For the stress-strain curve, the observed behavior is a typical result for a pseudoelastic material: a linear region where austenite is assumed to be deformed elastically is followed by a plateau where

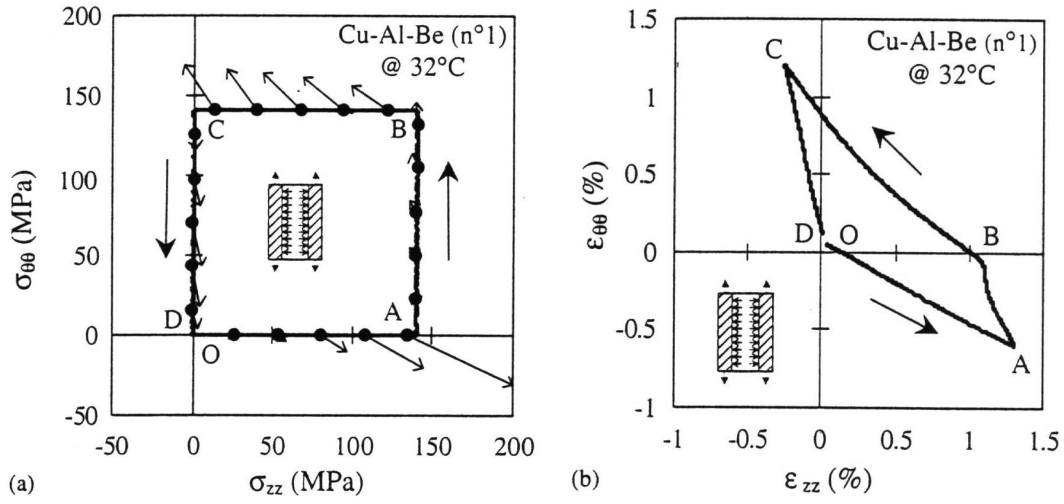

Figure 5.2: Stress-controlled box test. Note that large deviation for $\varepsilon_{\Theta\Theta}$ stems from elastic lateral contraction (Lexcellent et al. (2002)).

the austenite transforms into martensite accompanied by a deformation induced by the phase transition. When the specimen is unloaded, again a stage where the material behaves linearly can be observed, followed by the plateau where the backtransformation occurs. When only austenite is present, the specimen is elastically unloaded until the stress free state is reached. However, the temperature evolution does not conciliate with theoretical considerations. The austenite to martensite transformation is an exothermic process whereas the backtransformation is endothermic. An elastic loading is slightly endothermic due to the piezocaloric coupling. Following these considerations, the temperature would slightly decrease during the first stage of the loading, followed by a sudden temperature increase resulting from the forward transformation. During the first stage of the unloading, a slight temperature increase could be observed due to the piezocaloric coupling followed by a large decrease due to the backtransformation. This kind of behavior can not be observed at all in figure 5.4. During the mechanically linear stage, a temperature increase can be observed. When the plateau is reached, the temperature increase gets even smaller. At the time instance when the specimen is unloaded, the temperature decreases immediately. Again an approximately constant temperature is observed during the plateau-stage. It seems that an exothermal process is present during what is classically considered as

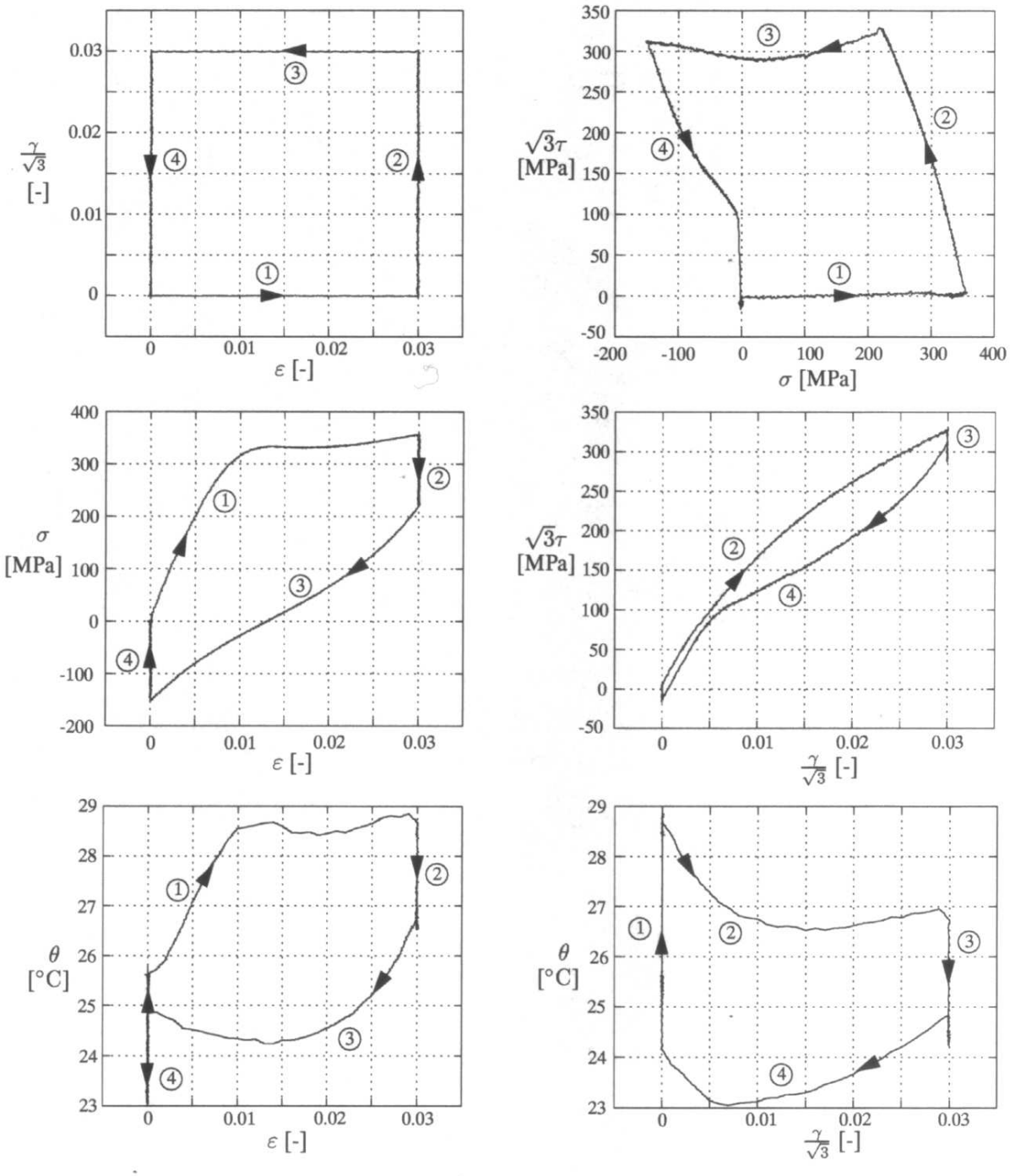

Figure 5.3: Multiaxial test on thin walled tube conducted by Helm (2001).

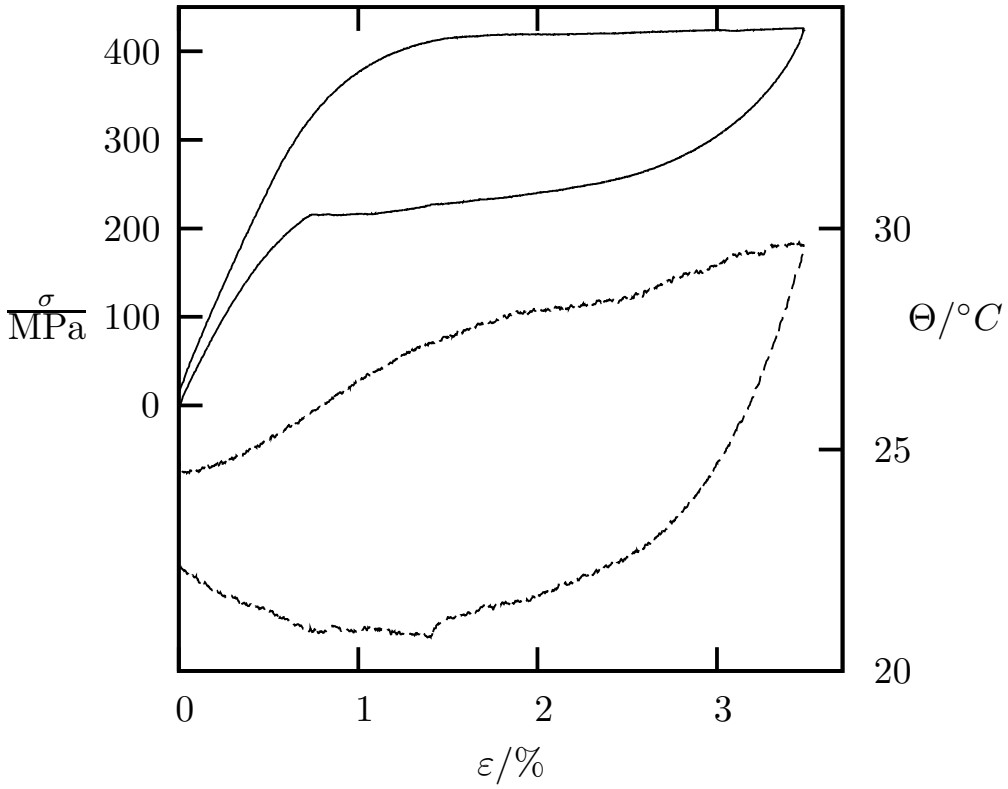

Figure 5.4: Stress σ and temperature Θ for a test in simple tension.

elastic loading of austenite and an endothermal process during what is classically considered as elastic unloading of martensite.

It is important to note that the behavior depicted in figure 5.4 has been observed by Lim, T.J. & McDowell, D.L. (1999) as well. It is also evident in figure 5.3: during stage 1 up to a stress of 300 MPa, a linear relation between stress and strain can be observed whereas the temperature increases drastically. When, still in stage 1, the typical non-linear behavior observed for SMA is present, the temperature is relatively constant. During stage 4, when the load is brought back to zero by removing the shear angle, the temperature increases when, according to common believe, the apparently elastic unloading, takes place. The increase is of a magnitude which can not be explained by the piezocaloric effect. However the heat exchange with the environment is a factor which is difficult to take into consideration.

In order to explain these phenomena, two approaches are proposed: the influence of the R-phase leads to this behavior (R) or the existence of twinned martensite at low stress levels (TM) serves as mechanism behind these phenomena. A further elaboration of these approaches yields the following:

- During the mechanically linear elastic loading, a strong endothermic process is present in the material. Possible reasons for this could be
  - (R) An austenite to R-Phase transition might lead to an endothermic process, as observed in the previous example. However, even though the influence of this type of transformation on the mechanical behavior is small, it would lead to an observable deviation from the linear behavior observed here (cf. Lim, T.J. & McDowell, D.L. (1999)).
  - (TM) An austenite to twinned martensite transition might be present. The local deformation due to the transformation from austenite to martensite is rather small and could easily be accommodated by the surrounding austenitic matrix.
- The second stage, within the classical context, is believed to reflect the transformation from austenite to martensite. Following the proposal above, it might be that
  - (R) The R-phase now transforms to martensite, leading to the release of the latent heat and the macroscopic deformation of the material.

(TM) The twinned martensite reorients due to the increased stress to a untwinned martensite. This process is to common believe, not accompanied by any considerable release or consumption of heat. Thus, during this stage, austenite to martensite and martensite to martensite transformations might occur at the same time.

– When unloading takes place, an immediate heat consumption can be observed. Furthermore, no sharp transition from an elastic region to a plateau is visible. Thus, one may conclude that an immediate transformation from untwinned martensite to austenite sets in when the specimen is unloaded. But this transformation must be accompanied by a relative large mass fraction which transforms from untwinned martensite to twinned martensite as the mechanical behavior indicates. When the load is decreased further, the transformation from twinned martensite to austenite takes place. However, the processes during unloading are more difficult to analyze and further detailed micromechanical investigations are necessary for a thorough development of a material model.

To conclude, the effects observed on the macroscopic scale are usually difficult to separate from each other. Heat exchange with the environment, having a large influence on the temperature and therefore altering the material properties considerably, leading to pseudo-viscous effects, overlays the effects which can be directly traced back to the material. Hence, a thorough modelling of the material behavior is only possible when detailed information about mass fractions of the phases involved, martensite variants present, and the caloric interaction of the specimen with its surrounding are available. Unfortunately, experimental investigations taking all aspects into consideration can be rarely found.

In the following, a frame which allows the distinction between twinned and untwinned martensite is developed. Such approaches exist (eg. Thamburaja (2005)), but either have the focus on the microscale or do not use the kinetic variable as a directed measure.

Basic features, such as the predicted martensite start temperature and the kinetics for the transition from austenite to martensite are discussed. Due to the uncertainties related to the backtransformation, no development leading to the concrete formulation describing the backtransformation is conducted.

The chapter is organized as follows: in the following section, basic consid-

erations leading to the introduction of tensorial transformation kinetics are discussed. In section 5.3, the approach is specialized to the case of SMA. In sections 5.4, 5.5, and 5.6, questions regarding the onset, kinetics and the backtransformation are discussed.

5.2 General considerations

The aim of this section is to derive a macroscopic description based on the derivations local to the discontinuity. Thus, a scale transition with appropriate homogenization assumptions must be introduced leading to a pair of tensorial variables describing the transformation kinetics macroscopically. Restriction for the transformation kinetics based on thermomechanical and micromechanical considerations have to be derived.

5.2.1 Scale transition

For the derivations in this section it has to be noted that a macroscopic description, independent of the local orientation of the phase interface, is desired. However, the local orientation may not, and under certain conditions must not, be discarded and taken into account in a averaged, global sense. Thus, the information concerning the existence of a local orientation of the phase interface characterized by its normal vector has to be transferred to the macroscopic scale. The introduced macroscopic internal variable may therefore not only bear scalar information about the mass fraction of the martensite, but also, up to a certain extend, statistical informations about the local orientations.

The main idea of the following procedure is based on the local dissipation at the phase boundary due to its movement. In section 2.4.9, the local dissipation at the phase boundary due to its movement is derived, leading to expression (2.263). This relation is adopted in the form

$$\zeta^{\Lambda} = \rho U_N \, \mathbf{n} \cdot [\boldsymbol{\mu}] \cdot \mathbf{n} \geq 0 \tag{5.1}$$

or

$$\zeta^{\Lambda} = (\rho U_N \, \mathbf{n} \otimes \mathbf{n}) : [\boldsymbol{\mu}] \geq 0. \tag{5.2}$$

The second order tensor $\rho U_N \, \mathbf{n} \otimes \mathbf{n}$ holds information about the local orientation of the transformation surface whereas the term $[\boldsymbol{\mu}]$ represents an orientation independent measure for the driving force of the discontinuity. It must be noted that $[\boldsymbol{\mu}]$ is not the local driving force for the movement of the discontinuity. The projection of this tensor in direction normal the phase boundary is identified as the driving force. However, a macroscopic description which does not hold any explicit knowledge of the local direction is derived in the following. Following the reasoning by Grinfeld (1991), the whole tensor $\boldsymbol{\mu}$ is used to *"characterize the state of the substance in the entire vicinity of a material particle, independently of the choice of any elementary area"*. This consideration by Grinfeld is supported by recent developments which introduce "mechanics in a material space" (cf. Maugin (1993), Kienzler & Herrmann (2000), and Kienzler & Maugin (2001)). There, a balance law is formulated using $\boldsymbol{\mu}$, leading to

$$\boldsymbol{\nabla}_0 \cdot \boldsymbol{\mu} + \mathbf{b} = \mathbf{0} \tag{5.3}$$

where $\mathbf{b}$ is a material force (cf. e.g. Maugin (1993)). Even though this approach is very attractive, it poses a completely new problem besides the thermal and mechanical description.

The preceding description has to be transferred to the macroscopic scale. This implies, that the definition of the macroscopic quantities is already based on the homogenization assumptions employed. The further derivations are based on the following assumption: the phases are assumed to be homogeneous, i.e. a field variable within a phase can be characterized by a single variable, usually the mean value of the field variable. A subscript α is used to denote a phase specific variable associated to phase α.

To simplify the notation, the following derivations are conducted under the presumption that only two phases coexist within the body under consideration at any time. For a body consisting of more phases, the approach described must be applied for each possible combination of phases. Restrictions on the internal variables are imposed by the requirement that the total mass of the body shall not change.

As stated before, the whole tensor $[\boldsymbol{\mu}]$ is used as the driving force for the progress of the phase transformation. Consequently, a thermodynamically conjugated tensorial measure has to be introduced as the associated thermodynamic flux. When the local form of the dissipation inequality (5.2) has to

be fulfilled, the relation has to hold in an averaged sense as well, i.e.

$$\zeta_g^{\Lambda} = \int_{\Lambda_0} \zeta^{\Lambda} \, \mathrm{d}A_0 = \int_{\Lambda_0} (\rho U_N \, \mathbf{n} \otimes \mathbf{n}) : [\boldsymbol{\mu}] \, \mathrm{d}A_0 \geq 0 \tag{5.4}$$

Introducing formally the definitions

$$\boldsymbol{\mu}^{\Delta} = \frac{1}{A_{\Lambda}} \int_{\Lambda_0} [\boldsymbol{\mu}] \, \mathrm{d}A_0 \tag{5.5}$$

for the mean driving force on the considered interface Λ_0 and

$$\dot{\boldsymbol{\xi}} = \frac{1}{M_{tot}} \int_{\Lambda_0} \rho U_N \, \mathbf{n} \otimes \mathbf{n} \, \mathrm{d}A_0, \tag{5.6}$$

where

$$A_{\Lambda} = \int_{\Lambda_0} \mathrm{d}A_0 \tag{5.7}$$

and M_{tot} denotes the total mass of the body under consideration, the dissipation inequality can be restated as

$$\boldsymbol{\mu}^{\Delta} : \dot{\boldsymbol{\xi}} \geq 0. \tag{5.8}$$

The assumption about the homogeneity of the phases is employed while deriving this relation.

The use of the whole tensor may be supported by the aspect that the approach with the tensorial variables can be tracked back to the classical approach. It can be shown that the trace of the variable $\dot{\boldsymbol{\xi}}$ describes the specific mass change

of the phase under consideration by

$$\begin{aligned}
\operatorname{tr}\left(\dot{\boldsymbol{\xi}}\right) &= \frac{1}{M_{tot}} \operatorname{tr}\left(\int_{\Lambda_0} \rho U_N \, \mathbf{n} \otimes \mathbf{n} \, \mathrm{d}A_0\right) \\
&= \frac{1}{M_{tot}} \int_{\Lambda_0} \rho U_N \operatorname{tr}\left(\mathbf{n} \otimes \mathbf{n}\right) \, \mathrm{d}A_0 \\
&= \frac{1}{M_{tot}} \int_{\Lambda_0} \rho U_N \, \mathrm{d}A_0 \\
&= \frac{\dot{M}}{M_{tot}} \\
&= \dot{\xi}
\end{aligned} \tag{5.9}$$

where $\dot{M} = \int_{\Lambda_0} \rho U_N \, \mathrm{d}A_0$ denotes the mass change and therefore ξ the mass fraction of the phase under consideration. Thus, the first invariant of $\dot{\boldsymbol{\xi}}$ is the scalar information about the change of the mass fraction of the phase, bearing no information about the orientation of the phase boundary. Even though such direct interpretations of other invariants, i.e. the invariants of the deviator, are more difficult to derive, one may conclude that other invariants bear information about the current orientation of the interfaces due to the definition of the tensor.

The aspect that the first invariant of $\boldsymbol{\xi}$ is of special importance is supported by the observation that for a purely hydrostatic stress state $\boldsymbol{\sigma} = -p\,\mathbf{1}$, the tensor $\boldsymbol{\mu}^{\Delta}$ collapses to $\boldsymbol{\mu}^{\Delta} = \mathbf{1}\, g^{\Delta}$. Here, g^{Δ} denotes the difference of the Gibbs free energy of the phases. Using this result in the form (5.8) of the dissipation inequality, the second order unit tensor in front of g^{Δ} acts as a trace operator, yielding the form of (5.8) for hydrostatic stress state as

$$g^{\Delta}\, \dot{\xi} \geq 0 \tag{5.10}$$

which coincides with classical formulations used in thermodynamics.

5.2.2 Kinetic relation

The aim of the remainder of this chapter is to develop a set of constitutive equations which describe the relation between the measures $\boldsymbol{\mu}^{\Delta}$ and $\boldsymbol{\xi}$. As a

first approach, a function $\dot{\boldsymbol{\xi}} = \dot{\boldsymbol{\xi}}(\dot{\boldsymbol{\mu}}^{\Delta}, \boldsymbol{\mu}^{\Delta}, \boldsymbol{\xi})$ is proposed. The use of the tensor $\boldsymbol{\xi}$ in the arguments for the desired relation is important. In case $\boldsymbol{\xi}$ is omitted, only situations where the probability for each orientation is equal, i.e. only spheroidal inclusions exist, can be considered. Furthermore, it is shown that its use is important to account for some situations dealing with SMA.

The basic development of this relation is based on the following observations:

- In order to initiate a macroscopic progress of the phase transformation, undercooling below the equilibrium temperature is necessary to induce the phase transition. For mechanically induced phase transitions, this leads to a hysteresis when a loading-unloading cycle is performed. This behavior can be observed in shape memory alloys where, in contrast to most steels, the transition from austenite to martensite and vice versa is primarily a time independent, martensitic transformation.

- The transformation is not time dependent. Thus, if the change of the driving force is zero, i.e. $\dot{\boldsymbol{\mu}}^{\Delta} = \mathbf{0}$, $\dot{\boldsymbol{\xi}} = \mathbf{0}$ should hold too. It should be noted at this point, that during phase transitions in SMA, a rate dependence can be observed macroscopically (cf. Iadicola & Shaw (2004)). However, this may be primarily due to the latent heat released during the transformation and conducted to the environment. As the heat conduction is a first order process, a rate dependence is introduced. Some authors claim that the rate effects observed can not completely be explained by thermal effects (Helm (2001)). Therefore, this questions still remains open.

In order to develop a relation between $\boldsymbol{\mu}$ and $\dot{\boldsymbol{\xi}}$, different approaches are considered:

- An approach solely based on thermodynamic considerations, leading to a rule which is similar to the "normality-rule" known from associated plasticity, is developed first.

- A deviation from the normality rule is also considered. This approach rather suits situations where the underlying microstructure, as e.g. the question which martensitic variants form at which stage, is predominant and leads to a violation of the rules developed focusing only on macroscopic thermodynamic aspects. Thus, based on the associated approach proposed before, different non-associated proposal are discussed.

The associated approach is based on the assumption that each subprocess maximizes the dissipation associated with itself. For the subprocess that describes the phase transition, the dissipation seek a maximum, i.e.

$$\boldsymbol{\mu}^{\Delta} : \dot{\boldsymbol{\xi}} \longrightarrow \text{Max.} \tag{5.11}$$

Furthermore, a threshold value

$$F^{\xi} = F^{\xi}(\boldsymbol{\mu}^{\Delta}, \boldsymbol{\xi}) = 0 \tag{5.12}$$

must be reached to induce the phase transformation. It is assumed that this condition holds during the complete phase transition. Thus, relations (5.11) and (5.12) constitute a constraint optimization problem which can be solved by introducing the Lagrange multiplier λ^{ξ} such that

$$\mathcal{L} = \boldsymbol{\mu}^{\Delta} : \dot{\boldsymbol{\xi}} - \lambda^{\xi} F^{\xi} \longrightarrow \text{Extr.} \tag{5.13}$$

Partial differentiating of $\mathcal{L}$ with respect to $\boldsymbol{\mu}^{\Delta}$ leads to

$$\frac{\partial}{\partial \boldsymbol{\mu}^{\Delta}} \left[\boldsymbol{\mu}^{\Delta} : \dot{\boldsymbol{\xi}} - \lambda^{\xi} F^{\xi} \right] = 0 \tag{5.14}$$

and finally to

$$\dot{\boldsymbol{\xi}} = \left\langle \lambda^{\xi} \right\rangle_{\xi} \frac{\partial F^{\xi}}{\partial \boldsymbol{\mu}^{\Delta}} \tag{5.15}$$

where

$$\left\langle x \right\rangle_{\xi} = \begin{cases} x & \text{if } F^{\xi} = 0 \\ 0 & \text{otherwise.} \end{cases} \tag{5.16}$$

Due to circumstances discussed in detail in section 5.2.2.1, it may be necessary to deviate from this purely thermodynamical approach. Thus, a new potential $P^{\xi} = P^{\xi}(\boldsymbol{\mu}^{\Delta}, \boldsymbol{\xi})$ is introduced in order to determine the direction of the evolution of $\boldsymbol{\xi}$, such that

$$\dot{\boldsymbol{\xi}} = \left\langle \lambda^{\xi} \right\rangle_{\xi} \frac{\partial P^{\xi}}{\partial \boldsymbol{\mu}^{\Delta}}. \tag{5.17}$$

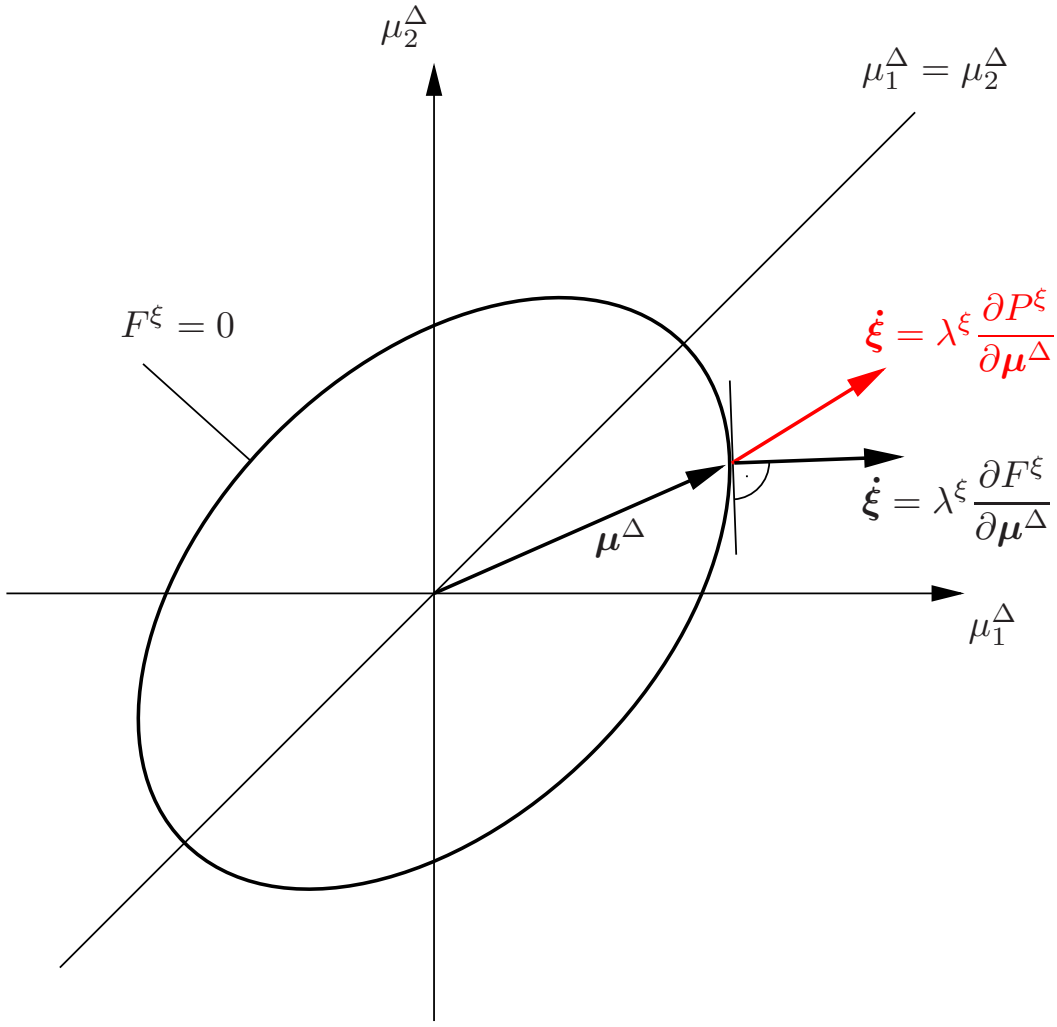

Figure 5.5: F^ξ and P^ξ in the $\boldsymbol{\mu}^\Delta$-space

The deviation from the normality rule for a two dimensional example is depicted in figure 5.5. Possible approaches for the choice of P^{ξ} are discussed in section 5.2.2.2 and 5.2.2.3. Making use of the decomposition

$$\dot{\boldsymbol{\xi}} = \frac{1}{3}\,\mathbf{1}\,\dot{\xi} + \dot{\boldsymbol{\xi}}' \tag{5.18}$$

with $\dot{\xi} = \mathrm{tr}\left(\dot{\boldsymbol{\xi}}\right)$ leads to

$$\dot{\xi} = \left\langle \lambda^{\xi} \right\rangle_{\xi} \mathrm{tr}\left(\frac{\partial P^{\xi}}{\partial \boldsymbol{\mu}^{\Delta}}\right) \tag{5.19}$$

and

$$\dot{\boldsymbol{\xi}}' = \left\langle \lambda^{\xi} \right\rangle_{\xi} \left(\frac{\partial P^{\xi}}{\partial \boldsymbol{\mu}^{\Delta}}\right)' . \tag{5.20}$$

The yet undetermined variable λ^{ξ} can be determined by use of the consistency condition $\dot{F}^{\xi} = 0$, i.e.

$$\dot{F}^{\xi} = \frac{\partial F^{\xi}}{\partial \boldsymbol{\mu}^{\Delta}} : \dot{\boldsymbol{\mu}}^{\Delta} + \frac{\partial F^{\xi}}{\partial \boldsymbol{\xi}} : \dot{\boldsymbol{\xi}} = 0. \tag{5.21}$$

The unknown multiplier λ^{ξ} can be determined as

$$\lambda^{\xi} = -\frac{\dfrac{\partial F^{\xi}}{\partial \boldsymbol{\mu}^{\Delta}} : \dot{\boldsymbol{\mu}}^{\Delta}}{\dfrac{\partial F}{\partial \boldsymbol{\xi}} : \dfrac{\partial P^{\xi}}{\partial \boldsymbol{\mu}^{\Delta}}}$$

loading finally to

$$\dot{\boldsymbol{\xi}} = -\frac{\partial P^{\xi}}{\partial \boldsymbol{\mu}^{\Delta}} \frac{\dfrac{\partial F^{\xi}}{\partial \boldsymbol{\mu}^{\Delta}} : \dot{\boldsymbol{\mu}}^{\Delta}}{\dfrac{\partial F}{\partial \boldsymbol{\xi}} : \dfrac{\partial P^{\xi}}{\partial \boldsymbol{\mu}^{\Delta}}}. \tag{5.22}$$

The deviation from the normality rule might lead to a violation of the requirement of thermodynamic consistency. Thus, employing the relation derived for $\dot{\boldsymbol{\xi}}$ so far, equation (5.8) may be restated as

$$\dot{\boldsymbol{\xi}} : \boldsymbol{\mu}^{\Delta} = -\frac{\partial P^{\xi}}{\partial \boldsymbol{\mu}^{\Delta}} : \boldsymbol{\mu}^{\Delta} \, \frac{\dfrac{\partial F^{\xi}}{\partial \boldsymbol{\mu}^{\Delta}} : \dot{\boldsymbol{\mu}}^{\Delta}}{\dfrac{\partial F}{\partial \boldsymbol{\xi}} : \dfrac{\partial P^{\xi}}{\partial \boldsymbol{\mu}^{\Delta}}} \geq 0, \tag{5.23}$$

leading to restriction on the choice of P^{ξ}.

In order to proceed, a further specification of the functions F^{ξ} and P^{ξ} is necessary. As a relatively general approach, it is assumed that a combination of the invariants has to reach a threshold which depends on the internal variables introduced. In the following, the functions

$$F^{\xi} = c_1 \, I_1^{\mu} + c_2 \sqrt{-J_2^{\mu}} + c_3 \sqrt[3]{J_3^{\mu}} - g(\boldsymbol{\xi}) \tag{5.24}$$

introducing the parameters c_1, c_2, and c_3 and

$$g(\boldsymbol{\xi}) = g_0 + g_1 \, I_1^{\xi} + g_2 \sqrt{-J_2^{\xi}} + g_3 \sqrt[3]{J_3^{\xi}} \tag{5.25}$$

with the parameters g_0, g_1, g_2, and g_3 are used. The invariants of the tensors $\boldsymbol{\mu}$ and $\boldsymbol{\xi}$ are specified by (2.23) and (2.27). In order to avoid overparameterization, $g_0 = 1$ is set. For P^{ξ}, three different cases are considered in the following.

5.2.2.1 Case 1: $P^{\xi} = F^{\xi}$

The determination of the derivatives yields

$$\begin{aligned} \frac{\partial F^{\xi}}{\partial \boldsymbol{\mu}^{\Delta}} &= c_1\,\mathbf{1} + c_2\,\frac{\boldsymbol{\mu}^{\Delta\prime T}}{2\,\sqrt{-J_2^{\mu}}} \\ &\quad + c_3\,\frac{1}{3\,\sqrt[3]{J_3^{\mu\,2}}}\left[\left(\boldsymbol{\mu}^{\Delta\prime}\cdot\boldsymbol{\mu}^{\Delta\prime}\right)^{T} + \frac{2}{3}\,J_2^{\mu}\,\mathbf{1}\right] \qquad (5.26) \\ -\frac{\partial F}{\partial \boldsymbol{\xi}} = \frac{\partial g}{\partial \boldsymbol{\xi}} &= g_1\,\mathbf{1} + g_2\,\frac{\boldsymbol{\xi}'^{T}}{2\,\sqrt{-J_2^{\xi}}} \\ &\quad + g_3\,\frac{1}{3\,\sqrt[3]{J_3^{\xi\,2}}}\left[\left(\boldsymbol{\xi}'\cdot\boldsymbol{\xi}'\right)^{T} + \frac{2}{3}\,J_2^{\xi}\,\mathbf{1}\right]. \qquad (5.27) \end{aligned}$$

Making use of

$$\frac{\partial F^{\xi}}{\partial \boldsymbol{\mu}^{\Delta}} : \dot{\boldsymbol{\mu}}^{\Delta} = c_1\,\dot{I}_1^{\mu} - c_2\,\frac{\dot{J}_2^{\mu}}{2\,\sqrt{-J_2^{\mu}}} + c_3\,\frac{\dot{J}_3^{\mu}}{3\,\sqrt[3]{J_3^{\mu\,2}}} \qquad (5.28)$$

leads to

$$\dot{\boldsymbol{\xi}} = \left[c_1\,\mathbf{1} + c_2\,\frac{\boldsymbol{\mu}^{\Delta\prime}}{2\,\sqrt{-J_2^{\mu}}} + c_3\,\frac{1}{\sqrt[3]{J_3^{\mu\,2}}}\left[\left(\boldsymbol{\mu}^{\Delta\prime}\cdot\boldsymbol{\mu}^{\Delta\prime}\right)^{T} + \frac{2}{3}\,J_2^{\mu}\,\mathbf{1}\right]\right]\,\lambda^{\xi} \qquad (5.29)$$

with

$$\begin{aligned}\lambda^{\xi} \;=\; & \left[c_1\, \dot{I}_1^{\mu} - c_2\, \frac{\dot{J}_2^{\mu}}{2\,\sqrt{-J_2^{\mu}}} + c_3\, \frac{\dot{J}_3^{\mu}}{3\,\sqrt[3]{J_3^{\mu\,2}}} \right] \\ & \left[3\, c_1\, g_1 + c_2\, g_2\, \frac{\boldsymbol{\xi}' : \boldsymbol{\mu}^{\Delta\,\prime}}{4\,\sqrt{J_2^{\xi}\, J_2^{\mu}}} + c_3\, g_2\, \frac{\mathrm{tr}\left(\boldsymbol{\xi}' \cdot \boldsymbol{\mu}^{\Delta\,\prime} \cdot \boldsymbol{\mu}^{\Delta\,\prime}\right)}{6\,\sqrt{-J_2^{\xi}}\,\sqrt[3]{J_3^{\mu\,2}}} \right. \\ & \left. + c_3\, g_3\, \frac{\mathrm{tr}\left(\boldsymbol{\xi}' \cdot \boldsymbol{\xi}' \cdot \boldsymbol{\mu}^{\Delta\,\prime} \cdot \boldsymbol{\mu}^{\Delta\,\prime}\right) - \frac{20}{9}\, J_2^{\xi} J_2^{\mu}}{9\,\sqrt[3]{J_3^{\xi\,2}}\,\sqrt[3]{J_3^{\mu\,2}}} \right]^{-1} . \end{aligned} \tag{5.30}$$

Using the decomposition (5.18), one may eventually formulate differential equations for ξ and $\boldsymbol{\xi}'$ as follows:

$$\dot{\xi} \;=\; 3\, c_1\, \lambda^{\xi} \tag{5.31}$$

$$\dot{\boldsymbol{\xi}}' \;=\; \left(c_2\, \frac{\boldsymbol{\mu}^{\Delta\,\prime}}{2\,\sqrt{-J_2^{\mu}}} + c_3\, \frac{1}{\sqrt[3]{J_3^{\mu\,2}}} \left[\left(\boldsymbol{\mu}^{\Delta\,\prime} \cdot \boldsymbol{\mu}^{\Delta\,\prime} \right)^{T} + \frac{2}{3}\, J_2^{\mu}\, \mathbf{1} \right] \right) \lambda^{\xi} . \tag{5.32}$$

Apart from the specifications for F^{ξ} and P^{ξ} done so far, a more general aspect should be discussed. Without reference to a choice for F^{ξ}, one may substitute the Lagrange multiplier in relation (5.20), providing that $\mathrm{tr}\left(\partial P^{\xi} / \partial \boldsymbol{\mu}^{\Delta}\right) \neq 0$ which is generally true for $P^{\xi} = F^{\xi}$, by the term derived from (5.19) leading to

$$\dot{\boldsymbol{\xi}}' = \frac{\dot{\xi}}{\mathrm{tr}\left(\frac{\partial P^{\xi}}{\partial \boldsymbol{\mu}^{\Delta}}\right)} \left(\frac{\partial P^{\xi}}{\partial \boldsymbol{\mu}^{\Delta}} \right)' . \tag{5.33}$$

This relation states that an evolution of $\dot{\boldsymbol{\xi}}'$ is only possible if $\dot{\xi}$ is nonzero. Relating this statement to the description of pseudoelastic and pseudoplastic shape memory alloys, no reorientation of the martensite is possible if $\xi = 1$. A possible approach to avoid this situation is to choose P^{ξ} such that $\mathrm{tr}\left(\partial P^{\xi} / \partial \boldsymbol{\mu}^{\Delta}\right) = 0$, rendering the substitution performed above impossible for this case. This aspect leads to the introduction of the non-associated rule discussed in the next sections.

5.2.2.2 Case 2: $P^\xi = F^\xi - c_1\, I_1^\mu\, I_1^\xi$

As stated above, P^ξ is now chosen such that for $\xi = 1$, a change of the deviatoric part of $\boldsymbol{\xi}$ is possible. One approach is to choose

$$P^\xi = F^\xi - c_1\, I_1^\mu\, I_1^\xi \tag{5.34}$$

which leads to

$$\begin{aligned}\frac{\partial P^\xi}{\partial \boldsymbol{\mu}^\Delta} &= c_1\, \mathbf{1}\,(1 - \mathrm{tr}\,(\boldsymbol{\xi})) + c_2\, \frac{\boldsymbol{\mu}^{\Delta\prime}}{2\,\sqrt{-J_2^\mu}}\cdot \\ &\quad + c_3\, \frac{1}{3\,\sqrt[3]{J_3^{\mu\,2}}} \left[\left(\boldsymbol{\mu}^{\Delta\prime} \cdot \boldsymbol{\mu}^{\Delta\prime} \right)^T + \frac{2}{3}\, J_2^\mu\, \mathbf{1} \right]. \end{aligned} \tag{5.35}$$

Solving for $\dot{\boldsymbol{\xi}}$ yields

$$\dot{\xi} = 3\, c_1\, (1 - \xi)\, \lambda^\xi \tag{5.36}$$

$$\dot{\boldsymbol{\xi}}' = \left(c_2\, \frac{\boldsymbol{\mu}^{\Delta\prime}}{2\,\sqrt{-J_2^\mu}} + c_3\, \frac{1}{\sqrt[3]{J_3^{\mu\,2}}} \left[\left(\boldsymbol{\mu}^{\Delta\prime} \cdot \boldsymbol{\mu}^{\Delta\prime} \right)^T + \frac{2}{3}\, J_2^\mu\, \mathbf{1} \right] \right) \lambda^\xi \tag{5.37}$$

with

$$\begin{aligned}\lambda^\xi &= \left[c_1\, \dot{I}_1^\mu - c_2\, \frac{\dot{J}_2^\mu}{2\,\sqrt{-J_2^\mu}} + c_3\, \frac{\dot{J}_3^\mu}{3\,\sqrt[3]{J_3^{\mu\,2}}} \right] \\ &\quad \left[3\, c_1\, g_1\, (1 - \xi) + c_2\, g_2\, \frac{\boldsymbol{\xi}' : \boldsymbol{\mu}^{\Delta\prime}}{4\,\sqrt{J_2^\xi J_2^\mu}} + c_3\, g_2\, \frac{\mathrm{tr}\left(\boldsymbol{\xi}' \cdot \boldsymbol{\mu}^{\Delta\prime} \cdot \boldsymbol{\mu}^{\Delta\prime} \right)}{6\,\sqrt{-J_2^\xi}\,\sqrt[3]{J_3^{\mu\,2}}} \right. \\ &\quad \left. + c_3\, g_3\, \frac{\mathrm{tr}\left(\boldsymbol{\xi}' \cdot \boldsymbol{\xi}' \cdot \boldsymbol{\mu}^{\Delta\prime} \cdot \boldsymbol{\mu}^{\Delta\prime} \right) - \frac{20}{9}\, J_2^\xi J_2^\mu}{9\,\sqrt[3]{J_3^{\xi\,2}}\,\sqrt[3]{J_3^{\mu\,2}}} \right]^{-1}. \end{aligned} \tag{5.38}$$

Two positive aspects can be noticed:

- The differential equation for ξ automatically satisfies the condition $0 \le \xi \le 1$.

- Even for $\xi = 1$, a reorientation of the martensite is possible.

The second remark holds also true for $\xi = 0$, which is considered non-physical within this context. Thus, a possible extension to circumvent this contradiction is discussed in the following section.

5.2.2.3 Case 3: $P^\xi = F^\xi - c_1\, I_1^\mu\, I_1^\xi - \left(c_2\sqrt{-J_2^\mu} + c_3\sqrt[3]{J_3^\mu}\right)(1 - f^\xi(I_1^\xi, J_2^\xi, J_3^\xi))$

Now, P^ξ is extended such that the deviatoric part of $\partial P^\xi / \partial \boldsymbol{\mu}^\Delta$ vanishes for $\xi = 0$. This can be achieved by using

$$\begin{aligned} P^\xi &= F^\xi - c_1\, I_1^\mu\, I_1^\xi - \left(c_2\sqrt{-J_2^\mu} + c_3\sqrt[3]{J_3^\mu}\right)(1 - f^\xi(I_1^\xi, J_2^\xi, J_3^\xi)) \\ &= c_1\, I_1^\mu\,(1-\xi) + f^\xi(I_1^\xi, J_2^\xi, J_3^\xi)\left(c_2\sqrt{-J_2^\mu} + c_3\sqrt[3]{J_3^\mu}\right) \end{aligned} \tag{5.39}$$

with the function $f^\xi(I_1^\xi, J_2^\xi, J_3^\xi)$ introduced such that $f^\xi(I_1^\xi = 0) = 0$. The simplest choice meeting the requirement stated above is $f^\xi(I_1^\xi, J_2^\xi, J_3^\xi) = \xi$. Other invariants might be incorporated to reflect situations where the reorientation process of the martensite is no longer possible. The choice can, within the framework of the application to shape memory alloys, be interpreted in a way that during the transformation from austenite to martensite, first only nonoriented martensite forms. During the transformation, gradually oriented martensite is formed by transformation from austenite to martensite as well as by orientation of nonoriented martensite.

This approach yields

$$\begin{aligned} \frac{\partial P^\xi}{\partial \boldsymbol{\mu}^\Delta} &= c_1\,\mathbf{1}\,(1-\xi) + c_2\,\frac{\boldsymbol{\mu}^{\Delta\prime}\, f^\xi}{2\sqrt{-J_2^\mu}} \\ &\quad + c_3\,\frac{f^\xi}{3\sqrt[3]{J_3^{\mu\,2}}}\left[\left(\boldsymbol{\mu}^{\Delta\prime}\cdot\boldsymbol{\mu}^{\Delta\prime}\right)^T + \frac{2}{3}\,J_2^\mu\,\mathbf{1}\right]. \end{aligned} \tag{5.40}$$

and finally

$$\dot{\xi} = 3\,c_1\,(1-\xi)\,\lambda^{\xi} \tag{5.41}$$

$$\dot{\boldsymbol{\xi}}' = \left(c_2\,\frac{\boldsymbol{\mu}^{\Delta\,\prime}}{2\,\sqrt{-J_2^{\mu}}} + c_3\,\frac{1}{\sqrt[3]{J_3^{\mu\,2}}}\left[\left(\boldsymbol{\mu}^{\Delta\,\prime}\cdot\boldsymbol{\mu}^{\Delta\,\prime}\right)^{T} + \frac{2}{3}\,J_2^{\mu}\,\mathbf{1}\right]\right) f^{\xi}\,\lambda^{\xi} \tag{5.42}$$

with

$$\lambda^{\xi} = \left[c_1\,\dot{I}_1^{\mu} - c_2\,\frac{\dot{J}_2^{\mu}}{2\,\sqrt{-J_2^{\mu}}} + c_3\,\frac{\dot{J}_3^{\mu}}{3\,\sqrt[3]{J_3^{\mu\,2}}}\right] \left[3\,c_1\,g_1\,(1-\xi) + c_2\,g_2\,f^{\xi}\,\frac{\boldsymbol{\xi}' : \boldsymbol{\mu}^{\Delta\,\prime}}{4\,\sqrt{J_2^{\xi}\,J_2^{\mu}}} + c_3\,g_2\,f^{\xi}\,\frac{\mathrm{tr}\left(\boldsymbol{\xi}'\cdot\boldsymbol{\mu}^{\Delta\,\prime}\cdot\boldsymbol{\mu}^{\Delta\,\prime}\right)}{6\,\sqrt{-J_2^{\xi}}\,\sqrt[3]{J_3^{\mu\,2}}} + c_3\,g_3\,f^{\xi}\,\frac{\mathrm{tr}\left(\boldsymbol{\xi}'\cdot\boldsymbol{\xi}'\cdot\boldsymbol{\mu}^{\Delta\,\prime}\cdot\boldsymbol{\mu}^{\Delta\,\prime}\right) - \frac{20}{9}\,J_2^{\xi}\,J_2^{\mu}}{9\,\sqrt[3]{J_3^{\xi\,2}}\,\sqrt[3]{J_3^{\mu\,2}}}\right]^{-1}. \tag{5.43}$$

The condition of thermodynamic consistency (5.23) may be written as

$$\dot{\boldsymbol{\xi}} : \boldsymbol{\mu}^{\Delta} = \lambda^{\xi}\left[c_1\,(1-\xi)I_1^{\mu} + c_2\,f^{\xi}\sqrt{-J_2^{\mu}} + c_3\,f^{\xi}\sqrt[3]{J_3^{\mu}}\right] = \lambda^{\xi}P^{\xi} \geq 0. \tag{5.44}$$

5.3 Further specifications

In order to derive expressions for F^{ξ} and P^{ξ} in terms of global stress and temperature, further assumptions are necessary. These are again related to the phase-specific behavior of the material and the homogenization.

The following assumptions are imposed for the remainder of this section:

- The assumption related to the homogeneity of the phases already introduced is still assumed to be valid.
- To separate the kinematic description from the material specific description, small strain measure are used. Taking into account the previous assumption, the strain in phase α is denoted by $\boldsymbol{e}^{\alpha}$ and the stress by $\boldsymbol{\Pi}^{\alpha}$.

- Based on relation (3.30) and the assumption that the specific heat at constant volume of the phases does not differ (as well as $\boldsymbol{\beta}_0$ and $\boldsymbol{\varphi}'_*$), the approach for the difference of Helmholtz free energy is chosen as

$$\varphi = \varphi_c + \frac{\mathbf{\Pi}^A : \boldsymbol{e}_r^A - \mathbf{\Pi}^M : \boldsymbol{e}_r^M}{2\rho} \tag{5.45}$$

with

$$\varphi_c = \Delta s(\Theta_0 - \Theta). \tag{5.46}$$

- It is assumed that the phase specific material behavior can be described by the relation (cf. equation (3.32))

$$\mathbf{\Pi}^\alpha = \mathbb{C}^\alpha : (\boldsymbol{e}_r^\alpha - \mathbf{1}\,\alpha_\Theta^\alpha\,(\Theta - \Theta_\Theta)) \tag{5.47}$$

where an additive decomposition of the strains

$$\boldsymbol{e}^\alpha = \boldsymbol{e}_r^\alpha + \boldsymbol{\kappa}^\alpha \tag{5.48}$$

is employed. $\boldsymbol{\kappa}^\alpha$ denotes the phase-specific strain due to the phase transformation, constant within the phase. Here,

$$\boldsymbol{\kappa}^A = \mathbf{0} \quad \text{and} \quad \boldsymbol{\kappa}^M = \boldsymbol{\kappa} \tag{5.49}$$

is used. $\boldsymbol{\kappa}$ is not yet determined or specified, a discussion related to this term can be found in section 5.5.

- A mixture rule for stresses and strains is used, i.e.

$$\mathbf{\Pi} = \xi\,\mathbf{\Pi}^M + (1-\xi)\,\mathbf{\Pi}^A \tag{5.50}$$

and

$$\boldsymbol{e} = \xi\,\boldsymbol{e}^M + (1-\xi)\,\boldsymbol{e}^A. \tag{5.51}$$

Furthermore, it is assumed that a variant of the Taylor assumption is valid such that the elastic strains in the phases are equal, i.e.

$$\boldsymbol{e}_r = \boldsymbol{e}_r^M = \boldsymbol{e}_r^A \tag{5.52}$$

To simplify the notation, it is assumed that the coordinate-system is chosen such that the global stress state $\mathbf{\Pi}$ can be expressed as a principal stress state

$$\mathbf{\Pi} = \begin{pmatrix} \sigma_1 & 0 & 0 \\ 0 & \sigma_2 & 0 \\ 0 & 0 & \sigma_3 \end{pmatrix}. \tag{5.53}$$

By introducing the abbreviations $\Xi = 1+(\alpha-1)\xi$ and $E^A = E$ and $E^M = \alpha\, E$ for the Young's moduli, the first invariant of $\boldsymbol{\mu}^{\Delta}$ can be expressed as

$$\begin{aligned} I_1^{\mu} \;=\; & \frac{(\alpha-1)\,\left(\sigma_1^2+\sigma_2^2+\sigma_3^2-2\,\nu\,(\sigma_2\,\sigma_3+\sigma_1\,\sigma_2+\sigma_1\sigma_3)\right)}{2\,E\,\Xi^2\,\rho} \\ & + \frac{\sigma_1\,(\alpha-1+2\,\alpha\,\kappa_{11})}{\Xi\,\rho} \\ & + \frac{\sigma_2\,(\alpha-1+2\,\alpha\,\kappa_{22})}{\Xi\,\rho} \\ & + \frac{\sigma_3\,(\alpha-1+2\,\alpha\,\kappa_{33})}{\Xi\,\rho} \\ & + 3\,\varphi_c \end{aligned} \tag{5.54}$$

For SMA, the ratio σ_i/E can be expected to be of a magnitude 10^{-2} or lower. Thus, I_1^{μ} can be approximately be expressed as

$$I_1^{\mu} = -\,\frac{\Sigma_1+\Sigma_2+\Sigma_3}{\Xi\,\rho} + 3\,\varphi_c \tag{5.55}$$

where the abbreviation $\Sigma_i = -\sigma_i\,(\alpha-1+2\,\alpha\,\kappa_{ii})$ is used. The corresponding expression for the second invariant is

$$J_2^{\mu} = -\,\frac{\left(\Sigma_1^2+2\,K_{12}\Sigma_1\Sigma_2+\Sigma_2^2+2\,K_{23}\Sigma_2\Sigma_3+\Sigma_3^2+2\,K_{13}\Sigma_1\Sigma_3\right)}{3\,\Xi^2\rho^2} \tag{5.56}$$

with

$$K_{ij} = \frac{1}{2} - \frac{6\,\alpha^2\,\kappa_{ij}}{(\alpha-1+2\,\alpha\,\kappa_{ii})(\alpha-1+2\,\alpha\,\kappa_{jj})}. \tag{5.57}$$

The expression for J_3^{μ} is omitted because the further derivations do not explicitly take this part into account.

5.4 Onset of the phase transition

In this and the following section, the transformation from austenite to martensite is discussed. Thus the term "onset of the phase transition" refers to the case where the martensite just begins to form within the austenitic matrix. Considering this, the state may be characterized by $\xi = 0$, thus $\Xi = 1$ follows. Using this, the invariants read

$$I_1^{\mu} = -\frac{\Sigma_1 + \Sigma_2 + \Sigma_3}{\rho} + 3\,\varphi_c \tag{5.58}$$

$$J_2^{\mu} = -\frac{\left(\Sigma_1^2 + 2\,K_{12}\Sigma_1\Sigma_2 + \Sigma_2^2 + 2\,K_{23}\Sigma_2\Sigma_3 + \Sigma_3^2 + 2\,K_{13}\Sigma_1\Sigma_3\right)}{3\,\rho^2} \tag{5.59}$$

In order to keep the focus on the basic aspects of the approach proposed, $c_3 = 0$ is chosen. Possible extension based on other choices are discussed in section 5.4.6.

5.4.1 Stress free state

For the stress free transformation,

$$\sigma_1 = \sigma_2 = \sigma_3 = 0 \tag{5.60}$$

holds. Thus,

$$F^{\xi} = 3\,c_1\,\varphi_c - 1 = 0 \tag{5.61}$$

follows and the martensite start temperature for the stress free state M_s^0 can be determined as

$$M_s^0 = \Theta_0 - \frac{1}{3\,\Delta s\,c_1}. \tag{5.62}$$

5.4.2 Simple tension and compression

Now,

$$\sigma_1 = \sigma, \;\; \sigma_2 = \sigma_3 = 0 \tag{5.63}$$

is set which leads to

$$F^{\xi} = c_1 \left(-\frac{\Sigma}{\rho} + 3\,\varphi_c \right) + c_2 \, \frac{1}{\rho\sqrt{3}} \sqrt{\Sigma^2} - 1 = 0, \tag{5.64}$$

introducing the abbreviation $\Sigma = \Sigma_1$. Defining a dimensionless temperature

$$\hat{\Theta} = \frac{\Theta - \Theta_0}{\Theta_0 - M_s^0} \tag{5.65}$$

which can be interpreted as a relative degree of undercooling as $\hat{\Theta}(\Theta_0) = 0$ and $\hat{\Theta}(M_s^0) = -1$ yields

$$-\;\; c_1 \, \frac{\Sigma}{\rho} + c_2 \, \frac{1}{\rho\sqrt{3}} \sqrt{\Sigma^2} = 1 + \hat{\Theta}. \tag{5.66}$$

An interpretation in a Clausius-Clapeyron diagram might be useful. The slope in the Clausius-Clapeyron diagram can be determined as

$$\frac{\partial \Sigma}{\partial \hat{\Theta}} = \frac{\sqrt{3} \;\; \rho}{-\sqrt{3}\, c_1 + \mathrm{sgn}(\Sigma) c_2}. \tag{5.67}$$

Due to the structure of relation (5.66), two different cases have to be considered when depicting the Clausius-Clapeyron diagram: the case $c_2 > 0$ and the case $c_2 < 0$. For $c_2 > 0$, the Clausius-Clapeyron diagram in the $\Sigma/\hat{\Theta}$-space is depicted in figure 5.6, for $c_2 < 0$ the Clausius-Clapeyron diagram can be found in figure 5.7. In order to clarify the influence and physical interpretation of the parameters introduced so far, an identification of the parameters c_1, c_2, and Δs in terms of experimentally measurable terms $\Sigma^+ = \Sigma(F^{\xi} = 0, \Sigma > 0)$, $\Sigma^- = \Sigma(F^{\xi} = 0, \Sigma < 0)$, Θ_0, and M_s^0 is given:

$$\Delta s \;\; = \;\; \frac{\Theta_0 - M_s^0}{2\, c_1} \tag{5.68}$$

$$c_1 \;\; = \;\; -(1 + \hat{\Theta})\, \rho \;\; \frac{\Sigma^+ + \Sigma^-}{2\, \Sigma^+ \Sigma^-} \tag{5.69}$$

$$c_2 \;\; = \;\; -(1 + \hat{\Theta})\, \rho \;\; \frac{\Sigma^+ - \Sigma^-}{2\, \Sigma^+ \Sigma^-}. \tag{5.70}$$

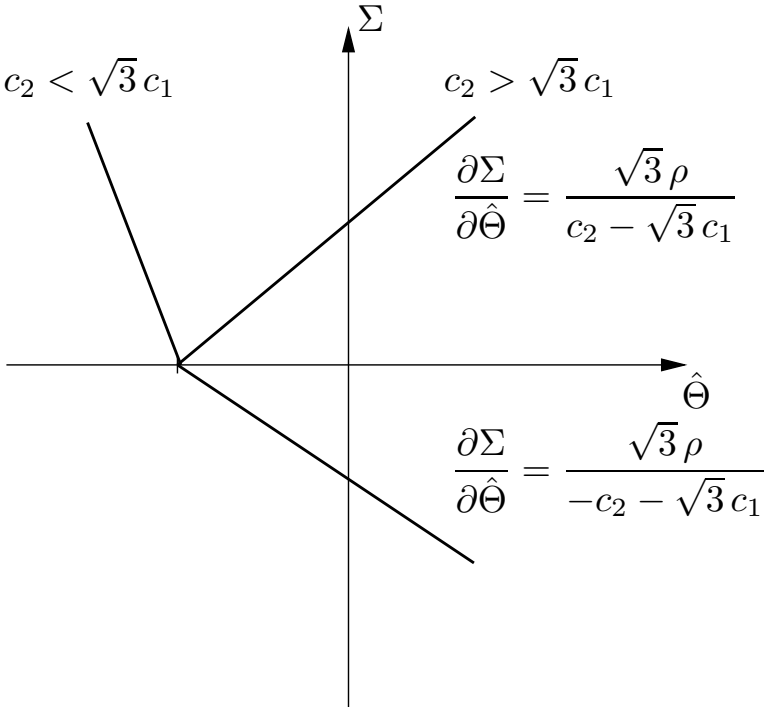

Figure 5.6: Clausius-Clapeyron diagram for test in simple tension, $c_2 > 0$.

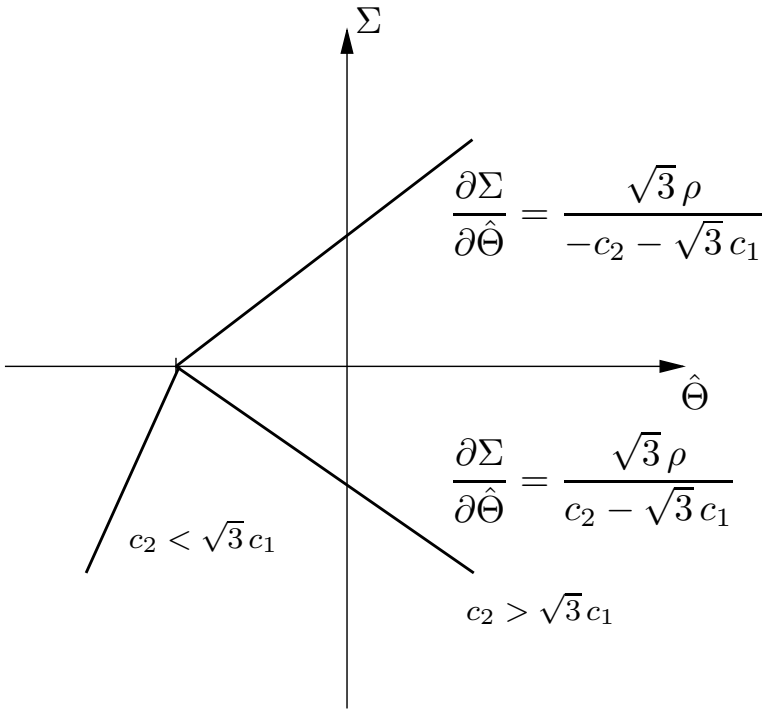

Figure 5.7: Clausius-Clapeyron diagram for test in simple tension, $c_2 < 0$.

Providing the experimentally measurable values of the undercooling $\Theta_0 - M_s^0$ and the stresses Σ^+ and Σ^-, the three parameters Δs, c_1, and c_2 can be determined.

5.4.3 Pure shear

Even though this example is implicitly included in the consideration concerning the two dimensional case in section 5.4.5 (as is the example before), it is included here due to its importance. Now,

$$\sigma_1 = \tau, \;\; \sigma_2 = -\tau, \;\; \sigma_3 = 0 \tag{5.71}$$

is set. Assuming isotropy related to the deformation induced by the transformation, i.e. $\kappa_{11} = \kappa_{22} = \kappa$, the invariants can be expressed as

$$I_1^\mu = \frac{\tau^2(\alpha - 1) + 6\,\mu\,\Xi^2\,\rho\,\varphi_c}{2\mu\Xi^2\rho} \tag{5.72}$$

$$J_2^\mu = -\tau^2\,\frac{1 - 2\alpha\,(1 + 2\kappa) + \alpha^2(1 + 4\kappa + 4\kappa^2 - 4\kappa_{12})}{\Xi^2\rho^2}. \tag{5.73}$$

Dropping the term containing τ^2 due to its magnitude in (5.72) and specializing for the onset $\Xi = 1$ leads to

$$I_1^\mu = 3\,\varphi_c \tag{5.74}$$

$$J_2^\mu = -\tau^2\,\frac{1 - 2\alpha\,(1 + 2\kappa) + \alpha^2(1 + 4\kappa + 4\kappa^2 - 4\kappa_{12})}{\rho^2}. \tag{5.75}$$

It is noteworthy that the first invariant solely depends on the chemical part of the Helmholtz free energy but not on the shear stress applied. Thus, a shear test may also prove useful to identify the material parameters. Using the above result in conjunction with relation (5.24), the condition to induce the transformation may be formulated as

$$3\,c_1\,\varphi_c + c_2\,\sqrt{\tau^2\,\frac{1 - 2\alpha\,(1 + 2\kappa) + \alpha^2(1 + 4\kappa + 4\kappa^2 - 4\kappa_{12})}{\rho^2}} = 1, \tag{5.76}$$

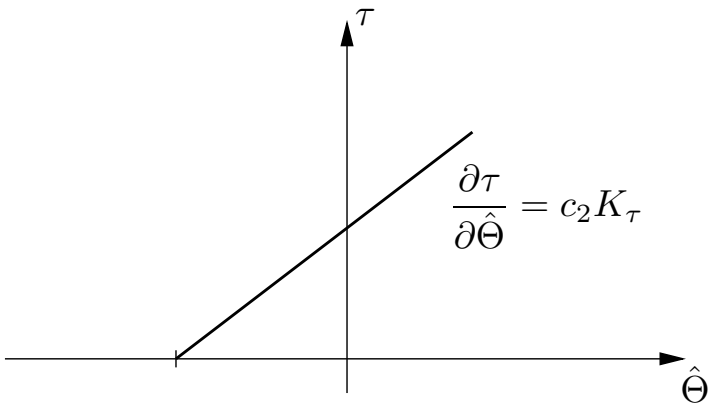

Figure 5.8: Clausius-Clapeyron Diagram for shear-test,
$K_\tau = \rho^{-1}\sqrt{1 - 2\alpha\,(1 + 2\kappa) + \alpha^2(1 + 4\kappa + 4\kappa^2 - 4\kappa_{12})}$.

or, using the dimensionless temperature $\hat{\Theta}$ and restricting to positive values for τ, as

$$c_2\,\tau\,\sqrt{\frac{1 - 2\alpha\,(1 + 2\kappa) + \alpha^2(1 + 4\kappa + 4\kappa^2 - 4\kappa_{12})}{\rho^2}} = 1 + \hat{\Theta}. \tag{5.77}$$

This result is depicted in figure 5.8. Again, a straight line can be observed in the Clausius-Clapeyron diagram. However, its slope does not depend on the parameter c_1.

5.4.4 Hydrostatic stress state

The statement made concerning the implicit inclusion of this case in the two dimensional example applies to this section as well. Now,[2]

$$\sigma_1 = \sigma_2 = \sigma_3 = p \tag{5.78}$$

is set. Using the assumption, that isotropy with respect to the induced deformation may be present, i.e. $\kappa_{11} = \kappa_{22} = \kappa_{33} = \kappa$, and dropping higher order

[2] p denotes a negative pressure. This sign convention is chosen to allow for simpler comparison with the results of other sections.

terms, the invariants read

$$I_1^\mu = \frac{3\,p\,(\alpha - 1 + 2\,\kappa\,\alpha)}{\Xi\,\rho} + 3\,\varphi_c \tag{5.79}$$

$$J_2^\mu = -4\,p^2\alpha^2\,\frac{\kappa_{12}^2 + \kappa_{23}^2 + \kappa_{13}^2}{\Xi^2\,\rho^2}. \tag{5.80}$$

Specializing to the onset of the transformation yields

$$I_1^\mu = \frac{3\,p\,(\alpha - 1 + 2\,\kappa\,\alpha)}{\rho} + 3\,\varphi_c \tag{5.81}$$

$$J_2^\mu = -4\,p^2\alpha^2\,\frac{\kappa_{12}^2 + \kappa_{23}^2 + \kappa_{13}^2}{\rho^2}. \tag{5.82}$$

It is generally believed that the onset of the transformation for SMA is not influenced by a superimposed hydrostatic stress. This behavior can only be achieved if by posing an additional restriction on the choice of the parameters,

$$\frac{c_1}{c_2} = -\frac{2}{3}\,\frac{\alpha\,\sqrt{\kappa_{12}^2 + \kappa_{23}^2 + \kappa_{13}^2}}{\alpha - 1 + 2\alpha\kappa}. \tag{5.83}$$

However, experimental results by Kakeshita et al. (1999) indicate, that this assumption, which is based more on theoretical considerations, might be not valid in all cases. For some SMA, a slight dependence of the hydrostatic part of the stress on the onset of the transformation exists.

5.4.5 Two dimensional stress-state

For the considered two-dimensional stress state,

$$\sigma_3 = 0 \tag{5.84}$$

is chosen. This leads to

$$I_1^\mu = -\frac{\Sigma_1 + \Sigma_2}{\rho} + 3\,\varphi \tag{5.85}$$

$$J_2^\mu = -\frac{\left(\Sigma_1^2 + 2\,K_{12}\Sigma_1\Sigma_2 + \Sigma_2^2\right)}{3\,\rho^2} \tag{5.86}$$

for the invariants. By introducing Σ_0, a scaled stress derived from the uniaxial simple tension case, such that

$$-c_1 \frac{\Sigma_0}{\rho} + c_2 \frac{1}{\rho\sqrt{3}}\Sigma_0 = 1 + \hat{\Theta} \tag{5.87}$$

holds, the transformation condition can be expressed as

$$F^{\xi} = -c_1 \left(\frac{\Sigma_1}{\Sigma_0} + \frac{\Sigma_2}{\Sigma_0}\right) + c_2 \sqrt{\left(\frac{\Sigma_1}{\Sigma_0}\right)^2 + 2\,K_{12}\,\frac{\Sigma_1}{\Sigma_0}\,\frac{\Sigma_2}{\Sigma_0} + \left(\frac{\Sigma_2}{\Sigma_0}\right)^2} - \left(\frac{c_2}{\sqrt{3}} - c_1\right) = \; 0 \tag{5.88}$$

Taking the square of this relation and rearranging yields

$$\boldsymbol{s} \cdot \boldsymbol{A} \cdot \boldsymbol{s}^T + 2\,\boldsymbol{a} \cdot \boldsymbol{s}^T - \left(\frac{c_2}{\sqrt{3}} - c_1\right)^2 = 0 \tag{5.89}$$

with $\boldsymbol{s} = (\Sigma_1/\Sigma_0, \Sigma_2/\Sigma_0)$,

$$\boldsymbol{A} = \begin{pmatrix} c_2^2 - c_1^2 & K_{12}\,c_2^2 - c_1^2 \\ K_{12}\,c_2^2 - c_1^2 & c_2^2 - c_1^2 \end{pmatrix}, \tag{5.90}$$

and

$$\boldsymbol{a} = \begin{pmatrix} c_1\,(c_1 - c_2/\sqrt{3}) \\ c_1\,(c_1 - c_2/\sqrt{3}) \end{pmatrix}. \tag{5.91}$$

Introduction of a translated coordinate-system

$$\hat{\boldsymbol{s}} = \boldsymbol{s} - (1,1)\,\frac{c_1(c_1 - c_2/\sqrt{3})}{2\,c_1^2 - c_2^2\,(1 + K_{12})} \tag{5.92}$$

leads to

$$\hat{\boldsymbol{s}} \cdot \boldsymbol{A} \cdot \hat{\boldsymbol{s}}^T + a = 0 \tag{5.93}$$

with

$$a = c_2^2 \left(\frac{c_2}{\sqrt{3}} - c_1 \right)^2 \frac{1 + K_{12}}{2\,c_1^2 - c_2^2\,(1 + K_{12})}. \tag{5.94}$$

Finally, the introduction of a coordinate system $\boldsymbol{x} = (x, y)$ which is rotated by an angle of 45° such that

$$x = \frac{1}{\sqrt{2}}\,(\hat{s}_1 + \hat{s}_2) \quad \text{and} \quad y = \frac{1}{\sqrt{2}}\,(-\hat{s}_1 + \hat{s}_2) \tag{5.95}$$

yields

$$\boldsymbol{x} \cdot \hat{\boldsymbol{A}} \cdot \boldsymbol{x}^T + a = 0 \tag{5.96}$$

with

$$\hat{\boldsymbol{A}} = \begin{pmatrix} -2\,c_1^2 + c_2^2(1 + K_{12}) & 0 \\ 0 & c_2^2(1 - K_{12}) \end{pmatrix}. \tag{5.97}$$

The structure of equation (5.96) and the resulting shape of the transformation condition can easily by analyzed (cf. Bronstein et al. (1997)). The following cases have to be considered:

- Zero-point or an intersection of beams.
  As the transformation condition should constitute a surface for a general three-dimensional situation, this case is considered degenerate here. In both situations, $a = 0$ holds, which leads to the restrictions

$$\begin{aligned} c_2 &\neq 0 \\ \frac{c_2}{\sqrt{3}} - c_1 &\neq 0 \\ K_{12} &\neq -1. \end{aligned} \tag{5.98}$$

- F^{ξ} forms an ellipse.
  In this case, $\hat{A}_{11}$ and $\hat{A}_{22}$ have to be of the same sign whereas a is nonzero and of opposite sign, i.e.

$$\hat{A}_{11}\,\hat{A}_{22} > 0 \;\text{ and }\; a\,\hat{A}_{11} < 0 \text{ (or, equivalently } a\,\hat{A}_{22} < 0). \tag{5.99}$$

The requirement that a should be nonzero can be satisfied by fulfillment of (5.98). The second condition in the equation above can be satisfied if

$$K_{12} > -1 \tag{5.100}$$

and, using relations (5.98a) and (5.98b),

$$K_{12} \neq 2 \left(\frac{c_1}{c_2}\right)^2 - 1. \tag{5.101}$$

The latter requirement can be geometrically interpreteded such that an ellipse of infinite diameter would be constructed if not obeyed. Taking into account that the condition $1 + K_{12} > 0$ has been derived already, this requirement may be adapted to

$$1 + K_{12} < 2 \left(\frac{c_1}{c_2}\right)^2 \tag{5.102}$$

The third requirement in equation (5.99) may be, using (5.102), expressed as

$$K_{12} > 1, \tag{5.103}$$

which is a stronger condition for the lower bound as the condition derived before. Assuming that the conditions for an ellipse hold, relation (5.96) can be rewritten to yield

$$\left(\frac{x}{r_x}\right)^2 + \left(\frac{y}{r_y}\right)^2 = 1 \tag{5.104}$$

with

$$r_x = \frac{c_2 \left(c_2/\sqrt{3} - c_1\right) \sqrt{1 + K_{12}}}{2\,c_1^2 - c_2^2\,(1 + K_{12})} \tag{5.105}$$

$$r_y = \left(c_2/\sqrt{3} - c_1\right) \sqrt{\frac{(1 + K_{12})(1 - K_{12})}{2\,c_1^2 - c_2^2\,(1 + K_{12})}} \tag{5.106}$$

- F^{ξ} forms an hyperbola.
  As the stress free state should be enclosed within the region where no transformation occurs, this case is considered a degenerate case for this application. In this case, $\hat{A}_{11}$ and $\hat{A}_{22}$ have to be of opposite sign and a nonzero which is already assured by the validity of requirements (5.98a)-(5.98c). This leads to the restriction

$$\hat{A}_{11}\,\hat{A}_{22} < 0. \tag{5.107}$$

- In case $\hat{A}_{11}$, $\hat{A}_{22}$, and a have the same sign, no real solutions can be found. This case should generally be avoided, its occurrence can be avoided by validity of one of the previous cases.

5.4.6 Closing remarks

Several examples for loadings and the influence of the parameters are presented in the preceding sections. Furthermore, some conditions related to the choice of the parameters have been derived if certain types of behavior can be observed. However, these conditions may overdetermine the parameters such that it is not possible to fulfill all restrictions imposed by the phenomena observed. It should be kept in mind that the initial approach (5.24) is the most simple combination of the invariants of the tensor $\boldsymbol{\mu}^{\Delta}$ and might be altered if necessary. Furthermore, certain assumption about the induced deformation have been made. These assumption may only be justified or disproven by the aid of thorough multiaxial experimental investigations at different temperatures. Those results are, in the quantity required for this task, not available nowadays.

5.5 Transformation kinetics

The derivations so far do not depend on a special choice of the strain induced by the phase transformation $\boldsymbol{\kappa}$, it could be treated as a variable. Thus, $\boldsymbol{\kappa}$ has not been fixed yet. Generally, it may by a function of the internal variable $\boldsymbol{\xi}$ and the applied stress. Unfortunately, not enough experimental data is available concerning this question for multiaxial situations. In order to proceed further, $\boldsymbol{\kappa}$ is treated as a constant regarding $\boldsymbol{\mu}^{\Delta}$ and $\boldsymbol{\xi}$. In order to keep the governing differential equations sufficiently simple to allow for an analytical treatment, only the case of simple tension is considered. Furthermore, $\hat{\Theta} = 0$,

$\kappa_{11} = const$, and $\kappa_{12} = \kappa_{13} = 0$ is set. Due to these simplifications, this section should be rather taken as an introductory example gaining first insight into the properties of the transformation kinetics rather than a complete and thorough investigation. The consideration are not elaborated further as measurements perpendicular to the loading axis are even necessary for the uniaxial case as these directions are influenced by the principal value of the tensor $\boldsymbol{\xi}$ perpendicular to the loading direction. Multiaxial experimental investigations on SMA are rare (Helm (2001), McNaney et al. (2003)) and their focus has not been on the thorough observation of the states perpendicular to the loading direction. Thus, in oder to make more specific assumptions about the measure involved, multiaxial experiments with a special emphasis on the discussed aspects are necessary.

From equations (5.41)-(5.43), it can be deduced that

$$\dot{\xi} = 3\,c_1(1-\xi)\,\lambda^{\xi} \tag{5.108}$$

$$\dot{\boldsymbol{\xi}}' = c_2\,\frac{f^{\xi}\,\boldsymbol{\mu}^{\Delta\prime}}{2\,\sqrt{-J_2^{\mu}}}\,\lambda^{\xi} \tag{5.109}$$

and

$$\lambda^{\xi} = \frac{-c_1 + \dfrac{c_2}{\sqrt{3}}}{3\,c_1\,g_1\,(1-\xi) + \dfrac{1}{2}\,c_2\,g_2\,f^{\xi}}\,\left(\frac{\Sigma}{\Xi}\right)^{\cdot} \tag{5.110}$$

holds when the approach

$$\boldsymbol{\xi} = \frac{1}{3}\begin{pmatrix} \xi+\xi' & 0 & 0 \\ 0 & \xi-\xi'/2 & 0 \\ 0 & 0 & \xi-\xi'/2 \end{pmatrix} \tag{5.111}$$

is used.

Considering the simplest approach for f^{ξ}

$$f^{\xi}(\xi) = \xi, \tag{5.112}$$

the differential equation for ξ can be solved to yield

$$\Sigma = (1+(\,\alpha-1)\xi)\left[\Sigma_0 + \frac{c_1\,\xi}{4}\,\frac{12\,c_1\,g_1(3+\xi(\xi-3)) + c_2\,g_2\,(3-2\xi)}{-c_1+\dfrac{c_2}{\sqrt{3}}}\right] \tag{5.113}$$

using the initial conditions $\Sigma(\xi = 0) = \Sigma_0$ and $\Xi(\xi = 0) = 1$. The stress reached at the end of the transformation can thus be calculated as

$$\Sigma(\xi = 1) = \alpha \left[\Sigma_0 + \frac{c_1}{4} \frac{12\, c_1\, g_1 + c_2\, g_2}{-c_1 + \dfrac{c_2}{\sqrt{3}}} \right]. \tag{5.114}$$

The slope at the onset of the transformation can be determined as

$$\frac{\partial \Sigma}{\partial \xi}(\xi = 0) = \frac{9\, c_1^2\, g_1}{-c_1 + \dfrac{c_2}{\sqrt{3}}} \tag{5.115}$$

whereas the slope at the end is

$$\frac{\partial \Sigma}{\partial \xi}(\xi = 1) = (\alpha - 1) \frac{3\, c_1 \left(c_1\, g_1 + \dfrac{1}{12}\, c_2\, g_2 \right)}{-c_1 + \dfrac{c_2}{\sqrt{3}}}. \tag{5.116}$$

By using these relation, the influence of the parameters g_1 and g_2 becomes clearer: g_1 influences the slope at the onset of the transformation whereas a combination of g_1 and g_2 governs this for $\xi = 1$.

As stated in section 5.1, this approach may be used to describe the process of reorientation when only martensite is present, i.e. for $\xi = 1$. In order to investigate this process further, $\xi = 1$ is assumed for the following and the differential equation for J_2^{ξ} is developed. For $\xi = 1$ and $f^{\xi}(\xi) = \xi$, λ^{ξ} reads

$$\lambda^{\xi} = 2 \frac{-c_1 + \dfrac{c_2}{\sqrt{3}}}{c_2\, g_2} \frac{\dot{\Sigma}}{\alpha} \tag{5.117}$$

A direct analytical analysis of the deviatoric part of $\boldsymbol{\xi}$ renders to be difficult. However, a differential equation for J_2^{ξ} can be derived as

$$\dot{J_2^{\xi}} = -\frac{c_2}{4} \sqrt{-J_2^{\xi}}\, \lambda^{\xi}. \tag{5.118}$$

The solution of the relation can be expressed as

$$\frac{J_2^\xi}{\sqrt{-J_2^\xi}} - \frac{J_{2\,1}^\xi}{\sqrt{-J_{2\,1}^\xi}} = -\frac{1}{4}\,\frac{-c_1 + \dfrac{c_2}{\sqrt{3}}}{g_2}\,\frac{\Sigma - \Sigma_1}{\alpha}. \tag{5.119}$$

where Σ_1 denotes the value of Σ at the end of the austenite to martensite transformation and begin of the reorientation. The reorientation may not proceed forever, thus the relation should reflect this. This is currently not the case and is an open question. But again it has to be noted, that experimental observations on this subject do not exist, thus a further specification is ruled out.

5.6 Backtransformation

The backtransformation from martensite to austenite may be described by a completely different set of functions g^ξ, F^ξ, and P^ξ with $\xi \in \{A, M\}$, implying that a complete new set of material parameters is used. This approach differs from the usual procedure where both transformations are treated in a symmetric fashion, i.e. as variants of essentially the same physical procedure. However, phenomena mentioned in section 5.1 indicate that the forward- and backtransformation are completely different processes. Again, it has to be noted that the lack of experimental investigations related to the approach proposed here render the further specification impossible.

5.7 Summary and Outlook

Even though the lack of experimental data left some important issues regarding the transformation kinetics open, the approach can be used to describe the twinning phenomenon. Furthermore, it is shown that it can be regarded as an extension of classical description stemming from thermodynamics.

6 Conclusion

Two approaches to describe the behavior of shape memory alloys are presented. Even though they describe the same material, the length scales and their problem statements lead to completely different solutions.

The micromechanical scheme is developed to capture the influence of inhomogeneities within the material on the martensitic transformation. A numerical scheme which captures the interfacial movement as well as the bulk behavior is developed. The qualitative influence of the size of inhomogeneities and the applied load can be verified.

The macroscopical approach has a completely different objective. Its aim is to describe macroscopically the behavior of SMA within a material law which could be implemented into an FE-code. Important characteristics can be verified using the proposed approach. However, due to the lack of experimental data, some questions remain open.

To close this monograph, the statement made in the introduction related to the choice of the modeling scale should be repeated: *such thing as THE right modeling scale which does not need any assumptions related to an underlying scale does not exist.*

A Specification of U, T, and $\hat{\mathbf{E}}$

The kernel functions used in the Somigliana identity can be stated for linear elastic, isotropic material behavior (cf . Gao & Davies (2000b)) as

$$\mathbf{U}(\mathbf{r},\ \tilde{\mathbf{r}}) = \frac{A}{r}\left(B\,\mathbf{1} + \boldsymbol{\nabla} r \otimes \boldsymbol{\nabla} r\right) = \frac{A}{r}\left(B\,\mathbf{1} + \frac{(\mathbf{r} - \tilde{\mathbf{r}}) \otimes (\mathbf{r} - \tilde{\mathbf{r}})}{r^2}\right) \tag{A.1}$$

with $r = |\mathbf{r} - \tilde{\mathbf{r}}|$,

$$A = \frac{1}{16\,\pi\,G(1-\nu)}, \tag{A.2}$$

and

$$B = 3 - 4\,\nu, \tag{A.3}$$

where G and ν denote shear modulus and Poisson's ration respectively. For the traction kernel **T**,

$$\mathbf{T}(\mathbf{r},\ \tilde{\mathbf{r}}, \mathbf{n}) = -\frac{2\,G\,A}{r^2}\left(C\left(\mathbf{n} \otimes \boldsymbol{\nabla} r - \boldsymbol{\nabla} r \otimes \mathbf{n}\right) + \mathbf{n} \cdot \boldsymbol{\nabla} r\left(C\,\mathbf{1} + 3\,\boldsymbol{\nabla} r \otimes \boldsymbol{\nabla} r\right)\right) \tag{A.4}$$

with

$$C = 1 - 2\,\nu \tag{A.5}$$

holds. For the volumetric term, a kernel **E** with the components

$$E_{ijk}(\mathbf{r},\ \tilde{\mathbf{r}}, \mathbf{n}) = \frac{U_{ij,k} + U_{ik,j}}{2}, \tag{A.6}$$

where $U_{ij,k}$ are the components of **U**, can be used to yield the components of $\hat{\mathbf{E}}$

$$\hat{E}_{ijk} = \mathbb{C}_{jkrs} E_{irs}. \tag{A.7}$$

$\mathbb{C}_{jkrs}$ denotes the components of the fourth order tensor of isotropic elasticity. Special care has to be taken when singularities occur. Procedures to deal with weak and strong singularities are described in Gao & Davies (2000b).

Bibliography

Aavatsmark, I. (1995): *Mathematische Einfürung in die Thermodynamik der Gemische*, Akademie Verlag 1995.

Allafi, J. (2002): *Mikrostrukturelle Untersuchungen zum Einfluß von thermomechanischen Behandlungen auf die martensitischen Phasenumwandlungen an einer Ni-reichen NiTi Formgedächtnislegierung* 2002, Ruhr-Universität Bochum.

Altenbach, J. & Altenbach, H. (1994): *Einführung in die Kontinuumsmechanik*, B.G. Teubner, Stuttgart 1994.

Baehr, H. (1966): *Thermodynamik*, Springer-Verlag 1966.

Ball, J. M. & James, R. D. (1987): *Fine phase mixtures and minimizers of energy*, in: Arch. Rat. Mech. Anal, Volume 100, 13–52.

Ball, J. M. & James, R. D. (1992): *Proposed experimental test of a theory of fine microstructure and the two well problem*, in: Phil. Trans. R. Soc. Lond. A, Volume 338, 389–450.

Barles, G., Soner, H. M. & Souganidis, P. E. (1993): *Front propagation and phase field theory*, in: SIAM J. Control and Optimization, Volume 31, 2, 439–469.

Başar, Y. & Weichert, D. (2000): *Nonlinear continuum mechanics of solids. Fundamental mathematical and physical concepts*, Springer-Verlag 2000.

Becker, E. & Bürger, W. (1975): *Kontinuumsmechanik*, B. G. Teubner, Stuttgart 1975.

Beer, G. (2001): *Programming the Boundary Element Method: An Introduction for Engineers*, John Wiley & Sons Inc 2001.

Berezovski, A. & Maugin, G. (2002): *Thermodynamics of Discrete Systems and Martensitic Phase Transition Simulation*, in: Technische Mechanik, Volume 22, 118–131.

Berezovski, A. & Maugin, G. A. (2003): *Simulation of wave and front propagation in thermoelastic materials with phase transformation*, in: Computational Materials Science, Volume 28, 2478–485.

Berezovski, A. & Maugin, G. A. (2005): *Stress-induced phase-transition front propagation in thermoelastic solids*, in: Eurpean Journal of Mechanics A/Solids, Volume 24, 1–21.

Betten, J. (1987): *Tensorrechnung für Ingenieure*, Teubner 1987.

Bowen, R. (1967): *Toward a Thermodynamics and Mechanics of Mixtures*, in: Arch. Rational Mech. Anal., Volume 24, 370–403.

Bowen, R. (1976): *Theory of Mixtures*, in: Eringen, C. (Ed.): *Mixtures and EM Field Theories*, Academic Press, New York, San Francisco, London 1976, Volume III of *Continuum Physics*, pp. 1–127.

Bowles, J. S. & Mackenzie, J. K. (1954): *Acta Metall.*, Volume 2, 129, 138, 224.

Bronstein, I. N., Semendjajew, A., Musiol, G. & Mühlig, H. (1997): *Taschenbuch der Mathematik*, Verlag Harri Deutsch 1997.

Bruhns, O. T. (2003): *Objective rates in finite elastoplasticity*, in: Miehe, C. (Ed.): *Computational mechanics of solid materials at large strains, Proceedings of IUTAM-Symposium, Stuttgart 2001*, Kluwer Academic Publ., Dordrecht 2003, pp. 151–160.

Bruhns, O. T., Xiao, H. & Meyers, A. (1999): *Self-consistent Eulerian rate type elasto-plasticity models based upon the logarithmic stress rate*, in: Int. J. Plast., Volume 15, 479–520.

Budyn, E., Zi, G., Moes, N. & Belytschko, T. (2004): *A method for multiple crack growth in brittle materials without remeshing*, in: International Journal for Numerical Methods in Engineering, In press.

Buratti, G., Huo, Y. & Müller, I. (2003): *Eshelby Tensor as a Tensor of Free Enthalpy*, in: Journal of Elasticity, Volume 72, 31–42.

Callen, H. (1970): *Thermodynamics*, 7 Edition, John Wiley & Sons, Inc. 1970.

Carlson, D. E. & Hoger, A. (1986): *The derivative of a tensor-valued function of a tensor*, in: Q. Appl. Math., Volume 44, 3, 409–423.

Carlson, N. N. & Miller, K. (1998a): *Design and Application of a Gradient-Weighted Moving Finite Element Code I: In one Dimension*, in: SIAM J. Sci. Comput., Volume 19, 3, 728–765, URL `http://www.siam.org/journals/sisc/19-3/26955.html`.

Carlson, N. N. & Miller, K. (1998b): *Design and Application of a Gradient-Weighted Moving Finite Element Code II: In two Dimensions*, in: SIAM J. Sci. Comput., Volume 19, 3, 766–798, URL `http://www.siam.org/journals/sisc/19-3/26956.html`.

Chessa, J. & Belytschko, T. (2004): *Arbitrary discontinuities in space-time finite elements by level sets and X-FEM*, in: International Journal for Numerical Methods in Engineering, .

Chessa, J., Smolinkski, P. & Belytschko, T. (2002): *The extended finite element method(XFEM) for solidification problems*, in: International Journal for Numerical Methods in Engineering, Volume 53, 1959–1977.

Eggeler, G., Allafi, J. K., Dlouhy, A. & Ren, X. (2003): *On the role of chemical and microstrictural heterogeneities in multistage martensitic transformations*, in: *ICOMAT'02*, 2003, pp. 673–676.

Eringen, A. C. (1967): *Mechanics of Continua*, John Wiley & Sons Inc 1967.

Eringen, A. C. (1975): *Continuum Physics Vol 2: Continuum Mechanics of Single-Substance Bodies*, 1975.

Eshelby, J. (1951): *The force on an elastic singularity*, in: Phil. Trans. Roy. Soc. London, Volume A 244, 87–112.

Eshelby, J. (1975): *The elastic energy-momentum tensor*, in: J. Elasticity, Volume 5, 321–335.

Foerster, A. & Kuhn, G. (1993): *Die Behandlung von großen Deformationen hyperelastischer Materialien mit der Randelementmethode*, in: Z. angew. Math. Mech., Volume 73, 7/8, 702–705.

Gao, X. W. & Davies, T. G. (2000a): *3D multi-region BEM with corners and edges*, in: International Jouranal of Solids and Structures, Volume 37, 1549–1560.

Gao, X. W. & Davies, T. G. (2000b): *Boundary Element Programming in Mechanics*, Cambridge University Press 2000.

Ghoussoub, J. & Leroy, Y. M. (2001): *Solid-fluid phase transformation within grain boundaries during compaction by pressure solution*, in: Journal of the Mechanics and Physics of Solids, Volume 49, 2385–2430.

Grinfeld, M. (1991): *Thermodynamic methods in the theory of heterogenous systems*, Longman Scientific & Technical 1991.

Gross, D., Kolling, S., Mueller, R. & Schmidt, I. (2003): *Configurational forces and their application in solid mechanics*, in: European Journal of Mechanics A/Solids, Volume 22, 669–692.

Gurtin, M. (1995): *The Nature of Configurational Forces*, in: Arch. Rat. Mech. Anal., Volume 131, 67–100.

Gurtin, M. & Podio-Guidugli, P. (1996): *On Configurational Inertial Forces at a Phase Interface*, in: Journal of Elasticity, Volume 44, 255–269.

Gurtin, M. E. (2000): *Configurational Forces as Basic Concepts of Continuum Physics*, Springer Verlag 2000.

Gurtin, M. E. & Fried, E. (1999): *Coherent Solid-State Phase Transitions with Atomic Diffusion: A Thermomechanical Treatment*, in: Journal of Statistical Physics, Volume 95, 5/6, 1361–1426.

Gurtin, M. E. & Jabbour, M. E. (2002): *Interface evolution in three-dimensions with curvature-dependent energy and surface diffusion: interface-controlled evolution, phase ransitions, epitaxial growth of elastic films*, in: Archive for Rational Mechanics and Analysis, Volume 163 (3), 171–208.

Gyarmati, I. (1970): *Non-equilibrium Thermodynamics*, Springer Verlag 1970.

Hahn, H. G. (1985): *Elastizitätstheorie*, Teubner 1985.

Heidug, W. & Lehner, F. (1985): *Thermodynamics of Coherent Phase Tranformations in Nonhydrostatically Stressed Solids*, in: Pure Appl. Geophys., Volume 123, 91–98.

Helm, D. (2001): *Formgedächtnislegierungen – Experimentelle Untersuchung, phänomenologische Modellierung und numerische Simulation der thermomechanischen Materialeigenschaften* 2001, Institut für Mechanik, Universität Gesamthochschule Kassel.

Hill, R. (1978): *Aspects of invariance in solid mechanics*, in: Adv. Appl. Mech., Volume 18, 1–75.

Hoger, A. (1986): *The material time derivative of logarithmic strain*, in: Int. J. Solids Structures, Volume 22, 9, 1019–1032.

Hornbogen, E. & Warlimont, H. (1991): *Metallkunde*, Springer-Verlag 1991.

Huang, R., Sukumar, N. & Prevost, J.-H. (2003): *Modelling quasi-static crack growth with the extended finite element method Part II: Numerical applications*, in: International Journal of Solids and Structures, Volume 40, 7539–7552.

Iadicola, M. A. & Shaw, J. A. (2004): *Rate and thermal sensitivities of unstable transformation behavior in a shape memory alloy*, in: International Journal of Plasticity, Volume 20, 577–605.

Kakeshita, T., Saburi, T. & Shimizu, K. (1999): *Effects of hydrostatic pressure and magnetic field on martensitic transformations*, in: Materials science and engineering A, , 21–39.

Kane, J., Kashava Kumar, B. & Saigal, S. (1990): *An Arbitrary Condensing, Noncondensing Solution Strategy for Large Scale, Multi-Zone Boundary Element Analysis*, in: Computer Methods in Applied Mechanics and Engineers, Volume 79.

Kienzler, R. & Herrmann, G. (2000): *Mechanics in Material Space*, Springer-Verlag Berlin, Heidelberg, New York 2000.

Kienzler, R. & Maugin, G. (2001): *Configurational Mechanics of Materials*, Springer Verlag, Wien 2001.

Knowles, J. K. (1995): *Dynamic thermoelastic phase transitions*, in: Int. J. Solids Structures, Volume 32, 17/18, 2703–2710.

Köhler, O. (1999): *Entwicklung eines effizienten Randintegralverfahrens für 2D, 3D und axialsymmetrische Probleme bei nichtlinearem Materialverhalten und großen Deformationen* 1999, Erlangen.

Kuprat, A. (2000): *Modeling Microstructure Evolution using Gradient-Weighted Moving Finite Elements*, in: SIAM J. Sci. Comput., Volume 22, 2, 535–560, URL `http://www.siam.org/journals/sisc/22-2/34837.html`.

Levitas, V. (2002): *Critical thought experiment to choose the driving force for interface propagation in inelastic materials*, in: Int. J. Plasticity, Volume 18, 1499–1525.

Lexcellent, C., Vivet, A., Bouvet, C., Calloch, S. & Blanc, P. (2002): *Experimental and numerical determinations of the initial surface of phase transformation under biaxial loading in some polycrystalline shape-memory alloys*, in: J. Mech. Phys. Solids, Volume 50, 2717–2735.

Lieberman, D. S., Wechsler, M. S. & Read, T. A. (1955): *On the theory of the formation of martensite*, in: Journal of Applied Physics, Volume 26, 473.

Lim, T.J. & McDowell, D.L. (1999): *Mechanical Behavior of an Ni-Ti Shape Memory Alloy Under Axial-Torsional Proportional and Nonproportional Loading*, in: Journal of Engineering Materials and Technology, Volume 121, 1, 9–18.

Luig, P., Knopik, A., Oberste-Brandenburg, C., Grabe, C., Bruhns, O.-T. & Predki, W. (2005): *Damping couplings with elements of pseudoelastic NiTi shape memory alloys*, in: Archive of Applied Mechanics, Submitted.

Lusk, M. (1996): *A Consideration of Curved Interfaces in Stress-Assisted Martensite Formation*, in: Journal of Elasticity, Volume 44, 271–284.

Marsden, J. & Hughes, T. (1983): *Mathematical Foundations of Elasticity*, Prentince-Hall, Englewood Cliffs, New Jersey 1983.

Maugin, G. (1993): *Material Inhomogeneities in Elasticity*, Chapman & Hall, London 1993.

Maugin, G. (2002): *Special Issue - Eshelbian Mechanics*, in: Mechanics Research Comunications, Volume 29, 6.

McNaney, J., Imbeni, V., Jung, Y., Papadopoulos, P. & Ritchie, R. (2003): *An experimental study of the superelastic effect in a shape-memory Nitinol alloy under biaxial loading*, in: Mechanics of Materials, Volume 35, 969–986.

Morill, B. (1972): *An Introduction to Equilibrium Thermodynamics*, Pergamon Press, Inc. 1972.

Müller, C. (2003): *Thermodynamic modeling of polycrystalline shape memory alloys at finite strains* 2003, Ruhr-Universität Bochum.

Muschik, W., Papenfuss, C. & H., E. (2001): *A sketch of continuum thermodynamics*, in: J. Non-Newtonian Fluid Mech., Volume 96, 255–290.

Oberste-Brandenburg, C. (1999): *Ein Materialmodell zur Beschreibung der Austenit-Martensit Phasentransformation unter Berücksichtigung der transformationsinduzierten Plastizität* 1999, Dissertation, Ruhr-Universität Bochum.

Oberste-Brandenburg, C. & Bruhns, O.-T. (2004): *A tensorial description of the transformation kinetics of the martensitic phase transformation*, in: Int. J. Plasticity, Volume 20, 2083–2109.

Ogden, R. (1984): *Non-Linear Elastic Deformations*, Dover 1984.

Otsuka, K. & Wayman, C. M. (1998): *Shape memory materials*, Cambridge University Press 1998.

Potrc, I., Alujevic, A. & Kuhn, G. (1987): *Thermo-Plasticity by Boundary Elements*, Volume 2, Springer - Verlag 1987.

Raniecki, B. & Bruhns, O. (1991): *Thermodynamic reference model for elastic-plastic solids undergoing phase transformations*, in: Arch. Mech., Volume 43, 2-3, 343–376.

Raniecki, B. & Lexcellent, C. (1999): *The Equilibrium Motion of the Martensitic Interface in Thick-walled Infinite Austenitic Plate*, in: Argoul, P., Frémond, M. & Nguyen, Q. (Eds.): *IUTAM Symposium on Variations of Domains and Free-Boundary Problems in Solid Mechanics (Solid Mechanics and Its Applications)*, Springer 1999, pp. 22IV–25IV.

Raniecki, B. & Tanaka, K. (1994): *On the Thermodynamic Driving Force for Coherent Phase Transformations*, in: Int. J. Engng Sci, Volume 32, 12, 1845–1858.

Russo, G. & Smereka, P. (2000): *A level-set method for the evolution of faceted crystals*, in: SIAM J. Sci. Comput., Volume 21, 6, 2073–2095.

Schade, H. (1970): *Kontinuumstheorie strömender Medien*, Springer-Verlag 1970.

Schmidt, I. & Gross, D. (1997): *The equilibrium shape of an elastically inhomogeneous inclusion*, in: J. Mech. Phys. Solids, Volume 45, 9, 1521–1549.

Sethian, J. A. (1998): *Level Set Methods*, Cambridge University Press 1998.

Shield, T. W. (1995): *Orientation dependence of the pseudoelastic behavior of single crystals of Cu-Al-Ni in tension*, in: J. Mech. Phys. Solids, Volume 43, 6, 869–895.

Šilhavý, M. (1997): *The Mechanics and Thermodynamics of Continuous Media*, Springer Verlag, Berlin, Heidelberg, New York 1997.

Simha, N. K. & Bhattacharya, K. (1999): *Edge effects on the propagation of phase boundaries*, in: Materials Science and Engineering, Volume A273-275, 241–244.

Simha, N. K. & Bhattacharya, K. (2000): *Kinetics of phase boundaries with edges and junctions in a three-dimensional multi-phase body*, in: J. Mech. Phys. Solids, Volume 48, 2619–2641.

Sukumar, N., Chopp, D. L., Moes, N. & Belytschko, T. (2001): *Modelling holes and inclusions by level sets in the extended finite-element method*, in: Comput. Methods Appl. Mech. Engrg, Volume 190, 6183–6200.

Sukumar, N. & H., P. J. (2003): *Modelling quasi-static crack growth with the extended finite element method Part I: Computer implementation*, in: International Journal of Solids and Structures, Volume 40, 7513–7537.

Sun, Q. P. (Ed.): *The formation of macrotwins in NiAl martensite*, 2001.

Taylor, J. E., Cahn, J. W. & Handwerker, C. A. (1992): *I-Geometric models of crystal growth*, in: Acta Metall. Mater., Volume 40, 7, 1443–1474.

Thamburaja, P. (2005): *Constitutive equations for martensitic reorientation and detwinning in shape-memory alloys*, in: Journal of the Mechanics and Physics of Solids, Volume 53, 825–856.

Truesdell, C. & Toupin, R. (1960): *The Classical Field Theories*, in: Flügge, S. (Ed.): *Handbuch der Physik*, Springer-Verlag Berlin 1960, Volume III, pp. 227–793.

Wechsler, M., Liebermann, D. & Read, T. (1953): *On the theory of the formation of martensite*, in: Trans. Am. Inst. Min. (Metall) Eng., Volume 197, 1503–1515.

Wilmanski, K. (1998): *Thermomechanics of Continua*, Springer Verlag 1998.

Xiao, H. (1997a): *A unified theory of representations for scalar-, vector- and second order tensor-valued anisotropic functions of vectors and second order tensors*, in: Arch. Mech., Volume 49, 6, 995–1039.

Xiao, H. (1997b): *On Isotropic Invariants of the Elasticity Tensor*, in: Journal of Elasticity, Volume 46, 115–149.

Xiao, H., Bruhns, O. T. & Meyers, A. (2000a): *The choice of objective rates in finite elastoplasticity: general results on the uniqueness of the logarithmic rate*, in: Proc. R. Soc. Lond. A, Volume 456, 1865–1882.

Xiao, H., Bruhns, O. T. & Meyers, A. (2000b): *A consistent finite elastoplasticity theory combining additive and multiplicative decomposition of the stretching and the deformation gradient*, in: Int. J. Plast., Volume 16, 143–177.

Mitteilungen aus dem Institut für Mechanik

Nr. 1 Theodor Lehmann: Dezember 1976
Große elasto-plastische Formänderungen

Nr. 2 Bogdan Raniecki/Klaus Thermann: Juni 1978
Infinitesimal Thermoplasticity and Kinematics of Finite Elastic-Plastic Deformations. Basic Concepts

Nr. 3 Wolfgang Krings: Januar 1976
Beitrag zur Finiten Element Methode bei linearem, viskoelastischem Stoffverhalten Stoffverhalten

Nr. 4 Burkhard Lücke: Januar 1976
Theoretische und experimentelle Untersuchen der zyklischen elastoplastischen Blechbiegung bei endlichen Verzerrungen

Nr. 5 Knut Schwarze: Februar 1976
Einfluß von Querschnittsverformungen bei dünnwandigen Stäben mit stetig gekrümmter Profilmittellinie

Nr. 6 Hubert Sommer: Januar 1977
Ein Beitrag zur Theorie des ebenen elastischen Verzerrungszustandes bei endlichen Formänderungen

Nr. 7 H. Stumpf/F. J. Biehl: März 1977
Die Methode der orthogonalen Projektionen und ihre Anwendungen zur Berechnung orthotroper Platten

Nr. 8 Albert Meyers: April 1977
Ein Beitrag zum optimalen Entwurf von schnellaufenden Zentrifugenschalen

Nr. 9 Berend Fischer: April 1977
Zur zyklischen, elastoplastischen Beanspruchen eines dickwandigen Zylinders bei endlichen Verzerrungen

Nr. 10 Wojciech Pietraszkiewicz: Mai 1977
Introduction to the Non-Linear Theory of Shells

Nr. 11 Wilfried Ullenboom: Juni 1977
Optimierung von Stäben unter nichtperiodischer dynamischer Belastung

Nr. 12 Jürgen Güldenpfennig: Juli 1977
Anwendung eines Modells der Vielkristallplastizität auf ein Problem gekoppelter elastoplastischer Wellen

Nr. 13 Pawel Rafalski: März 1978
Minimum Principles in Plasticity

Nr. 14 Peter Hilgers: Juli 1978
Der Einsatz eines Mikrorechners zur hybriden Optimierung und Schwingungsanalyse

Nr. 15 Hans-Albert Lauert: August 1979
Optimierung von Stäben unter dynamischer periodischer Beanspruchung bei Beachtung von Spannungsrestriktionen

Nr. 16 Martin Fritz: Juli 1979
Berechnund der Auflagerkräfte und der Muskelkräfte des Menschen bei ebenen Bewegungen aufgrund von kinematographischen Aufnahmen

Nr. 17 H. Stumpf/F. J. Biehl: Dezember 1979
Approximations and Error Estimates in Eigenvalue Problems of Elastic Systems with Application to Eigenvibrations of Orthotropic Plates

Nr. 18 Uwe Kohlberg: Juli 1979
Variational Principles and theirNumerical Application to Geometrically Nonlinear v. Karman Plates

Nr. 19 Heinz Antes: Januar 1980
Über Fehler und Möglichkeiten ihrer Abschätzung bei numerischen Berechnungen von Schalentragwerken

Nr. 20 Czeslaw Wozniak: März 1980
Large Deformations of Elastic and Non-Elastic Plates, Shells and Rods

Nr. 21 Maria K. Duszek: Juni 1980
Problems of Geometrically Non-Linear Theory of Plasticity

Nr. 22 Burkhard von Bredow: Dezember 1980
Optimierung von Stäben unter stochastischer Erregung

Nr. 23 Jürgen Preuss: Februar 1981
Optimaler Entwurf von Tragwerken mit Hilfe der Mehrzielmethode

Nr. 24 Ekkehard Großmann: Februar 1981
Kovarianzanalyse mechanischer Zufallsschwingungen bei Darstellung der mehrfachkorrelierten Erregungen durch stochastische Differentialgleichungen

Nr. 25 Dieter Weichert: März 1981
Variational Formulation and Solution of Boundary-Value Problems in the Theory of Plasticity and Application to Plate Problems

Nr. 26 Wojciech Pietraszkiewicz: Juni 1981
On Consistent Approximations in the Geometrically Non-Linear Theory of Shells

Nr. 27 Georg Zander: September 1981
Zur Bestimmung von Verzweigungslasten dünnwandiger Kreiszylinder unter kombinierter Längs- und Torsionslast

Nr. 28 Pawel Rafalski: September 1981
An Alternative Approach to the Elastic-Viscoplastic Initial-Boundary Value Problem

Nr. 29 Heinrich Oeynhausen: November 1981
Verzweigungslasten elastoplastisch deformierter, dickwandiger Kreiszylinder unter Innendruck und Axialkraft

Nr. 30 F.-J. Biehl: Dezember 1981
Zweiseitige Eingrenzung von Feldgrößen beim einseitigen Kontaktproblem

Nr. 31 Maria K. Duszek: Juni 1982
Foundations of the Non-Linear Plastic Shell Theory

Nr. 32 Reinhard Piltner: Juli 1982
Spezielle finite Elemente mit Löchern, Ecken und Rissen unter Verwendung von analytischen Teillösungen

Nr. 33 Petrisor Mazilu: Dezember 1982
Variationsprinzipe der Thermoplastizität I. Wärmeausbreitung und Plastizität

Nr. 34 Helmut Stumpf: Dezember 1982
Unified Operator Description, Nonlinear Buckling and Post-Buckling Analysis of Thin Elastic Shells

Nr. 35 Bernd Kaempf: März 1983
Ein Exremal-Variationsprinzip für die instationäre Wärmeleitung mit einer Anwendung auf thermoelastische Probleme unter Verwendung der finiten Elemente

Nr. 36 Alfred Kraft: Juli 1983
Zum methodischen Entwurf mechanischer Systeme im Hinblick auf optimales Schwingungsverhalten

Nr. 37 Petrisor Mazilu: August 1983
Variationsprinzipe der Thermoplastizität II. Gekoppelte thermmomechanische Prozesse

Nr. 38 Klaus-Detlef Mickley: November 1983
Punktweise Eingrenzung von Feldgrößen in der Elastomechanik und ihre numerische Realisierung mit Fundamental-Splinefuntionen

Nr. 39 Lutz-Peter Nolte: Dezember 1983
Beitrag zur Herleitung und vergleichende Untersuchung geometrisch nichtlinearer Schalentheorien unter Berücksichtigung großer Rotationen

Nr. 40 Ulrich Blix: Dezember 1983
Zur Berechnung der Einschnürung von Zugstäben unter Berücksichtigung thermischer Einflüsse mit Hilfe der Finite-Element-Methode

Nr. 41 Peter Becker: Februar 1984
Zur Berechnung von Schallfeldern mit Elemtmethoden

Nr. 42 Diemar Bouchard: Februar 1984
Entwicklung und Anwendung eines an die Diskrete-Fourier-Transformation angepaßten direkten Algorithmus zur Bestimmung der modalen Parameter linearer Schwingungssysteme

Nr. 43 Uwe Zdebel: Dezember 1984
Theoretische und experimentelle Untersuchungen zu einem thero-plastischen Stoffgesetz

Nr. 44 Jan Kubik: April 1985
Thermodiffusion Flows in a Solid with a Dominant Constituent

Nr. 45 Horst J. Klepp: Juni 1985
Über die Gleichgewichtslagen und Gleichgewichtsbereiche nichtlinearer autonomer Systeme

Nr. 46 J. Makowski/L.-P. Nolte/H. Stumpf: Juli 1985
Finite In-Plane Deformations of Flexible Rods - Insight into Nonlinar Shell Problems

Nr. 47 Franz Karl Labisch: August 1985
Grundlagen einer Analyse mehrdeutiger Lösungen nichtlinearer Randwertprobleme der Elastostatik mit Hilfe von Variationsverfahren

Nr. 48 J. Chroscielewski/L.-P. Nolte: Oktober 1985
Strategien zur Lösung nichtlinearer Probleme der Strukturmechanik und ihre modulare Aufbereitung im Konzept MESY

Nr. 49 Karl-Heinz Bürger: Dezember 1985
Gewichtsoptimierung rotationssymmetrischer Platten unter instationärer Erregung

Nr. 50 Ulrich Schmid: Februar 1987
Zur Berechnung des plastischen Setzens von Schraubenfedern

Nr. 51 Jörg Frischbier: März 1987
Theorie der Stoßbelastung ortotroper Platten und ihr experimentelle Überprüfung am Beispiel einer unidirektional verstärkten CFK-Verbundplatte

Nr. 52 W. Tampczynski: Juli 1987
Strain history effect in cyclic plasticity

Nr. 53 Dieter Weichert: Dezember 1987
Zum Problem geometrischer Nichtlinearitäten in der Plastizitätstheorie

Nr. 54 Heinz Antes/Thomas Meise/Thomas Wiebe: Januar 1988
Wellenausbreitung in akustischen Medien Randelement-Prozeduren im 2-D Frequenzraum und im 3-D Zeitbereich

Nr. 55 Wojciech Pietraszkiewicz: März 1988
Geometrically non-linear theories of thin elastic shells

Nr. 56 Jerzy Makowski/Helmut Stumpf: April 1988
Finite strain theory of rods

Nr. 57 Andreas Pape: Mai 1988
Zur Beschreibung des transienten und stationären Verfestigungsverhaltens von Stahl mit Hilfe eines nichtlinearen Grenzflächenmodells

Nr. 58 Johannes Groß-Weege: Juni 1988
Zum Einspielverhalten von Flächentragwerken

Nr. 59 Peihua LIU: Juli 1988
Optimierung von Kreisplatten unter dynamischer nicht rotationssymmetrischer Last

Nr. 60 Reinhard Schmidt: August 1988
Die Anwendung von Zustandsbeobachtern zur Schwingungsüberwachung und Schadensfrüherkennung auf mechanische Konstruktionen

Nr. 61 Martin Pitzer: Juli 1988
Vergleich einiger FE-Formulierungen auf der Basis eines inelastischen Stoffgesetzes

Nr. 62 Jerzy Makowski/Helmut Stumpf: Dezember 1988
Geometric structure of fully nonlinear and linearized Cosserat type shell theory

Nr. 63 O. T. Bruhns: Januar 1989
Große plastische Formänderungen - Bad Honnef 1988

Nr. 64 Khanh Chau Le/Helmut Stumpf/Dieter Weichert: Juli 1989
Variational principles of fracture mechanics

Nr. 65 Guido Obermüller: Juni 1989
Ein Beitrag zur Strukturoptimierung unter stochastischen Lasten

Nr. 66 Herbert Diehl: Juni 1989
Ein Materialmodell zur Berechnung von Hochgeschwindigkeitsdeformationen metallischer Werkstoffe unter besonderer Berücksichtigung der Schädigung durch Scherbänder

Nr. 67 Michael Geis: November 1989
Zur Berechnund ebener, elastodynamischer Rißprobleme mit der Randelementmethode

Nr. 68 Günter Renker: November 1989
Zur Identifikation nichtlinearer strukturmechanischer Systeme

Nr. 69 Berthold Schieck: November 1989
Große elastische Dehnungen in Schalen aus hyperelastischen inkompressiblen Materialien

Nr. 70 Frank Szepan: Dezember 1989
Ein elastisch-viskoplastisches Stoffgesetz zur Beschreibung großer Formänderungen unter Berücksichtigung der thermomechanischen Kopplung

Nr. 71 Christian Scholz: Dezember 1989
Ein Beitrag zur Gestaltsoptimierung druckbelasteter Rotationsschalen

Nr. 72 J. Badur/H. Stumpf: Dezember 1989
On the influence of E. and F. Cosserat on modern continuum mechanics and field theory

Nr. 73 Werner Fornefeld: Januar 1990
Zur Parameteridentifikation und Berechnung von Hochgeschwindigkeitsdeformationen metallischer Werkstoffe anhand eines Kontinuums-Damage-Modells

Nr. 74 J. Saczuk/H. Stumpf: April 1990
On statical shakedown theorems for non-linear problems

Nr. 75 Andreas Feldmüller: April 1991
Ein thermoplastisches Stoffgesetz isotrop geschädigter Kontinua

Nr. 76 Ulfert Rott: April 1991
Ein neues Konzept zur Berechnung viskoplastischer Strukturen

Nr. 77 Thomas Heinrich Pingel: Juli 1991
Beitrag zur Herleitung und numerischen Realisierung eines mathematischen Modells der menschlichen Wirbelsäule

Nr. 78 O. T. Bruhns: Dezember 1991
Große plastische Formänderungen - Bad Honnef 1991

Nr. 79 J. Makowski/J. Chroscielewski/H. Stumpf:
Computational Analysis of Shells Undergoing Large Elastic Deformation Part I:Theoretical Foundations

Nr. 80 J. Chroscielewski/J. Makowski/H. Stumpf:
Computational Analysis of Shells Undergoing Large Elastic Deformation Part II: Finite Element Implementation

Nr. 81 R. H. Frania/H. Waller: Mai 1992
Entwicklung und Anwendung spezieller finiter Elemente für Kerbspannungsprobleme im Maschienebau

Nr. 82 B. Bischoff-Beiermann: Juli 1992
Zur selbstkonsistenten Berechnung von Eigenspannungen in polykristallinem Eis unter Berücksichtigung der Monokristallanisotropie

Nr. 83 J. Pohé: Februar 1993
Ein Beitrag zur Stoffgesetzentwicklung für polykristallines Eis

Nr. 84 U. Kikillus: Mai 1993
Ein Beitrag zum zyklischen Kiechverhalten von Ck 15

Nr. 85 T. Guo: Juni 1993
Untersuchung des singulären Rißspitzenfeldes bei stationärem Rißwachstum in verfestigendem Material

Nr. 86 Achim Menne: Januar 1994
Identifikation der dynamischen Eigenschaften von hydrodynamischen Wandlern

Nr. 87 Uwe Folchert: Januar 1994
Identifikation der dynamischen Eigenschaften Hydrodynamischer Kopplungen

Nr. 88 Jörg Körber: April 1994
Ein verallgemeinertes Finite-Element-Verfahren mit asymptotischer Stabilisierung angewendet auf viskoplastische Materialmodelle

Nr. 89 Peer Schieße: April 1994
Ein Beitag zur Berechnung des Deformationsverhaltens anisotrop geschädigter Kontinua unter Berücksichtigung der thermoplastischen Kopplung

Nr. 90 Egbert Schopphoff: Juli 1994
Dreidimensionale mechanische Analyse der menschlichen Wirbelsäule

Nr. 91	Christoph Beerens: Zur Modellierung nichtlinearer Dämpfungsphänomene in der Strukturmechanik	Juli 1994
Nr. 92	K. C. Le/H. Stumpf: Finte elastoplasticity with microstructure	November 1994
Nr. 93	O. T. Bruhns: Große plastische Formänderungen - Bad Honnef 1994	Dezember 1994
Nr. 94	Armin Lenzen: Untersuchung von dynamischen Systemen mit der Singulärwertzerlegung - Erfassung von Strukturveränderungen	Dezember 1994
Nr. 95	J. Makowski/H. Stumpf: Mechanics of Irregular Shell Structures	Dezember 1994
Nr. 96	J. Chroscielewski/J. Makowski/H. Stumpf: Finte Elements for Irregular Nonlinear Shells	Dezember 1994
Nr. 97	W. Krings/A. Lenzen/u. a.: Festschrift zum 60. Geburtstag von Heinz Waller	Februar 1995
Nr. 98	Ralf Podleschny: Untersuchung zum Instabilitätsverhalten scherbeanspruchter Risse	April 1995
Nr. 99	Bernd Westerhoff: Eine Untersuchung zum geschwindigkeitsabhängigen Verhalten von Stahl	Juli 1995
Nr. 100	Marc Mittelbach: Simulation des Deformations- und Schädigungsverhaltens beim Stoßversuch mit einem Kontinuums-Damage-Modell	Dezember 1995
Nr. 101	Ulrich Hoppe: Über grundlegende Konzepte der nichtlinearen Kontinuumsmechanik und Schalentheorie	Mai 1996
Nr. 102	Marcus Otto: Erweiterung des Kaustikenverfahrens zur Analyse räumlicher Spannungskonzentrationen	Juni 1996
Nr. 103	Horst Lanzerath: Zur Modalanalyse unter Verwendung der Randelementemethode	Juli 1996
Nr. 104	Andreas Wichtmann: Entwicklung eines thermodynamisch konsistenten Stoffgesetzes zur Beschreibung der Reckalterung	August 1996
Nr. 105	Bjarne Fossa: Ein Beitrag zur Fließflächenmessung bei vorgedehnten Stoffen	Oktober 1996
Nr. 106	Khanh Chau Le: Kontinuumsmechanisches Modellieren von Medien mit veränderlicher Mikrostruktur	Dezember 1996
Nr. 107	Holger Behrens: Nichtlineare Modellierung und Identifikation hydrodynamischer Kupplungen mit allge- meinen diskreten Modellansätzen	Januar 1997
Nr. 108	Johannes Moosheimer: Gesteuerte Schwingungsdämpfung mit Elektrorheologischen Fluiden	Juli 1997
Nr. 109	Dirk Klaus Anding: Zur simultanen Bestimmung materialabhängiger Koeffizienten inelastischer Stoffgesetze	Oktober 1997
Nr. 110	Stephan Weng: Ein Evolutionsmodell zur mechanischen Analyse biologischer Strukturen	Dezember 1997

Nr. 111 Michael Straßberger: Dezember 1997
Aktive Schallreduktion durch digitale Zustandsregelung der Strukturschwingungen mit Hilfe piezokeramischer Aktoren

Nr. 112 Hans-Jörg Becker: Dezember 1997
Simultation des Deformationsverhaltens polykristallinen Eises auf der Basis eines monokristallinen Stoffgesetzes

Nr. 113 Thomas Nerzak: Dezember 1997
Modellierung und Simulation der Ausbreitung adiabatischer Scherbänder in metallischen Werkstoffen bei Hochgeschwindigkeitsdeformationen

Nr. 114 O. T. Bruhns: März 1998
Große plastische Formänderungen

Nr. 115 Jan Steinhausen: August 1998
Die Beschreibung der Dynamik von Antriebssträngen durch Black-Box-Modelle hydrodynamischer Kupplungen

Nr. 116 Thomas Pandorf: August 1998
Experimentelle und numerische Untersuchungen zur Kerbspitzenbeanspruchung bei schlagbelasteten Biegeproben

Nr. 117 Claus Oberste-Brandenburg: Juni 1999
Ein Materialmodell zur Beschreibung der Austenit-Martensit Phasentransformation unter Berücksichtigung der transformationsinduzierten Plastizität

Nr. 118 Michael Märtens: Dezember 1999
Regelung mechanischer Strukturen mit Hilfe piezokeramischer Stapelaktoren

Nr. 119 Dirk Kamarys: Dezember 1999
Detektion von Systemveränderungen durch neue Identifikationsverfahren in der experimentellen Modalanalyse

Nr. 120 Wolfgang Hiese: Januar 2000
Gültigkeitskriterien zur Bestimmung von Scherbruchzähigkeiten

Nr. 121 Peter Jaschke: Februar 2000
Mathematische Modellierung des Betriebsverhaltens hydrodynamischer Kupplungen mit hybriden Modellansätzen

Nr. 122 Stefan Müller: Februar 2000
Zum Einsatz von semi-aktiven Aktoren zur optimalen Schwingungsreduktion in Tragwerken

Nr. 123 Dirk Eichel: Juni 2000
Zur Kondensation strukturdynamischer Aufgaben mit Hilfe von Polynommatrizen

Nr. 124 Andreas Bürgel: August 2000
Bruchmechanische Kennwerte beim Wechsel im Versagensverhalten dynamisch scherbeanspruchter Risse

Nr. 125 Daniela Lürding: März 2001
Modellierung großer Deformationen in orthotropen, hyperelastischen Schalenstrukturen

Nr. 126 Thorsten Quent: Mai 2001
Ein mikromechanisch begründetes Modell zur Beschreibung des duktilen Verhaltens metallischer Werkstoffe bei endlichen Deformationen unter Berücksichtigung von Porenschädigung

Nr. 127 Ndzi C. Bongmba: Mai 2001
Ein finites anisotropes Materialmodell auf der Basis der Hencky-Dehnung und der logarithmischen Rate zur Beschreibung duktiler Schädigung

Nr. 128 Henning Schütte: August 2001
Ein finites Modell für spröde Schädigung basierend auf der Ausbreitung von Mikrorissen

Nr. 129 Henner Vogelsang: Dezember 2001
Parameteridentifikation für ein selbstkonsistentes Stoffmodell unter Berücksichtigung von Phasentransformationen

Nr. 130 Jörn Mosler: Dezember 2002
Finite Elemente mit sprungstetigen Abbildungen des Verschiebungsfeldes für numerische Analysen lokalisierter Versagenszustände

Nr. 131 Karin Preusch: Mai 2003
Hierarchische Schalenmodelle für nichtlineare Kontinua mit der p-Version der Finite-Element Methode

Nr. 132 Christoph Müller: August 2003
Thermodynamic modeling of polycrystalline shape memory alloys at finite strains

Nr. 133 Martin Heiderich: Juni 2004
Ein Beitrag zur zerstörungsfreien Schädigungsanalyse

Nr. 134 Raoul Costamagna: Juli 2004
Globale Materialbeziehungen für das geklüftete Gebirge

Nr. 135 Markus Böl: Januar 2005
Numerische Simulation von Polymernetzwerken mit Hilfe der Finite-Elemente-Methode

Nr. 136 Gregor Kotucha: August 2005
Regularisierung von Problemen der Topologieoptimierung unter Einbeziehung von Dichtegradienten

Nr. 137 Michael Steiner: Februar 2006
Deformations- und Versagensverhalten innendruckbeanspruchter Stahlrohre durch Stoßbelastung

Nr. 138 Dirk Bergmannshoff: Dezember 2006
Das Instabilitätsverhalten zug-/scherbeanspruchter Risse bei Variation des Belastungspfades

Nr. 139 Olaf Schilling: Januar 2007
Über eine implizite Partikelmethode zur Simulation von Umformprozessen

Nr. 140 Jörn Mosler: Mai 2007
On the numerical modeling of localized material failure at finite strains by means of variational mesh adaption and cohesive elements

Nr. 141 Rainer Fechte-Heinen: Juni 2007
Mikromechanische Modellierung von Formgedächtnismaterialien

Nr. 142 Christian Grabe: Juni 2007
Experimental testing and parameter identification on the multidimensional material behavior of shape memory alloys

Nr. 143 Markus Peters: Juli 2007
Modellierung von Rissausbreitung unter Verwendung der p-Version der XFEM mit einer adaptiven Integrationsmethode

Nr. 144 Claus Oberste-Brandenburg: Juli 2007
Thermomechanical modeling of shape memory alloys at diffent length scales

Mitteilungen aus dem Institut für Mechanik
RUHR-UNIVERSITÄT BOCHUM
Nr. 144

978-3-935892-19-3